FLUID AND THERMAL INDUCED VIBRATION IN THIN SLENDER TUBE

Thesis

Submitted in partial fulfillment of the requirements for the degree of

DOCTOR OF PHILOSOPHY

by

NARASIMHA MARAKALA

(Reg.No.: ME05P04)

DEPARTMENT OF MECHANICAL ENGINEERING,

NATIONAL INSTITUTE OF TECHNOLOGY KARNATAKA,

SURATHKAL, MANGALORE-575 025, INDIA

DECEMBER, 2012

NATIONAL INSTITUTE OF TECHNOLOGY KARNATAKA, SURATHKAL

D E C L A R A T I O N

by the Ph.D. Research Scholar

I hereby *declare* that the Research Thesis entitled **"FLUID AND THERMAL INDUCED VIBRATION IN THIN SLENDER TUBE"** Which is being submitted to the **National Institute of Technology Karnataka, Surathkal** in partial fulfillment of the requirements for the award of the Degree of **Doctor of Philosophy** in **Mechanical Engineering** is a *bonafide report of the research work carried out by me*. The material contained in this Research Thesis has not been submitted to any University or Institution for the award of any degree.

ME05P04 NARASIMHA MARAKALA

(Register Number, Name & Signature of the Research Scholar)

Department of **Mechanical Engineering**

Place: NITK-Surathkal

Date:

NATIONAL INSTITUTE OF TECHNOLOGY KARNATAKA, SURATHKAL

C E R T I F I C A T E

This is to *certify* that the Research Thesis entitled **"FLUID AND THERMAL INDUCED VIBRATION IN THIN SLENDER TUBE"** submitted by **NARASIMHA MARAKALA** (Register Number: **ME05P04)** as the record of the research work carried out by him, is *accepted as the Research Thesis submission* in partial fulfillment of the requirements for the award of degree of **Doctor of Philosophy**.

Dr.Appu Kuttan K.K	Dr.Ravikiran Kadoli
Professor	Professor
Dept. of Mechanical Engineering	Dept. of Mechanical Engineering

Research Guides

(Name and Signature with Date and Seal)

Chairman - DRPC

(Signature with Date and Seal)

ACKNOWLEDGEMENTS

The satisfaction and happiness that accompanies the successful completion of any task would be incomplete without the expression of gratitude and appreciation to the people who made this research project work possible.

With due respects I would like to express and keep on record my sincere thanks and gratitude to my guides **Dr.Appu Kuttan K.K.**, Professor and **Dr.Ravikiran Kadoli,** Professor, Department of Mechanical Engineering for their invaluable guidance and for being a constant source of enthusiasm and inspiration throughout this project. Their support and encouragement has made me to gain additional knowledge in my career.

I sincerely thank the Head of the Department **Dr. G.C.Mohan Kumar,** faculty members and other staff of the Department of Mechanical Engineering, NITK, for their timely help and support during this project.

I am grateful to the management of my parent institution, NMAM Institute of Technology, Nitte, for permitting me to carry out this research work at NITK.

I wish to place on record my sincere thanks to Head of the Department and other colleagues of the Department of Mechanical Engineering, NMAM Institute of Technology, Nitte, who extended their whole hearted support to carry out the research work.

I whole heartedly thank my friends at NITK, Mr.Umashankar, Mr. Praveen Mallik, Mr.Kondaiah and Mr.Karthik Rao who extended their whole hearted support and help in developing the necessary computer programme, in conducting the experiments and in the preparation of the thesis.

Lastly I thank all those who have helped me either directly or indirectly during my research work.

NARASIMHA MARAKALA

ABSTRACT

Thin beam and thin walled circular tubes are widely found in various structural engineering applications. For example, satellites, rockets where the propellant is transferred through connecting pipe lines, micro heat exchanger pipe used in refrigeration and air conditioning system, air craft fuel ducts, etc. Invariably the structure experiences fluid load due to inertia effect of the fluid, thermal loads due to heat conduction and convection and dynamic loads due to inertia effect of the structural element. The pipelines conveying high velocity internal flow may experience severe flow induced vibration due to fluid pipeline interaction. Therefore response of the pipe to fluid load and inertia load is very important for the safe design and operation.

The present study is focused on the dynamic response of slender cantilever pipe oriented in the horizontal and vertical direction conveying air at different pressure. The objective of this work is to formulate the equation of motion using Newtonian's approach and finite element solution of this equation that helps to study the effect of boundary conditions, flow velocity, fluid pressure on the free vibration characteristics of the cantilevered pipe conveying air. The FORTRAN codes are written based on the finite element formulation. This code is validated with problems reported in archival journals. The experimental set-up was fabricated in the laboratory and experiments were conducted to study the response of the cantilever tube in horizontal and vertical orientation at different lengths, conveying air with different pressure. Certain important observations which are concluded from this work are (i) increasing the length of cantilever tube will increase the amplitude of transverse displacement and decrease the fundamental frequency of tube, irrespective of its orientation and (ii) increasing the pressure will increase amplitude of transverse response of cantilever tube and but the frequency remains same. These experimental observations are compared with the numerically obtained results.

To understand the thermally induced oscillations, it is essential to solve the heat transfer and structural problems simultaneously by coupling the temperature distribution and the structural displacement. The second order linear differential equation of motion with damping and thermal load as forcing function is presented. In the present study, spatial and time variation of convection that arises due to motion of

beam is interpreted based on the physical understanding of the nature of air currents that are established due to motion of tube. Thus, the forced convective heat transfer coefficient is computed using Reynold's number, Prandlt number and Nusselt number. Fourth order Runge-Kutta method is used to determine the transient response of the tube being subjected to heat source. The dynamic response of the tube is studied for various heating rates and different diameters of tube. The analysis showed that the rate of vibration is governed by the natural frequency of the tube and convective heat transfer coefficient. The displacement histories, which were initiated due to initial displacement, with the passage of time exhibited an initial decrease in the displacement and gradually increased to a maximum value depending on the heating rate and the magnitude of the sustained oscillations, were governed by the fact that the heat removed by convection balance the internal heating. Experimental studies were also carried out on thermally induced vibration of internally heated cantilever tube with tip mass and cantilevered U-tube with and without tip mass. The experimental results on the displacement response are found to agree reasonably well with the theoretical results. The important observations from the study conducted were, lowering the heating rate leading to larger time to attain steady state amplitude and vice- versa and also there exists a threshold heating rate to produce thermal induced motion for the tube.

According to available literature, combined effect of fluid flow and thermal effect on the vibration of pipe has not been studied rigorously. In the present work, experimental and theoretical study of fluid and thermal induced vibration has been carried out on thin tube. The experiments are conducted for different end mass, length of the tube as well as the air passing through the tube at different temperature and pressure. The natural frequencies are calculated theoretically using finite element formulation and compared with the experimental results. It is observed from the study that the increase in pressure tends to increase the frequency due to increase in stiffness and increase in temperature tends to decrease the frequency due to softening effect of tube.

CONTENTS

LIST OF FIGURES

LIST OF TABLES

NOMENCLATURE

A	Cross section area of tube, m^2
A_c	Surface area for convection, m^2
a	Magnification factor for convection
a_c	Acceleration
a_{fx}	Acceleration of fluid in x-axis, m/sec^2
a_{fy}	Acceleration of fluid in y-axis
a_{fz}	Acceleration of tube in z-axis
a_p	Acceleration of pipe
a_{pz}	Acceleration of pipe in z-axis
B	Damping coefficient
b	Width of the beam, m
c	Velocity of propagation of longitudinal waves, m/sec
c_p	Specific heat, J/kg^0C
D	External diameter of the tube, m
D_c	Outside diameter of cement coating, m
$\{d\}$	Nodal displacement vector
$\{\dot{d}\}$	Nodal velocity vector
dA	Elemental Cross section area, m^2
dt	Small change in time
dx	Small element length
E	Young's modulus, N/m^2
E_c	Elastic modulus of cement, N/m^2
E_s	Elastic modulus of steel, N/m^2
F	Shear force, N
F_T	Total force
$F(t)$	Forcing function due to thermal moment, Nm
$\bar{F}_Q^e$	Elemental thermal force vector

F_{tot}	Total forcing function for the entire tube, Nm
$F\delta s$	Reaction forces of the pipe on the fluid normal to the fluid element
F^*	Thermal force between point a and b
f	Arbitrary function
G^e	Elemental damping matrix
$[G]_{ns\max}$	Global damping matrix
g	Acceleration due to gravity, m/s^2
H	Thickness of tube, m
h_{avg}	Average convective heat transfer coefficient
h_c	Natural convective heat transfer coefficient, $W/m^2\ ^0C$
$h(t)$	Forced convection heat transfer coefficient
I	Moment of inertia of beam cross section, m^4
K_p^e	Elemental fluid pressure matrix
K_{cap}^e	Elemental capacitance matrix
K_{comb}^e	Elemental conduction and/or convection matrix
K_f^e	Elemental fluid stiffness matrix
K_s^e	Elemental structural stiffness matrix
K_t^e	Elemental pipe tension matrix
K_{st}^e	Total elemental stiffness matrix
$[K]$	Stiffness matrix
$[K_{3D}]$	Stiffness matrix for 3-D beam element
$[K]_{ns\max}$	Global stiffness matrix
K_{conv_last}	Elemental end convection matrix
k	Thermal conductivity of material, W/m^0K
k_{air}	Thermal conductivity of air
k_x	Thermal conductivity of material along length of the tube

L	Length of the tube, m
l	Element length, m
l_{seg}	Segmental length, m
M	Bending moment, N-m
M^e	Elemental mass matrix
$[M]$	Mass matrix
$[M]_{ns\max}$	Global mass matrix
M_T	Thermal bending moment, Nm
M_{Ti}, M_{Tj}	Thermal bending moment at nodes i and j
m	Mass of pipe, kg
m_e	Equivalent mass of tube with tip mass, kg
m_f	Mass of fluid, kg
m_T	Non dimensional thermal moment
m_{tip}	Tip mass, kg
$N_{1,2,3,4}$	Hermite shape function
$N_{i,}N_j$	Linear shape function
N_H	Hermitian interpolation functions
N_L	Linear interpolation (shape) functions
N_L^T	Test function
N_{uD}	Nusselt number
$N(u)$	Linear function
P	Perimeter of boundary surface, m^2
Pr	Prandlt number
P_{rS}	Prandlt number at instantaneous temperature
p	Fluid pressure, N/m^2
$\bar{p}$	Mean pressure, N/m^2
Q	Heat flux, W/m^2

Q_T	Transverse shear force
q	Rate of conductive heat transfer
q_s	Wall shear stress
$\dot{q}$	Internal heat generation rate per unit volume, W/m^3
$\dot{q}_c$	Rate of convective heat transfer
q_x	Heat flux in x direction, W/m^2
R	Average tube radius, m
R_i	Inner radius of tube, m
R_0	Outer radius of tube, m
R_{eD}	Reynolds number
r	Position vector
S	Internal perimeter of the pipe
s	Curvilinear coordinate
T	Temperature of surface, ^{0}C
$[T]$	Rotation transformation matrix
$\left[T^{'}\right]$	Transformation matrix
$[T_x],\left[T_y\right],[T_z]$	Transformation matrix in x, y and z axis
$\{T\}_a,\{T\}_b$	Temperature at points a and b
$\bar{T}$	Mean applied tension
T_0	Longitudinal Tension in pipe
T_1, T_2	Nodal temperatures, ^{0}C
T_B	Temperature on bottom surface of beam, ^{0}C
T_i	Instantaneous temperature, ^{0}C
T_m	Perturbation temperature, ^{0}C
T_s	Surface temperature, ^{0}C
T_T	Temperature on top surface of beam, ^{0}C

T_∞	Ambient temperature, ^{0}C
T_{avg}	Average temperature, ^{0}C
t	Time, sec
t_c	Cement coating thickness, m
t_s	Steel pipe thickness, m
U	Steady flow velocity of the fluid, m/s
u	Dummy variable of integration
V	Non-dimensional transverse deflection
V_o	Velocity of the oscillating tube
$\bar{V}$	Displacement at the tip of the tube, m
V_f	Velocity of the centre of the fluid element
V_p	Velocity of the pipe element
v_{st}	Static displacement, m
W^T	Hermite interpolation (shape) function
$[W]$	Hermite interpolation matrix
w	Lateral deflection in the z direction, m
w^e	Deflection vector
x	Position along x-axis
y	Moment arm about z-axis, m
y_i	Thickness at i^{th} layer measured along the y axis, m
z	Moment arm about y-axis, m

Greek Letters

α	Coefficient of thermal expansion, / ^{0}C
ΔT	Change in temperature, ^{0}C
Δt	Time interval
ξ	Damping ratio
ρ	Mass density, Kg/m^3

ρ_a	Density of air at ambient temperature, Kg/m^3
ρ_c	Density of cement, Kg/m^3
ρ_g	Density of pure gas, Kg/m^3
ρ_s	Density of steel, Kg/m^3
v_{dyn}	Dynamic displacement, m
δs	Element thickness of fluid and pipe
ω_n	Natural frequency, rad/s
τ	Non dimensional time
ν	Poisson's ratio
ϕ	Radial position angle
Ψ	State space damping matrix
Θ	State space stiffness matrix
υ	Transverse deflection in the y direction, m
τ	Unit vector tangential to the pipe
μ	Viscosity of the air at ambient temperature
φ	Constant in central difference method
Ω	Domain
σ	Stefan – Boltzmann constant
θ	Slope
θ_{x1}, θ_{x2}	Rotation about X-axis at i and j node
θ_{y1}, θ_{y2}	Rotation about Y-axis at i and j node
θ_{z1}, θ_{z2}	Rotation about Z-axis at i and j node
Γ	Convective heat loss from surface
χ, β, γ	Angles of rotation about x, y and z axes

CHAPTER 1
INTRODUCTION

1.1 GENERAL INTRODUCTION AND OUTLINE OF THE THESIS

Petrochemical industries, chemical processing plants and power generating industries require vessels and pipes for storage and transportation of fluids at high pressure and temperature. The miniaturization of many appliances in bio-medical, chemical and computer technology has brought an increased demand for high performance heat dissipating devices. There are many research work (Paidoussis 1998 and Thornton 1993) on micro scale level has already been started in recent years which are mostly concentrated on hydrodynamic and heat transfer characterization. There is still much variation in the results between the various experimental and numerical results. The variation exists because of experimental error like external disturbance, reliability of the instrument or due to some of the assumptions made in the theoretical work like assuming flow as laminar. Every experimental case studied inherently has trouble of isolating the vibrations due to pressure fluctuations alone. Uncontrollable factors such as pump noise, clamps and bends in the pipe and irregularities in the cylindrical geometry also contribute to the overall vibration sensed by the accelerometer. Conditions are fairly extreme and difficult to control at a micro scale in the case of gas flow in slender pipe.

The study of flow induced vibration of slender structures has been the objective of study for quite few decades. This may be partly due to the increase in the need for stability and reliability. It has now become increasingly important to understand and able to predict the dynamic behavior of fluid flow in a slender structure. Unlike the pipelines found in mechanical equipments, nuclear reactor, heat exchanger, steam generator, ocean mining pipe and drill rigs (Xia et al. 2004, Khulief et al. 2007 and Paidoussis 1998), the vibration of a slender structure induced by cross flow dynamic behaviors for structures of axial flow is relatively new phenomenon, although most of the failures are associated with the cases of cross flow dynamics. The quest for fundamental understanding of fluid-thermal- structure interaction and its

application in several areas of engineering, researchers analyze the problem through modeling and experiment. The vibration of axially moving slender beams or cylinders in fluid has been studied by several investigators (Taleb and Misra 1981 and Lin and Quio 2008).

Fluid induced vibration in pipes has important application in the oil transportation. In an important application such as host sonar sensor that are towed on the sea surface are sufficiently submerged to avoid wave induced vibration which has extremely long (1 kilometer or longer) array of several parallel cylinders. These pipes sense acoustic signal directed at the end and redirected from the sea bed strata. The accuracy of the signal which can be affected by vibration is of extreme importance. In this case pipeline is subjected to both fluid induced vibration as well as thermal induced vibration. The piping system used for transfer of highly pressurized gas often operate under time varying condition imposed by the pumps and valve operations and thus it may experience severe vibration. Examples of such problems are flow induced vibration of a pipeline supported above ground level as well as conveying internal flow.

Changes in the temperature of pipe produce thermal stresses which cause displacement of the pipe. Cyclic changes in the temperature of the beam induce transverse vibration. Thermal load can arises in structures that are subjected to rapid nonuniform radiant surface heating. For example, a spacecraft when passing from earth's shadow into sunlight is subjected to a sudden change in heating on one side. A nonuniform heating cause the temperature difference through cross section of the structure. The temperature difference induces a structural deformation away from the sun which may induce a low frequency transient vibration. Rapid non uniform surface heating is not the only cause for temperature difference through the cross section of the structure. A structure with internal heat generation in the earth's atmosphere can experience a temperature difference through the cross section caused by non uniform heat at the structure surface.

The combined effect of fluid induced vibration and thermal induced vibration has been investigated to a lesser extent. In this research project, it is planned to

investigate the vibration of the pipeline induced due to thermal and fluid loading. When a heated fluid under pressure passes through the pipeline, heating of the pipeline takes place and also heat dissipates from the surface of the pipeline through convection. The effect of thermal load and fluid load on the response of the system will be investigated in the present research work. Finite element model to numerically compute the structural vibration due to thermal and fluid induced vibration has been formulated. An experimental model is fabricated in the laboratory to correlate the experimental results with numerical results obtained through finite element method. The experimental results are presented graphically.

First chapter deals with the general introduction to fluid structure interaction of thin slender pipes and thermal induced vibration, basic concepts and relevant equation on fluid induced and thermal induced vibration problems, previous research work, scope and objective of the work. The Chapter 2 covers the details about experimental setup, results and analysis on the experimental results due to fluid structure interaction. Experiments were conducted for different length of pipe, different flow velocity and different orientation of the pipe such as vertical and horizontal. The results are presented graphically and discussed in detail.

The Chapter 3 explains the finite element formulation for the fluid structure interaction problem. The numerically computated results are verified with the results available in the literature and results are in agreement with an error of 1% for simply supported pipe and 12% for cantilever pipe. The referred literature Lee and Oh (2003) has followed spectral element method, which is similar to present one dimensional FE analysis method. Hence the error for simply supported pipe is less (1%). But another referred literature Sinha et al. (2001) has followed one dimensional FE analysis with different approach. Hence the error is more for cantilever pipe (12%). Finite element code developed in Chapter 3 is used for the experimental setup parameters and results are presented in Chapter 4. The results obtained through finite element method are cross verified with the experimental results and presented in this Chapter.

The Chapter 5 presents dynamic behavior of a heated tube using thermal model. The determination of the convective heat transfer coefficient for a stationary vertical tube with internal heating and kept in the still air under laboratory conditions were carried out. The results shows similar trend as reported in literature. For a heating rate between 7.5 W and 15 W, the model predicted reasonably close to experimental transient temperature distribution and steady state. It was noted that amplitude of vibration decreases on the tube and natural frequency and heat transfer coefficient increases during forced convection.

The Chapter 6 and 7 deals with theoretical and experimental studies on thermally induced vibration of the tube with and without tip mass. For the range of heating rates between 6 W to 12 W, the model was used to predict the transient temperature distribution and hence steady state temperature. The Chapter 8 presents theoretical and experimental studies on thermally induced vibration of the U-tubes. Natural frequency of the U-tube was obtained experimentally and compared with the theoretically results.

The Chapter 9 discusses about the combined effect of fluid thermal-structure interaction on the vibration of thin pipe experimentally and theoretically. The Chapter 10 concludes with summary of the thesis report, conclusions and scope for the future work.

1.2 BASICS ON FLUID INDUCED VIBRATION

Piping systems are widely utilized to convey fluids in many industrial fields. Examples include risers in offshore plants, fuel pipes in engine systems, heat transfer pipes in power generation plants, chemical plant piping, etc. The instability problem of these pipes conveying fluid is highly complex and a challenging task for modeling and analysis. The flow-induced vibration effect in fluid flowing pipes are generated through fluid-structure interaction (FSI) are normally observed in the garden hose pipe as well by holding the fingers on the pipe. If this effect increases beyond limit, pipe line failure will take place similar to the incident of Trans Arabian Pipeline (TAPLINE) (www.almashriq.hiof.no)

The fluid-structure interaction vibration can also be observed in a running fan, transmission lines, aircraft wings, etc., which involves the flow of air external to the surface. This is the case of external fluid-structure interaction (FSI) problem. If vibration will increase beyond limit, failure will takes place. The historical example is that of the Tacoma narrows bridge failure on November 7, 1940 (www.wikipedia.org)

With regard to the instability mechanism of slender pipes conveying fluid, there are two different cases: (i) unstable vibration caused by the fluid flow when the flow velocity surpasses a critical value and (ii) vibration due to oscillating fluid flow and two-phase fluid flow (Kaneko et al., 2008). In the present work only case (i) is considered. A thorough discussion on the vibration due to flow pressure internally dealt in detail in Chapter 2 to 4.

1.2.1 VARIOUS TYPES OF FLUID STRUCTURE INTERACTION PROBLEMS

The various classes of problems under the head of fluid structure interaction are detailed by Blevins (2001) and the same is represented in Figure 1.1 and 1.2. In this thesis, the subject of steady fluid with elastic instability is taken up for study.

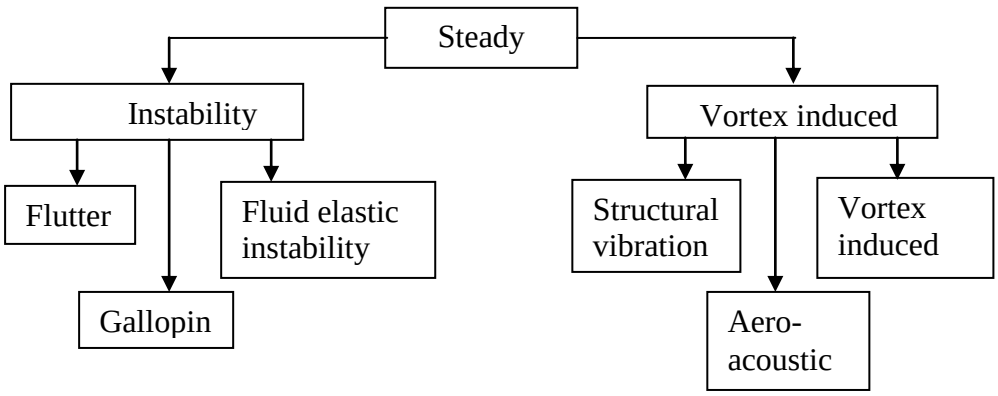

Fig.1.1 Steady case FSI types.

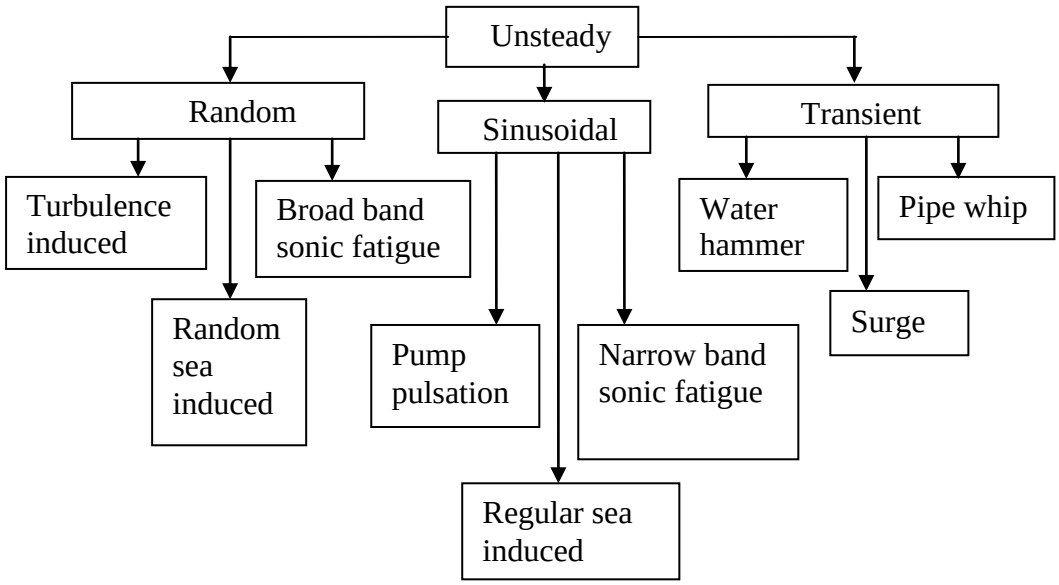

Fig.1.2 Unsteady case FSI types.

1.2.2 BASIC EQUATIONS IN FLUID STRUCTURE INTERACTION

The pipe may be modeled as a beam if the forces are considered only in $x-z$ plane (Refer Fig. 1.5). Forces causing radial expansion and contraction of the pipe and forces in other directions are not considered. A beam resists transverse loads mainly through bending action. Bending produces compressive stresses on one side of the beam and tensile stresses in the other. The fluid motion and pipe motion are coupled through the condition that the displacement of the flowing fluid in the pipe follows the deformation of the pipe and is accounted through the kinetic energy of the system.

If gravity, internal damping, externally imposed tension and pressurization effects are either absent or neglected, the equation for motion of the cantilever pipe shown in Figure 1.3 takes the simple form (Paidoussis 1998).

$$EI\frac{\partial^4 w}{\partial x^4}+m_f U^2\frac{\partial^2 w}{\partial x^2}+2m_f U\frac{\partial^2 w}{\partial x\partial t}+(m_f+m)\frac{\partial^2 w}{\partial t^2}=0, \qquad (1.1)$$

where EI is the flexural rigidity of the pipe, m_f is the mass of fluid per unit length flowing with a steady flow velocity U, m is the mass of the pipe per unit length, and w is the lateral deflection of the pipe; x and t are the axial coordinate and time

respectively. The fluid forces are modeled in terms of a plug flow model, which is the simplest possible form of the slender body approximation for the problem at hand. This equation will be derived in various ways and forms. One of the ways is the Newtonian approach, which is discussed below following the details given in the book by Paidoussis (1998).

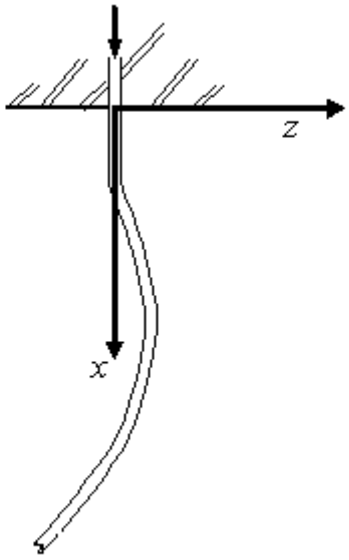

Fig.1.3 A cantilevered continuously flexible pipe conveying fluid (Paidoussis 1998).

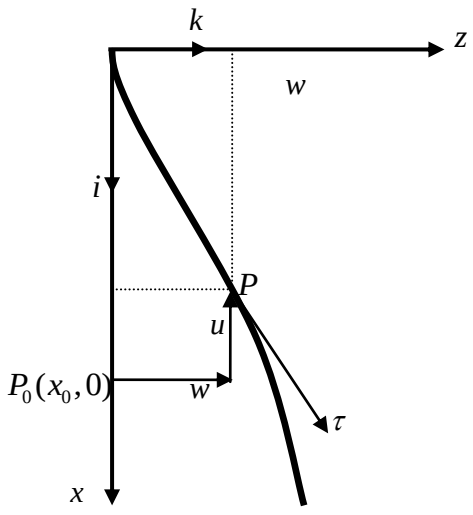

Fig.1.4. Euler coordinate system (x, z) and the deflection of a point $P(x, z)$ and the deflection of u and w.

Consider, a uniform pipe of length, L, internal perimeter, S, flow-area, A, mass per unit length, m, and flexural rigidity, EI, conveying fluid of mass per unit length, m_f, with mean axial flow velocity, U. Figure 1.4 shows the Euler coordinate system to describe the deflection of point on the pipe. The flow in the pipe is fully developed plug flow. Consider the undisturbed axis of the pipe to be vertical, along the x-axis, and the effect of gravity to be generally non-negligible. The flow velocity may be subject to small perturbations imposed externally, so that $\frac{dU}{dt} \neq 0$ generally.

The pipe is considered to be slender, and its lateral motions, $w(x,t)$ to be small and of long wavelength compared to the diameter; so the curvilinear coordinate s along the centerline of the pipe and the coordinate x may be used interchangeably. Consider the elements δs of the fluid and the pipe, as shown in Figure 1.5.

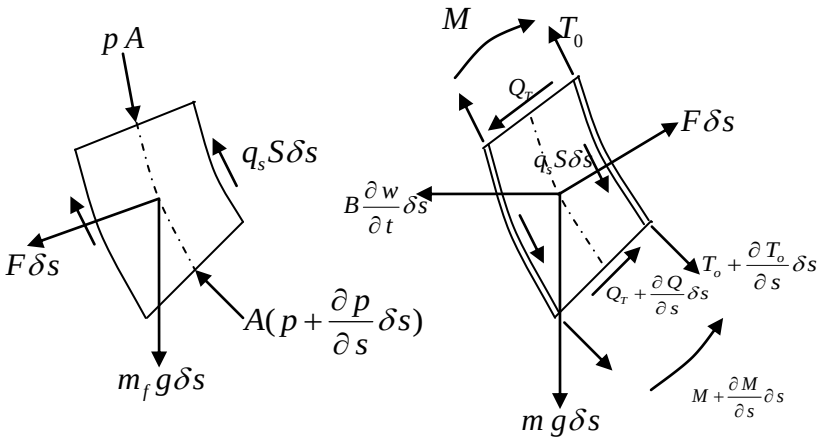

(a) (b)

Fig.1.5 (a) Forces acting on an element of the fluid; (b) forces and moments on the corresponding element of the pipe.

The fluid element shown in the Figure 1.5 is subjected to: (i) pressure forces, where the pressure $p = p(s,t)$ because of frictional losses, (ii) reaction forces of the pipe on the fluid normal to the fluid element $F\delta s$, and tangential to it is $q_s S\delta s$, associated with the wall-shear stress q_s; (iii) gravity forces $m_f g\delta s$ in the x-

direction. Applying Newton's second law in the x and z directions for the fluid and pipe elements, results in following equations.

From the free body diagram shown in Figure 1.5(a), the summation of forces along x-axis (considering equilibrium of equations along x-axis) is zero. Hence, $\sum F_x = 0$. Therefore,

$$-q_s S\delta s \cos\theta + F\delta s \sin\theta + m_f g\delta s - A\frac{\partial p}{\partial x}\delta s \cos\theta = m_f a_{fx}\delta s, \tag{1.2}$$

where, $\cos\theta = 1$, $\sin\theta = \theta$ [$\because$ 'θ' is small]

$$\Rightarrow \quad -q_s S\delta s + F\delta s\theta + m_f g\delta s - A\frac{\partial p}{\partial x}\delta s\theta = m_f a_{fx}\delta s,$$

$$\therefore \quad -q_s S + F\frac{\partial w}{\partial x} + m_f g - A\frac{\partial p}{\partial x} = m_f a_{fx}. \qquad [\because '\theta' = \frac{\partial w}{\partial x} \text{ is the slope}] \tag{1.3}$$

Similarly considering equilibrium of equations along z-axis,

$$-q_s S\delta s \sin\theta - F\delta s \cos\theta - A\frac{\partial p}{\partial x}\delta s \sin\theta = m_f a_{fz}\delta s, \tag{1.4}$$

$$\Rightarrow -q_s S\frac{\partial w}{\partial x} - F - A\frac{\partial}{\partial x}\left(p\frac{\partial w}{\partial x}\right) = m_f a_{fz}. \tag{1.5}$$

From the free body diagram shown in Figure 1.5(b), the summation of forces along x-axis (considering equilibrium of equations along x-axis) is zero. Hence, $\sum F_x = 0$. Therefore,

$$m g\delta s + q_s S\delta s \cos\theta + \frac{\partial T_o}{\partial x}\delta s \cos\theta - F\delta s \sin\theta = 0,$$

$$\Rightarrow \quad \delta s(m g + q_s S + \frac{\partial T_o}{\partial x} - F\theta) = 0,$$

$$\therefore\ m g + q_s S + \frac{\partial T_o}{\partial x} - F\frac{\partial w}{\partial x} = 0\,. \tag{1.6}$$

Similarly considering equilibrium of equations along z-axis,

$$-B\frac{\partial w}{\partial t}\delta s + q_s S\delta s \sin\theta + F\delta s \cos\theta + \frac{\partial T_o}{\partial x}\delta s \sin\theta + \frac{\partial Q}{\partial x}\cos\theta\,\delta s = m\, a_{pz}\delta s,$$

$$\therefore -B\frac{\partial w}{\partial t}+q_s S\frac{\partial w}{\partial x}+F+\frac{\partial}{\partial x}\left(T_o\frac{\partial w}{\partial x}\right)+\frac{\partial Q}{\partial x}=m\,a_{pz}, \tag{1.7}$$

where, a_f = acceleration of fluid,

a_p = acceleration of pipe.

Considering equilibrium of equations for shear force and bending moment,

$$Q_T=\frac{\partial M}{\partial x}=-\left(E+E*\frac{\partial}{\partial t}\right)I\frac{\partial^3 w}{\partial x^3}, \tag{1.8}$$

where T_o is the longitudinal tension, Q_T is the transverse shear force, and M is the bending moment and damping due to friction with the surrounding fluid as $B\frac{\partial w}{\partial t}$. The subscript f in equation (1.3) indicates the acceleration of the fluid and subscript p in equation (1.7) that of the pipe**.**

Basic assumption of fluid flow is plug flow, where fluid flow as infinitely flexible rod travelling through the pipe, all points of the fluid having a velocity U relative to the pipe. Velocity of pipe V_p is in terms of the unit vectors in x and z-directions is

$$V_p=\frac{\partial r}{\partial s}=x\,i+z\,k, \tag{1.9}$$

where r is the position vector to a point measured from the origin. Velocity of the centre of the fluid element V_f is

$$V_f=V_p+U\tau, \tag{1.10}$$

where τ is the unit vector tangential to the pipe,

$$\tau=\frac{\partial x}{\partial s}i+\frac{\partial z}{\partial s}k. \tag{1.11}$$

Consequently,

$$V_f=\left(\frac{\partial}{\partial t}+U\frac{\partial}{\partial s}\right)(x\,i+z\,k)\equiv\frac{D\,r}{D\,t}, \tag{1.12}$$

$$V_f=\frac{\partial x}{\partial t}i+\frac{\partial z}{\partial t}k+U\left(\frac{\partial x}{\partial s}i+\frac{\partial z}{\partial s}k\right),$$

$$V_f = \frac{\partial x}{\partial t} i + \frac{\partial z}{\partial t} k + U \frac{\partial x}{\partial s} i + U \frac{\partial z}{\partial s} k,$$

where, $\frac{D(.)}{Dt}$ is the material derivative for the fluid element. Recalling that $z = w$ and that $\frac{\partial x}{\partial s} \approx 1$ and $\frac{\partial x}{\partial t} \approx 0$ in accordance with the assumptions made, gives

$$V_f = \frac{D r}{D t} = U i + \left[\frac{\partial w}{\partial t} + U \frac{\partial w}{\partial s} \right] k. \tag{1.13}$$

In a similar manner, the acceleration is found to be

$$a_f = \frac{D^2 r}{D t^2} = \frac{D}{D t}\left(\frac{D r}{D t} \right) = \frac{D}{D t}(U i) + \frac{D}{D t}\left[\left(\frac{\partial w}{\partial t} + U \frac{\partial w}{\partial s} \right) k \right],$$

$$\Rightarrow \frac{d U}{d t} i + \left[\left\{ \frac{\partial}{\partial t}\left(\frac{\partial w}{\partial t} \right) + U \frac{\partial}{\partial s}\left(\frac{\partial w}{\partial t} \right) \right\} + \left\{ \frac{\partial}{\partial t}\left(U \frac{\partial w}{\partial s} \right) + U \frac{\partial}{\partial s}\left(U \frac{\partial w}{\partial s} \right) \right\} \right] k,$$

$$\Rightarrow \frac{d U}{d t} i + \frac{\partial^2 w}{\partial t^2} k + U \frac{\partial^2 w}{\partial s \partial t} k + U \frac{\partial^2 w}{\partial s \delta t} k + \frac{\partial w}{\partial s} \frac{\partial U}{\partial t} k + U^2 \frac{\partial^2 w}{\partial s^2} k + \frac{\partial w}{\partial s} \frac{\partial U}{\partial t} k,$$

$$\Rightarrow \frac{d U}{d t} i + \left[\frac{\partial^2 w}{\partial t^2} + 2U \frac{\partial^2 w}{\partial s \partial t} + U^2 \frac{\partial^2 w}{\partial s^2} + 2 \frac{\partial w}{\partial s} \frac{\partial U}{\partial t} \right] k,$$

$$\therefore a_f = \frac{d U}{d t} i + \left[\frac{\partial}{\partial t} + U \frac{\partial}{\partial s} \right]^2 w k. \tag{1.14}$$

From equation (1.13) and (1.14) we get,

$$a_{fx} = \frac{d U}{d t}, \quad a_{fz} = \left[\frac{\partial}{\partial t} + U \frac{\partial}{\partial x} \right]^2 w, \quad a_{pz} = \frac{\partial^2 w}{\partial t^2}; \tag{1.15}$$

In the above equation (1.15), last term is the lateral acceleration of the pipe. Combining equation (1.4), (1.6), (1.7) and (1.11); one obtains

$$\left(E \frac{\partial}{\partial t} + E \right) I \frac{\partial^4 w}{\partial x^4} - \frac{\partial}{\partial x}\left[(T_o - p A) \frac{\partial w}{\partial x} \right] + m_f \left[\frac{\partial}{\partial t} + U \frac{\partial}{\partial x} \right]^2 w + B \frac{\partial w}{\partial t} + m \frac{\partial^2 w}{\partial t^2} = 0 . \tag{1.16}$$

Also, adding equations (1.3) and (1.5), and using equation (1.15) yields

$$\frac{\partial}{\partial x}(T_o - p A) = m_f \frac{d U}{d t} - (m_f + m) g, \tag{1.17}$$

which integrated from x to L gives

$$\left(T_o - pA\right)\Big|_{x=L} - \left(T_o - pA\right) = \left[m_f \left(\frac{dU}{dt} \right) - \left(m_f + m \right) g \right] \left(L - x \right). \tag{1.18}$$

If the flexible pipe discharges the fluid to atmosphere at $x = L$, the pipe tension T_o which is then entirely due to fluid friction is zero at $x = L$; unless there is an externally applied tension, denoted by $\bar{T}$. The pressure, p at $x = L$ will also be zero unless the pipe does not discharge to atmosphere, in which case there may be a mean pressure $\bar{p}$ at $x = L$. Thus, $\bar{T}$ and $\bar{p}$ would act uniformly over the total length of the pipe, which yields $T_o = 2\nu \bar{p} A$ (internal pressurization induces an additional tensile force, which for thin pipe is equal to $T_o = 2\nu \bar{p} A$).

Hence, rearranging equation (1.18) with T_o and $\bar{T}$ and substituting $T_o = 2\nu \bar{p} A$ at $x = L$,

$$T_o - pA = \left(\bar{T} + T_o - \bar{p} A \right)_{x=L} + \left[\left(m_f + m \right) g - m_f \left(\frac{dU}{dt} \right) \right] \left(L - x \right),$$

$$T_o - pA = \delta \left[\bar{T} - \bar{p} A \left(1 - 2\nu \right) \right] + \left[\left(m_f + m \right) g - m_f \left(\frac{dU}{dt} \right) \right] \left(L - x \right). \tag{1.19}$$

$$\therefore \left(E \frac{\partial}{\partial t} + E \right) I \frac{\partial^4 w}{\partial x^4} + \left[m_f U^2 - \delta \left[\bar{T} - \bar{p} A \left(1 + 2\nu \right) \right] - \left\{ \left(\left(m_f + m \right) g - m_f \frac{dU}{dt} \right) \left(L - x \right) \right\} \right] \frac{\partial^2 w}{\partial x^2}$$
$$+ 2 m_f U \frac{\partial^2 w}{\partial x \partial t} + \left(m_f + m \right) g \frac{\partial w}{\partial x} + B \frac{\partial w}{\partial t} + \left(m_f + m \right) \frac{\partial^2 w}{\partial t^2} = 0, \tag{1.20}$$

where, $\delta = 0$ signifies that there is no constraint to axial motion at $x = L$ (i.e. cantilever pipe) then equation (1.20) becomes

$$\therefore \left(E \frac{\partial}{\partial t} + E \right) I \frac{\partial^4 w}{\partial x^4} + \left[m_f U^2 + \left\{ \left(\left(m_f + m \right) g - m_f \frac{dU}{dt} \right) \left(L - x \right) \right\} \right] \frac{\partial^2 w}{\partial x^2}$$
$$+ 2 m_f U \frac{\partial^2 w}{\partial x \partial t} + \left(m_f + m \right) g \frac{\partial w}{\partial x} + B \frac{\partial w}{\partial t} + \left(m_f + m \right) \frac{\partial^2 w}{\partial t^2} = 0, \tag{1.21}$$

where, $\delta = 1$ signifies that there is constraint to axial motion at $x = L$ (i.e. simply supported pipe) then the equation (1.21) is,

$$\therefore \left(E\frac{\partial}{\partial t}+E\right)I\frac{\partial^4 w}{\partial x^4}+\left[m_f U^2-\bar{T}+\bar{p}A(1-2\nu)-\left\{\left(\left(m_f+m\right)g-m_f\frac{dU}{dt}\right)(L-x)\right\}\right]\frac{\partial^2 w}{\partial x^2} \quad (1.22)$$
$$+2m_f U\frac{\partial^2 w}{\partial x\partial t}+\left(m_f+m\right)g\frac{\partial w}{\partial x}+B\frac{\partial w}{\partial t}+\left(m_f+m\right)\frac{\partial^2 w}{\partial t^2}=0\,.$$

Further if gravity and dissipation effects are either absent or neglected and U is constant, then equation (1.22) simplifies to the governing equation of motion for a pipe in the transverse direction is given as,

$$EI\frac{\partial^4 w}{\partial x^4}+\left[m_f U^2-\bar{T}+\bar{p}A(1-2\nu)\right]\frac{\partial^2 w}{\partial x^2}+2m_f U\frac{\partial^2 w}{\partial x\partial t}+(m_f+m)\frac{\partial^2 w}{\partial t^2}=0, \quad (1.23)$$

where E is the modulus of elasticity of the pipe, I is the area moment of inertia of the pipe, A is the fluid flow area of the pipe, ρ is the density of fluid, m_f is the fluid mass per unit length, m is the pipe mass per unit length and U is the velocity of fluid.

The detailed description of each term in equation (1.23) has been mentioned in Sinha et al. (2001). The first and fourth terms are stiffness and inertia terms whereas the second and third terms are fluid forces dependent on the flow velocity. They are required to change the direction of flow in deformed section of pipe during vibration and for rotation of fluid element respectively. The second term is equivalent to the axial compression term which increases with velocity. Hence, this term is responsible for decreasing the frequency of pipe with increase in flow velocity compared to the frequencies of the pipe completely filled with stagnant fluid. The third term is a mixed derivative that causes an asymmetric distortion in the classical mode shapes. Piping instability occurs at the critical velocity of the fluid in the pipe.

1.2.3 PREVIOUS RESEARCH WORK ON FLUID STRUCTURE INTERACTION

As mentioned in the section 1.2.3, a number of studies have been conducted to assess the relationship between the fluid flow velocity, pressure of fluid flowing through a pipe and its accompanying dynamic response. These researchers explained this problem using numerical and/or experimental techniques. This section discusses on what has been done in each of these areas.

Theoretical and Experimental investigation on the vibration of pipe conveying fluid

Most numerical studies on FSI phenomenon focus to study the effect of flow velocity and effect of fluid pressure of the pipe conveying the fluid. Long (1955) investigated analytically and experimentally the free transverse vibrations for the fundamental mode of single span tube containing a flowing fluid for several end conditions like simply supported, fixed, fixed-simple and fixed-free ends. For theoretical analysis an approximate solution of the differential equation of motion was proposed with an infinite power series. For experimental investigation, low carbon steel seamless tube with 1 inch (0.0254 m) OD and 0.037 inches (0.9398 mm) thickness for the above end conditions were constructed. Two, type A-5 SR4, strain gauges were mounted on the tube to pick up the strain in the vibrating tube and a brush BL-310 strain amplifier and BL-201 magnetic direct-inking oscillograph were used to record the vibration. The free vibration was started with no velocity and an initial displacement by hanging weight at the mid span. They observed that a slight decrease in frequency and no decaying vibration with an increase in flow rate for simply supported, fixed and fixed-simple ends. For a cantilever pipe, a decaying vibration and a slight frequency decrease due to flowing fluid was indicated.

Naguleswaran and Williams (1968) made theoretical and experimental investigation on lateral vibration of a pipe conveying fluid. For theoretical study they used exact solution and approximate solution for pinned-pinned span, fixed- fixed span and pinned-fixed span condition and compared the results as a variation of natural frequency and phase difference between the ends of the span as a function of flow speed. For experimental investigation, a neoprene tube was clamped at each end to a rigid copper tube and initial tension was induced by suitably loading one copper tube before fixing. Two capacitance pick–ups were used to detect the vibration and flow speed was calculated from the weight of water delivered in a measured interval of time. They conducted the experiment for various fluid pressure and speed and found that straight cantilever pipes fail about at large amplitude when the flow velocity exceeds critical velocity. Hills and Swanson (1970) studied the effect of

adding lumped mass on the vibration of cantilever tube conveying fluid. In this investigation an analytical solution is presented using Galerkin's method. The value of the critical velocity were determined without lumped mass and with lumped mass. This theoretical study is verified with the data obtained from the experiment. The experiment set up consists of latex surgical cantilever tube of inside diameter between 3 to 32 inches (0.0762 to 0.8128 m) and 9 to 32 inches (0.2286 to 0.8128 m) and wall thickness between 1 to 16 inches (0.0254 to 0.4064 m) and 1 to 8 inches (0.0254 to 0.2032 m) with lumped mass. They found that the addition of lumped mass reduces the value of the critical velocity.

Hill and Davis (1974) studied effect of initial forces on vibration and stability of a curved, clamped and fluid conveying tube using the finite element technique. They developed the equation of motion by modifying the equilibrium equation of a curved elastic tube including initial pressure, inertial effect of the tube and flowing fluid. The initial force was considered by pressurizing the fluid through the tube at a constant velocity. Calculations were carried out using derived equation to verify the effect of flowing fluid and pressure on natural frequency of circular arcs of 180, 360 and 540 degree, S, L and spiral configuration of fluid conveying tube with and without initial forces. They concluded that (i) buckling of tube occurs without initial force, while with initial force no buckling occurs (ii) without initial force, the arcs buckled out of plane with the bucking velocity increasing with the increasing angle and effect of pressure to lower the buckling velocities. Paidoussis and Laithier (1976) derived the equation of motion for the pipe conveying fluid by means of Timoshenko beam theory using finite difference technique and variational method and compared the results obtained from Euler-Bernoulli theory. This theory incorporates the effect of transverse and rotational inertia. They also verified the results with the experimental data. Experimental set up consists of two separate silicon rubber short tube hanging vertically downward as a cantilever beam. The dimensionless critical flow velocities and corresponding frequencies are obtained and compared with the above two theoretical analysis. From this study, they confirmed that the Euler-Bernouli theory is quite inadequate for predicting condition of very short pipe

conveying fluid, while the Thimoshenko beam theory is considerably more successful.

Holmes (1978) developed an equation representing the nonlinear dynamic behavior of a simply supported pipe conveying fluid to study the local and global stability of the equilibrium position. This numerical study showed that the sustained flutter motions are impossible when pipe is supported at both the ends. Rousselet and Herrmann (1981) examined the plane motion of a cantilever pipe conveying fluid near the critical velocity. Generally, for finite amplitudes of oscillation, the flow velocity is affected by the transverse motion of the pipe. Hence they derived the equation of motion for fluid and pipe, which will be coupled through non linear terms. For this they considered a continuous cantilevered pipe hanging vertically, connected to a reservoir containing fluid so that fluid enters into the pipe at the top end and discharged tangentially at the free end into the atmosphere. From this theoretical analysis they concluded that for small amplitude, linear terms dominate and for larger amplitude non- linear term dominates. Edelstein et al. (1986) developed a finite element computation method for predicting the response of a cantilevered tube conveying fluid and verified with experimental data. In this paper a numerical method which consists of non linear equation has been presented to characterize tube response for flow velocity larger than critical speed. To make quantitative comparison, tests were performed on a polyethylene tube, hanging vertically downward with 0.375 inches (0.009525 m) OD, 0.625 inches (0.01587 m), and wall thickness 27 inches (0.6858 m) length conveying fluid. Tube displacement at the free end is measured for different flow velocities. They observed that the response amplitudes at sub critical flow velocities are very small and it increase drastically at the critical flow velocity.

Paidoussis et al. (1986) re-examined the dynamics and stability of short tubes conveying fluids by means of Timoshenko beam theory, with refined fluid mechanics model, referred as Timoshenko-Refined-Flow theory for clamped-clamped and cantilevered end conditions. They derived the equation and analyzed theoretically. For experimental analysis cantilever pipe made of silicone rubber with 15.60 mm outside and 6.35 mm inside diameter was considered. An optical-fiber sensor is used to

measure the displacement and frequency was measured from the oscillation-time traces recorded on the oscilloscope. The experiments were conducted for various flow velocities, measured by standard means. They found that theoretical critical flow velocity and corresponding critical frequencies agree better with the experimental data than the result obtained by the other theory. Hence they concluded that the refined fluid mechanics model is more suitable for analyzing the dynamics of a short tube conveying fluid. Lin and Tsai (1996) presented a finite element approach for nonlinear vibration analysis for Timoshenko pipes conveying fluid. This approach makes use of the concept of fictitious loads for dynamic analysis of cantilever pipes conveying fluid with supercritical flow velocities. The formulation of this approach were verified by comparing the analysis results with those available in the previous technical papers for slender and short beam undergoing large deformation. They found that numerical simulation results from this approach were in good agreement with those obtained from exact solution for large deformation analysis of a slender beam and for short beam, excellent agreement has been observed when compared with the ANSYS analysis.

Bar-Avi (2000) developed an analytical model for the non linear response of fluid conveying risers. It is nonlinear differential equations of motion of riser conveying an internal fluid including the aspects like nonlinearities due to geometry (due to drag force), internal and external fluid pressure and internal fluid velocity and acceleration. They considered an actual riser of 100 m length, 0.21 m outside diameter and 0.2 m internal diameter for calculation. The response of the riser to different environmental condition and different physical parameters like without external loading, considering wave and current excitation, base and top excitation was investigated. Also, response in the presence (at 300 m/sec) and absence of internal fluid flow was compared. They found that (i) natural frequency of riser decreases with increase in fluid flow velocity, (ii) in the absence of internal velocity, the displacement of riser reaches a steady state equilibrium position, while in the presence of internal flow it will keep oscillating due to the flow induced vibration, (iii) for wave and current excitation, in the absence of internal flow the riser oscillates with small amplitude and for nonzero flow it oscillates with larger amplitude, (iv) for base

and top excitation, the response with internal flow is larger than one without flow and frequency of excitation coincides with the natural frequency resulting in high amplitude for both case (with and without flow), (v) for accelerating fluid, the response was clearly nonlinear. Wang et al. (2001) studied theoretically and experimentally the flow induced vibrations of a fixed-fixed elastic cylinder with large aspect ratio for free vibration by considering 2-dimensional laminar flow. For theoretical analysis, structural vibration was modeled by Euler-Bernoulli beam theory coupled with Navier-Stokes equation. The experimental work was performed on 6 mm diameter, 350 mm length pipe made up of acrylic material cylinder. They analyzed for two different cases (i) at resonance (ii) at off-resonance. The results are compared with experimental measurements obtained under identical conditions. Differences between these results were examined and a correction formula is derived.

Lee and Oh (2003) considered simply-supported pipeline conveying high velocity internal flow, experience severe flow induced vibration due to fluid-pipeline interaction. They predicted accurate flow induced vibrations using spectral element model (i.e. using one dimensional finite element for the uniform structure member, regardless of its length) than classical finite element model. They formulated equation of motion by considering fluid and pipe elements individually and then converted into spectral element formulation to solve equation of motion. Numerical results were compared with the analytical results detailed in Blevins (2001) at different conditions like empty pipeline, stagnant fluid and pipe line conveying fluid at different velocities and at different pipe axial tension. They concluded that by increasing the fluid velocity, frequency of pipe will decrease. Zou et al. (2005) studied fluid induced vibration of composite natural gas pipelines using Ritz method. They developed a state variable model for the analysis of fluid induced vibration of composite pipe line systems for various boundary conditions like cantilever, simply-supported, fixed-fixed. A steel pipe with fiber reinforced composite to get high strength and less weight in sub-sea applications was used for the analysis. They investigated the influence of fluid velocity, internal pressure and initial tension on pipeline vibration frequency. This analysis showed that increasing the fluid velocity and pressure decreases the vibration frequency, but increasing the pre-tension force increases the

pipes natural frequency for all boundary conditions. These results were compared with finite element analysis using ANSYS software with eight node isotropic 3D solid (SOLID 45) and mesh density of 20 (in the circumferential direction) × 200 (in the axial direction) × 2 (in the radial direction).

Paidoussis and Semler (1998) examined theoretically and experimentally the planar dynamics of a fluid conveying cantilever pipe with a small mass attached at the free end. Experiments were conducted with five silicon rubber tube with eight end masses of various weights. The pipe was hung vertically and fluid flow supplied from the reciprocating pump through accumulator and flow straightener. The flow rate was measured using Omega FMG-700 magnetic flow meter and displacement of pipe was measured with a optical tracking system (Optron 806a). Experiments were conducted by increasing the flow rate from zero until onset of flutter (Hopf bifurcation), where the pipe begins to oscillate. Further increase in flow rate gave second bifurcation, where the motion becomes chaotic. From the experimental investigation, they concluded that (i) two successive bifurcations were detected in the presence of end mass (ii) after second bifurcation, three dimensional chaotic oscillations were observed (ii) with no end mass, only the first bifurcation was observed. To investigate the above case theoretically, a non linear equation was derived using Finite Difference Method (FDM) and Incremental Harmonic Balance method (IBH) to calculate the required parameter. Rinaldi and Paidoussis (2010), studied theoretically and experimentally, the dynamics of a flexible cantilevered pipe fitted with a special end-piece. They observed that (i) the dynamics in the flow going straight through, unimpeded, and emerging at the free end as a jet is similar to that of a pipe with no end-piece, the system loses stability by flutter at high enough flow velocity, and then develops more complex oscillatory patterns at higher flow (ii) the dynamics in the straight-through path blocked, so that the flow is discharged radially from a number of holes perpendicular to the pipe, the system remains stable over the full range of flow velocities.

Sinha et al. (2001) studied the results of a modal experiment on an open ended cantilever pipe conveying fluid and using finite element method. For experimental

work, a cantilever pipe conveying fluid made of aluminium of 1010 mm length, 22.85 mm outer and 19.65 mm inner diameter was used. The critical velocity estimated to be of the order of 350 m/s. A small instrumented hammer was used for the excitation of the pipe. The force sensor (PCB 208A02) and an accelerometer were used for the measurement of exciting force and the response of the pipe respectively. The experiments were conducted for (i) empty pipe (ii) pipe filled with stagnant water (iii) pipe conveying water at a flow velocity of 0.55 m/s and 1.1 m/s. The modal parameter i.e. natural frequencies and modal damping was measured for the above case. These results were compared with the result obtained from FEM. They observed that an additional inertia of the fluid jet at the free end of the pipe is required to simulate the experimental natural frequency values. Hence, this additional inertia has to be accounted in the governing equation of motion for the cantilever pipe conveying fluid. Kuiper and Metrikine (2008) described the dynamic stability of a submerged cantilever pipe conveying fluid from free end to fixed end as one of the unresolved issue in the area of Fluid-Structure interaction. Every experimental case studied inherently has trouble of isolating the vibrations due to pressure fluctuations alone. Uncontrollable factors such as pump noise, clamps and bends in the pipe and irregularities in the cylindrical geometry also contribute to the overall vibration sensed by the accelerometer. It is also difficult to eliminate variation at high flow velocities-which affects the fully developed nature of the flow. Consequently, it is difficult to determine the effect of fully developed flow on the vibrations of a pipe. The summary of these literatures are summarized in the table 1.1.

The aforementioned research papers and books have helped in understanding the subject of dynamics of pipes conveying fluid as well as numerical solution procedure.

Table 1.1: Table summary of fluid induced vibration literature review.

Sl.No.	Author Name and year	Summary
1	Ashley and Haviland(1950)	Theoretically describe the vibration characteristics of the Trans-Arabian pipeline.
2	Bar-Avi (2000)	Developed an analytical model for the non linear response of fluid conveying risers and found that

		Natural frequency of riser decreases with increase in fluid flow velocity.
3	Blevins (2001)	Studied empty pipeline, stagnant fluid and pipe line conveying fluid at different velocities and at different pipe axial tension and concluded that by increasing the fluid velocity, frequency of pipe will decrease.
4	Edelstein et al. (1986)	Developed a finite element computation method for predicting the response of a cantilevered tube conveying fluid and verified with experimental data.
5	Guo et al.(2010)	Developed a modified equation of motion by including centrifugal force term for laminar and turbulent flow profile.
6	Hill and Davis (1974)	Studied effect of initial forces on vibration and stability of a curved, clamped and fluid conveying tube using the finite element technique.
7	Hills and Swanson (1970)	Studied the effect of adding lumped mass on the vibration of cantilever tube conveying fluid and found that the addition of lumped mass reduces the value of the critical velocity.
8	Holmes (1978)	Developed a equation representing the nonlinear dynamic behavior of a simply supported pipe conveying fluid to study the local and global stability of the equilibrium position.
9	Karagiozis et al. (2005)	Studied non-linear stability of a cylindrical shell subjected to internal flow by means of linear Fluid structure interaction model.
10	Kuiper and Metrikine (2008)	Described the dynamic stability of a submerged cantilever pipe conveying fluid from free end to fixed end as one of the unresolved issue in the area of Fluid-Structure interaction.
11	Lee and Oh (2003)	Studied simply-supported pipeline conveying high velocity internal flow and predicted accurate flow induced vibrations using spectral element model.
12	Lin and Tsai (1996)	Presented a finite element approach for nonlinear vibration analysis for Timoshenko pipes conveying fluid.
13	Long (1955)	Investigated analytically and experimentally the free transverse vibrations for the fundamental mode of single span tube containing a flowing fluid for several end conditions like simply supported, fixed, fixed-simple and fixed-free ends.
14	Modarres-Sadeghi	Theoretically investigated the 2-D and 3-D

	et al.(2008)	flutter of cantilever pipe conveying fluid.
15	Modarres-Sadeghi et al.(2008)	Studied experimentally and theoretically the dynamic behavior of vertical clamped- clamped cylinder.
16	Naguleswaran and Williams (1968)	Theoretical and experimental investigation on lateral vibration of a pipe conveying fluid for pinned-pinned span, fixed- fixed span and pinned-fixed span condition.
17	Namkong et al. (2005)	Developed combined formulation which incorporate both fluid and structure equation of motion into a single coupled variational equation.
18	Paidoussis and Laithier (1976)	Derived the equation of motion for the pipe conveying fluid by means of Timoshenko beam theory using finite difference technique and variational method and compared the result with the results obtained from Euler-Bernoulli theory.
19	Paidoussis and Semler (1998)	Examined theoretically and experimentally the planar dynamics of a fluid conveying cantilever pipe with a small mass attached at the free end.
20	Paidoussis et al. (1986)	Examined the dynamics and stability of short tubes conveying fluids by means of refined fluid mechanics model, referred as Timoshenko-Refined-Flow theory.
21	Païdoussis et al. (2005)	Studied non-linear dynamic vibration of horizontal cantilever pipe conveying pipe.
22	Païdoussis et.al (2002)	Studied experimental behavior of cantilever cylinder and energy transfer of motion without solving the equation of motion.
23	Païdoussis et.al (2008)	Developed theoretical model for the dynamics of a hanging tubular cantilever pipe conveying fluid downward and then upward in the container.
24	Rinaldi and Paidoussis (2010)	Studied theoretically and experimentally, the dynamics of a flexible cantilevered pipe fitted with a special end-piece.
25	Rousselet and Herrmann (1981)	Examined the plane motion of a cantilever pipe conveying fluid near the critical velocity.
26	Sinha et al. (2001)	Studied the results of a modal experiment on an open ended cantilever pipe conveying fluid and their analytical simulation using Finite Element Method.
27	Srejith et al (2004)	Developed finite element formulation for fully coupled dynamic equation of motion to include the effect of fluid structure interaction and applied to a pipeline system used in nuclear reactor.

28	Wang et al. (1998)	Studied the influence of flow velocity on natural frequency using solid-liquid coupling dynamic equation.
29	Wang et al. (2001)	Studied theoretically and experimentally the flow induced vibrations of a fixed-fixed elastic cylinder with large aspect ratio for free vibration by considering 2-dimensional laminar flow.
30	Zou et al. (2005)	Studied analytically fluid induced vibration of composite natural gas pipelines and investigated the influence of fluid velocity, internal pressure and initial tension on pipeline vibration frequency.

1.3 BASICS ON THERMAL INDUCED VIBRATION

Structural components subjected to thermal conditions like, high temperature, high heating rate are common in the field of aerospace, nuclear, casting, forging, radiant burner, heat exchanger etc. The heating of the structure may be due to sudden exposure to very large amount of heat which is typical in rocket launching, spacecraft structural element subjected to radiant heating, nuclear reactor components are subjected to gradual heating or internal heat generation. It is well known that the topic of thermal induced vibration is of great concern. In spite of the availability of sufficient analytical studies on the thermal induced motion of beams and plates, it is found that the effect of boundary condition has not been dealt with. It is also noted that the convection effect were not included as part of heat transfer boundary condition. In this thesis, an attempt has been made using finite element formulation for an Euler-Bernoulli beam subjected to thermal load. The dynamic displacement and dynamic thermal moment of the beam is taken into consideration that temperature gradient independent as well as depend on the beam displacement.

1.3.1 PROBLEM DEFINITION

Consider a solid tube fixed at one end and free at the other kept in still air under laboratory conditions, heated by means of external heat source or electric current causing temperature variation along the length of the tube and continuously loosing heat to the surrounding from the surface and end face by means of convective

heat transfer. The generalized work domain for heat transfer problem is shown in Figure 1.6. The various parameters considered are as follows,

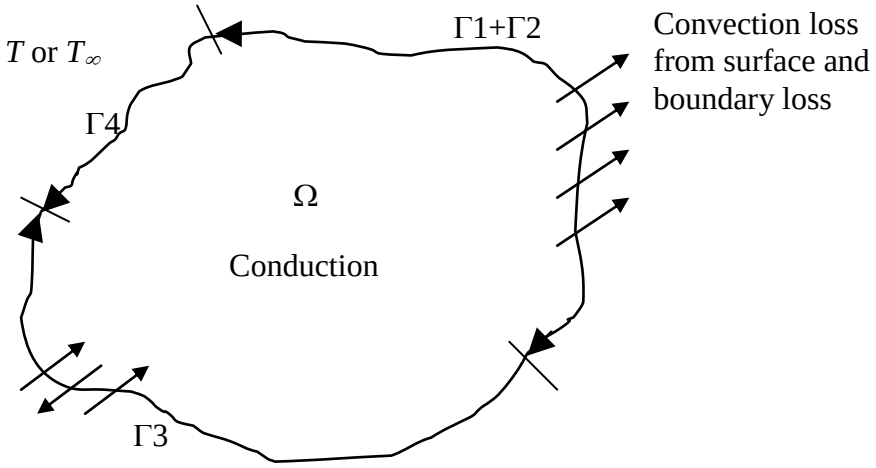

Fig 1.6 Generalized work domain for heat transfer problem

For the formulation of differential equation, the following domain and boundary conditions are used.

1. Internal heat will be generated because of supply of electric current, nuclear reaction, etc. and is time dependent, Ω. It is also referred to as change in internal energy.
2. Heat transfer from fixed end to tip by conduction, Ω.
3. Convective heat loss from surface, Γ_1.
4. Heat loss by convection from the end surface, Γ_2.
5. Heat influx or efflux, Γ_3.

The following assumptions are made for the formulation of differential equation.

1. Thickness of tube is small and hence the temperature gradient through the thickness is neglected.
2. There is no temperature variation around the circumference of the tube.
3. Radiation heat transfer occurring inside and outside the tube surfaces is neglected.
4. Convection inside the tube is neglected.

5. The thermal conductivity and specific heat do not vary with temperature and time.
6. At any cross section the natural convection on the surface of the tube is assumed to be axisymmetric.

1.3.2 FORMULATION OF THE HEAT CONDUCTION EQUATION WITH CONVECTION

The generalized energy equation for the system is written as:

Energy into the element - Energy out of element + Energy generated within the element = Change in internal energy

For the three dimensional system in cylindrical coordinates as shown in Figure 1.7 the governing differential energy equation is written as,

$$\left(\frac{1}{r}\frac{\partial T}{\partial r}+\frac{\partial}{\partial r}\left(\frac{\partial T}{\partial r}\right)+\frac{\partial^2 T}{\partial \phi^2}+\frac{\partial^2 T}{\partial x^2}\right)k+\dot{q}=\rho c_p\frac{\partial T}{\partial t}. \tag{1.24}$$

Hence, from the assumptions we have,

$$\frac{1}{r}\frac{\partial T}{\partial r}+\frac{\partial}{\partial r}\left(\frac{\partial T}{\partial r}\right)=0 \quad \text{and} \quad \frac{\partial^2 T}{\partial \phi^2}=0; \tag{1.25}$$

Therefore, the governing differential energy equation in 3-D reduces to a simple one dimensional form as

$$k\frac{\partial^2 T}{\partial x^2}+\dot{q}=\rho c_p\frac{\partial T}{\partial t}, \tag{1.26}$$

and adding the term to take care heat transfer due to convection,

$$kA\frac{\partial^2 T}{\partial x^2}+\dot{q}A=\rho c_p A\frac{\partial T}{\partial t}+\dot{q}_c P, \tag{1.27}$$

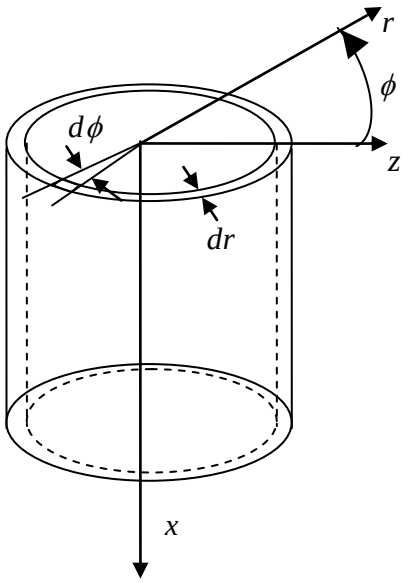

Fig.1.7 Cylindrical tube in 3-D coordinate system

where, $\dot{q}_c = h_c(T - T_\infty)$ or $-k\dfrac{\partial T}{\partial x} = h_c(T - T_\infty)$; (1.28)

P is the perimeter of boundary surface, ρ is the mass density, c_p is the specific heat, and $\dot{q}$ is the internal heat generation rate per unit volume.

The possible boundary and initial conditions are:

1. Initial condition $T(x,t) = T_\infty$ on Γ_4.
2. Boundary condition $\dot{q}_c = -k\dfrac{\partial T}{\partial x}$ on Γ_1.
3. Loss of heat by convection from the ends of one dimensional body, Γ_2.

Figure 1.8 shows the tube with various heat transfer boundary conditions. Consider a small element dx through which the heat q_x is flowing in x direction at any time instant due to conduction.

Heat influx, $q_x = -k_x\dfrac{\partial T}{\partial x}$. (1.29)

At the same time the heat flowing out of the element is given as q_{x+dx}

Heat efflux, $q_{x+dx} = -\left(k_x\dfrac{\partial T}{\partial x} + k_x\dfrac{\partial}{\partial x}\left(\dfrac{\partial T}{\partial x}\right)dx\right)$. (1.30)

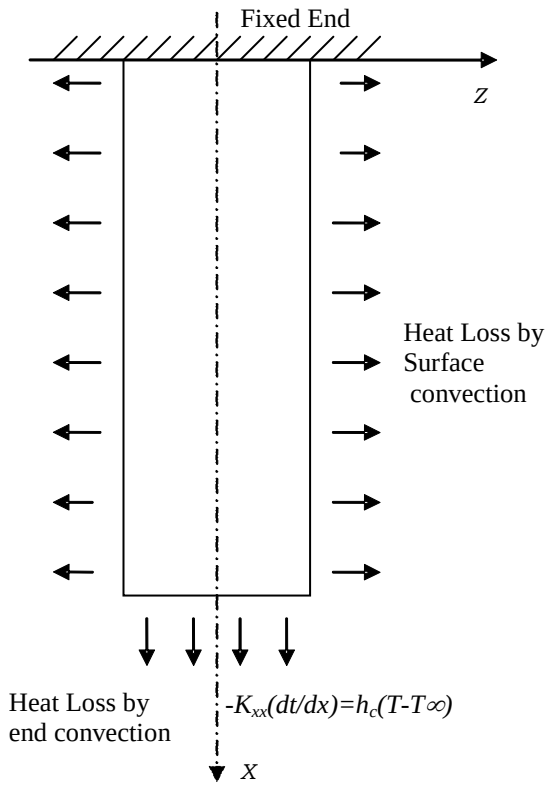

Fig.1.8 Tube with various heat transfer boundary conditions

Hence, substituting in Equation (1.27), the various initial and boundary conditions and rearranging,

$$q_x A dt + A\dot{q} dx dt = \rho c_p \partial T A dx + \dot{q}_c P dt dx + q_{x+dx} A dt. \tag{1.31}$$

Therefore,

$$k_x \frac{\partial}{\partial x}\left(\frac{\partial T}{\partial x}\right) A dx dt + \dot{q} A dx dt = \rho c_p A dx dT + \dot{q}_c P dt dx.$$

Dividing by *dxdt*

$$k_x A \frac{\partial}{\partial x}\left(\frac{\partial T}{\partial x}\right) + \dot{q} A = \rho c_p A \frac{dT}{dt} + \dot{q}_c P.$$

Hence, the governing equation in one dimension considering heat conduction and boundary condition as heat loss due to convective heat transfer can be written as

$$k_x A \frac{\partial}{\partial x}\left(\frac{\partial T}{\partial x}\right) + \dot{q} A = \rho c_p A \frac{dT}{dt} + \dot{q}_c P. \tag{1.32}$$

1.3.3. PREVIOUS RESEARCH WORK ON THERMAL INDUCED VIBRATION

Many researchers have studied thermal induced vibration. The first paper to address thermally induced vibration was published by Boley (1956) showed that when a beam is subjected to rapid external heating, a time dependent thermal moment develops due to temperature difference between the heated and unheated sides. The time dependent thermal moment act as a forcing function induces a structural deformation. Boley (1972) showed that, if the thermal response time is same order of magnitude or less than the structural response time, for a low mass, flexible structure, it is prone to thermal vibration. Flexible structures with a low fundamental frequency of vibration are used in spacecraft for booms and to support solar panels. Thus thermally induced vibrations have occurred as a problem associated with the spacecraft. Thornton (1996) presents a chronology of thermally induced vibration research with application to spacecraft.

Thornton and Foster (1992) conducted experiments investing thermally induced bending vibration in a vacuum. Thornton and Kim (1993) developed a mathematical model to investigate dynamic behavior of roll-out solar arrays used in Humble Space Telescope. Murozono and Thornton (1998) studied thermally induced quasi-static bending- torsion deformation in the context of local buckling of the bubble space telescope solar arrays. Thornton and et al. (1995) investigated the effect of self shadowing on the behavior of space station solar arrays. Thermally induced vibration of a spinning aircraft boom were studied by Gulick and Thornton (1995). Johnston (1999) conducted a detailed investigation of thermal induced motion of rigid panel solar arrays. Beam (1969) is credited with producing the first thermal induced vibration in the laboratory. These were torsional vibration produced by radiant surface heating. Rimrott and Abdel Sayed (1977) presented thermally induced bending vibration in the laboratory. Both of these investigations are land mark in the study of thermally induced vibrations. But neither was the first to produce thermal induced vibration in the laboratory. The first published experimental data on thermal induced vibration was by Baker (1936), although he did not understand by the time that vibration he observed was due to temperature difference through the thickness of the

test beam. Baker stated that vibrations were excited by the force between the air and the wire due to thermal action of the moving hot wire on the surrounding air. Baker did not give any insight into how or why the beam began to vibrate. Baker classifies the beam undergoing thermally induced vibration as a self induced vibration. Murozono (1995) showed that a vibration in convection coefficient around the circumference of the beam would cause a thermally induced vibration.

Blandino and Thornton (2001) have reviewed chronologically the contributions of various researchers to study thermally induced vibrations. They have carried out the detailed study of a thermally induced vibration caused by internal heating. Tran et al. (2007) analysed the structural intensity pattern of thin isentropic and laminated composite plates which are subjected to thermally induced vibration. Kidawa-Kukla (1997) has proved the frequency of the thermally induced beam vibration is a multiple of harmonic motion frequency of the heat source and then resonance can occur in the system. Hong et al. (2005) analysed the thermally induced vibration of a thermal sleeve using computational Generalized Differential Quadrature (GDQ) method for calculating the natural frequency displacement and thermal stresses. Kidawa-Kukla (2003) analysed the temperature distribution and transverse vibration of beam induced by using the property of the Green functions. Seibert and Rice (1973) have carried out studies on thermally induced vibration of a simply supported beam with heat input on one surface using (i) the one dimension heat conduction equations and including thermoelastic coupling and uncoupling terms for Bernouilli-Euler and Timoshenko beams as well as (ii) two dimension heat conduction equation in conjunction with uncoupled thermoelastic governing equations for thin and thick beams. Kraus (1996) has presented numerical results on the quasi-static response and dynamic response as a function of inertia parameter for simply supported thin non-shallow spherical shells whose inside surface is insulated and suddenly applied heat flux on to its outer surface. Lyons (1966) suggested that the best practical way of providing sudden heat input to beams, plates and shells is by instantaneously supply of electrical energy and by gamma radiation. Associated governing equation of motion for infinitely long cylindrical shell and the displacement response solution has been presented. Kim (1998) has presented an

analytical and experimental investigation of the thermal creak phenomenon by developing a generic model of a thermal creak element to understand the mechanism and to identify the key parameters. The model captures the thermoelastic response, the friction behavior, and the dynamic response of a system. Key parameters that govern the response and quantify the parameters correlated with the energy storage, energy release and energy propagation were identified and the dynamic response was parametrically studied to qualitatively understand the range of behaviors.

Blandino and Thornton (2000) in their recently published article have given the experimental results and theoretical model for calculating the natural and forced convective heat transfer coefficient as function of position along the beam length and velocity for a vertical vibrating beam. Wang and Mai (2005) have given a solution method for the one-dimensional transient heat conduction problems for non-homogeneous material by using finite element method. The summary of these literatures are summarized in the table 2.2.

Table 2.2: Table summary of thermal induced vibration literature review.

Sl.No.	Author Name and year	Summary
1	Baker (1936)	Stated that vibrations were excited by the force between the air and the wire due to thermal action of the moving hot wire on the surrounding air and classifies the beam undergoing thermally induced vibration as a self induced vibration.
2	Beam (1969)	Credited with producing the first thermal induced vibration in the laboratory.
3	Blandino and Thornton (2000)	Published article have given the experimental results and theoretical model for calculating the natural and forced convective heat transfer coefficient as function of position along the beam length and velocity for a vertical vibrating beam.

4	Blandino and Thornton (2001)	Carried out the detailed study of a thermally induced vibration caused by internal heating.
5	Boley (1956)	Showed that when a beam is subjected to rapid external heating, a time dependent thermal moment develops due to temperature difference between the heated and unheated sides.
6	Boley (1972)	Showed that, if the thermal response time is same order of magnitude or less than the structural response time, for a low mass, flexible structure, it is prone to thermal vibration.
7	Boley and Barbe(1957)	Carried out studies on the thermally induced vibrations of beams and plates subjected to gradual heating. They have studied the effect of thickness to width ratio on the dynamic maximum displacement for rectangular plate subjected to step heating.
8	Carne(1937)	Experimentally determined the natural convection heat transfer coefficient for a vertical cylinder by using steam as heat source and taking in account the heat loss by radiation by using a correction factor.
9	Chen and Yuh(1980)	Carried out studies to examine effect of heat and mass transfer characteristics of natural convection flow along a vertical cylinder under the combined buoyancy force effect of thermal and species diffusion.
10	Frisch(1970)	Studied thermally induced vibrations of long thin walled cylinders of open section and derived equations to describe the coupled non-planar transverse and torsional vibrations are presented.
11	Friswell et al.	They showed that thermally induced vibrations

	(1997)	can be damped using currently available smart structure technology, provided temperature effects are properly accounted for in the control law.
12	Graham(1970)	States that the boom subjected to solar radiation may experience unstable bending oscillations if the boom is pointed away from the sun.
13	Gulick and Thornton (1995)	Studied thermally induced vibration of a spinning aircraft boom.
14	Gupta et al. (2007)	Studied the effect of thermal gradient on vibration of non-homogeneous orthotropic rectangular plate having bidirectional parabolically varying thickness using Rayleigh- Ritz procedure.
15	Hama et al. (1959)	Investigated theoretically as well as experimentally the effect of axisymmetric free-convection temperature field along a vertical thin brass cylinder heated by means of electric current.
16	Hong et al. (2005)	Analysed the thermally induced vibration of a thermal sleeve using computational Generalized Differential Quadrature (GDQ) method for calculating the natural frequency displacement and thermal stresses.
17	Johnston (1999)	Conducted a detailed investigation of thermal induced motion of rigid panel solar arrays.
18	Kidawa-Kukla (1997)	Proved the frequency of the thermally induced beam vibration is a multiple of harmonic motion frequency of the heat source and then resonance can occur in the system.
19	Kidawa-Kukla (2003)	Analysed the temperature distribution and transverse vibration of beam induced by using the property of the Green functions.
20	Kim (1998)	Presented an analytical and experimental

		investigation of the thermal creak phenomenon by developing a generic model of a thermal creak element to understand the mechanism and to identify the key parameters.
21	Ko and Kim(2003)	Carried out coupled thermal–structural analysis on spinning thin-walled composite beam appendages, which includes the interaction between structural deformations and incident heating
22	Kong et al. (2010)	Experimentally investigated fluctuating characteristics, natural frequency and thermal strains of the thermally-induced vibration at various thermal environment conditions.
23	Kraus (1996)	Presented numerical results on the quasi-static response and dynamic response as a function of inertia parameter for simply supported thin non-shallow spherical shells whose inside surface is insulated and suddenly applied heat flux on to its outer surface.
24	Lee and Kwon (2008)	Developed a spectral element model for accurate prediction of the dynamic characteristics of an axially moving thin uniform plate subjected to sudden thermal loadings on its surfaces.
25	Lyons (1966)	Suggested that the best practical way of providing sudden heat input to beams, plates and shells is by instantaneously supply of electrical energy and by gamma radiation.
26	Manolis and Beskos(1981)	Reviewed the work of Boley by using Laplace Transform and method of Papoulis in order to obtain thermally induced vibrations of beam subjected rapid heating.
27	Murozono	Showed that a vibration in convection coefficient

	(1995)	around the circumference of the beam would cause a thermally induced vibration.
28	Murozono and Thornton (1998)	Studied thermally induced quasi-static bending-torsion deformation in the context of local buckling of the bubble space telescope solar arrays.
29	Rajeev Kumar et al. (2005)	Derived finite element model based on first-order shear deformation theory for an isoparametric shell element for the active control of thermally induced vibration of laminated composite antenna reflector with piezoelectric sensors and actuators.
30	Rimrott and Abdel Sayed (1977)	Presented thermally induced bending vibration in the laboratory.
31	Seibert and Rice (1973)	Carried out studies on thermally induced vibration of a simply supported beam with heat input on one surface.
32	Silver(2001)	Presented method to measure and characterize the stability of a precision deployable truss for thermally induced spontaneous vibrations.
33	Stroud and Mayers(1971)	Evaluated dynamic stresses and deformations of a rapidly heated rectangular plate using the dynamic thermo-elastic variational principle.
34	Thornton (1996)	Presents a chronology of thermally induced vibration research with application to spacecraft.
35	Thornton et al. (1995)	Investigated the effect of self shadowing on the behavior of space station solar arrays.
36	Thornton and Foster (1992)	Conducted experiments investing thermally induced bending vibration in a vacuum.
37	Thornton and Kim (1993)	Developed a mathematical model to investigate dynamic behavior of roll-out solar arrays used in

		Humble Space Telescope.
38	Tran et al. (2007)	Analysed the structural intensity pattern of thin isentropic and laminated composite plates which are subjected to thermally induced vibration.
39	Wang and Mai (2005)	Developed a solution method for the one-dimensional transient heat conduction problems for non-homogeneous material by using finite element method.
40	Yu(1969)	Analysed thermally induced vibration and flutter of a flexible boom without twisting and showed that bending oscillations were stable if the boom was pointed away from the sun and unstable if it was pointed towards the sun.

1.4 SCOPE FOR RESEARCH

The combined effect of fluid induced vibration and thermal induced vibration has not been investigated to this day. In this research, it is planned to investigate the vibration of the pipeline induced through thermal and fluid loading. The studies involve investigating the effect of fluid flow pressure on the natural frequencies of vibration. When a heated fluid passes through the pipeline, heating of the pipeline takes place and also heat dissipates from the surface of the pipeline through convection. This leads to thermal induced vibration in pipes. The effect of thermal and fluid induced vibration on the natural frequency of the system has been investigated. A mathematical model has developed to predict the thermal structure behavior of an internal heated beam and fluid flow induced vibration. Combined effect of thermally induced and fluid flow induced vibration has been investigated. One dimensional finite element model with Newtonian approach has been developed considering the numerical model for the fluid and thermal induced vibration of the beam. An experimental model has been fabricated in the laboratory, various experiments were conducted and results are presented.

1.5 OBJECTIVE OF THE WORK

From the literature review it is observed that not much work has been reported on the response of structure due to combined loading of thermal, fluid, fluid inertia and structure inertia. Hence the present work focuses in this area and set out the following objectives. To visualize the problem, an experimental and theoretical analysis is contemplated.

Theoretical and numerical study of fluid-flow induced vibration of pipes

- To derive the equation of motion by considering fluid velocity, pressure, damping, pipe tension, structural stiffness, pipe and fluid mass, Coriolis (mixed derivative) effects.
- Finite element formulation for the structural equation of motion with fluid flow.
- Validation of the code using referred journal and to study the effect of structural boundary conditions, flow velocity and fluid flow pressure on fluid flow induced vibration of pipes numerically.

Experimental response of cantilever pipe conveying compressed air for flow induced vibration

- To obtain experimental displacement response of cantilever pipe with the flow of air at different pressure and for varying lengths.
- To verify theoretically natural frequency and displacement response of the cantilever tube conveying compressed air at different pressure and for varying lengths.

Theoretical and experimental study of thermal induced vibration of pipes

- Experimental and theoretical investigation of heat transfer coefficient for tube under typical laboratory conditions.
- Theoretical modeling and numerical studies on thermally induced vibrations of an internally heated tube.

- To theoretically model the convection heat transfer for an internally heated oscillating cantilever tube based on Reynold's number, Prandtl number and Nusselt number.
- To simulate through theoretical model the dynamic response of the vertical cantilever tube with and without tip mass.
- To find effect of changing the length and diameter of the tube on the thermally induced vibrations.
- Theoretical modeling of thermally induced vibrations of an internally heated tube with tip mass and experimental validation.
- To simulate through theoretical model, the thermally induced vibration of the vertical cantilever tube with tip mass.
- To study experimentally the phenomenon of thermally induced vibration of vertical cantilever tube with tip mass and validate the theoretical model.
- Experimental investigation of thermally induced vibrations of an internally heated twin tube with and without tip mass.
- To study the effect of length of tube, tube diameter, and heating rate on the amplitude of thermal vibration.

Combined effect of fluid and thermal induced vibration

- To obtain experimental displacement response and natural frequency of cantilever tube conveying hot compressed air at different pressure and temperature.
- To verify theoretically natural frequency of the cantilever tube conveying hot compressed air at different pressure and temperature with that obtained experimentally.

CHAPTER 2

EXPERIMENTAL RESPONSE ANALYSIS OF A THIN SLENDER CANTILEVER TUBE CONVEYING COMPRESSED AIR

2.1 EXPERIMENTAL SET UP

The experiment was conducted on a cantilever tube set up conveying compressed air which is shown in Figure 2.1. The laser pick-up was used for the measurement of the response of the tube. The compressed air was supplied near the clamped location and response was obtained using laser pick-up at the tip of tube. The programming was done to acquire response signals through LabVIEW 8.5 with the block diagram as shown in Figure 2.2. The experiments were carried out under the following conditions: (1) tube with different positions – horizontal and vertical, (2) tube conveying air at different pressures and hence different velocities (3) different lengths of cantilever tube conveying air.

The test specimen used for the experiment was a stainless steel SS304 tube 800 mm long with 2.5 mm external diameter and 0.25 mm thickness. For the preliminary analysis, an experimental setup was fabricated in the laboratory. The one end of the tube was fixed and the other end left free in open atmosphere. The test specimen was enclosed in a box having 300 mm of width, 300 mm of length and 1100 mm of height. The box has wooden frames with glass pane to complete as a closed box . The wall of the box was prevented cross current of air from atmosphere on the response of the tube and clamped support was provided for holding the tube.

The reciprocating compressor was used for supplying compressed air. The supply pressure was controlled by the pressure regulator. The arrangement was suitable for generating high pressure air, which was passed through pressure regulator into test specimen (cantilever tube). Due to this high pressure air, the transient and steady state response of the tube were obtained. This response was sensed by using laser pick-up of LG10A65PU in the form of voltage signal. The sensor head was located approximately 90 mm from the tip of tube. The sensor was positioned such that the laser beam reflected off a point near the center of the tip of tube. The output

of the laser sensor was 5 Volt (Direct Current). This sensor was connected to the displacement indicator, which was then connected to NI high speed USB 9234 voltage module for data acquisition. Then it was connected to personal computer for displaying the output in LabVIEW 8.5 and the data was saved. The block diagram shown in Figure 2.2 indicates sensor, filter, and data acquisition card and start/stop button. The Figures 2.3 and 2.4 shows the photographs of the setup for vertical and horizontal orientations of the tube respectively.

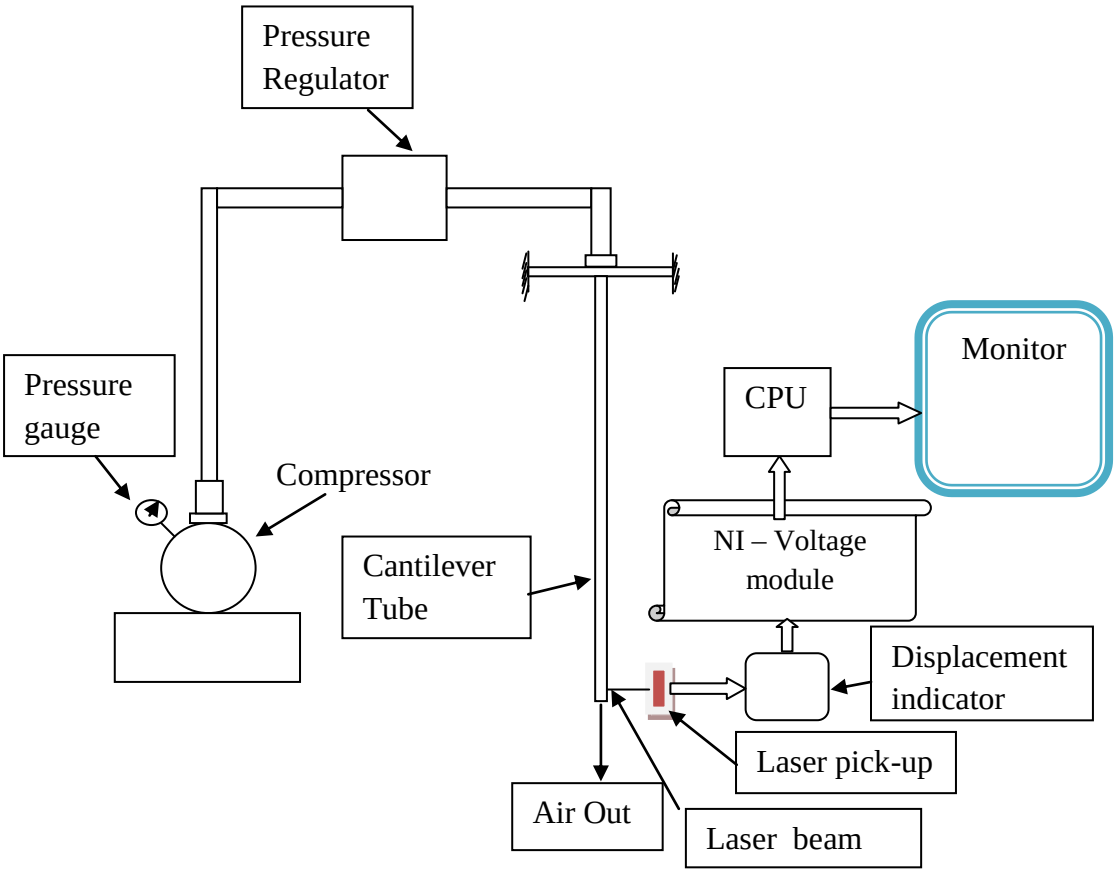

Fig. 2.1 Experimental set-up block diagram.

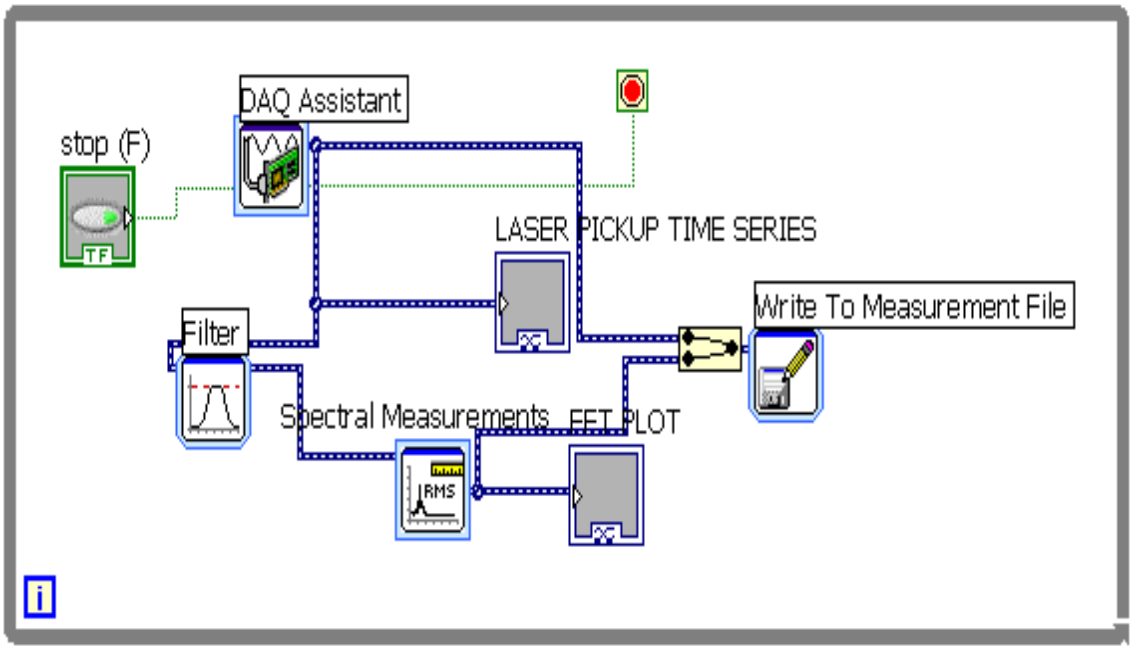

Fig.2.2 Block diagram of LabVIEW 8.5.

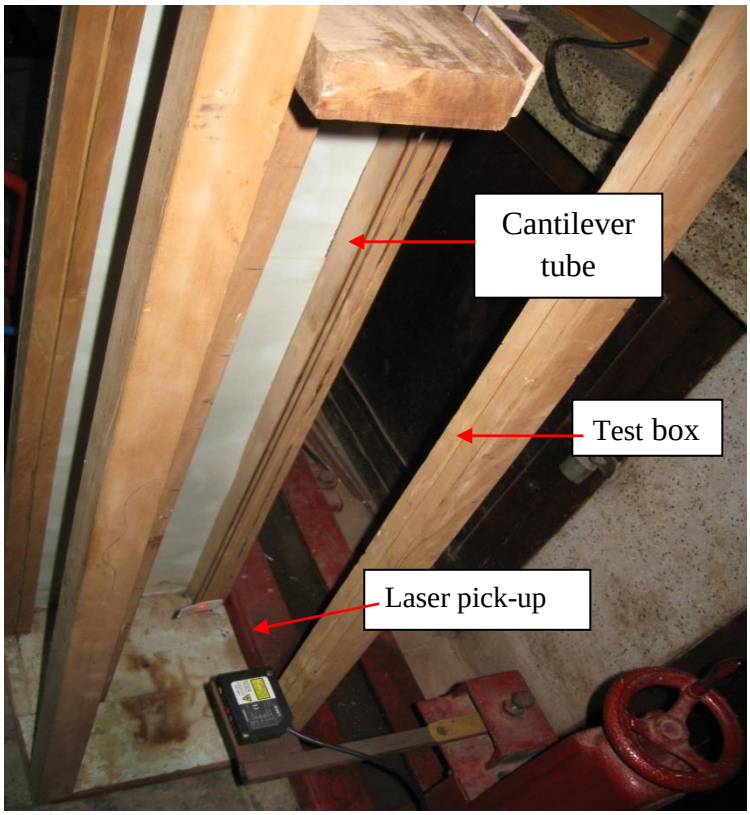

Fig. 2.3 Experimental test box with test specimen and laser pick-up sensor.

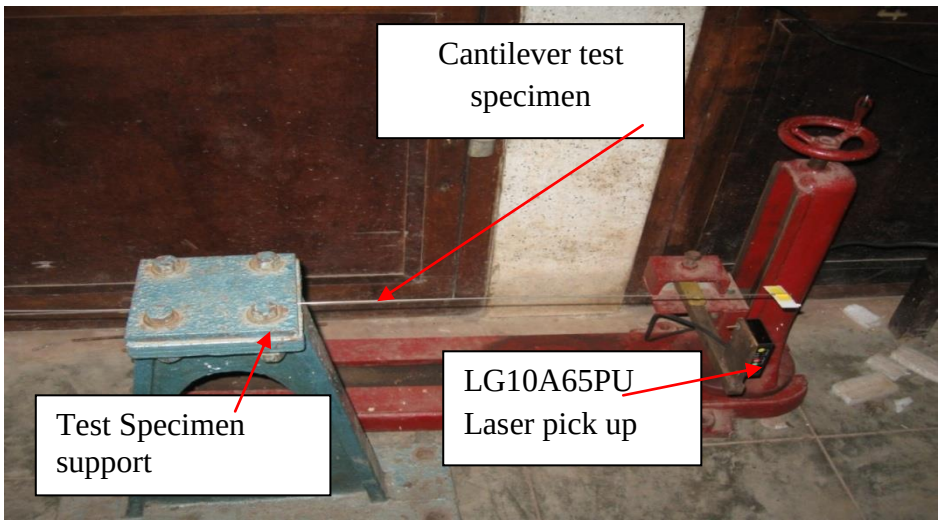

Fig.2.4 Experimental set up - horizontal cantilever tube.

2.2 EXPERIMENTAL RESULTS AND DISCUSSION FOR VERTICAL CANTILEVER TUBE CONVEYING COMPRESSED AIR

Figure 2.5 shows the response of the tube to the flow of compressed air at 4 bar pressure. With the flow of compressed air through the tube, the tube responds immediately by undergoing deflection as shown in Figure 2.6. The flow of air through the tube was maintained for about 300 sec. Once the tube deflects to the maximum, the deflections tend to decay about the deflected position but due to continued flow of air, the tube undergoes further transverse deflection about the deflected position. The deflections or oscillations about the deflected position are lesser in magnitude. The moment the flow of air is cut off, the transverse deflection immediately becomes zero and the tube attains the initial position. The response of the tube i.e. average displacement over time 200 seconds is 8 mm and the amplitude of oscillations about the deflected position is between +4.5 mm to −3.5 mm. The fundamental frequency of this configuration is 2.0 Hz, which is shown in Figure 2.7.

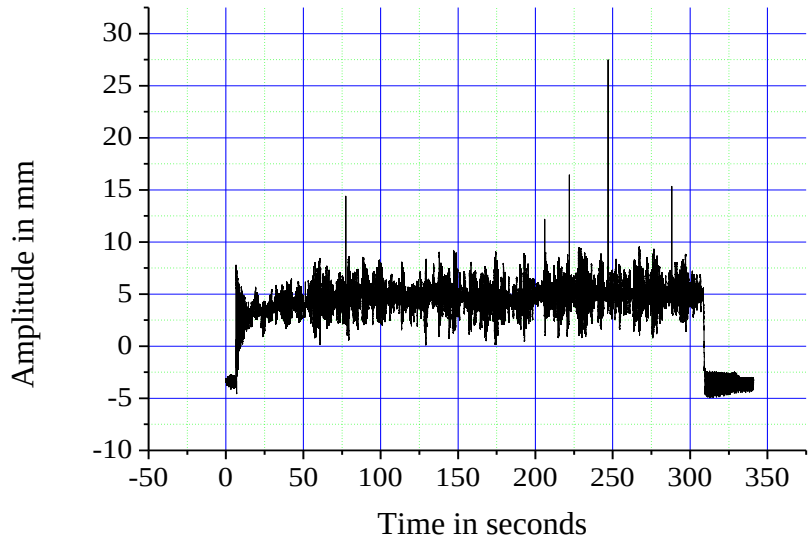

Fig.2.5 Response of cantilever tube of span 800 mm with compressed air at 4 bar.

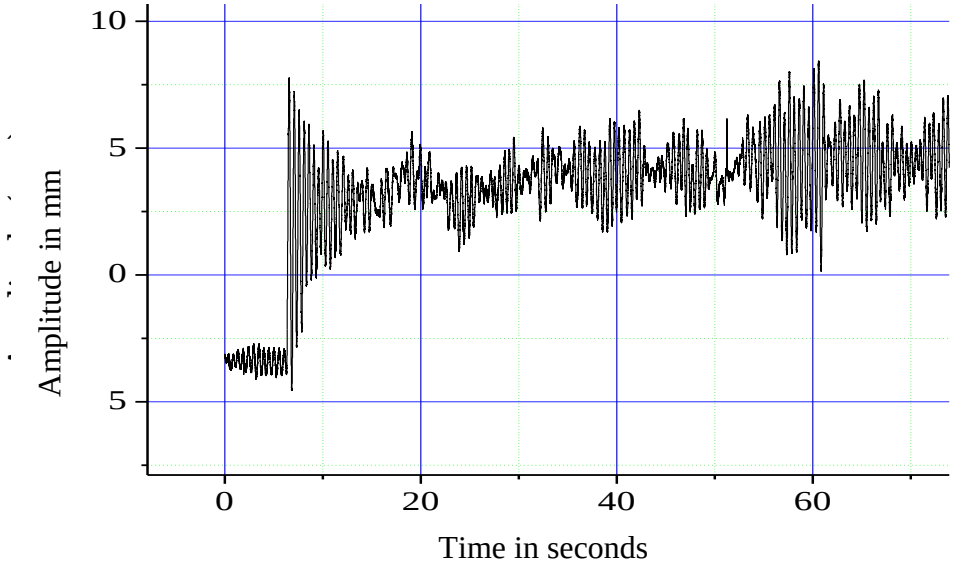

Fig. 2.6 A blow-up of Figure 2.5.

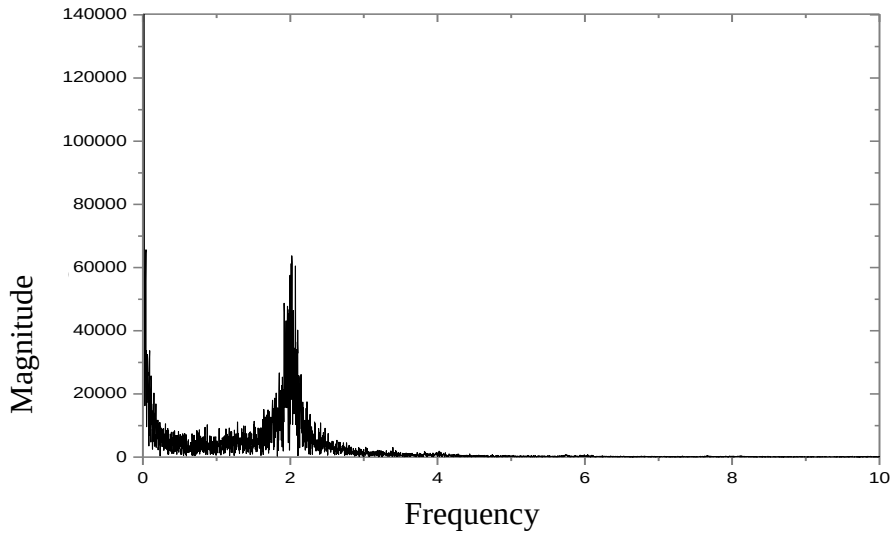

Fig.2.7 FFT frequency response of cantilever tube of span 800 mm with compressed air at 4 bar.

Similarly Figures 2.8 to 2.12 shows the response of the tube and fundamental frequency graph for 800 mm length of tube while maintaining air pressure of 5 bar and 6 bar. The average displacement and fundamental frequencies of these conditions are tabulated in the Table 2.1. The experiments are also conducted for 700 mm, 600mm, 500 mm length of tube by conveying air at pressure of 4 bar, 5 bar and 6 bar. The average displacement and fundamental frequencies of these conditions are also tabulated in the Table 2.1.

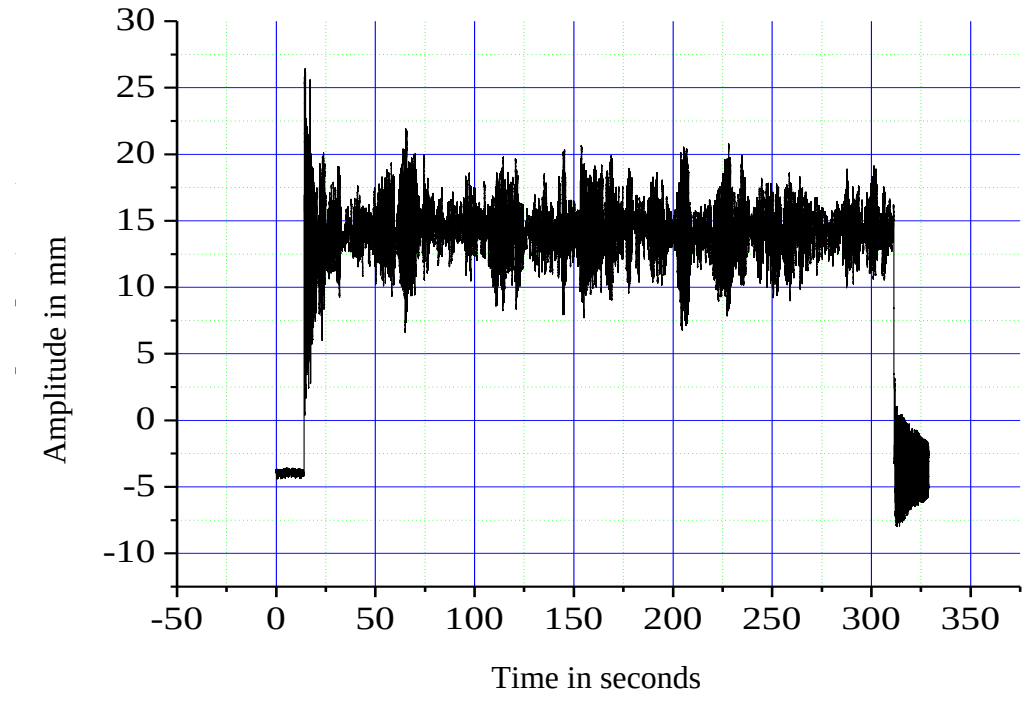

Fig.2.8 Response of cantilever tube of span 800 mm with compressed air at 5 bar.

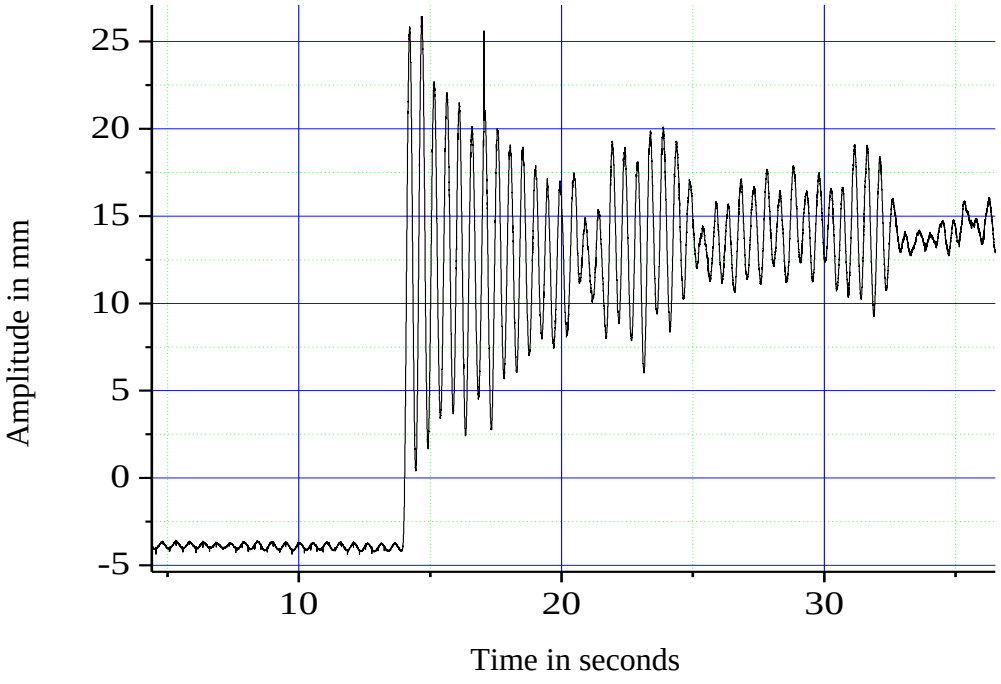

Fig.2.9 A blow-up of Figure 2.8.

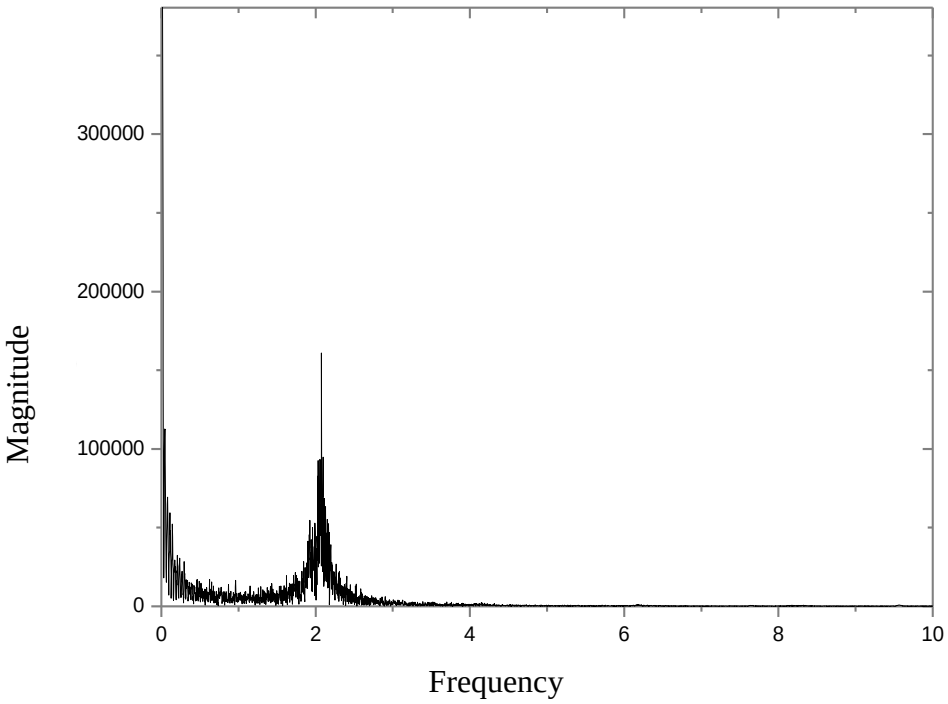

Fig.2.10 FFT frequency response of cantilever tube of span 800 mm with compressed air at 5 bar.

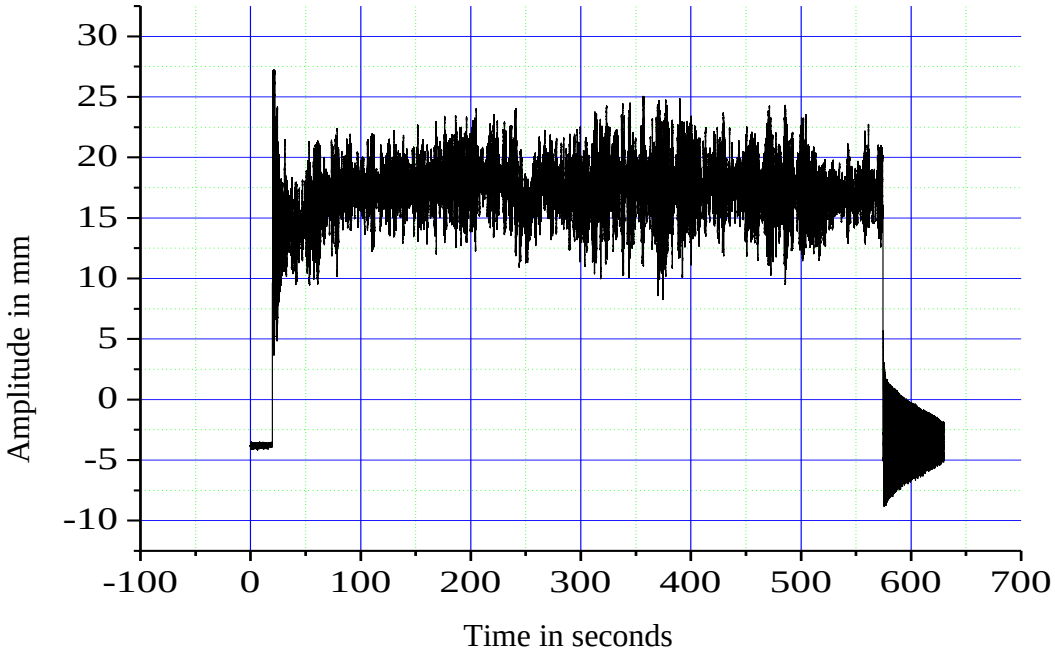

Fig.2.11 Response of cantilever tube of span 800 mm with compressed air at 6 bar.

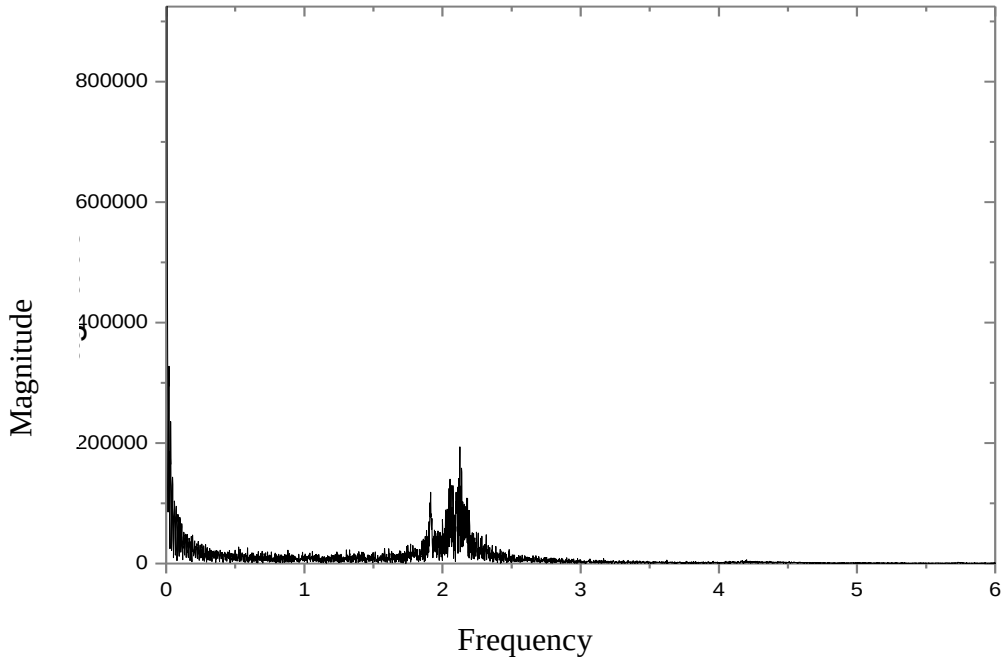

Fig.2.12 FFT frequency response of cantilever tube of span 800 mm with compressed air at 6 bar.

2.3 EXPERIMENTAL RESULTS AND DISCUSSION FOR HORIZONTAL CANTILEVER TUBE CONVEYING COMPRESSED AIR

Figure 2.13 shows the response of the tube to the flow of compressed air at 4 bar pressure. With the flow of compressed air through the tube, the tube responds immediately by undergoing deflection. The flow of air through the tube was maintained for about 200 seconds. Once the tube deflects to the maximum, the deflections tend to decay about the deflected position, but due to continued flow of air, the tube undergoes further transverse deflection about the deflected position. The deflections or oscillations about the deflected position are lesser in magnitude. The moment the flow of air is cut off, the transverse deflection immediately becomes zero and the tube attains the initial position. The response of the tube, i.e. average displacement over time 200 seconds was 16.8 mm and the amplitude of oscillations about the deflected position was in between +20.0 mm to +10.5 mm. The fundamental frequency of this configuration was 2 Hz, which is shown in Figure 2.14.

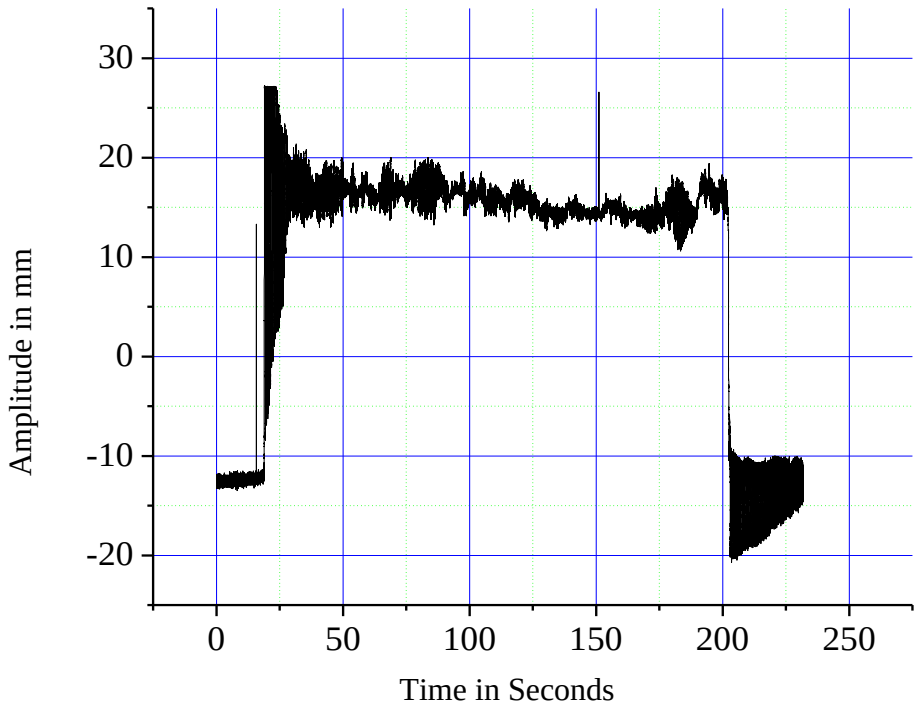

Fig.2.13 Response of cantilever tube of span 800 mm with compressed air at 4 bar.

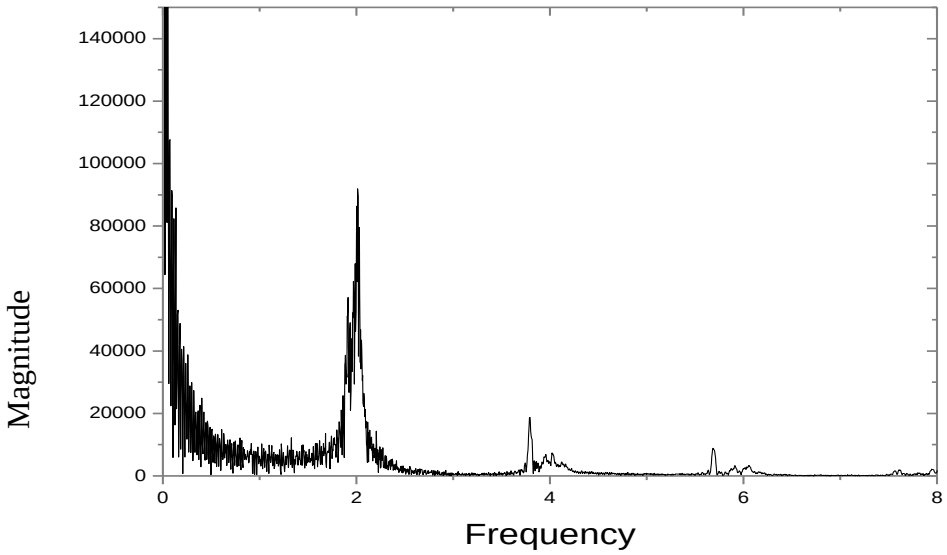

Fig.2.14 FFT frequency response of cantilever tube of span 800 mm with compressed air at 4 bar.

Similarly Figures 2.15 to 2.18 shows the response of the tube and fundamental frequency graph for 800 mm length of tube while maintaining air pressure of 5 bar and 6 bar. The average displacement and fundamental frequencies of these conditions are tabulated in the Table 2.2. The experiments are also conducted for 700 mm, 600mm, 500 mm length of tube by conveying air at pressure of 4 bar, 5 bar and 6 bar. The response of the tube and fundamental frequency graph for these conditions are represented in the Figures 2.19 to 2.38. The average displacement and fundamental frequencies of these conditions are also tabulated in the Table 2.2.

It is observed that the increase in air pressure tends to increase the average displacement and frequency of the tube. As the length of tube increases, the displacement increases and frequency decreases. But the change in frequency is not much significant due to small range of air pressure variation. This effect is same for both vertical and horizontal configuration. The horizontal configurations have larger mean displacements but smaller amplitudes of vibration due to gravity effect.

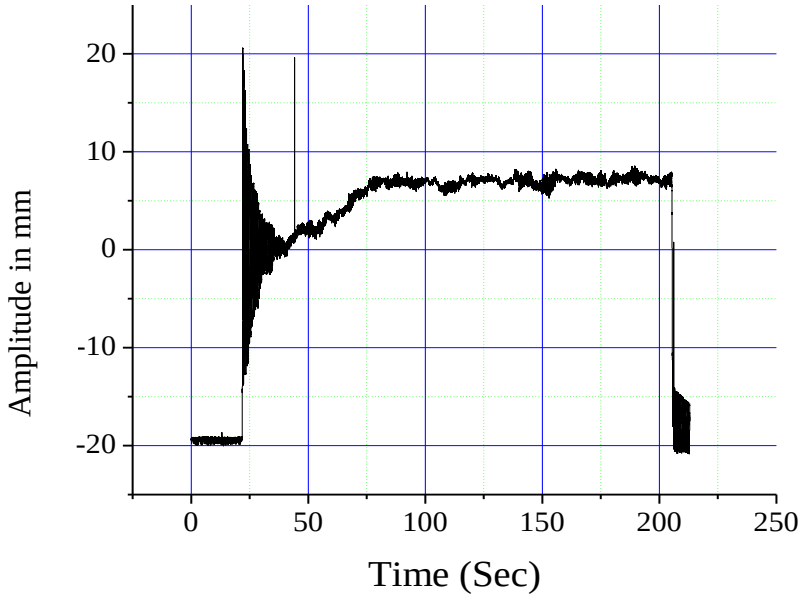

Fig.2.15 Response of cantilever tube of span 800 mm with compressed air at 5 bar.

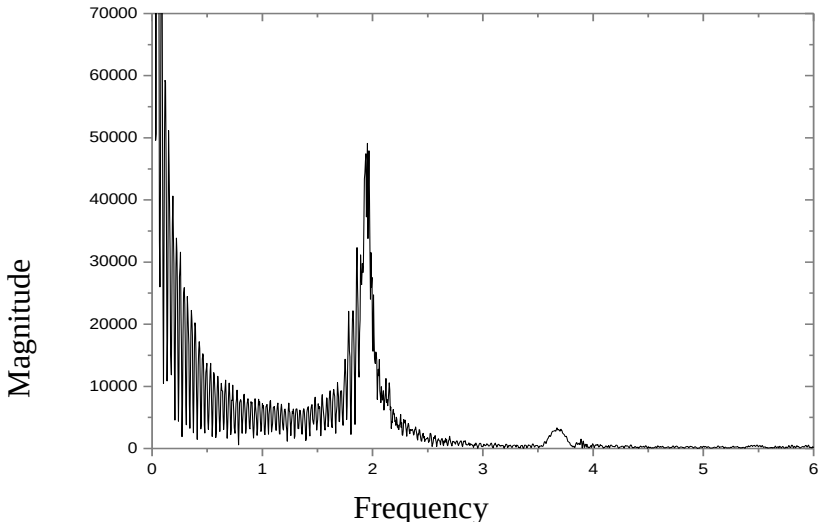

Fig.2.16 FFT frequency response of cantilever tube of span 800 mm with compressed air at 5 bar.

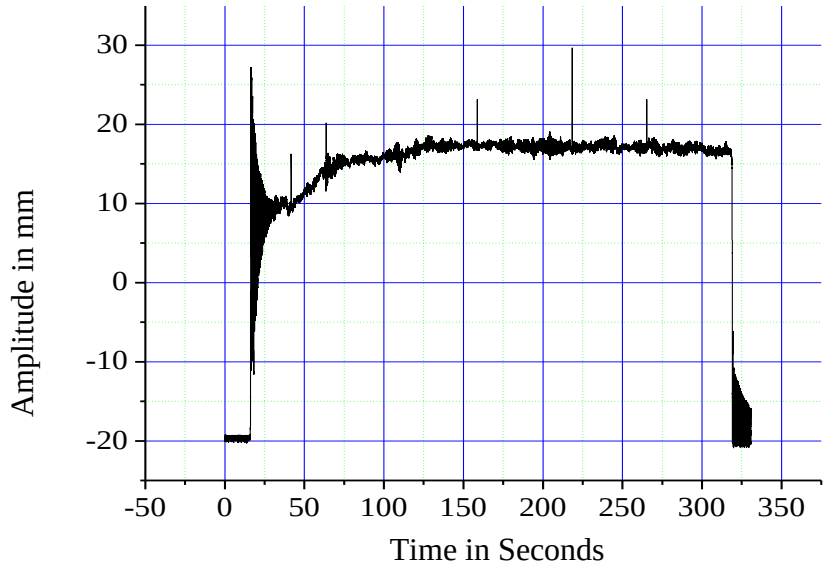

Fig.2.17 Response of cantilever tube of span 800 mm with compressed air at 6 bar.

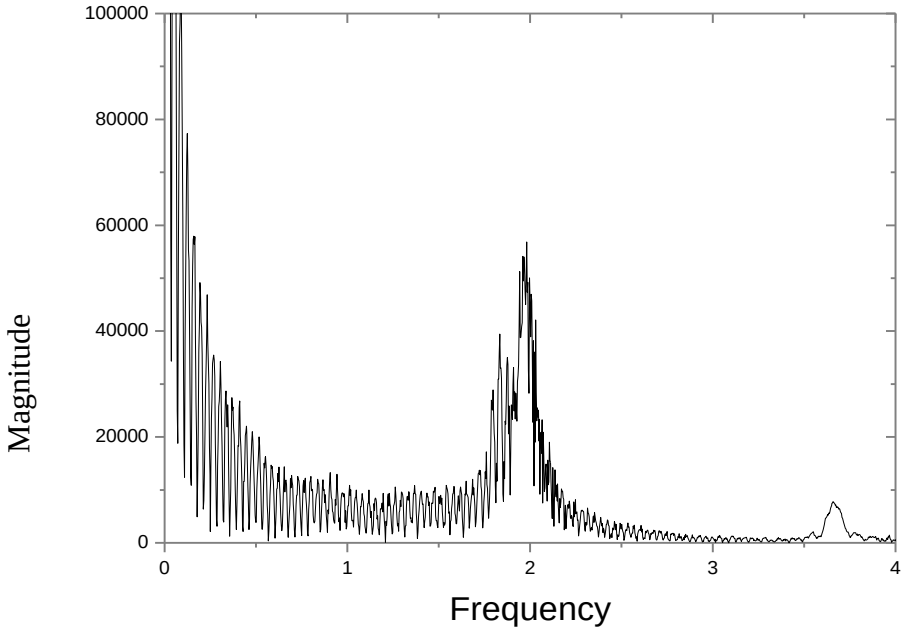

Fig.2.18 FFT frequency response of cantilever tube of span 800 mm with compressed air at 6 bar.

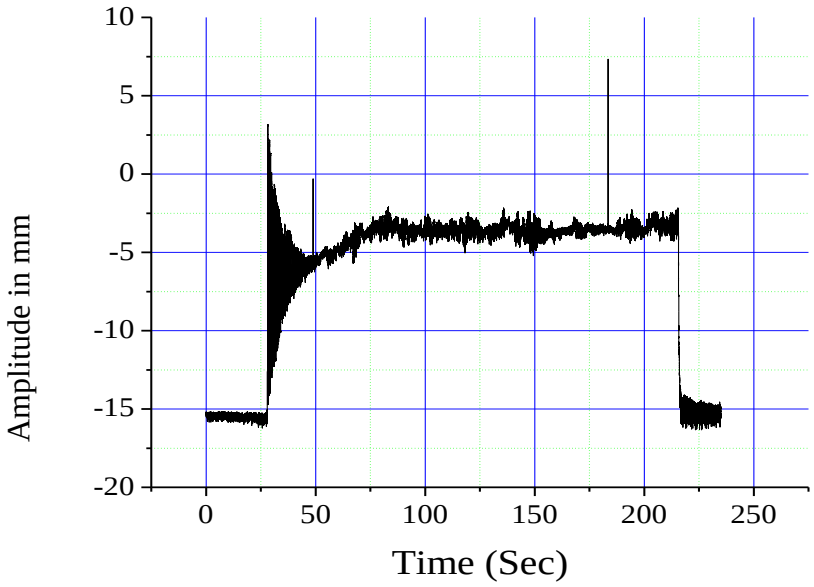

Fig.2.19 Response of cantilever tube of span 700 mm with compressed air at 4 bar.

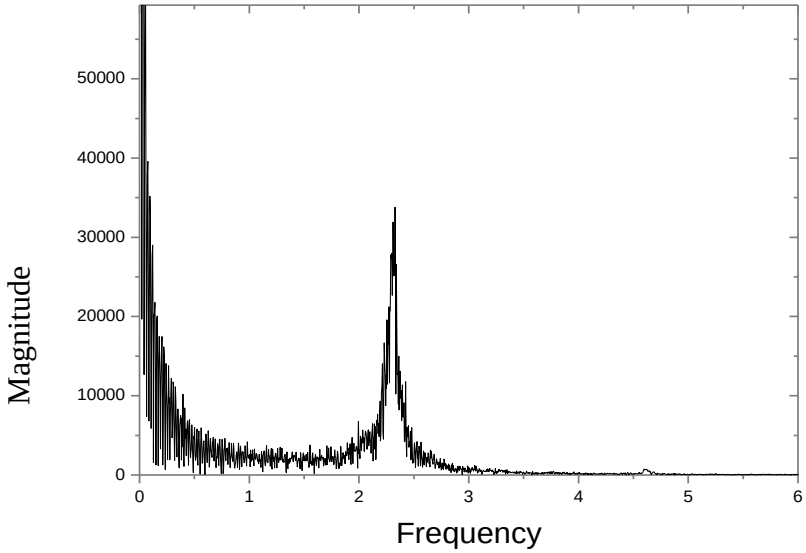

Fig.2.20. FFT frequency response of cantilever tube of span 700 mm with compressed air at 4 bar.

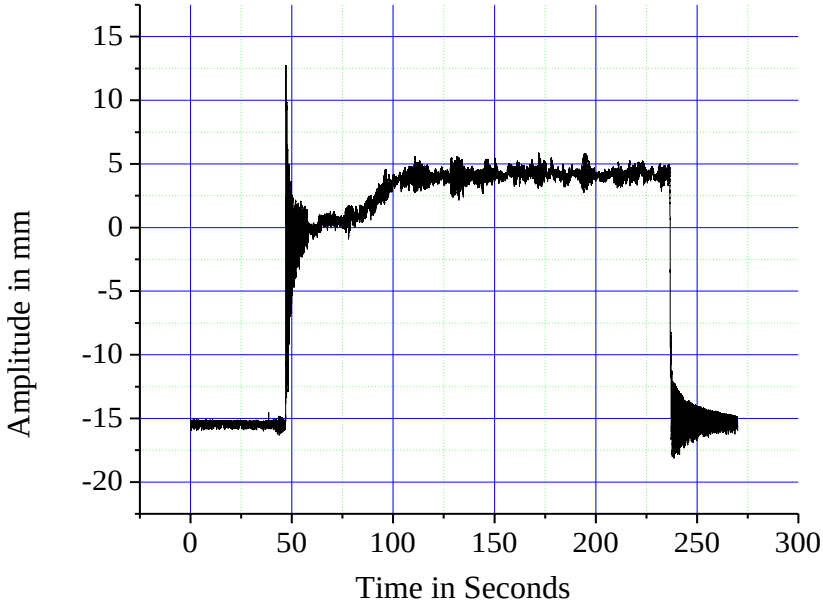

Fig.2.21 Response of cantilever tube of span 700 mm with compressed air at 5 bar.

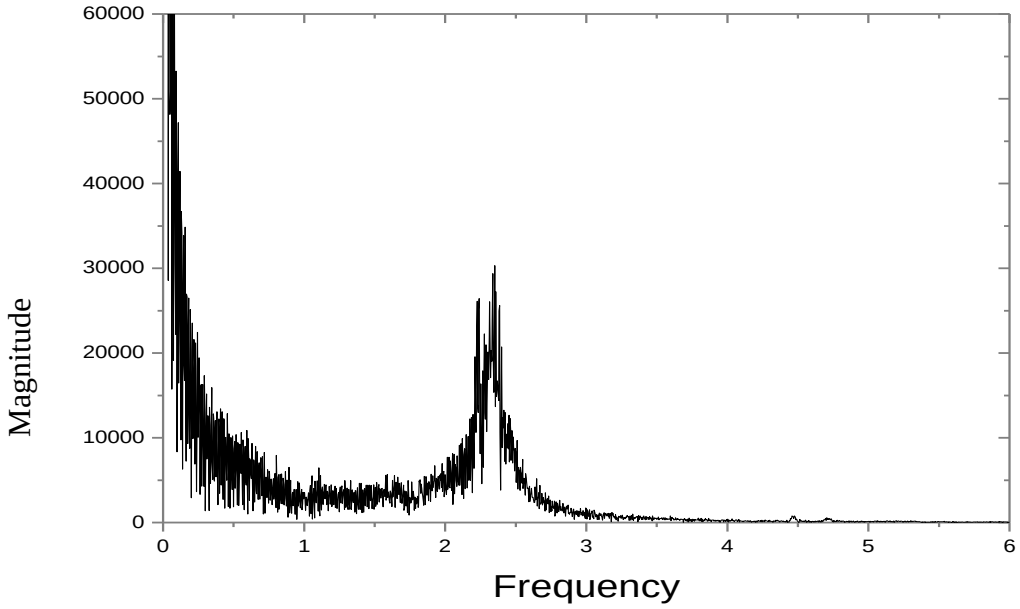

Fig.2.22 FFT frequency response of cantilever tube of span 700 mm with compressed air at 5 bar.

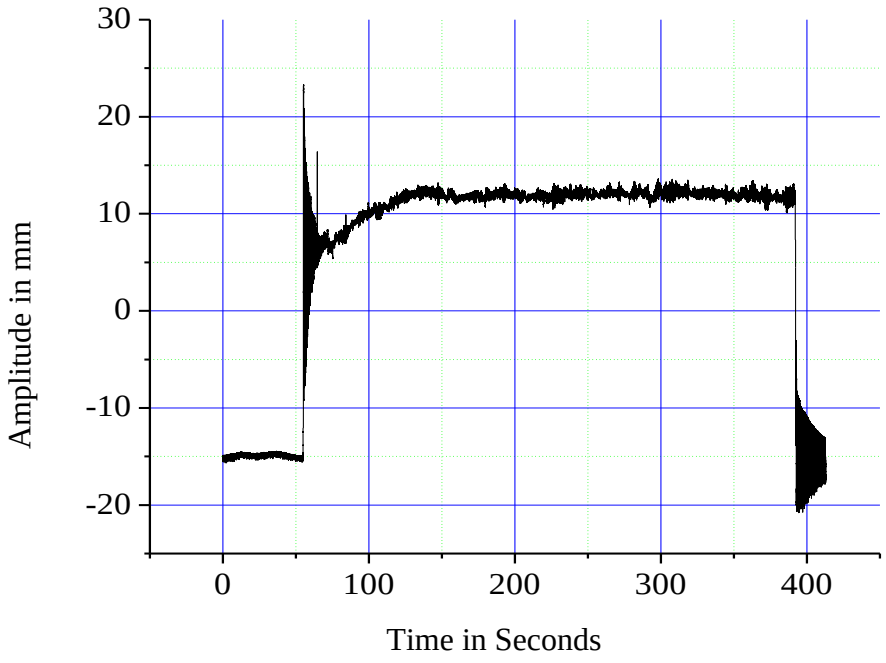

Fig.2.23 Response of cantilever tube of span 700 mm with compressed air at 6 bar.

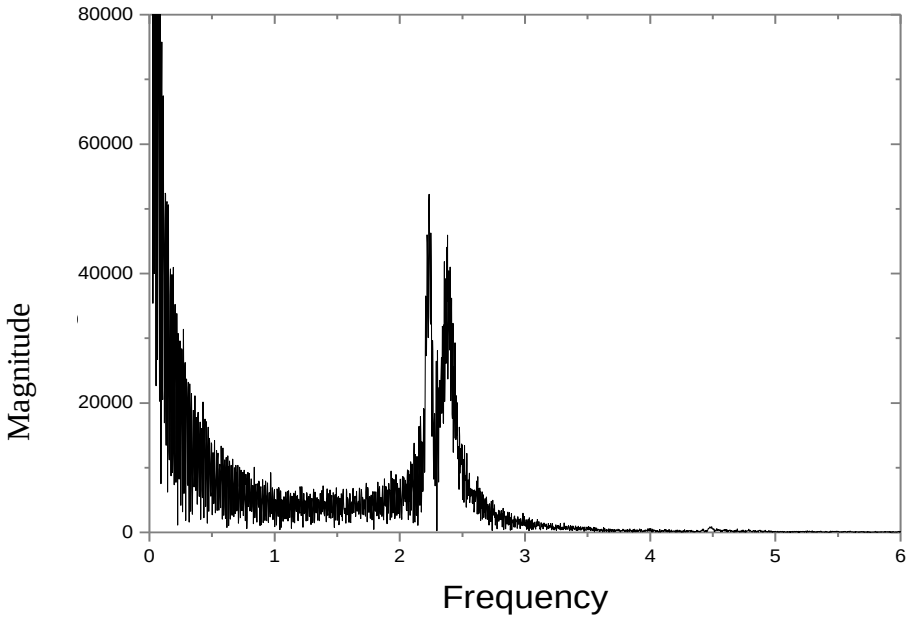

Fig.2.24 FFT frequency response of cantilever tube of span 700 mm with compressed air at 6 bar.

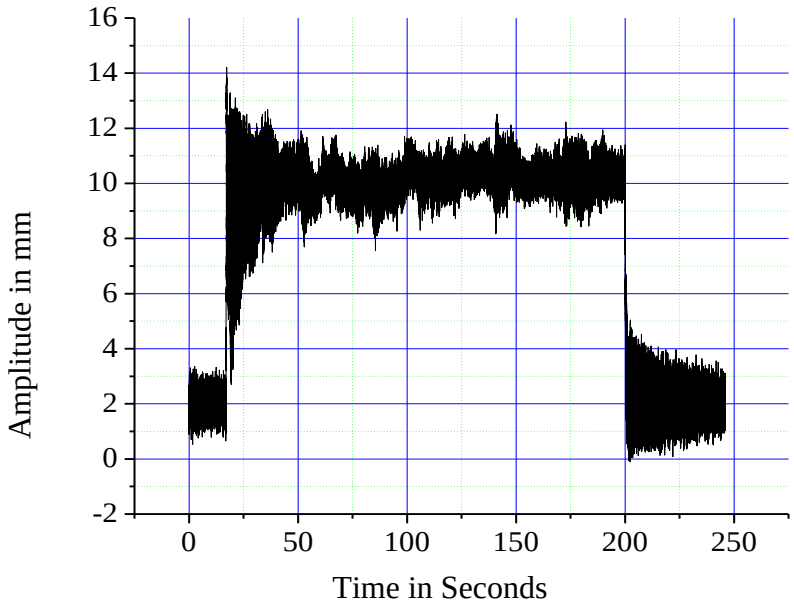

Fig.2.25 Response of cantilever tube of span 600 mm with compressed air at 4 bar.

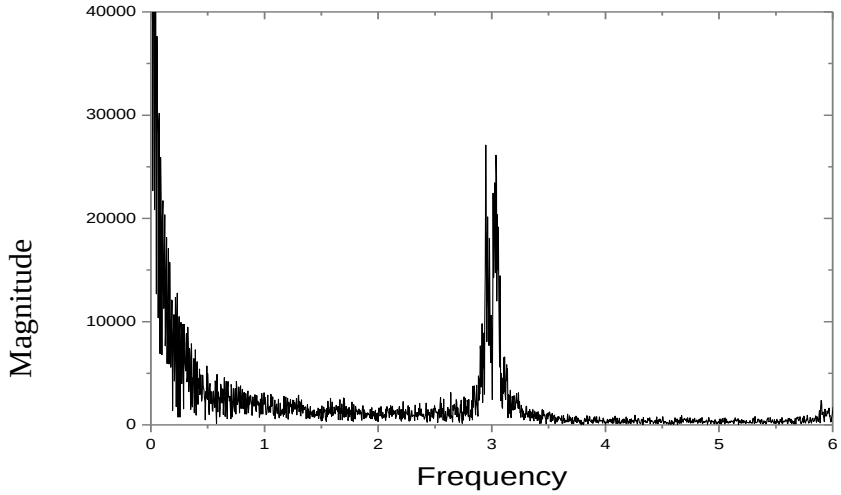

Fig.2.26 FFT frequency response of cantilever tube of span 600 mm with compressed air at 4 bar.

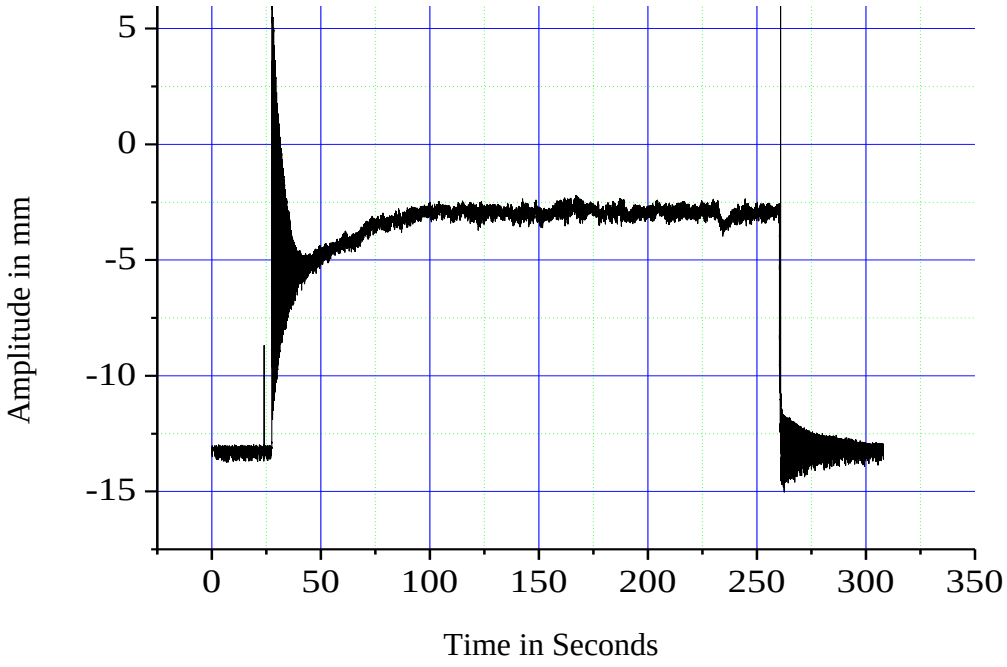

Fig.2.27 Response of cantilever tube of span 600 mm with compressed air at 5 bar.

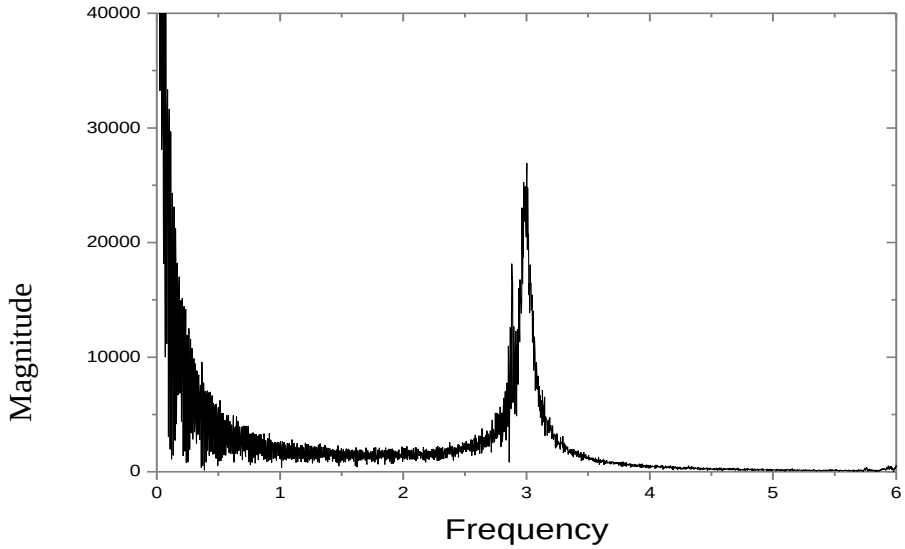

Fig.2.28 FFT frequency response of cantilever tube of span 600 mm with compressed air at 5 bar.

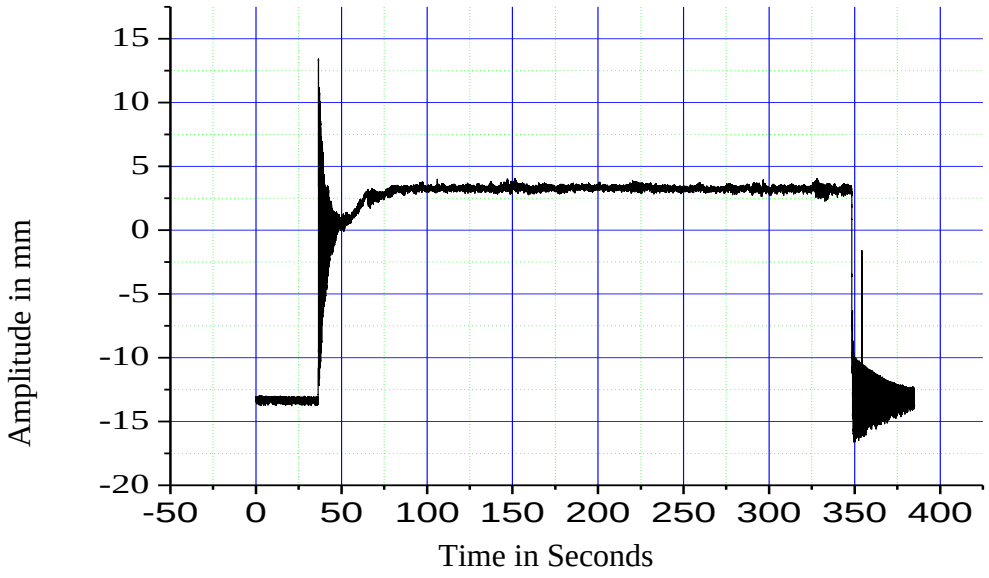

Fig.2.29 Response of cantilever tube of span 600 mm with compressed air at 6 bar.

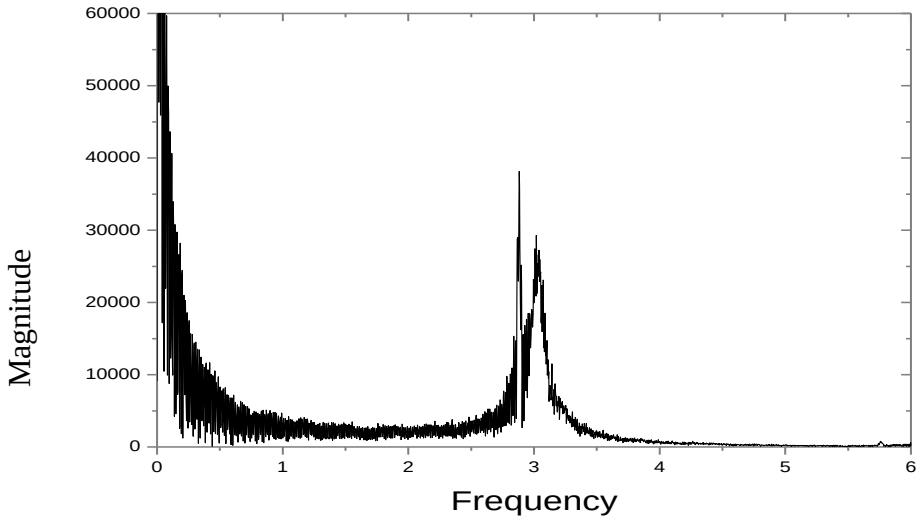

Fig.2.30 FFT frequency response of cantilever tube of span 600 mm with compressed air at 6 bar.

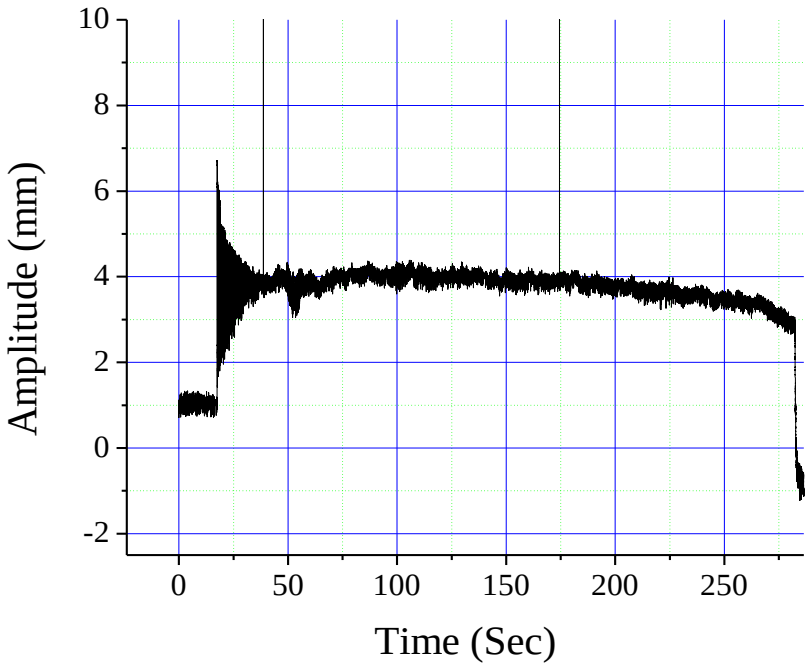

Fig.2.31 Response of cantilever tube of span 500 mm with compressed air at 4 bar.

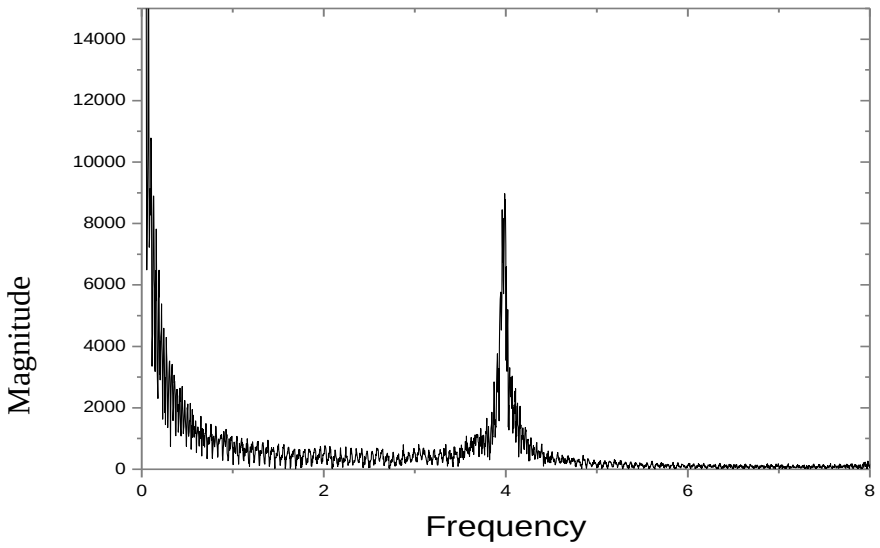

Fig.2.32 FFT frequency response of cantilever tube of span 500 mm with compressed air at 4 bar.

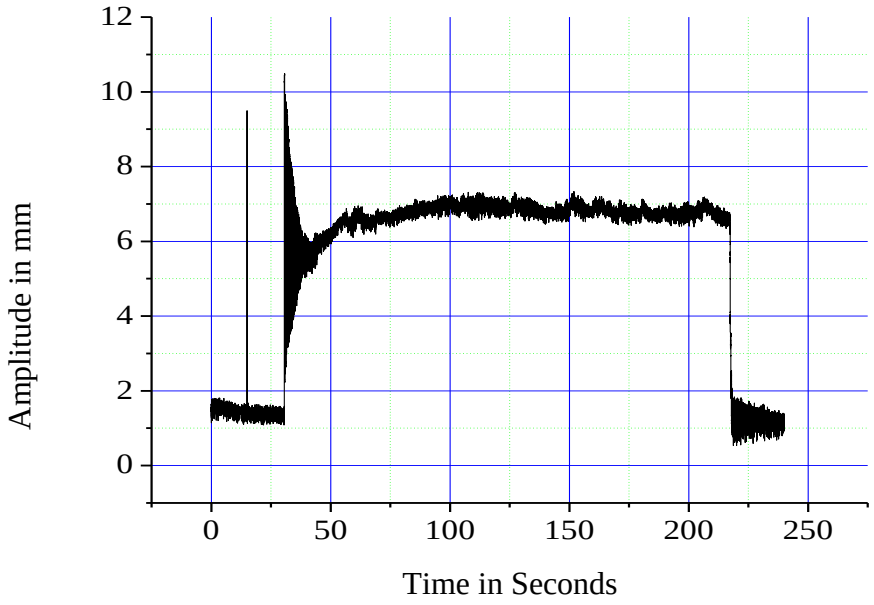

Fig.2.33 Response of cantilever tube of span 500 mm with compressed air at 5 bar.

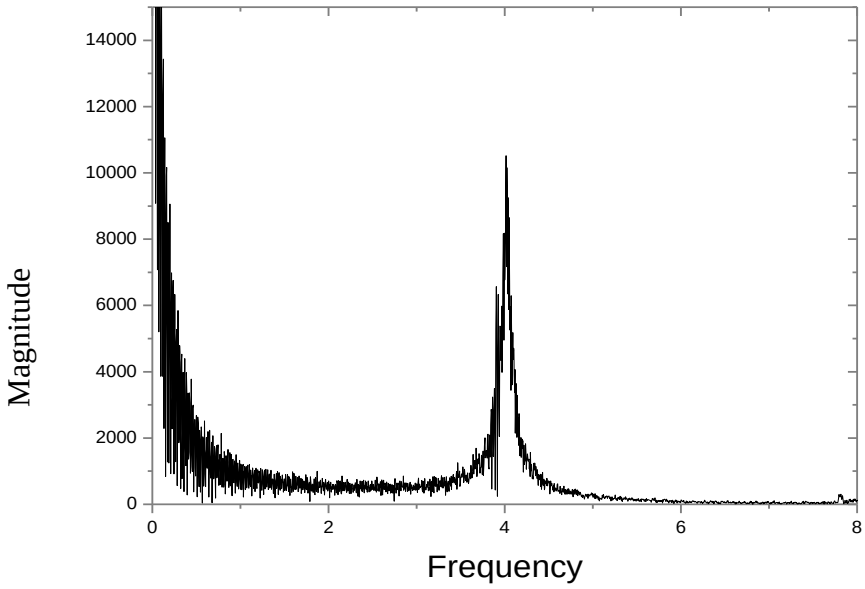

Fig. 2.34 FFT frequency response of cantilever tube of span 500 mm with compressed air at 5 bar.

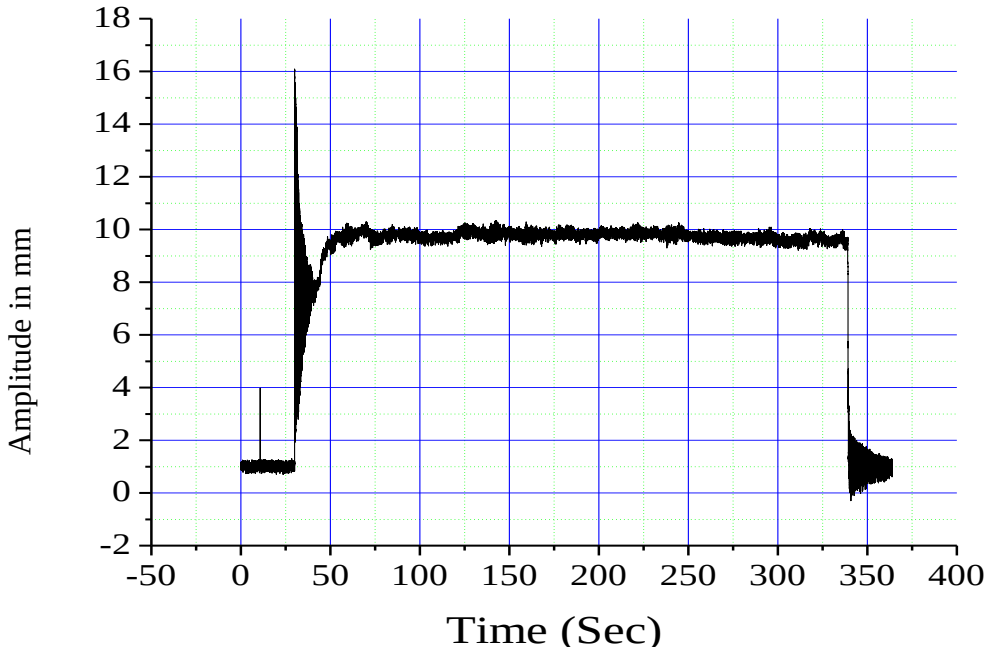

Fig.2.35 Response of cantilever tube of span 500 mm with compressed air at 6 bar.

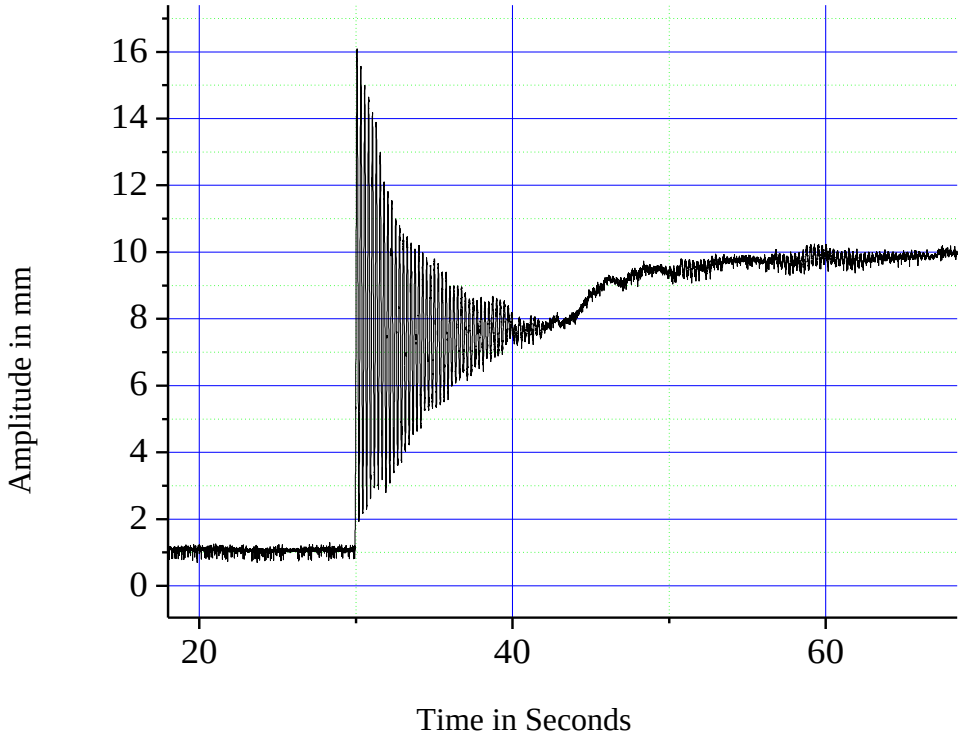

Fig.2.36 A blow-up of Figure 2.35.

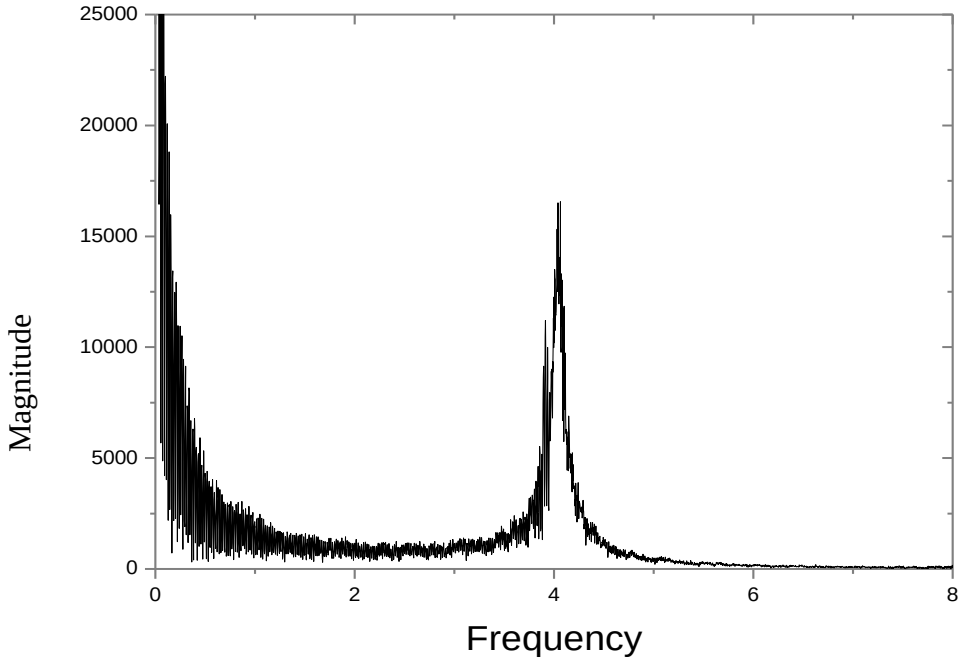

Fig. 2.37 FFT frequency response of cantilever tube of span 500 mm with compressed air at 6 bar.

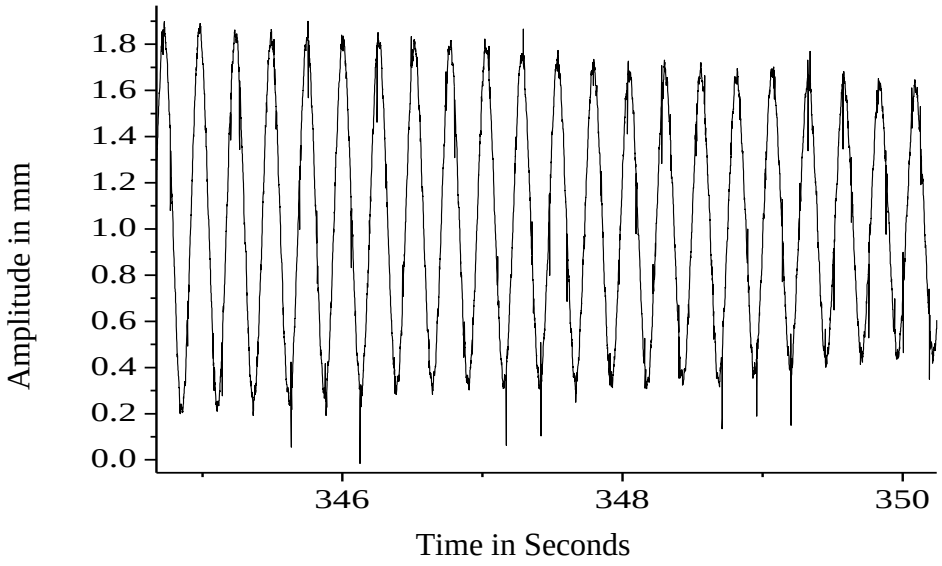

Fig.2.38 A blow-up of Figure 2.36 (341 – 353 sec).

2.3 SUMMARY

The average displacement and frequencies of cantilever tube conveying air at various pressure and tube length were obtained from the response curve and are tabulated in Table (2.1) and (2.2) and also shown in Figures 2.39, 2.40, 2.41 and 2.42. The increase in air pressure tends to increase the average displacement and frequency of the tube. As the length of tube increases, the average displacement also increases but frequency decreases. This effect is same for both vertical and horizontal configuration. The horizontal configurations have larger mean displacements but smaller amplitudes of vibration due to gravity effect.

Damping ratio was computed using logarithmic decrement from the transient response of the displacement. For logarithmic decrement method refer Appendix A. It was observed from the Figure 2.43 that fluid flowing velocity has a significant effect on damping. The damping ratio decreases with increase in pressure in all length of the tube namely 800, 700, 600, and 500 mm length. This is because of reduction in the system stiffness due to opposing action of flow as the velocity of air flow increases

according to equation of motion (Sinha et al.,2001). It was also observed that length of the tube also affects the damping ratio. Since the deflection is directly proportional to length of the tube and damping factor is directly proportional to deflection, as the length of the tube reduces damping factor also decreases. This effect is same for both horizontal and vertical configuration. The experiments were repeated for the same parameters and similar results were obtained. Figure 2.44 indicates the error bar for 800 mm pipe length at various pressures. This figure shows that repeatability of experiments is good.

Table 2.1 Displacement, frequency and damping factor with variation in pressure and length for vertical cantilever tube conveying compressed air.

S.No.	Tube length (mm)	Pressure (bar)	Avg. of displacement over time 200 sec.(mm)	Frequency (Hz)	Damping factor ζ
1	800	6	21.0	2.20	0.00692
		5	19.0	2.10	0.0168
		4	8.0	2.00	0.0245
2	700	6	17.5	2.50	0.0072
		5	10.4	2.45	0.0098
		4	6.3	2.35	0.0143
3	600	6	8.4	3.20	0.0021
		5	5.6	3.10	0.0035
		4	3.1	3.00	0.0046
4	500	6	6.0	4.00	0.0021
		5	3.4	3.90	0.0031
		4	2.2	3.90	0.0046

Table 2.2 Displacement, frequency and damping factor with variation in pressure and length for horizontal cantilever tube conveying compressed air.

S.No.	Tube length (mm)	Pressure (bar)	Avg. of displacement over time 200 sec.(mm)	Frequency (Hz)	Damping factor ζ
1	800	6	37.0	2.00	0.0053
		5	26.4	1.90	0.0073
		4	16.8	1.90	0.0091
2	700	6	27.0	2.35	0.0086
		5	19.4	2.35	0.014
		4	12.0	2.35	0.024
3	600	6	16.6	3.00	0.0035
		5	10.3	3.00	0.015
		4	6.2	2.90	0.022
4	500	6	8.9	4.10	0.0045
		5	5.7	4.10	0.0093
		4	3.0	4.00	0.0115

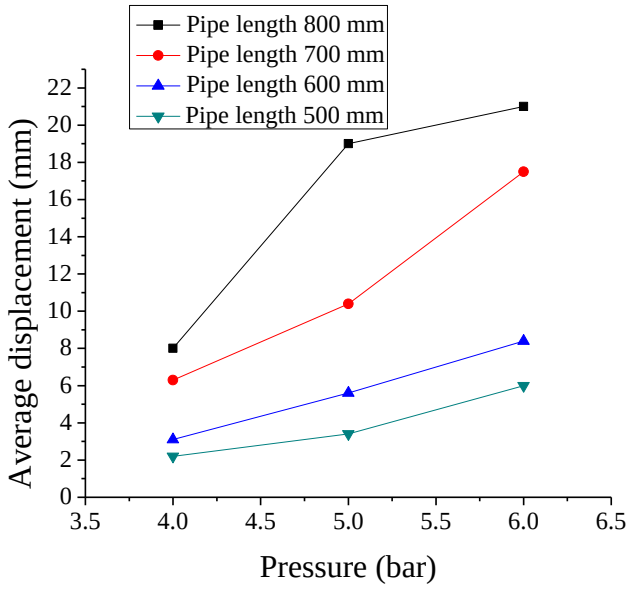

Fig. 2.39 Average displacement of vertical cantilever tube for various flow pressure and length of tube.

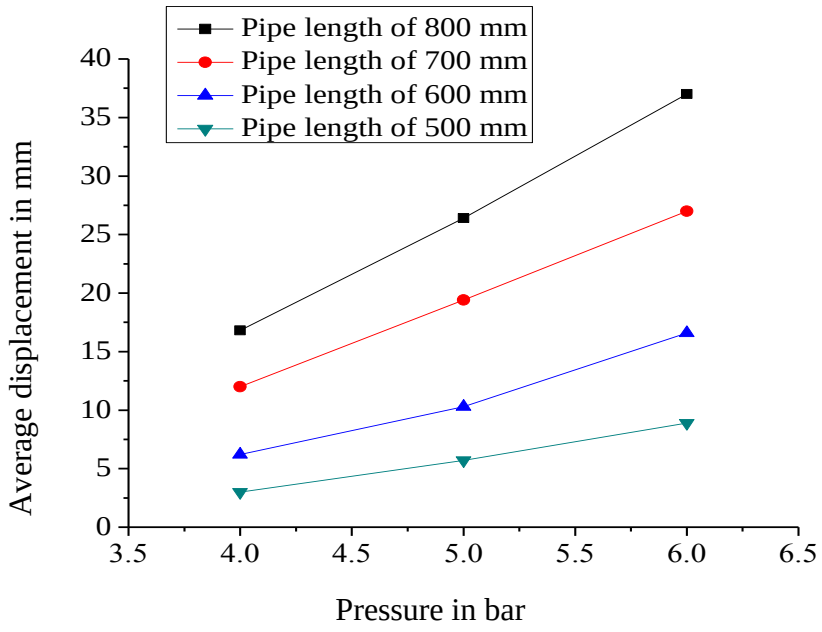

Fig. 2.40 Average displacement of horizontal cantilever tube for various flow pressure and length of tube.

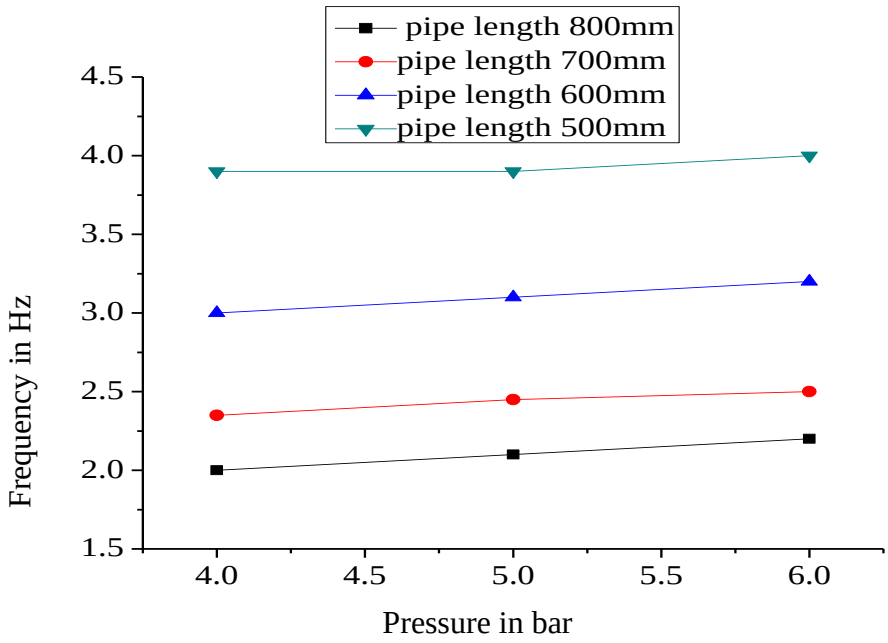

Fig. 2.41 Frequency of vertical cantilever tube for various flow pressure and length of tube.

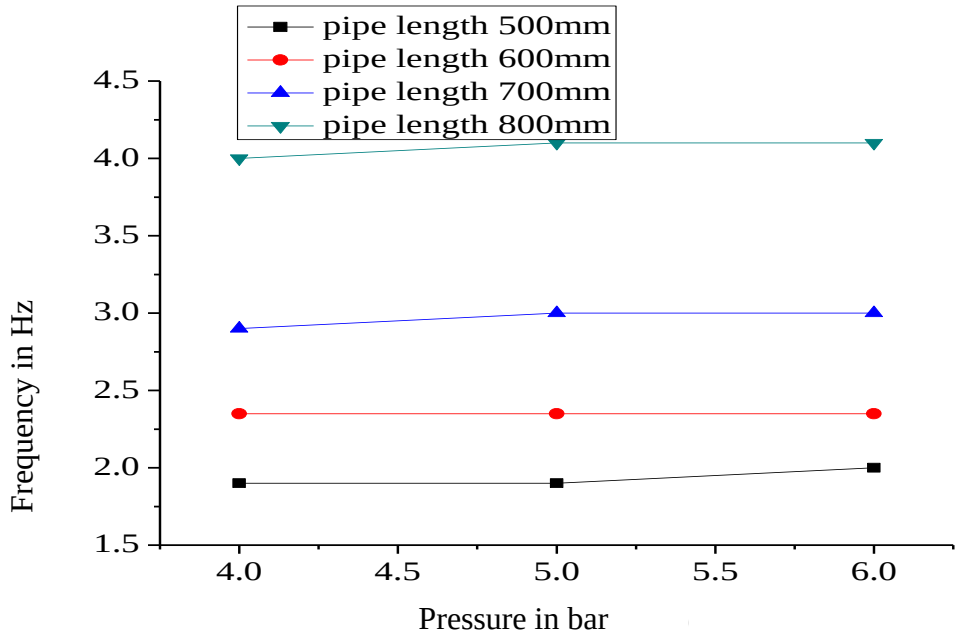

Fig. 2.42 Frequency of horizontal cantilever tube for various flow pressure and length of tube.

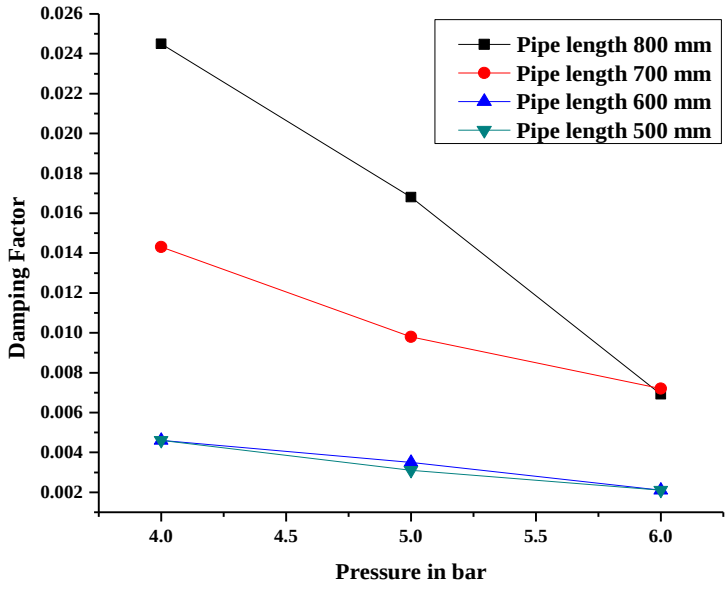

Fig. 2.43 Damping ratio of vertical cantilever tube for various flow pressure and length of tube.

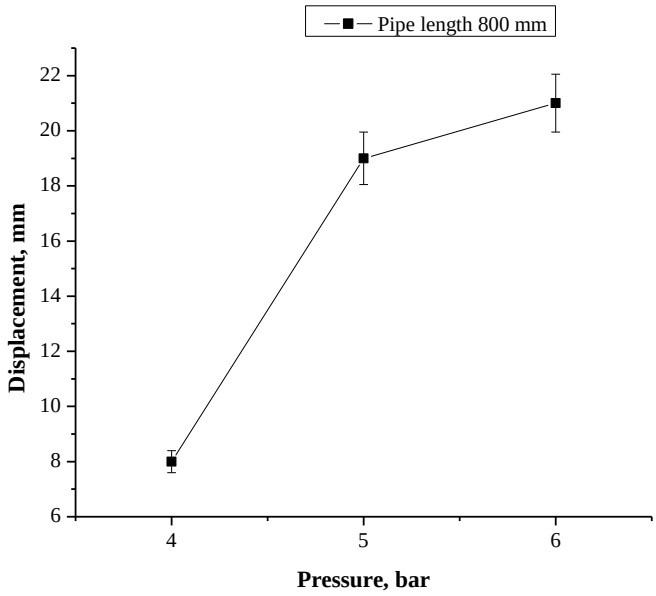

Fig. 2.44. Error bar for tube displacement of 800 mm length of pipe and at various pressure.

CHAPTER 3

FINITE ELEMENT FORMULATION AND SOLUTION FOR TUBE CONVEYING FLUID

3.1 INTRODUCTION

The evaluation of the natural frequency of the tube is found by using the finite element idealization as illustrated in Figure 3.1. The theoretical model based on finite element considers the tube as one-dimensional problem. Applying the Galerkin's approach i.e. multiply equation (1.23) by the shape function W^T, then integrating over the entire domain and equating to zero (Reddy, 2005, Sheshu, 2003 and Logan, 2002). The weak form of Eq.1.23 is as follows,

$$\int_0^l W^T\left(EI\frac{\partial^4 w}{\partial x^4}+\left[m_f U^2-\bar{T}+\bar{p}A(1-2\nu)\right]\frac{\partial^2 w}{\partial x^2}+2m_f U\frac{\partial^2 w}{\partial x\partial t}+(m_f+m)\frac{\partial^2 w}{\partial t^2}\right)dx=0. \tag{3.1}$$

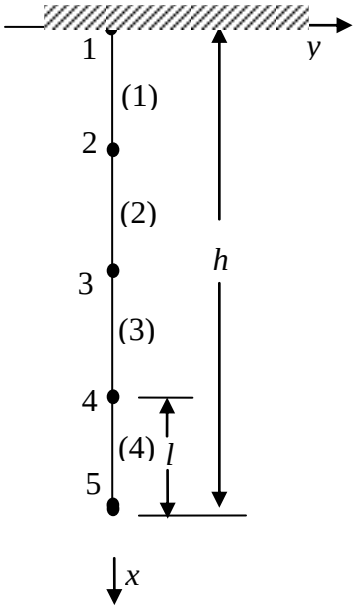

Fig.3.1 Finite element idealization of tube.

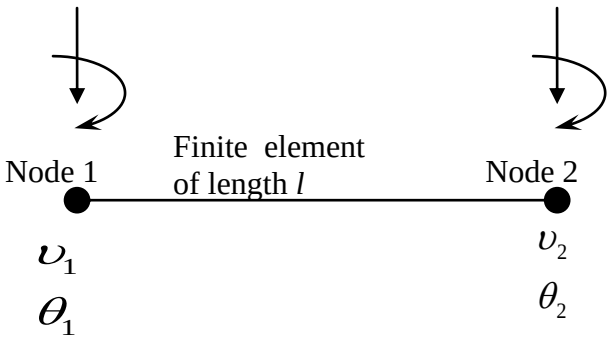

Fig.3.2 One-dimension beam (tube) element and nodal degrees of freedom.

In finite element (FE) modeling, the decrease in the frequency of pipes conveying fluid is generally occur due to the damping of the fluid mass. The second term of equation (3.1) is incorporated into the model as additional added mass to the pipe due to fluid flow which decreases the pipe stiffness. This thesis brings out the experiment results of on an open-ended cantilever tube conveying fluid and their numerical simulation using the FE method. Figure 3.2 illustrate a typical element with nodal values.

3.2 EVALUATION OF EACH TERM IN THE WEAK FORM OF THE DIFFERENTIAL EQUATION

Considering first term of Eq.(3.1)

$$\int_0^l \left(E\,I\,W^T \frac{\partial}{\partial x}\left(\frac{\partial^3 w}{\partial x^3}\right)\right) d\,x,$$

and applying integration by parts gives

$$\left[E\,I\,W^T \frac{\partial^3 w}{\partial x^3}\right]_0^l - E\,I \int_0^l \frac{\partial^3 w}{\partial x^3}\frac{\partial\, W^T}{\partial x}\, d\,x.$$

Appling once again integration by parts gives

$$\left[E\,I\,W^T \frac{\partial^3 w}{\partial x^3}\right]_0^l - \left[E\,I \frac{\partial\, W^T}{\partial x}\frac{\partial^2 w}{\partial x^2}\right]_0^l + E\,I \int_0^l \left(\frac{\partial^2 W^T}{\partial x^2}\frac{\partial^2 w}{\partial x^2}\right) d\,x. \qquad (3.2)$$

Evaluation of 2nd term of Eq.(3.1)

$$\int_0^l \left(W^T \left[m_f U^2 - \bar{T} + \bar{p} A(1-2\nu) \right] \frac{\partial^2 w}{\partial x^2} \right) dx. \tag{3.3}$$

Considering fluid flow term of equation (3.3)

$$\int_0^l \left(W^T m_f U^2 \frac{\partial^2 w}{\partial x^2} \right) dx,$$

and applying integration by parts gives

$$\left[m_f U^2 W^T \frac{\partial w}{\partial x} \right]_0^l - m_f U^2 \int_0^l \left(\frac{\partial W^T}{\partial x} \frac{\partial w}{\partial x} \right) dx. \tag{3.4}$$

Considering tube axial tension term of equation (3.3)

$$-\int_0^l \left(W^T \bar{T} \frac{\partial^2 w}{\partial x^2} \right) dx,$$

and applying integration by parts gives

$$-\left[\bar{T} W^T \frac{\partial w}{\partial x} \right]_0^l + \bar{T} \int_0^l \left(\frac{\partial W^T}{\partial x} \frac{\partial w}{\partial x} \right) dx. \tag{3.5}$$

Considering fluid pressure term of equation (3.3)

$$\int_0^l \left(W^T \bar{p} A(1-2\nu) \frac{\partial^2 w}{\partial x^2} \right) dx.$$

and applying integration by parts gives

$$\left[W^T \bar{p} A(1-2\nu) \frac{\partial w}{\partial x} \right]_0^l - \bar{p} A(1-2\nu) \int_0^l \left(\frac{\partial W^T}{\partial x} \frac{\partial w}{\partial x} \right) dx. \tag{3.6}$$

Considering the damping (third) term of Eq.(3.1)

$$\int_0^l \left(W^T 2 m_f U \frac{\partial}{\partial x} \left(\frac{\partial w}{\partial t} \right) \right) dx,$$

and applying integration by parts gives

$$\left[2m_f U W^T \frac{\partial w}{\partial t}\right]_0^l - 2m_f U \int_0^l \left(\frac{\partial W^T}{\partial x}\frac{\partial w}{\partial t}\right) dx. \tag{3.7}$$

Considering the mass (fourth) term of Eq.(3.1)

$$\int_0^l \left(W^T (m_f + m)\frac{\partial^2 w}{\partial t^2}\right) dx,$$

and applying integration by parts gives

$$\left[\left(m_f + m\right) W^T \frac{\partial w}{\partial t}\right]_0^l - \left(m_f + m\right)\int_0^l \left(\frac{\partial W^T}{\partial t}\frac{\partial w}{\partial t}\right) dx. \tag{3.8}$$

The Weak form of the governing equation is given by considering equation (3.2) to (3.8)

$$\int_0^l \left(\begin{array}{l} E I \frac{\partial^2 W^T}{\partial x^2}\frac{\partial^2 w}{\partial x^2} - m_f U^2 \frac{\partial W^T}{\partial x}\frac{\partial w}{\partial x} + \bar{T}\int_0^l \left(\frac{\partial W^T}{\partial x}\frac{\partial w}{\partial x}\right) - \\ \bar{p} A\left(1-2\nu\right)\int_0^l \left(\frac{\partial W^T}{\partial x}\frac{\partial w}{\partial x}\right) - 2m_f U \frac{\partial W^T}{\partial x}\frac{\partial w}{\partial t} - \left(m_f + m\right)\frac{\partial W^T}{\partial t}\frac{\partial w}{\partial t} \end{array} \right) dx = 0 . \tag{3.9}$$

Finite element equation of motion

$$\Rightarrow \sum_{n=1}^{8}\left[\left(\mathbf{K}_s^e + \mathbf{K}_f^e + \mathbf{K}_t^e + \mathbf{K}_p^e\right)\mathbf{w}^e + \mathbf{G}^e\dot{\mathbf{w}} + \mathbf{M}^e\ddot{\mathbf{w}}\right] = 0, \tag{3.10}$$

where, $\mathbf{K}_s^e = \int_0^l E I \left(\frac{\partial^2 W^T}{\partial x^2}\frac{\partial^2 w}{\partial x^2}\right) dx,$

$$\mathbf{K}_f^e = \int_0^l m_f U^2 \left(\frac{\partial W^T}{\partial x}\frac{\partial w}{\partial x}\right) dx,$$

$$\mathbf{K}_t^e = \int_0^l \bar{T}\left(\frac{\partial W^T}{\partial x}\frac{\partial w}{\partial x}\right) dx,$$

$$\mathbf{K}_p^e = \int_0^l \bar{p}\, A(1-2\nu)\left(\frac{\partial W^T}{\partial x}\frac{\partial w}{\partial x}\right)dx,$$

$$\mathbf{G}^e = \int_0^l 2m_f U\left(W^T \frac{\partial}{\partial x}\left(\frac{\partial w}{\partial t}\right)\right)dx,$$

$$\mathbf{M}^e = \int_0^l \left((m_f + m)W^T \frac{\partial^2 w}{\partial t^2}\right)dx.$$

The finite element equation of motion can be written as

$$\mathbf{M}^e\ddot{\mathbf{w}}^e + \mathbf{G}^e\dot{\mathbf{w}}^e + \left(\mathbf{K}_s^e + \mathbf{K}_f^e + \mathbf{K}_t^e + \mathbf{K}_p^e\right)\mathbf{w}^e = 0,$$

$$\Rightarrow \mathbf{M}^e\ddot{\mathbf{w}}^e + \mathbf{G}^e\dot{\mathbf{w}}^e + \left(\mathbf{K}_s^e + \mathbf{K}_f^e + \mathbf{K}_t^e + \mathbf{K}_p^e\right)\mathbf{w}^e = 0,$$

$$\Rightarrow \mathbf{M}^e\ddot{\mathbf{w}}^e + \mathbf{G}^e\dot{\mathbf{w}}^e + \mathbf{K}_{st}^e\mathbf{w}^e = 0\,. \qquad (3.11)$$

where, $\mathbf{K}_{st}^e = \mathbf{K}_s^e + \mathbf{K}_f^e + \mathbf{K}_t^e + \mathbf{K}_p^e$,

'$\mathbf{K}_{st}^e$' is known as total stiffness matrix.

3.3 DERIVATION OF STRUCTURAL ELEMENT

Stiffness matrix

'$\boldsymbol{K}_s^e$' is known as structural stiffness matrix

$$\boldsymbol{K}_s^e = \int_0^l E\,I\left(\frac{\partial^2 W^T}{\partial x^2}\frac{\partial^2 w}{\partial x^2}\right)dx,$$

$$K_s^e = E\,I\int_0^l \frac{\partial^2}{\partial x^2}\left(W^T\right)\frac{\partial^2}{\partial x^2}\left([W]\{d\}\right)dx,$$

$$K_s^e = E\,I\int_0^1 \left(\begin{bmatrix} \dfrac{\partial^2 N_1}{\partial x^2} \\ \dfrac{\partial^2 N_2}{\partial x^2} \\ \dfrac{\partial^2 N_3}{\partial x^2} \\ \dfrac{\partial^2 N_4}{\partial x^2} \end{bmatrix} \begin{bmatrix} \dfrac{\partial^2 N_1}{\partial x^2} & \dfrac{\partial^2 N_2}{\partial x^2} & \dfrac{\partial^2 N_3}{\partial x^2} & \dfrac{\partial^2 N_4}{\partial x^2} \end{bmatrix} \begin{Bmatrix} \upsilon_1 \\ \theta_1 \\ \upsilon_2 \\ \theta_1 \end{Bmatrix} \right) d\,x,$$

where, $W^T = \begin{bmatrix} N_1 \\ N_2 \\ N_3 \\ N_4 \end{bmatrix}$ and $w^e = [W]\{d\} \Rightarrow [N_1\, N_2\, N_3\, N_4] \begin{Bmatrix} \upsilon_1 \\ \theta_1 \\ \upsilon_2 \\ \theta_1 \end{Bmatrix}$;

N_1, N_2, N_3 and N_4 are Hermite shape functions,

$$N_1 = 1 - \frac{3x^2}{l^2} + \frac{2x^3}{l^3}; \qquad N_2 = x - \frac{2x^2}{l} + \frac{x^2}{l^2};$$

$$N_3 = \frac{3x^2}{l^2} - \frac{2x^3}{l^3}; \qquad N_4 = -\frac{x^2}{l} + \frac{x^2}{l^2};$$

which are used to develop the various finite element matrices, where l is the length of the tube element. Using the Hermite shape functions, the stiffness matrix is evaluated as

$$K_s^e = E\,I\int_0^1 \left(\begin{bmatrix} \dfrac{-6}{l^2} + \dfrac{12x}{l^3} \\ \dfrac{-4}{l} + \dfrac{6x}{l^2} \\ \dfrac{6}{l^2} - \dfrac{12x}{l^3} \\ \dfrac{-2}{l} + \dfrac{6x}{l^2} \end{bmatrix} \begin{bmatrix} \dfrac{-6}{l^2} + \dfrac{12x}{l^3} & \dfrac{-4}{l} + \dfrac{6x}{l^2} & \dfrac{6}{l^2} - \dfrac{12x}{l^3} & \dfrac{-2}{l} + \dfrac{6x}{l^2} \end{bmatrix} \begin{Bmatrix} \upsilon_1 \\ \theta_1 \\ \upsilon_2 \\ \theta_1 \end{Bmatrix} \right) d\,x.$$

The coefficients are evaluated by integrals, we get

$$\boldsymbol{K_s^e} = \frac{E\,I}{l^3}\begin{bmatrix} 12 & 6l & -12 & 6l \\ 6l & 4l^2 & -6l & -2l^2 \\ -12 & -6l & 12 & -6l \\ 6l & 2l^2 & -6l & 4l^2 \end{bmatrix}. \tag{3.12}$$

Fluid element matrix

$\boldsymbol{K_f^e}$ is known as fluid stiffness matrix

$$K_f^e = \int_0^l m_f U^2 \left(\frac{\partial W^T}{\partial x} \frac{\partial w}{\partial x} \right) dx,$$

$$K_f^e = m_f U^2 \int_0^l \frac{\partial}{\partial x}\left(W^T\right) \frac{\partial}{\partial x}\left([W]\{d\}\right) dx,$$

$$K_f^e = m_f U^2 \int_0^1 \left(\begin{bmatrix} \frac{\partial N_1}{\partial x} \\ \frac{\partial N_2}{\partial x} \\ \frac{\partial N_3}{\partial x} \\ \frac{\partial N_4}{\partial x} \end{bmatrix} \begin{bmatrix} \frac{\partial N_1}{\partial x} & \frac{\partial N_2}{\partial x} & \frac{\partial N_3}{\partial x} & \frac{\partial N_4}{\partial x} \end{bmatrix} \begin{Bmatrix} \upsilon_1 \\ \theta_1 \\ \upsilon_2 \\ \theta_1 \end{Bmatrix} \right) dx,$$

On evaluation of the above expression results in

$$\boldsymbol{K_f^e} = \frac{m_f U^2}{30l}\begin{bmatrix} 36 & 3l & -36 & 3l \\ 3l & 4l^2 & -3l & -l^2 \\ -36 & -3l & 36 & -3l \\ 3l & -l^2 & -3l & 4l^2 \end{bmatrix}. \tag{3.13}$$

Tube tension matrix

$\boldsymbol{K_t^e}$ is known as tube tension matrix

$$K_t^e = \int_0^1 \overline{T} \left(\frac{\partial W^T}{\partial x} \frac{\partial w}{\partial x} \right) dx,$$

$$K_t^e = \overline{T}\int_0^1 \left(\begin{bmatrix} \frac{\partial N_1}{\partial x} \\ \frac{\partial N_2}{\partial x} \\ \frac{\partial N_3}{\partial x} \\ \frac{\partial N_4}{\partial x} \end{bmatrix} \begin{bmatrix} \frac{\partial N_1}{\partial x} & \frac{\partial N_2}{\partial x} & \frac{\partial N_3}{\partial x} & \frac{\partial N_4}{\partial x} \end{bmatrix} \begin{Bmatrix} \upsilon_1 \\ \theta_1 \\ \upsilon_2 \\ \theta_1 \end{Bmatrix} \right) dx.$$

The coefficients are evaluated by integrals,

$$\boldsymbol{K_t^e} = \frac{\overline{T}}{30l} \begin{bmatrix} 36 & 3l & -36 & 3l \\ 3l & 4l^2 & -3l & -l^2 \\ -36 & -3l & 36 & -3l \\ 3l & -l^2 & -3l & 4l^2 \end{bmatrix}. \tag{3.14}$$

Fluid pressure matrix

$\boldsymbol{K_p^e}$ is known as fluid pressure matrix

$$K_p^e = \int_0^1 \overline{p}A(1-2\nu)\left(\frac{\partial W^T}{\partial x} \frac{\partial w}{\partial x} \right) dx,$$

$$K_p^e = \overline{p}A(1-2\nu)\int_0^1 \left(\begin{bmatrix} \frac{\partial N_1}{\partial x} \\ \frac{\partial N_2}{\partial x} \\ \frac{\partial N_3}{\partial x} \\ \frac{\partial N_4}{\partial x} \end{bmatrix} \begin{bmatrix} \frac{\partial N_1}{\partial x} & \frac{\partial N_2}{\partial x} & \frac{\partial N_3}{\partial x} & \frac{\partial N_4}{\partial x} \end{bmatrix} \begin{Bmatrix} \upsilon_1 \\ \theta_1 \\ \upsilon_2 \\ \theta_1 \end{Bmatrix} \right) dx.$$

The coefficients are evaluated by integrals,

$$\boldsymbol{K_p^e} = \frac{\overline{p}A(1-2\nu)}{30l} \begin{bmatrix} 36 & 3l & -36 & 3l \\ 3l & 4l^2 & -3l & -l^2 \\ -36 & -3l & 36 & -3l \\ 3l & -l^2 & -3l & 4l^2 \end{bmatrix}. \tag{3.15}$$

Fluid damping matrix

$\boldsymbol{G^e}$ is known as fluid damping matrix

$$G^e = \int_0^l 2m_f U\left(W^T \frac{\partial}{\partial x}\left(\frac{\partial w}{\partial t}\right)\right)dx,$$

$$G^e = 2m_f U\int_0^l\left(W^T \frac{\partial}{\partial x}\left([W]\{\dot{d}\}\right)\right)dx,$$

$$G^e = 2m_f U\int_0^l\left(\begin{bmatrix} N_1 \\ N_2 \\ N_3 \\ N_4 \end{bmatrix}\begin{bmatrix} \frac{\partial N_1}{\partial x} & \frac{\partial N_2}{\partial x} & \frac{\partial N_3}{\partial x} & \frac{\partial N_4}{\partial x} \end{bmatrix}\frac{\partial}{\partial x}\begin{Bmatrix} \dot{\upsilon}_1 \\ \dot{\theta}_1 \\ \dot{\upsilon}_2 \\ \dot{\theta}_1 \end{Bmatrix}\right)dx.$$

The coefficients are evaluated by integrals, we get

$$\boldsymbol{G^e} = \frac{m_f U}{30}\begin{bmatrix} 30 & 6l & 30 & -6l \\ -6l & 0 & 6l & -l^2 \\ -30 & -6l & 30 & 6l \\ 6l & l^2 & -6l & 6 \end{bmatrix}. \qquad (3.16)$$

Mass matrix

$\boldsymbol{M^e}$ is known as mass matrix

$$M^e = \int_0^l\left(\left(m_f + m\right)W^T \frac{\partial^2}{\partial t^2}(w)\right)dx,$$

$$M^e = \left(m_f + m\right)\int_0^l\left(W^T \frac{\partial^2}{\partial t^2}\left([W]\{\ddot{d}\}\right)\right)dx,$$

$$M^e = \left(m_f + m\right)\int_0^l\left(\begin{bmatrix} N_1 \\ N_2 \\ N_3 \\ N_4 \end{bmatrix}\begin{bmatrix} N_1 & N_2 & N_3 & N_4 \end{bmatrix}\frac{\partial^2}{\partial t^2}\begin{Bmatrix} \ddot{\upsilon}_1 \\ \ddot{\theta}_1 \\ \ddot{\upsilon}_2 \\ \ddot{\theta}_1 \end{Bmatrix}\right)dx.$$

On evaluation of the above integrals results in

$$\boldsymbol{M}^{e}=\left(\frac{\left(m_f+m\right)l}{420}\right)\begin{bmatrix} 156 & 22l & 54 & -13l \\ -22l & 4 & 13l & -3l^2 \\ 54 & 13l & 156 & -22l \\ -13l & 3l^2 & -22l & 4l^2 \end{bmatrix}. \tag{3.17}$$

Add the fluid pressure, velocity, tube tension, structural matrices to get total stiffness matrix. Assemble the element stiffness, damping, and mass matrices to get global matrices.

3.4 STATE-SPACE ANALYSIS

Solution of the above equation of motion (Eq.3.11) can be carried out by placing the equations in the state-space form. i.e. converting the second order finite element motion equation into first order (Zou et al. 2005). The state vector is defined to be,

$$\left\{\zeta\left(t\right)\right\}=\left[\left\{d\left(t\right)\right\}^{T}\left\{\dot{d}\left(t\right)\right\}^{T}\right]^{T}.$$

Correspondingly, the state-space form of the equations of motion is represented by

$$\left[\Theta\right]\left\{\dot{\zeta}\right\}-\left[\psi\right]\left\{\zeta\right\}=0, \tag{3.18}$$

$$\text{where, }\left[\Theta\right]=\begin{bmatrix}\left[K\right]_{nsmax} & 0 \\ 0 & \left[-M\right]_{nsmax}\end{bmatrix}_{nsmax2},\qquad \left[\psi\right]=\begin{bmatrix} 0 & \left[K\right]_{nsmax} \\ \left[K\right]_{nsmax} & \left[G\right]_{nsmax}\end{bmatrix}_{nsmax2};$$

$$\left[\mathbf{K}\right]_{nsmax}=\left[\left[\mathbf{K}_s^e\right]+\left[\mathbf{K}_f^e\right]+\left[\mathbf{K}_t^e\right]+\left[\mathbf{K}_p^e\right]\right]_{nsmax},$$

$$[\mathbf{K}]_{nsmax}=\left(\left(\frac{EI}{l^3}\right)+\left(\frac{m_fU^2}{30l}\right)+\left(\frac{\bar{T}}{30l}\right)+\left\{\frac{\bar{p}A(1-2\nu)}{30l}\right\}\right)\begin{bmatrix}120 & 15l & -120 & 15l & 0 & 0 & 0 & 0\\ 15l & 16l^2 & -15l & -l^2 & 0 & 0 & 0 & 0\\ -120 & -15l & 240 & 0 & -120 & 15l & 0 & 0\\ 15l & -l^2 & 0 & 32l^2 & -15l & -l^2 & 0 & 0\\ 0 & 0 & -120 & -15l & 240 & 0 & -120 & 15l\\ 0 & 0 & 15l & -l^2 & 0 & 32l^2 & -15l & -l^2\\ 0 & 0 & 0 & 0 & -120 & -15l & 120 & -15l\\ 0 & 0 & 0 & 0 & 15l & -l^2 & -15l & 16l^2\end{bmatrix},$$

$$[\mathbf{M}]_{nsmax}=\left\{\frac{(m_f+m)l}{420}\right\}\begin{bmatrix}156 & 22l & 54 & -13l & 0 & 0 & 0 & 0\\ 22l & 4l^2 & 13l & -3l^2 & 0 & 0 & 0 & 0\\ 54 & 13l & 312 & 0 & 54 & -13l & 0 & 0\\ -13l & -3l^2 & 0 & 8l^2 & 13l & -3l^2 & 0 & 0\\ 0 & 0 & 54 & 13l & 312 & 0 & 54 & -13l\\ 0 & 0 & -13l & -3l^2 & 0 & 8l^2 & 13l & -3l^2\\ 0 & 0 & 0 & 0 & 54 & 13l & 156 & -22l\\ 0 & 0 & 0 & 0 & -13l & -3l^2 & -22l & 4l^2\end{bmatrix},$$

$$[\mathrm{G}]_{nsmax}=\left\{\frac{m_fU}{30}\right\}\begin{bmatrix}-30 & 6l & 30 & -6l & 0 & 0 & 0 & 0\\ -6l & 0 & 6l & -l^2 & 0 & 0 & 0 & 0\\ -30 & -6l & 0 & 12l & 30 & -6l & 0 & 0\\ 6l & l^2 & -12l & 0 & 6l & -l^2 & 0 & 0\\ 0 & 0 & -30 & -6l & 0 & 12l & 30 & -6l\\ 0 & 0 & 6l & l^2 & -12l & 0 & 6l & -l^2\\ 0 & 0 & 0 & 0 & -30 & -6l & 30 & 6l\\ 0 & 0 & 0 & 0 & 6l & l^2 & -6l & 0\end{bmatrix}.$$

$$C_1=\left(\frac{EI}{l^3}\right)+\left(\frac{m_fU^2}{30l}\right)+\left(\frac{\bar{T}}{30l}\right)+\left\{\frac{\bar{p}A(1-2\nu)}{30l}\right\},\ C_2=\left\{\frac{(m_f+m)l}{420}\right\},\ C_3=\left\{\frac{m_fU}{30}\right\};$$

$$[\Theta] = \begin{bmatrix}
120C_1 & 15lC_1 & -120C_1 & 15lC_1 & 0 & 0 & 0 & 0 \\
15lC_1 & 16l^2C_1 & -15lC_1 & -l^2C_1 & 0 & 0 & 0 & 0 \\
-120C_1 & -15lC_1 & 240C_1 & 0 & -120C_1 & 15lC_1 & 0 & 0 \\
15lC_1 & -l^2C_1 & 0 & 32l^2C_1 & -15lC_1 & -l^2C_1 & 0 & 0 \\
0 & 0 & -120C_1 & -15lC_1 & 240C_1 & 0 & -120C_1 & 15lC_1 \\
0 & 0 & 15lC_1 & -l^2C_1 & 0 & 32l^2C_1 & -15lC_1 & -l^2C_1 \\
0 & 0 & 0 & 0 & -120C_1 & -15lC_1 & 120C_1 & -15lC_1 \\
0 & 0 & 0 & 0 & 15lC_1 & -l^2C_1 & -15lC_1 & 16l^2C_1 \\
0 & 0 & 0 & 0 & 0 & 0 & 0 & 0 \\
0 & 0 & 0 & 0 & 0 & 0 & 0 & 0 \\
0 & 0 & 0 & 0 & 0 & 0 & 0 & 0 \\
0 & 0 & 0 & 0 & 0 & 0 & 0 & 0 \\
0 & 0 & 0 & 0 & 0 & 0 & 0 & 0 \\
0 & 0 & 0 & 0 & 0 & 0 & 0 & 0 \\
0 & 0 & 0 & 0 & 0 & 0 & 0 & 0
\end{bmatrix}$$

$$\begin{bmatrix}
0 & 0 & 0 & 0 & 0 & 0 & 0 & 0 \\
0 & 0 & 0 & 0 & 0 & 0 & 0 & 0 \\
0 & 0 & 0 & 0 & 0 & 0 & 0 & 0 \\
0 & 0 & 0 & 0 & 0 & 0 & 0 & 0 \\
0 & 0 & 0 & 0 & 0 & 0 & 0 & 0 \\
0 & 0 & 0 & 0 & 0 & 0 & 0 & 0 \\
0 & 0 & 0 & 0 & 0 & 0 & 0 & 0 \\
0 & 0 & 0 & 0 & 0 & 0 & 0 & 0 \\
156C_2 & 22lC_2 & 54C_2 & -13lC_2 & 0 & 0 & 0 & 0 \\
22lC_2 & 4l^2C_2 & 13lC_2 & -3l^2C_2 & 0 & 0 & 0 & 0 \\
54C_2 & 13lC_2 & 312C_2 & 0 & 54C_2 & -39C_2 & 0 & 0 \\
-13lC_2 & -3l^2C_2 & 0 & 8l^2C_2 & 13lC_2 & -3l^2C_2 & 0 & 0 \\
0 & 0 & 54C_2 & 13lC_2 & 312C_2 & 0 & 54C_2 & -13lC_2 \\
0 & 0 & -13lC_2 & -3l^2C_2 & 0 & 8l^2C_2 & 13lC_2 & -3l^2C_2 \\
0 & 0 & 0 & 0 & 54C_2 & 13lC_2 & 156C_2 & -22lC_2 \\
0 & 0 & 0 & 0 & -13lC_2 & -3l^2C_2 & -22lC_2 & 4l^2C_2
\end{bmatrix} \quad (3.19)$$

$$
[\Psi] = \begin{bmatrix}
0 & 0 & 0 & 0 & 0 & 0 & 0 & 0 \\
0 & 0 & 0 & 0 & 0 & 0 & 0 & 0 \\
0 & 0 & 0 & 0 & 0 & 0 & 0 & 0 \\
0 & 0 & 0 & 0 & 0 & 0 & 0 & 0 \\
0 & 0 & 0 & 0 & 0 & 0 & 0 & 0 \\
0 & 0 & 0 & 0 & 0 & 0 & 0 & 0 \\
0 & 0 & 0 & 0 & 0 & 0 & 0 & 0 \\
0 & 0 & 0 & 0 & 0 & 0 & 0 & 0 \\
120C_1 & 15lC_1 & -120C_1 & 15lC_1 & 0 & 0 & 0 & 0 \\
15lC_1 & 16l^2C_1 & -15lC_1 & -l^2C_1 & 0 & 0 & 0 & 0 \\
-120C_1 & -15lC_1 & 240C_1 & 0 & -120C_1 & 15lC_1 & 0 & 0 \\
15lC_1 & -l^2C_1 & 0 & 32l^2C_1 & -15lC_1 & -l^2C_1 & 0 & 0 \\
0 & 0 & -120C_1 & -15lC_1 & 240C_1 & 0 & -120C_1 & 15lC_1 \\
0 & 0 & 15lC_1 & -l^2C_1 & 0 & 32l^2C_1 & -15lC_1 & -l^2C_1 \\
0 & 0 & 0 & 0 & -120C_1 & -15lC_1 & 120C_1 & -15lC_1 \\
0 & 0 & 0 & 0 & 15lC_1 & -l^2C_1 & -15lC_1 & 16l^2C_1
\end{bmatrix}
$$

$$
\begin{bmatrix}
120C_1 & 15lC_1 & -120C_1 & 15lC_1 & 0 & 0 & 0 & 0 \\
15lC_1 & 16l^2C_1 & -15lC_1 & -l^2C_1 & 0 & 0 & 0 & 0 \\
-120C_1 & -15lC_1 & 240C_1 & 0 & -120C_1 & 15lC_1 & 0 & 0 \\
15lC_1 & -l^2C_1 & 0 & 32l^2C_1 & -15lC_1 & -l^2C_1 & 0 & 0 \\
0 & 0 & -120C_1 & -15lC_1 & 240C_1 & 0 & -120C_1 & 15lC_1 \\
0 & 0 & 15lC_1 & -l^2C_1 & 0 & 32l^2C_1 & -15lC_1 & -l^2C_1 \\
0 & 0 & 0 & 0 & -120C_1 & -15lC_1 & 120C_1 & -15lC_1 \\
0 & 0 & 0 & 0 & 15lC_1 & -l^2C_1 & -15lC_1 & 16l^2C_1 \\
-30C_3 & 6lC_3 & 30C_3 & -6lC_3 & 0 & 0 & 0 & 0 \\
-6lC_3 & 0 & 6lC_3 & -l^2C_3 & 0 & 0 & 0 & 0 \\
-30C_3 & -6lC_3 & 0 & 12lC_3 & 30C_3 & -6lC_3 & 0 & 0 \\
6lC_3 & l^2C_3 & -12lC_3 & 0 & 6lC_3 & -l^2C_3 & 0 & 0 \\
0 & 0 & -30C_3 & -6lC_3 & 0 & 12lC_3 & 30C_3 & -6lC_3 \\
0 & 0 & 6lC_3 & l^2C_3 & -12lC_3 & 0 & 6lC_3 & -l^2C_3 \\
0 & 0 & 0 & 0 & -30C_3 & -6lC_3 & 30C_3 & 6lC_3 \\
0 & 0 & 0 & 0 & 6lC_3 & l^2C_3 & -6lC_3 & 0
\end{bmatrix} \quad (3.20)
$$

3.5 SOLUTION OF THE FINITE ELEMENT EQUATION

Numerical results are presented in this chapter based on the finite element formulation for equation of motion of pipe conveying fluid. The codes are written for finite element formulation using the FORTRAN compiler. Numerical exercises are presented for pipe with different boundary conditions like simply supported (SS), clamped simply supported (CS) and clamped- free (CF) for the analysis of natural frequency when the pipe is subjected to different fluid pressures and velocities. The free vibration frequency of pipe with internal flow has been validated with the spectral element approach solution given by Lee and Oh (2003). The finite element approach for the free vibration of pipe conveying fluid with different boundary conditions has been validated with the results reported by Zou et al. (2005).

3.5.1 STEEL PIPE

Case (a): Table 3.1 lists the natural frequencies of simply-supported pipe under different axial tension. The results obtained from present finite element calculations are being compared with analytical results of Blevins (2001) and results reported by Lee and Oh (2003) by spectral finite element pipe.

Case (b): Table 3.2 presents a comparison of the natural frequencies of pipe conveying fluid at various velocities for a given initial pipe tension. The natural frequencies for isotropic steel pipe are compared with the analytical results detailed in Blevins (2001) and numerical results detailed in Lee and Oh (2003) at different conditions like empty pipeline, pipe line conveying fluid at various flow velocities and pipe axial tension. It is observed that there is very close comparison between these values (i.e. within 0.01% to 0.9% of error).

3.5.2 ALUMINIUM PIPE

Table 3.3 shows the analytical and numerical natural frequencies of cantilevered pipe compared with the report of Sinha et al. (2001) by spectral finite element. The natural frequencies for aluminium pipe are also compared with the analytical results detailed in Blevins (2001) and numerical results detailed in Sinha et

al. (2001) at different conditions like empty pipeline, stagnant fluid and fluid velocity 0.55 m/s and 1.1 m/s. It is observed that there is close comparison with 11% error.

Table 3.1 Comparison of the natural frequencies of the empty simply supported pipeline obtained by FEM with the exact analytical results for different axial tensions.

Axial tension T_o (N)	Natural freq. (Hz)	Analytical (Blevins, 2001)	50 Elements (Lee and Oh, 2003)	50 Elements (Present)	20 Elements (Present)	10 Elements (Present)	%Error w.r.t. Lee and Oh, (2003)
0.00	ω_1	1.4717	1.4717	1.47142	1.47142	1.47143	0.019
	ω_2	5.8869	5.8869	5.88569	5.88573	5.88632	0.020
	ω_3	13.2455	13.2455	13.2428	13.2433	13.2499	0.020
	ω_{10}	147.172	147.187	147.158	147.723	163.317	0.009
4.95	ω_1	13.6224	13.6224	13.6210	13.6210	13.6210	0.010
	ω_2	27.7178	27.7178	27.7148	27.7148	27.7149	0.010
	ω_3	42.7328	42.7328	42.7279	42.7280	42.7305	0.011
	ω_{10}	200.000	200.012	199.981	201.437	212.724	0.009
7.63	ω_1	16.8781	16.8781	16.8763	16.8763	16.8763	0.010
	ω_2	34.1390	34.1390	34.1353	34.1353	34.1354	0.010
	ω_3	52.1514	52.1514	52.1457	52.1458	52.1480	0.011
	ω_{10}	223.450	223.460	223.428	223.826	235.183	0.009

Table 3.2 Comparison of the natural frequencies of the simply-supported pipeline conveying internal flow obtained by finite element (FEM) results for different flow speeds when initial tension T_0 = 7.63 N.

Flow speed m/s	Natural freq.(Hz)	50 Elements (Lee and Oh, 2003)	50 Elements (Present)	20 Elements (Present)	10 Elements (Present)	% Error w.r.t. Lee and Oh, (2003)
0.00	ω_1	13.5606	13.5644	13.5644	13.5644	0.02
	ω_2	27.4288	27.4363	27.4363	27.4364	0.03
	ω_3	41.9009	41.9122	41.9123	41.91405	0.03
	ω_{10}	179.5381	179.5807	179.8986	189.0270	0.02
3.07	ω_1	13.2425	13.2458	13.2458	13.2458	0.02
	ω_2	26.8159	26.8227	26.8227	26.8230	0.03
	ω_3	41.0324	41.0427	41.0429	41.0456	0.02
	ω_{10}	177.8216	177.8620	178.2027	187.5333	0.02
16.49	ω_1	0.0000	0.0000	0.0000	0.0000	0.00
	ω_2	3.0180	3.0299	3.0303	3.0364	0.40
	ω_3	9.6139	9.6284	9.6328	9.6970	0.15
	ω_{10}	126.7586	126.8032	127.9461	143.9294	0.03
16.80	ω_1	0.0000	0.8772	0.8773	0.87980	-
	ω_2	0.9648	0.8772	0.8773	0.87980	0.90
	ω_3	7.7819	7.7312	7.7358	7.8031	0.65
	ω_{10}	124.6570	124.6299	125.8120	142.0962	0.02
16.97	ω_1		0.0000	0.0000	0.0000	-
	ω_2		0.2299	0.2287	0.2112	-
	ω_3	Not	6.4813	6.4860	6.5553	-
	ω_{10}	available	123.3411	124.5448	141.0095	-
17.02	ω_1		0.0000	0.0000	0.0000	-
	ω_2		0.7885	0.7883	0.7848	-
	ω_3	Not	6.1014	6.1062	6.1762	-
	ω_{10}	available	122.9794	124.1895	140.7046	-

Table 3.3 Analytical and numerical natural frequencies of cantilever pipe.

Case 1: Empty pipe

Natural Frequency (Hz)	Analytical	Sinha et al. (2001)	Present method	% Error w.r.t. Sinha et al. (2001)
1st	18.70	18.43	21.01	10.9
2nd	118.53	122.5	131.71	10.0
3rd	334.57	336.5	368.86	9.3
4th	659.86	-	723.33	8.8

Case 2: Pipe with static water.

Natural Frequency (Hz)	Analytical	Sinha et al. (2001)	Present method	% Error w.r.t. Sinha et al. (2001)
1st	13.02	13.12	14.67	11.2
2nd	82.54	82.50	91.95	10.2
3rd	232.96	229.6	257.53	9.5
4th	459.44	455.0	505.01	9.0

Case 3: Pipe with water flow velocity = 0.55 m/s.

Natural Frequency (Hz)	Analytical	Sinha et al. (2001)	Present method	% Error w.r.t. Sinha et al. (2001)
1st	13.00	12.44	14.67	11.3
2nd	82.53	81.88	91.95	10.2
3rd	232.96	226.2	257.53	9.5
4th	459.44	440.7	505.01	9.0

Case 4: Pipe with water flow velocity = 1.1 m/s.

Natural Frequency (Hz)	Analytical	Sinha et al. (2001)	Present method	% Error w.r.t. Sinha et al. (2001)
1st	12.94	11.81	14.67	11.8
2nd	82.53	81.00	91.95	10.2
3rd	232.96	222.8	257.53	9.5
4th	459.44	435.9	505.01	9.0

3.5.3 COMPOSITE PIPE

The use of pipes made of composite materials for applications in oil fields has become an acceptable practice. Piping systems used for transfer of highly pressurized gas often operate under time-varying conditions, imposed by pumps and valves operations and thus may experience severe vibration induced loading. Examples of such problems are flow-induced vibration of a pipeline supported above ground level as well as conveying internal flow.

In this section, cement coated steel pipe and its geometry and material properties has been used for study and these are referred from Zou et al. (2005).

Table 3.4 (a) Specifications of the cement coated steel pipe (Geometry of pipeline).

Quantity	Symbol	value
Outside diameter	D	1.0668 m
Pipe thickness	t_s	0.0342 m
Cement coating thickness	t_c	0.030175 m
Outside diameter of cement coating	D_c	1.12776 m
Cross-section area of pipe	A	0.783844 m
Span length	L	59.1312 m

Table 3.4 (b) Specifications of the cement coated steel pipe (Material properties).

Density of steel	ρ_s	7850 kg/m^3
Density of cement	ρ_c	3043.508 kg/m^3
Density of pure gas	ρ_g	2.864 kg/m^3
Elastic modulus of steel	E_s	2e11 N/m^2
Elastic modulus of cement	E_c	2.4e10 N/m^2

Table 3.4 (c) Specifications of the cement coated steel pipe (Design parameters).

Design pressure	p	9.253e6 N/m^2
Residual tension	T_o	8896 N
Content gas velocity	V	4.59 m/s
Poisson's ratio	ν	0.312
Gas viscosity	μ	1.01019744 kgs/m^2

The natural frequeny for the simply supported, cantilever and clamped-simply supported pipelines reported by Zou et al. (2005) are compared with the present finite element results and are provided in Tables 3.5, 3.6, and 3.7 respectively. There is a good comparison of result for simply supported and clamped simply supported with the percentage error of 0.12% and for the clamped free the percentage of error is about 25%. The error is more in the present method because this method follows one dimensional FE analysis. But the referred literature Zou et al.(2005) has employed finite element program ANSYS software using 8 node isotropic 3D solid elements for analysis. This is more accurate than present method. Hence more error (25%) for cantilever pipe conveying gas in the present method. And it is also observed that (i) the natural frequency decreases with increase in fluid velocity and pressure. (ii) natural frequency increases with increase in initial tension.

Table 3.5 Analytical and numerical natural frequencies of simply-supported composite pipe conveying natural gas.

Mode	Structural frequency (Hz) Pipe without fluid			
	Analytical	Zou et al. (2005)	Present (FEM)	% Error w.r.t. Zou et al. (2005)
1	0.7382	0.72173	0.7390	0.11
2	2.9526	2.9083	2.9561	0.12
3	6.6435	6.5048	6.6512	0.11
4	11.8106	11.565	11.8243	0.12

Table 3.6 Analytical and numerical natural frequencies of clamped-free composite pipe conveying natural gas.

Mode	Structural frequency (Hz) pipe without fluid				Structural frequency (Hz) pipe with fluid pressure of 3 MPa			
	Analytical	Zou et al. (2005)	Present (FEM)	% Error	Analytical	Zou et al. (2005)	Present (FEM)	% Error
1	0.2630	0.2587	0.2633	0.11	0.0000	0.0000	0.0598	-
2	1.6480	1.6125	1.6499	0.11	1.1003	1.1194	1.4963	25.1
3	4.6144	4.5395	4.6198	0.12	4.0907	5.3254	4.9542	6.90
4	9.0424	8.8523	9.0529	0.12	8.4016	9.3538	9.7684	4.20

Table 3.7 Analytical and numerical natural frequencies of clamped-simply supported composite pipe conveying natural gas.

Mode	Structural frequency (Hz) Pipe without fluid			
	Analytical	Zou et al. (2005)	Present (FEM)	% Error w.r.t. Zou et al. (2005)
1	1.1532	1.1255	1.1545	0.12
2	3.7369	3.6861	3.7413	0.12
3	7.7968	7.6147	7.8059	0.12
4	13.333	13.094	13.3485	1.11

Influences on fluid velocity, internal pressure and initial tension

In order to observe the fundamental theoretical influence of one parameter at a time (i.e., the influence of the fluid velocity, internal pressure and initial tension) on fundamental frequency, when considering one parameter, the others are assumed to be zero. Therefore, three cases were considered to investigate the influence of (a) fluid velocity, (b) internal pressure, and (c) initial tension. The frequency of vibration results reported by Zou et al. (2005) for the simply supported, cantilever and clamped-simply supported pipelines are compared with the present finite element results and are provided in the Figures 3.3 to 3.11.

Influence of the fluid velocity (while keeping $p = 0$ and $T_o = 0$)

The first three vibration frequencies as a function of fluid velocities for a simply-supported, clamped-free and clamped-simply supported pipe were determined and are shown in Figures (3.3), (3.4) and (3.5). It can be see from the figures that increasing the fluid velocity decreases the vibration frequency of the pipeline for all the considered boundary conditions considered in the study. The velocity reaches to a critical value at which the first frequency becomes zero, thus indicating that the pipe will buckle (Zou et al., 2005). The lowest critical velocity is observed for the clamped-free pipe and the highest critical velocity for the clamped-simply supported pipe. i.e. increasing the flow speed tends to lower the natural frequencies. When the flow speed reaches the critical value, the first natural frequency vanishes in the beginning and the divergence starts to occur.

Influence of the internal pressure (while keeping $U = 0$ and $T_o = 0$)

The relationship between the internal pressure and vibration frequency for the simply supported, clamped-free and clamped-simply supported pipes are shown in Figures (3.6), (3.7) and (3.8). These figures show that increase of internal pressure decreases the natural frequency of the pipe as similar to velocity.

Influence of the pre-tensioning (while keeping $U = 0$ and $p = 0$)

The dependency of the vibration frequency to pre-tensioning (also called the initial pipe tensioning) force (T_o) of the pipe was evaluated and compared with the finite element results for all above mentioned boundary conditions, and the results are shown in Figures (3.9), (3.10) and (3.11). The figures show that increase of pre-tension increases the vibration frequency of the pipeline due to increase in stiffness of the pipe.

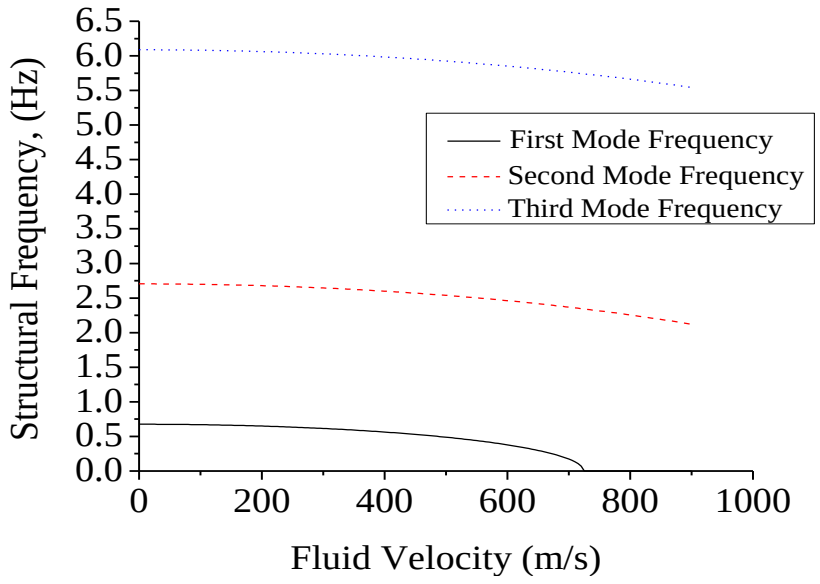

Fig.3.3 Variation of the first three fundamental frequencies as a function of fluid velocities for the simply-supported pipe.

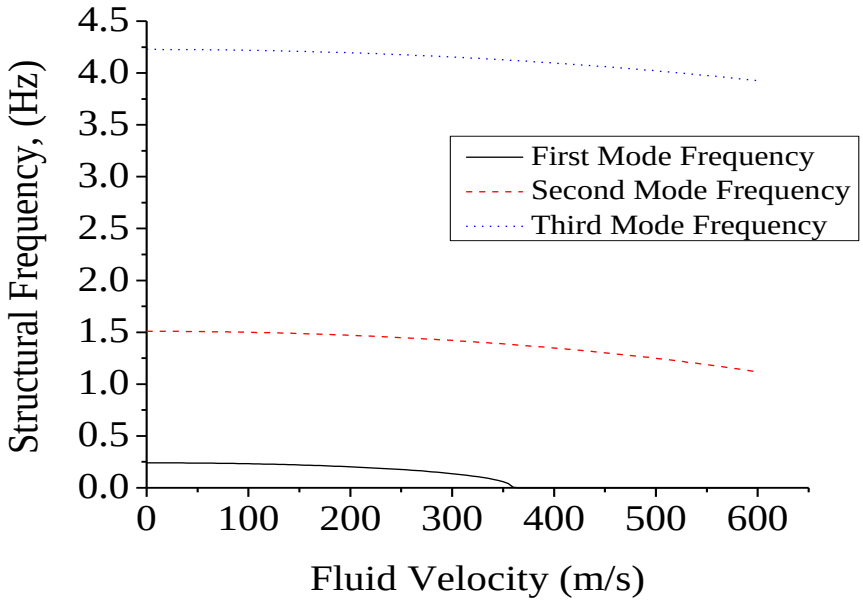

Fig.3.4 Variation of the first three fundamental frequencies as a function of fluid velocities for the clamped-free pipe.

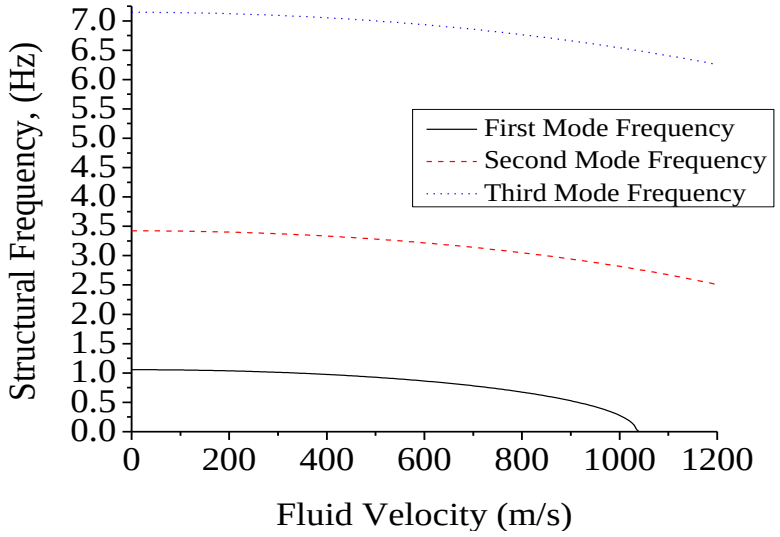

Fig.3.5 Variation of the first three fundamental frequencies as a function of fluid velocities for the clamped-hinged pipe.

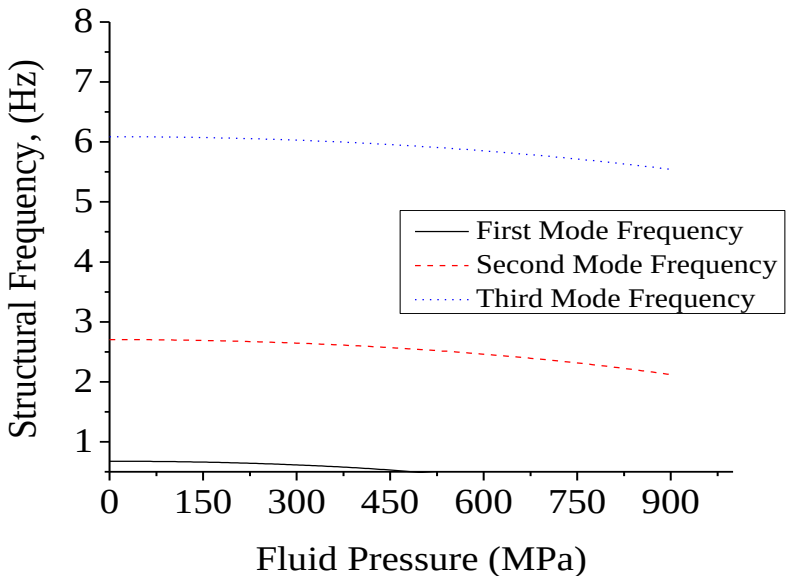

Fig.3.6 Influence of the internal pressure on the fundamental frequencies of the simply-supported pipe.

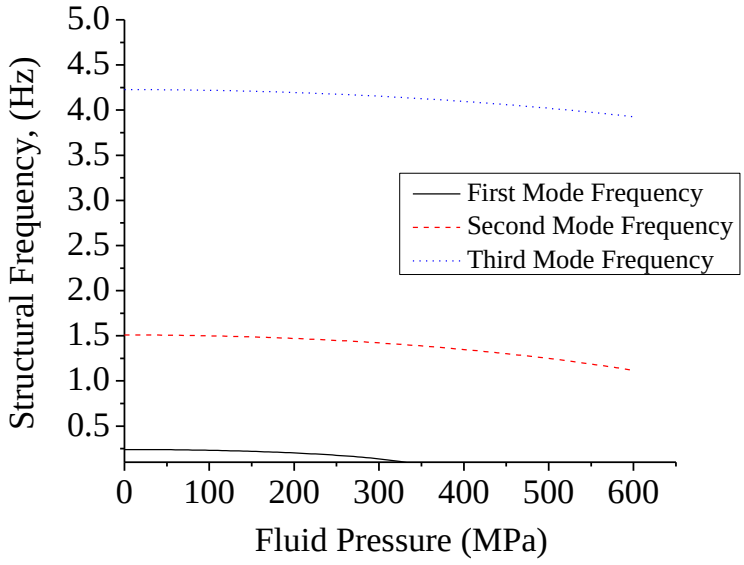

Fig.3.7 Influence of the internal pressure on the fundamental frequencies of the clamped-free pipe.

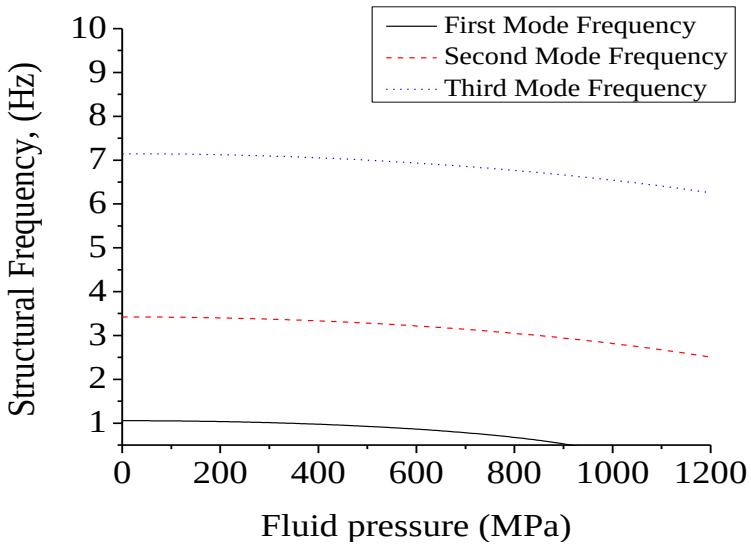

Fig.3.8 Influence of the internal pressure on the fundamental frequencies of the clamped-hinged pipe.

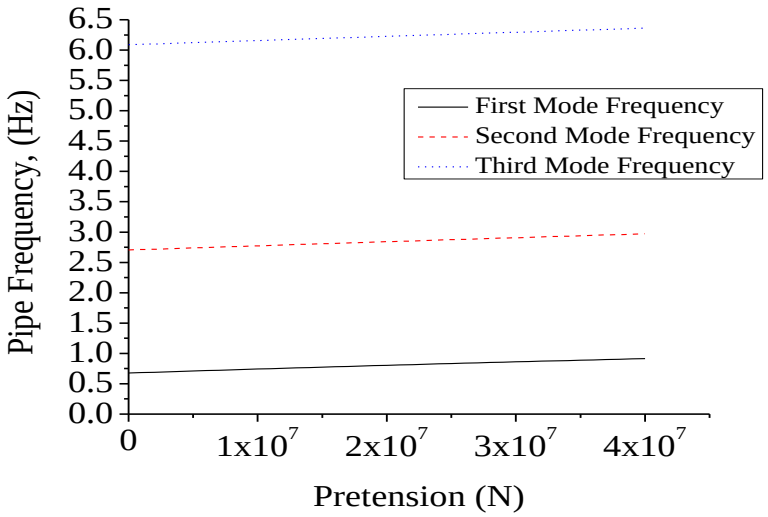

Fig.3.9 Influence of pre-tensioning force on the fundamental frequencies of the simply-supported pipe.

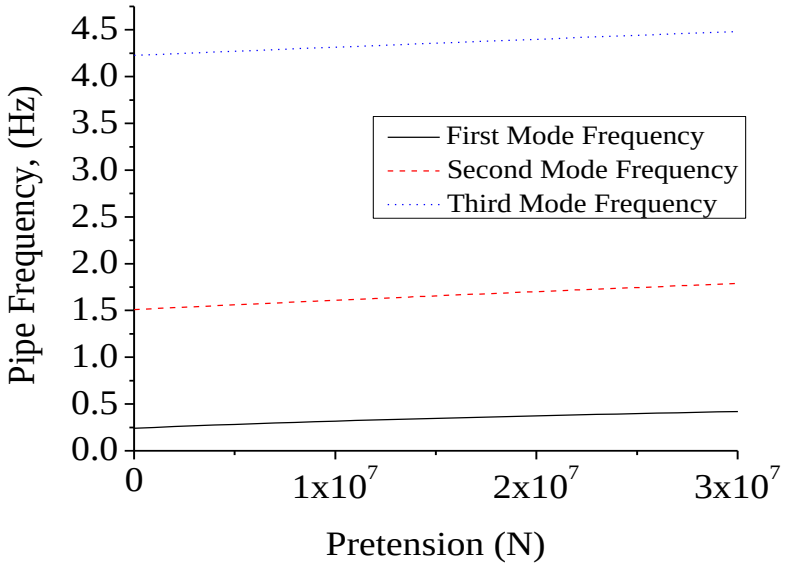

Fig.3.10 Influence of pre-tensioning force on the fundamental frequencies of the clamped-free pipe.

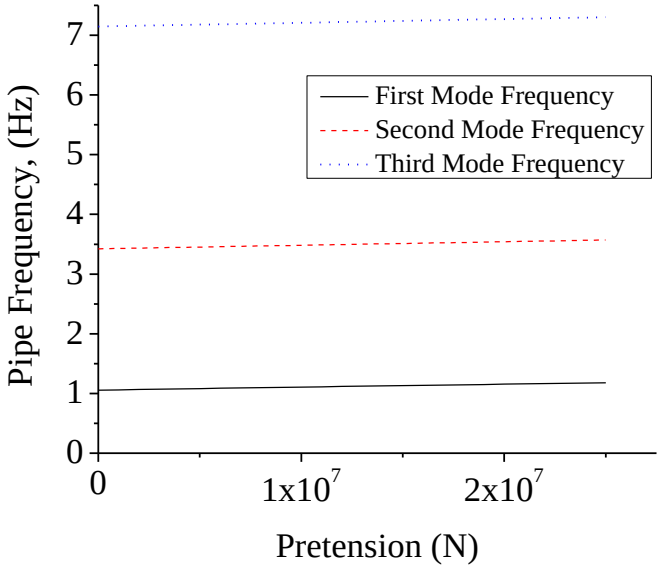

Fig.3.11 Influence of pre-tensioning force on the fundamental frequencies of the clamped-simply supported pipe.

3.6 SUMMARY

In this chapter the Finite element formulation of fluid conveying pipe is verified with the results available in the literature. The natural frequencies for isotropic steel pipe are compared with the analytical results detailed in Blevin (2001) and numerical results detailed in Lee and Oh (2003). The natural frequencies for isotropic aluminium pipe are also compared with the analytical results detailed in Blevins (2001) and numerical results detailed in Sinha et al. (2001). It is observed that there is close comparison between these values. Similarly natural frequencies are compared with numerical results obtained by Zou et al. (2005) for cement coated steel pipe for the simply supported, cantilever and clamped-simply supported pipeline. There is a good comparison of result for simply supported and clamped simply supported with the percentage error of 0.12% and for the clamped free pipe the percentage of error is about 25%. Also it is also observed that (i) the natural frequency decreases with increase in fluid velocity and pressure (ii) natural frequency increases with increase in initial tension.

The next chapter discusses about the numerical computation of natural frequency using the finite element method and comparison of the experimental results obtained from education model fabricated in the laboratory.

CHAPTER 4

COMPARISION OF THE EXPERIMENTAL AND THEORETICAL RESULTS ON DYNAMIC BEHAVIOUR OF THIN SLENDER TUBE CONVEYING COMPRESSED AIR

4.1 INTRODUCTION

The parameters used for the numerical computation are diameter of the tube, D = 3.0 mm, mass flow rate of the air, m_f = 0.0578 kg/s, Young's modulus, E = 261x10^9 Pascal, Mass moment of inertia, I = 2.825 mm^4, External tension $\overline{T}$ =7.361 x10^{-6} N/m, pressure of the air, $\overline{p}$ = 4, 5, or 6 bar, Area of the tube, A = 3.13x 10^{-6} m^2, Poisons ratio, ν = 0.3 and tube mass per unit length, m = 0.03 kg/m. Eigenvalues are computed based on these parameters in the educational experimental model and results are compared in this chapter. Computation details are explained in Appendix B and C. An experimental setup was fabricated to test time response and frequency response of a thin slender cantilever tube carrying compressed air at vertical orientation. Laser sensor and LabVIEW software were used to analyze experimental results and analysis details are discussed in chapter 2.

Θ -matrix constant terms in equation (3.19) were computed as below,

$$C_1 = \left[\frac{EI}{l^3}\right] + \left[\frac{m_f U^2}{30l}\right] + \left[\frac{\overline{T}}{30l}\right] + \left[\frac{\overline{p}}{30l} A(1-2\nu)\right],\ C_2 = \left[\frac{(m_f + m)l}{420}\right] \tag{4.1}$$

and results are shown in Table 4.1. Computation details are given in Appendix B.

ψ -matrix constant terms in equation (3.20) were computed as below,

$$C_1 = \left[\frac{EI}{l^3}\right] + \left[\frac{m_f U^2}{30l}\right] + \left[\frac{\overline{T}}{30l}\right] + \left[\frac{\overline{p}}{30l} A(1-2\nu)\right], \qquad C_3 = \left[\frac{m_f U}{420}\right] \tag{4.2}$$

and results are shown in Table 4.2. Computation details are given in Appendix C.

Table 4.1 Computed constant values of Θ matrix for the different tube length, velocity and pressure of the flow.

	l = 500 mm		l = 600 mm		l = 700 mm		l = 800 mm	
	C_1	C_2	C_1	C_2	C_1	C_2	C_1	C_2
U =28.88 m/s $\bar{p}$ = 4 bar	41.6	0.003	24.9	0.004	16.5	0.005	11.7	0.006
U =40.8 m/s $\bar{p}$ = 5 bar	43.3	0.003	26.9	0.004	18.5	0.005	13.7	0.006
U =57.6 m/s $\bar{p}$ = 6 bar	47.7	0.003	30.98	0.004	22.58	0.005	17.7	0.006

Table 4.2 Computed constant values of ψ matrix for the different tube length, velocity and pressure of the flow.

	l = 500 mm	l = 600 mm	l =700 mm	l =800 mm
	C_3	C_3	C_3	C_3
U =28.88 m/s $\bar{p}$ = 4 bar	0.0558	0.0558	0.0558	0.0558
U = 40.8 m/s $\bar{p}$ = 5 bar	0.0788	0.0788	0.0788	0.0788
U = 57.6 m/s $\bar{p}$ = 6 bar	0.1114	0.1114	0.1114	0.1114

The parameters such as Young's modulus, mass flow rate, pressure and initial velocity were measured physically and used to compute such as, Young's modulus was determined from universal testing machine, pressure was measured from pressure gauge, etc, However, air flow velocity was theoretically calculated and experimentally measured. Theoretical velocities determined from basic Bernoulli's equation for different air pressure are represented in Figure 4.1. The velocity

$U = \sqrt{2\frac{p}{\rho}}$, where p is supply pressure and ρ is density of air. These values are used to compute structural load due to air flow. Air flow rate was measured experimentally by collecting air inside a spherical balloon for known time interval. Experimentally measured air flow rates deviated by about 4.8% from theoretically computed. Other linear dimensions were measured using micrometer and tool maker microscope.

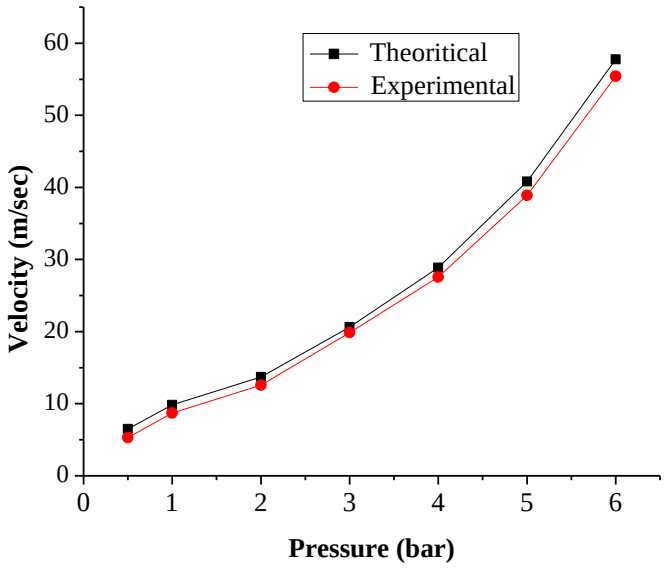

Fig 4.1 Theoretical and experimental velocities at different pressure.

4.2 NUMERICAL COMPUTED RESULTS

All parameters used in finite element method computation were obtained from experimental setup as indicated in Appendix B and C. Using $[\Theta]$ and $[\psi]$ are defined in equation (3.19) and (3.20) respectively in equation (3.18), $[\Theta]\{\dot{\zeta}\} - [\psi]\{\zeta\} = 0$, gives $\dot{\zeta} = [\Theta]^{-1}[\psi]\{\zeta\} = [A]\{\zeta\}$ and it becomes eigenvalue problem for the matrix $[A]$. The eigenvalues were then computed for different tube lengths and velocities as presented in appendix C (using MATLAB code). Table 4.3 gives the fundamental

natural frequency obtained form eigenvalues. Actual experimental results deviated up to a maximum of 13% from FEM model investigations.

Table 4.3 Natural frequency with the variation in velocity, pressure of the flow and length of tube.

Pressure (bar)	Velocity (m/s)	Length (mm)	Natural Frequency (Hz)		% Error
			FEM	Experimental	
4	28.8	500	4.24	3.7	12.7
		600	3.42	3.0	12.3
		700	2.53	2.35	7.0
		800	2.1	2.0	4.7
5	40.8	500	4.47	3.9	12.7
		600	3.53	3.1	12.2
		700	2.7	2.45	9.3
		800	2.32	2.1	6.6
6	57.6	500	4.5	4.0	11.1
		600	3.63	3.2	11.8
		700	2.8	2.5	10.7
		800	2.43	2.2	9.5

4.3 RESPONSE GRAPHS

Vibration responses for pulse input and step input were obtained from eigenvalues in state space equation (3.19), $\dot{x} = [A]x$, where x is the state vector and $[A]$ is the state matrix. System's transient response for impulse input and step input were obtained respectively, using MATLAB commands. It was observed that for 500 mm length and at different air flow rates unstable resonance occurred. Response curves of slender tube for various operating conditions are shown in figures 4.2 to 4.12. Figure 4.2 indicated that at 800 mm length and 4 bar pressure, very good damped response was obtained, clearly illustrating steady state response reached very

fast to both pulse input as well as step input. At higher pressure (5 bar or 6 bar), response were stable and with in 15 seconds steady state value was achieved as shown in Figure 4.3 and 4.4.

Figure 4.5 indicated instability at 700 mm with pressure of 4 bar perhaps due to violent vibration with higher amplitude, as the pressure increased to 5 bar or 6 bar, the response got stable as shown in figure 4.6 and 4.7 i.e, for 5 bar, steady state reaches within 5 seconds whereas 6 bar within 10 seconds. Similar response phenomenon was observed for 600 mm length of tube as indicated in Figure 4.8 to 4.10. The response time to reach the steady state was very less, in this case, approximately 6 seconds. For 500 mm length of tube it was observed that the system goes to unstable for all the pressure or fluid velocity of the flow (Refer Figures 4.11 to 4.13).

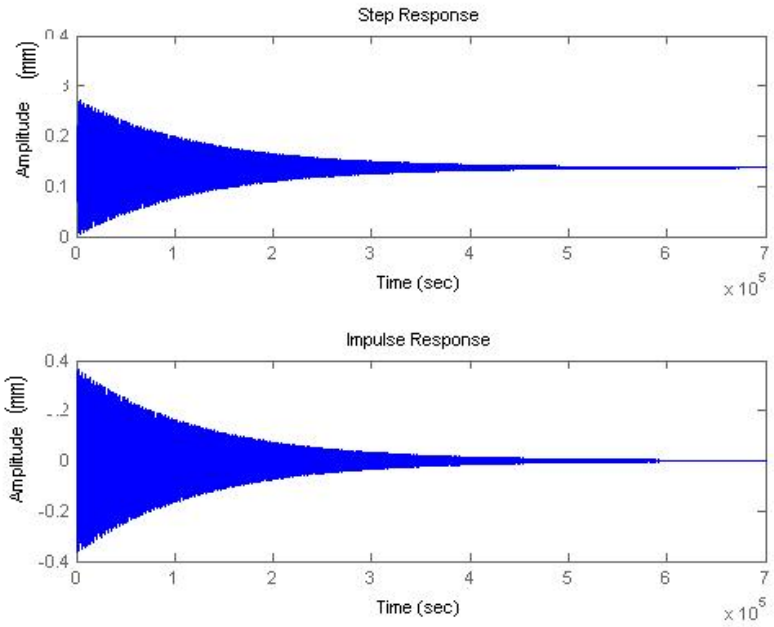

Fig. 4.2 Response of a cantilever tube with velocity 28.88 m/s, pressure 4 bar and length 800 mm.

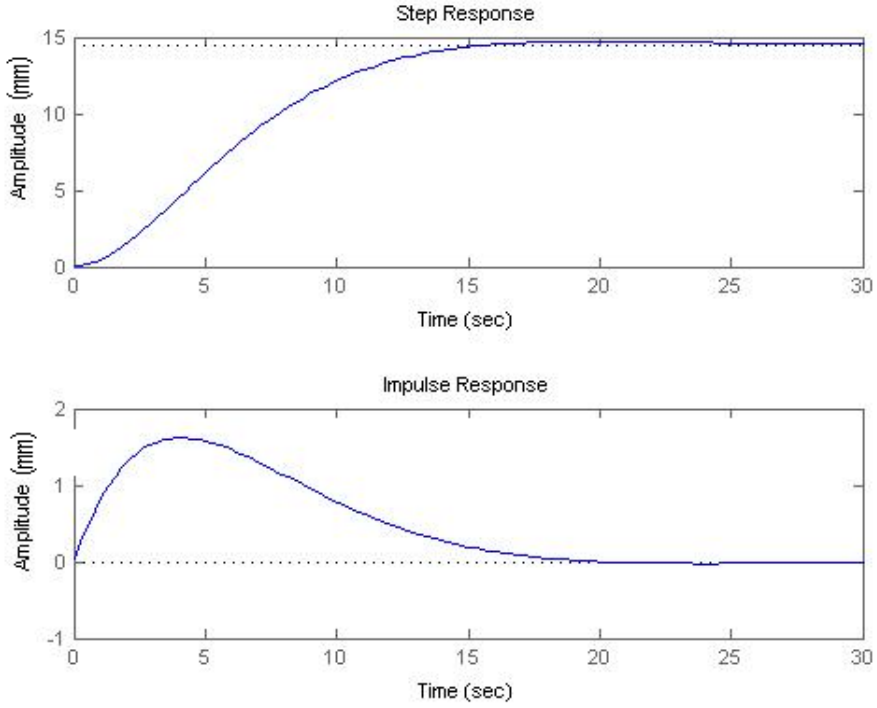

Fig. 4.3 Response of a cantilever tube with velocity 40.8 m/s, pressure 5bar and length 800 mm.

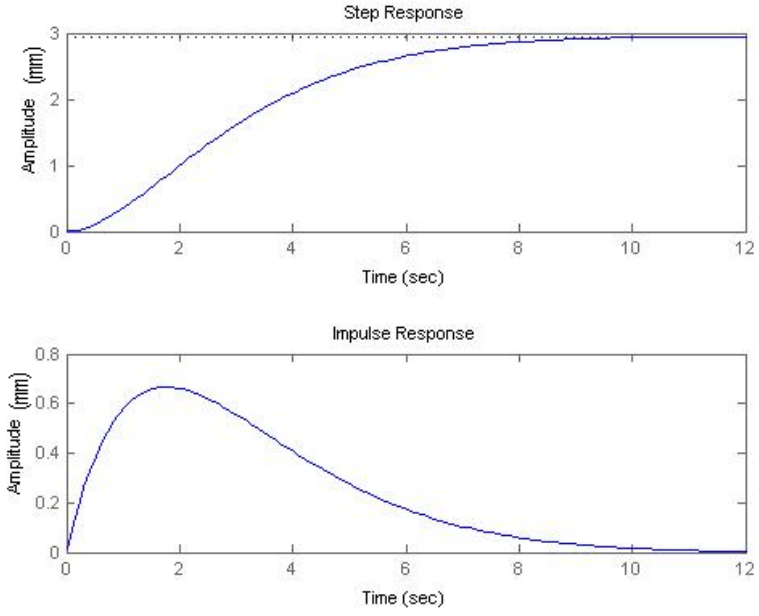

Fig. 4.4 Response of a cantilever tube with velocity 57.6 m/s, pressure 6 bar and length 800 mm.

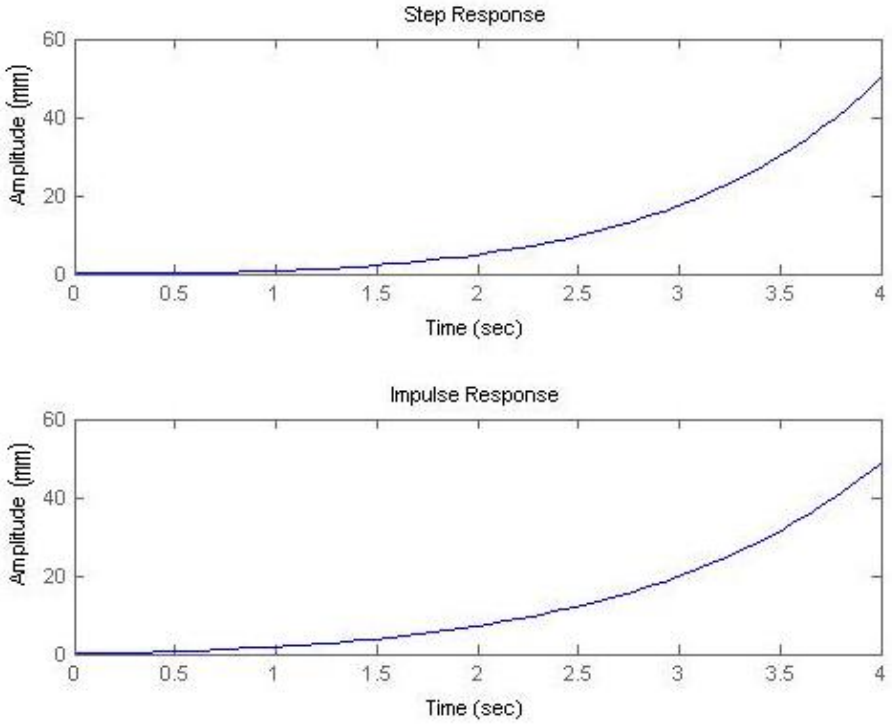

Fig. 4.5 Response of a cantilever tube with velocity28.88 m/s, pressure 4 bar and length 700 mm.

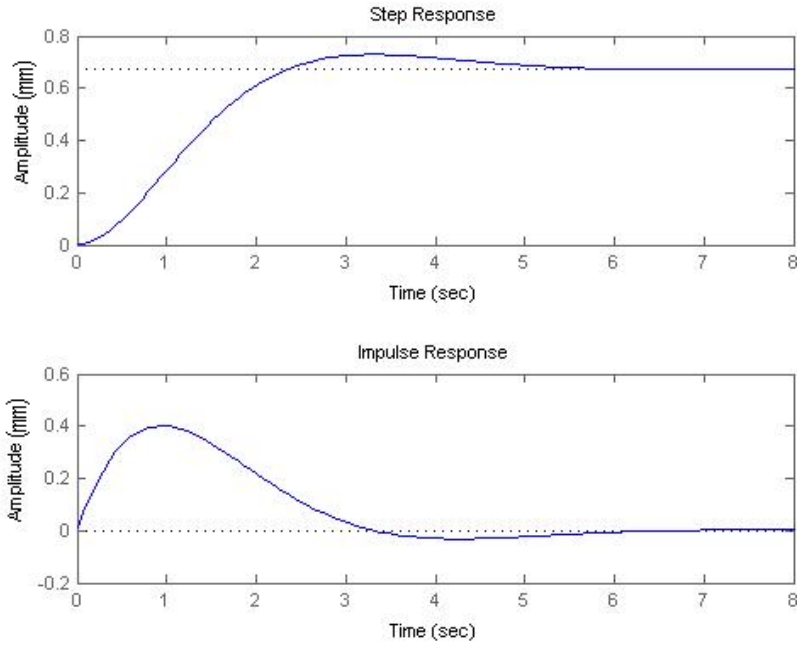

Fig. 4.6 Response of a cantilever tube with velocity 40.8 m/s, pressure 5 bar and length 700 mm.

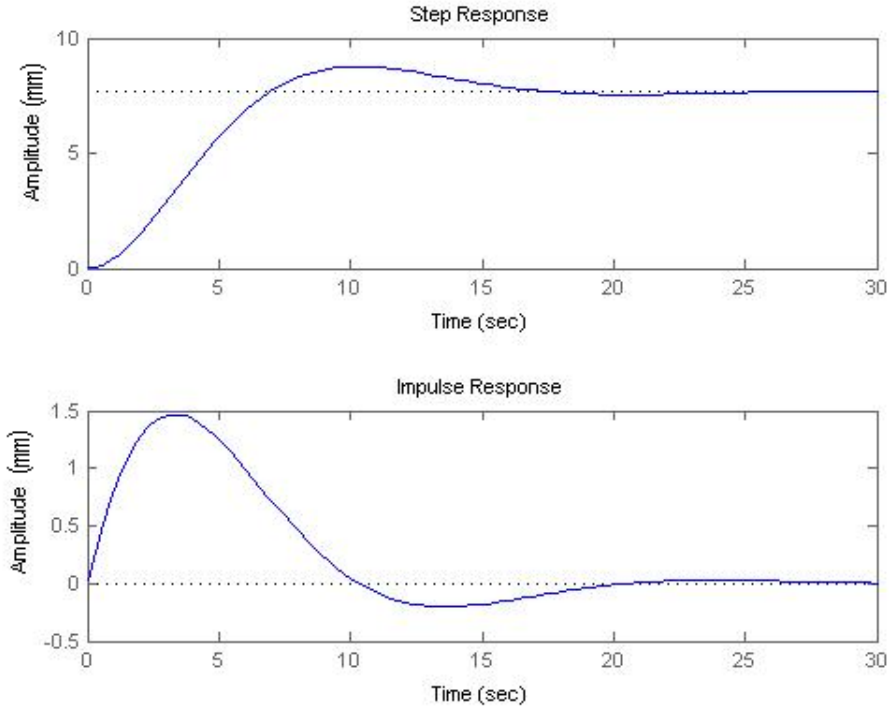

Fig. 4.7 Response of a cantilever tube with velocity 57.6 m/s, pressure 6 bar and length 700 mm.

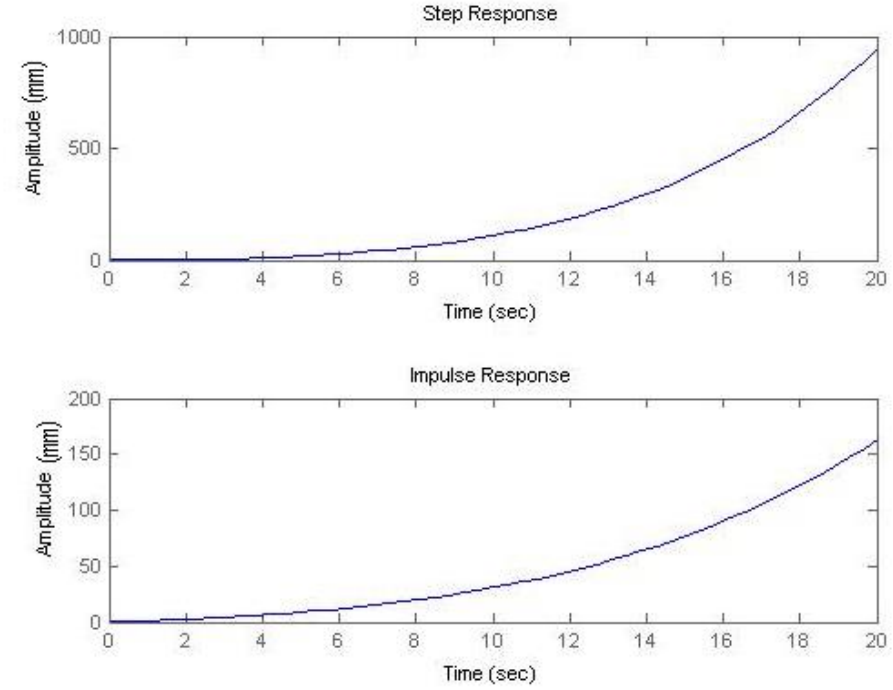

Fig. 4.8 Response of a cantilever tube with velocity 57.6 m/s, pressure 4 bar and length 600 mm.

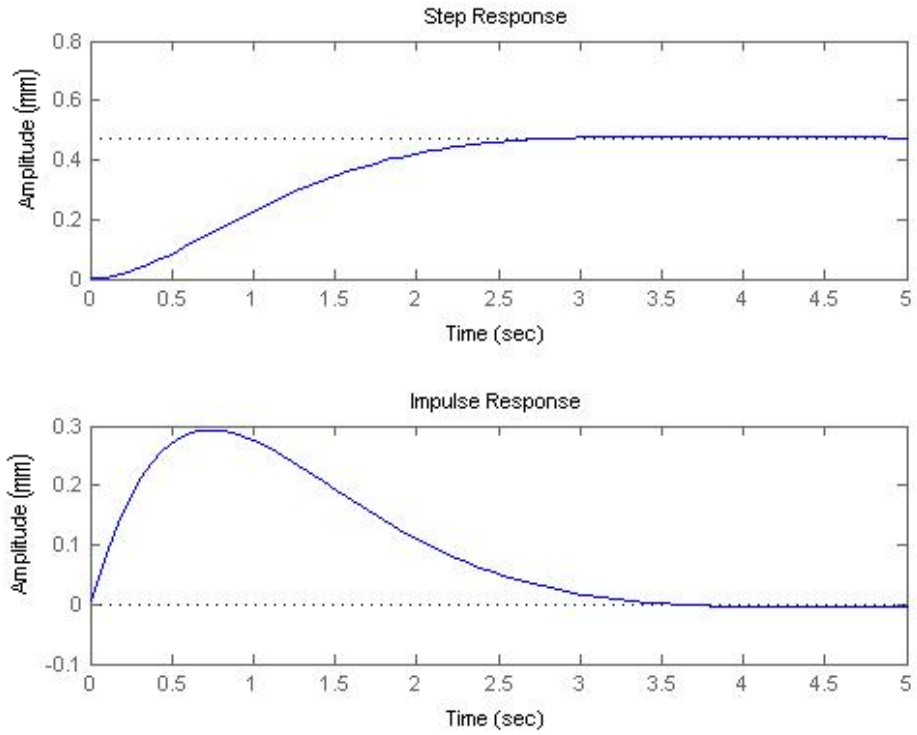

Fig. 4.9 Response of a cantilever tube with velocity 40.8 m/s, pressure 5bar and length 600 mm.

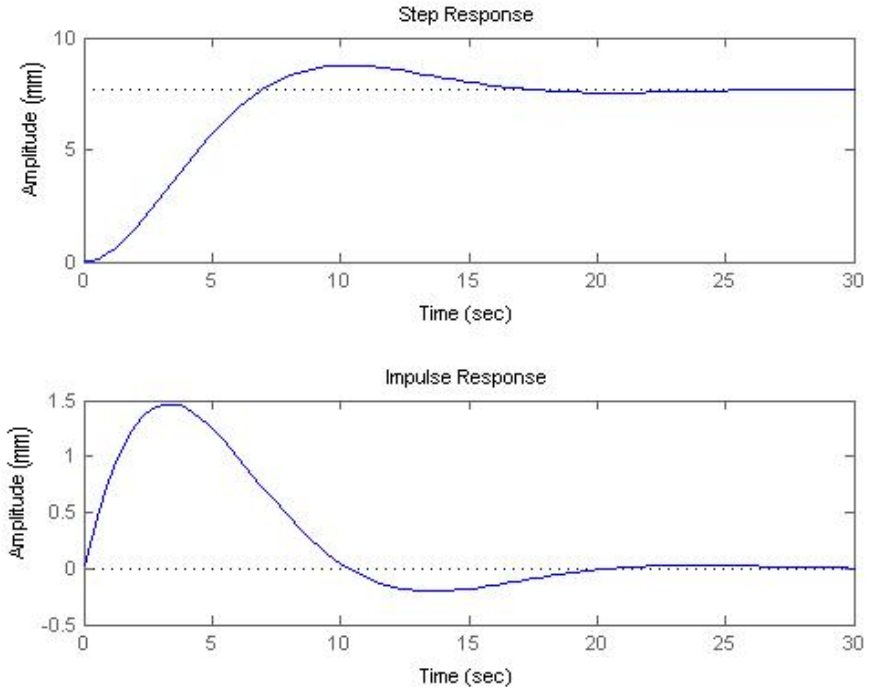

Fig.4.10 Response of a cantilever tube with velocity 40.8 m/s, pressure 6bar and length 600 mm.

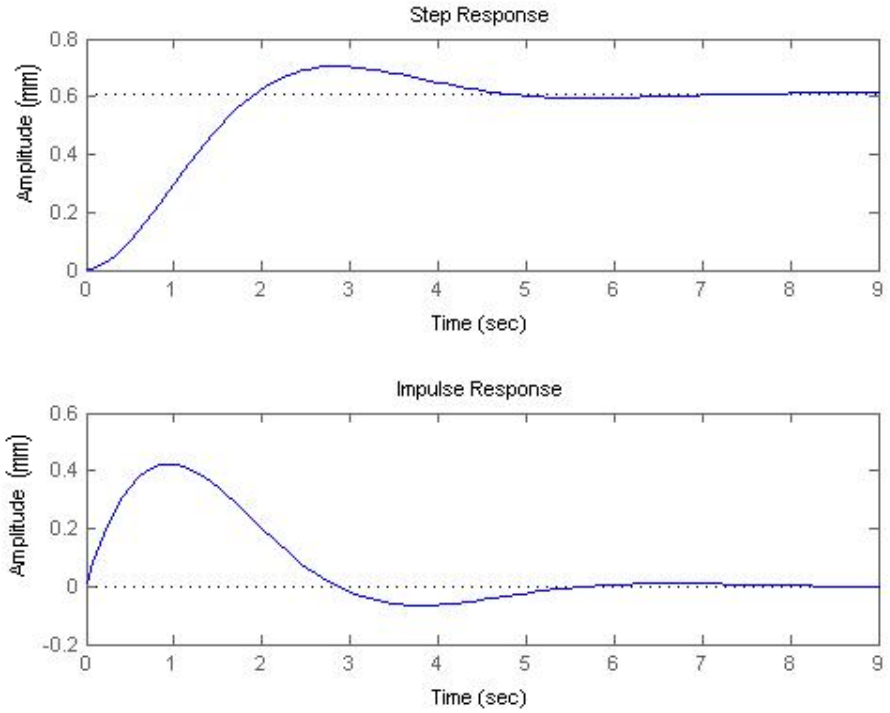

Fig. 4.11 Response of a cantilever tube with velocity 28.88m/s, pressure 4 bar and length 500 mm.

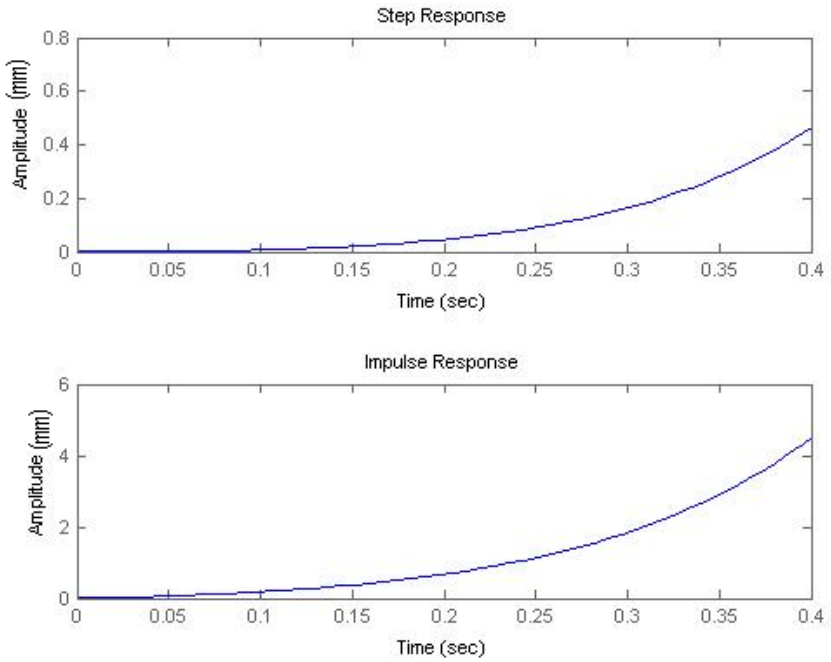

Fig. 4.12 Response of a cantilever tube with velocity 40.8 m/s, pressure 5 bar and length 500 mm.

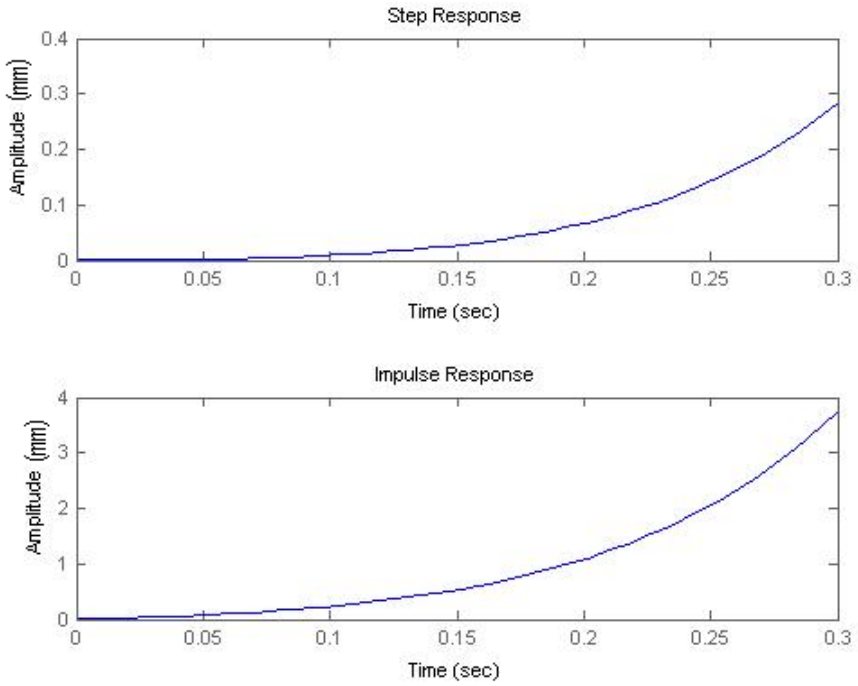

Fig. 4.13 Response of a cantilever tube with velocity 57.6 m/s, pressure 6 bar and length 500 mm.

4.4 COMPARISION OF RESPONSE CURVE GRAPHS

Figure 4.14 and 4.15 compares theoretical and experimental responses of the slender tube conveying air for various operating conditions like air pressure and length of pipe. For 500 mm length of tube with 5 bar air pressure average displacement is about 3mm (theoretical) and about 3.4 mm (experimental) as shown in Figure 4.14. Similarly for 600 mm length of tube with 6 bar air pressure average displacement is about 8.5 mm (theoretical) and about 8.4 mm (experimental) as shown in Figure 4.15. Inferentially as tube length and/or pressure increases displacement also increases.

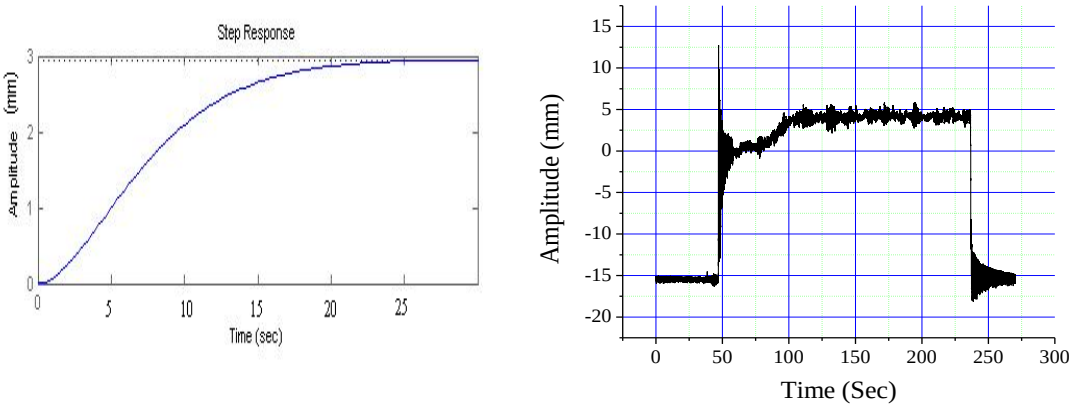

(a)Theoretical (b) Experimental

Fig. 4.16 Response of tube for 500 mm length of tube and 5 bar pressure.

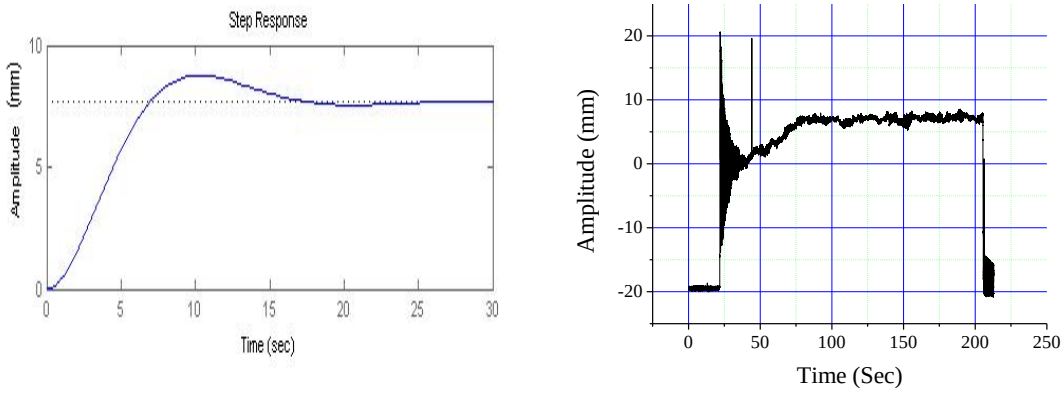

(a)Theoretical (b) Experimental

Fig. 4.15 Response of tube for 600 mm length of tube and 6 bar pressure.

4.5 CONCLUSION

Theoretical analyses were conducted to investigate the effect of various influencing parameters such as fluid velocity, pressure and tube length on natural frequency and response of tube conveying compressed air. The results obtained from experiment agree favorably with those obtained through finite element analysis. The length of tube is an important parameter in the amplitude of vibration for cantilever tube. Whatever may be the length, there may be a critical velocity of flow beyond which amplitude of vibration increases.

CHAPTER 5

TRANSIENT HEAT TRANSFER IN VERTICAL TUBE - A THEORETICAL AND EXPERIMENTAL STUDY

5.1 INTRODUCTION

In most heat transfer analysis, it is essential to predict the time taken by the structural component, which is at high temperature to cool down to ambient temperature or the time required to attain a steady state temperature if it is being supplied with continuous heat. Vital parameter that is required as input, to such numerical computation is convective heat transfer coefficient. Determining the proper convective heat transfer coefficient is the fundamental in many thermal analyses like evaluation of thermal stresses, thermally induced vibrations, etc. To estimate the natural convective heat transfer coefficient for a body kept in still air is very complex. There are numerous analytical models developed over the years to describe the transient behavior of commonly encountered geometries. Mathematical model must exhibit a high degree of flexibility in approximating temperature dependence of material encountered in high temperature environments. Numerical method such as finite-element method for solving temperature distribution is of great importance. Blandino and Thornton (2000) in their published article have given the experimental results and theoretical model for calculating the convective heat transfer coefficient for a vertical vibrating tube. This chapter describes a detailed study on the determination of the convective heat transfer coefficient for an internally heated stationary vertical tube kept in still air under laboratory conditions. Here an effort is made to develop a finite element model capable of describing the thermal transients for a vertical cylindrical tube kept in still air under laboratory conditions. The chapter describes a finite-element method in conjunction with experimental validation to solve the system of time-dependent equations that govern the transient temperature distribution and hence may be used to predict the steady state temperature distribution for the structure. The purpose of this study is to determine the magnitude of the

natural heat transfer coefficients for a uniformly heated vertical tube subjected to still air natural convection. The coefficients are determined experimentally as a function of time and position along the length of the structure. The experiments are carried out using two different setups. The section 5.4 explains experiments conducted on a tube of 38 mm diameter and 510 mm long with internal surface heating, and section 5.6 explains experiments carried out on a tube of 3 mm diameter and 500 mm long with internal heating.

5.2 THEORETICAL MODEL

5.2.1 ASSUMPTIONS

The cylindrical tube is heated uniformly by means of resistance heating. Following assumptions are made to derive the partial differential equation for the temperature along the length of the tube. (i) the temperature varies along the length of the tube due to variation in convective heat transfer. (ii) temperature gradient through the tube wall is neglected. (iii) radiation heat transfer inside the tube and external radiation are neglected. (iv) convection inside the tube is neglected. (v) the thermal conductivity, density and specific heat do not vary with temperature. (vi) at any cross section of the tube the natural convection on the surface of the tube is assumed to be axisymmetric i.e. temperature is assumed to be constant in circumferential direction.

5.2.2 EQUATION OF THERMAL CONDUCTION OF HEAT IN AN ISOTROPIC SOLID WITH CONVECTION

Figure 5.1 shows a vertical tube fixed at the top which is heated internally. Heat is conducted along the length of the tube and heat is lost by convection from the surface to the surrounding. Heat is also lost by convection from the end face. The associated governing equation for this problem is (Refer equation (1.32)):

$$kA\left(\frac{\partial^2 T}{\partial x^2}\right)+\dot{q}A=\rho c_p A\frac{\partial T}{\partial t}+\frac{h_c P}{A}(T-T_\infty), \tag{5.1}$$

where, h_c is the convective heat transfer coefficient, P is the perimeter of boundary surface, A is the cross sectional area and T_∞ is the ambient temperature of

surrounding. The initial condition specifies the temperature distribution at time zero, this is

$$T(x,0) = T_\infty, \tag{5.2}$$

and the boundary condition is the heat loss by convection at the end face,

$$-kA\frac{\partial T}{\partial x} = h_c A(T - T_\infty). \tag{5.3}$$

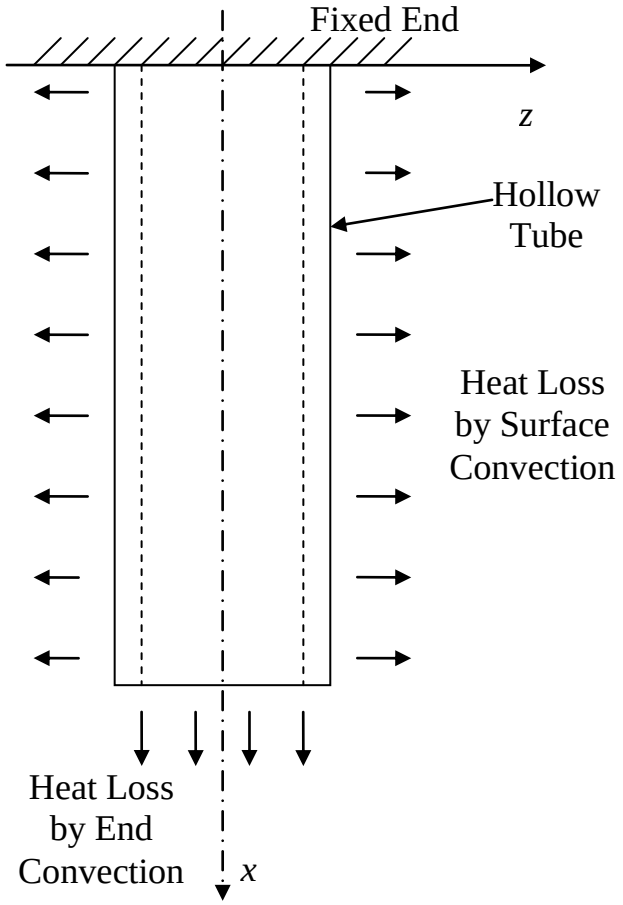

Fig.5.1 A vertical hollow tube showing various boundary conditions.

5.2.3 FINITE-ELEMENT FORMULATION

The theoretical model based on finite element method considers the cylindrical tube as one-dimensional problem as shown in Figure 5.2. Thus, the radial temperature distribution is not accounted for and circumferential temperature distribution is also

constant. Following are the procedure detailed in Lewis et al., 2004 based on the Galerkin's approach, equation (5.1) is multiplied by the test function N_L^T, integrating over the entire domain Ω and equating to zero, as follows

$$-\int_{\Omega} N_L^T \left[kA\frac{\partial^2 T}{\partial x^2} - \rho c_p A\frac{\partial T}{\partial t} - h_c P(T - T_\infty) + \dot{q}A \right] dx = 0. \tag{5.4}$$

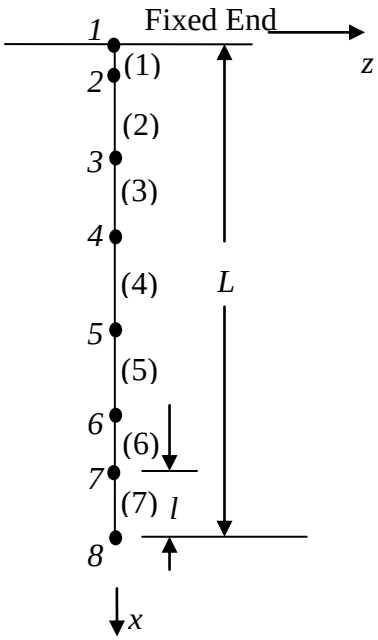

Fig. 5.2 Finite element idealization of beam for thermal analysis.

The weak form of the heat transfer governing equation for the tube with heat conduction and heat loss by convection along the tube is as follows:

$$\begin{aligned} -N_L^T kA\frac{\partial T}{\partial x}\bigg|_0^l + \int kA\frac{\partial T}{\partial x}\frac{\partial N_L^T}{\partial x}dx + \int N_L^T h_c PT dx \\ + \int N_L^T \rho c_p A\frac{dT}{dt}dx - \int N_L^T h_c PT_\infty dx - \int N_L^T \dot{q}A dx = 0. \end{aligned} \tag{5.5}$$

Linear shape functions

$$N_i = 1 - \frac{x}{l}, \quad \text{and} \quad N_j = \frac{x}{l}; \tag{5.6}$$

are used to develop the finite element matrices where l is the length of the element.

$$\left\{\frac{k_x A}{l}\begin{bmatrix}1 & -1\\ -1 & 1\end{bmatrix}+\frac{h_c Pl}{6}\begin{bmatrix}2 & 1\\ 1 & 2\end{bmatrix}+\begin{bmatrix}0 & 0\\ 0 & h_c A\end{bmatrix}\right\}\begin{Bmatrix}T_1\\ T_2\end{Bmatrix}+\frac{\rho c_p Al}{6}\begin{bmatrix}2 & 1\\ 1 & 2\end{bmatrix}\begin{Bmatrix}\dot{T}_1\\ \dot{T}_2\end{Bmatrix} \quad (5.7)$$

$$=\frac{\dot{q}Al}{2}\begin{Bmatrix}1\\ 1\end{Bmatrix}+\frac{h_c PlT_\infty}{2}\begin{Bmatrix}1\\ 1\end{Bmatrix}+h_c AT_\infty\begin{Bmatrix}0\\ 1\end{Bmatrix},$$

$$\left[\mathbf{K}_{\text{comb}}+\mathbf{K}_{\text{cap}}+\mathbf{K}_{\text{conv\_last}}\right]\{T\}+\left[\mathbf{K}_{\text{cap}}\right]\{\dot{T}\}=\{\mathbf{F}\}, \quad (5.8)$$

$$\mathbf{K}^e_{\text{comb}}T+\mathbf{K}^e_{\text{cap}}\dot{T}=\bar{\mathbf{F}}^e_Q. \quad (5.9)$$

In equation (5.7), the third term on LHS and third term on RHS are considered for the node of the elements involving boundary flux terms. $\mathbf{K}^{\text{e}}_{\text{comb}}$ = combination of elemental conduction and convection matrices, $\mathbf{K}^e_{\text{cap}}$ = elemental capacitance matrix, $\bar{\mathbf{F}}^e_Q$ = force vector. The finite element solution of time dependent field problems produces a system of linear first order differential equations in time domain. Equation (5.9) must be solved for the variation of temperature in space and time domain. The values of temperature can be calculated using the mean value theorem to give

$$\left[\mathbf{K}_{\text{cap}}+\varphi\,\Delta t\,\mathbf{K}^e_{\text{comb}}\right]\{T\}_b=\left[\left[\mathbf{K}_{\text{cap}}+(1-\varphi)\,\Delta t\,\mathbf{K}_{\text{comb}}\right]\{T\}_a+\Delta t(1-\varphi)\mathbf{F}_b+\varphi\,\mathbf{F}_a\right], \quad (5.10)$$

where, a and b are two points in time interval Δt where the temperature is evaluated and φ is equal to ½ for central difference method. The final system of equations has the general form

$$[A]\{T\}_b=[B]\{T\}_a+\{F^*\}. \quad (5.11)$$

5.3 DATA REDUCTION FOR NATURAL CONVECTION

During the experiments, the temperature data was recorded at different locations along the length of the tube. To determine the heat transfer coefficients, the tube was divided into segments and an energy balance was performed on each segment. The experimentally measured temperature at the centre of each segment was assumed to be the average temperature of the segment end temperatures. Figure 5.3 shows a typical segment. Each segment acted like a heater loosing heat to surroundings through convection.

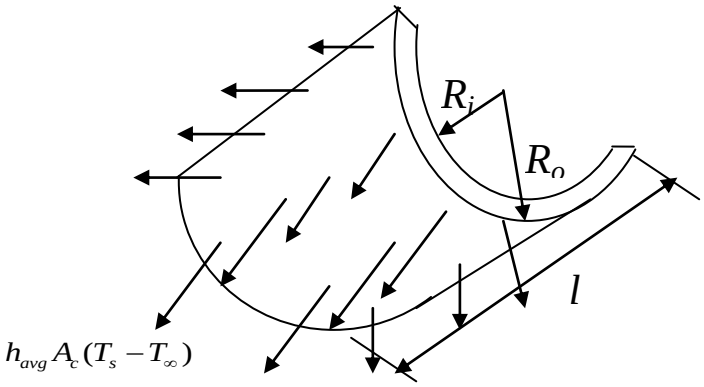

Fig.5.3 A typical segment of tube showing heat transfer from the surface.

In Figure 5.3 h_{avg} is the average convective heat transfer coefficient, l is the segment length, T_s is the surface temperature, T_∞ is the ambient temperature, R_o and R_i are the outer and inner radii of the tube respectively. Using the equation given by Incropera and DeWitt, 2002 the first law expression for the segment in Figure 5.3 is written as

$$\dot{q}_c = \dot{Q} A_c = h_{avg} A_c (T_s - T_\infty), \qquad (5.12)$$

where, $\dot{q}_c$ is the heat transfer by convection, $\dot{Q}$ is the heat supplied by heater per unit area, A_c is the surface area for convection. Equation (5.12) assumes that radiation heat transfer is small compared to the convection heat transfer. Hence, the average natural convection heat transfer coefficient for tube was determined from the prescribed heat input, measured surface temperature, and the ambient temperature.

5.4 EXPERIMENTAL SETUP – TUBES INTERNAL SURFACE SUBJECTED TO SURFACE HEATING

The test specimen used for the experiment was a copper tube 510 mm long with 38 mm external diameter and 4 mm wall thickness. Seven thermocouples were mounted on the tube at various points (Refer Table 5.1) along the length to measure the temperature at these points on the tube. The eighth thermocouple was used to measure the ambient temperature and it was located inside the test box.

Table.5.1: Position of thermocouples on the tube from top.

Thermocouple number	T2	T3	T4	T5	T6	T7
Distance from top, mm	20	110	210	310	410	460

The test specimen was enclosed in a wooden test box 250 mm wide, 250 mm long and 800 mm high with front glass door. The test box performs several functions. The wall of the box prevent cross currents from affecting the convection heat transfer from the surface of the tube and provide clamped support for holding the tube. The sketch of the test rig is shown in Figure 5.4.

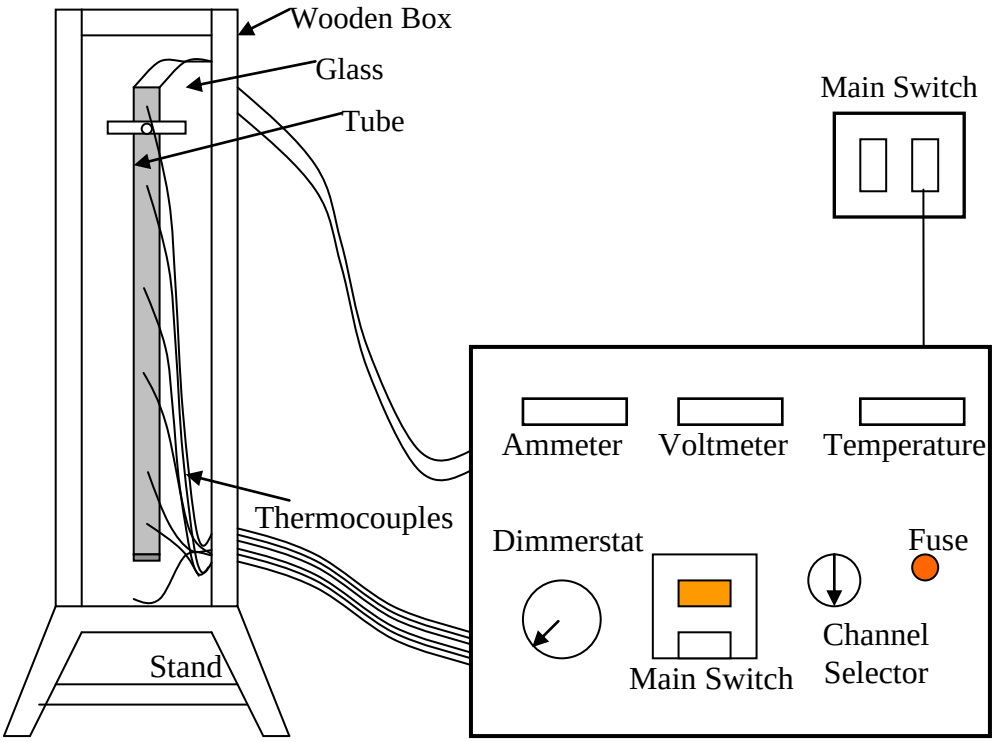

Fig. 5.4 Experimental Setup.

An AC power supply was used to supply the current to the test specimen. Voltage supply was controlled by means of an autotransformer (dimmer). The voltmeter and ammeter were used to measure the amount of power being supplied to the test specimen. A digital thermometer was used to take the temperature readings.

The objective of the experiment was to gather temperature data during natural convection and to find out the time the specimen takes to attain steady state condition. The tube was heated by means of a rod heater of 20 mm outer diameter and 480 mm long kept inside the copper tube. This is equivalent to surface heating. The current and voltage were adjusted to 1 ampere and 100 volts respectively in order to get heating rate of 100 Watts. The following data are used for the analysis: thermal conductivity (at 100°C), k = 370 W/m.K, specific heat (0-100°C) c_p = 388 J/kg.K and density ρ = 8490 Kg/m^3.

5.5 RESULTS AND DISCUSSION

5.5.1 RESULTS

For the heating rate of 100 Watts, the temperature variation on the tube surface with respect to time is shown in the Figure 5.5(a). It can be seen from Figure 5.5(a) that the tube reaches the steady state after 56 min and later the variation of temperature with respect to time is negligible.

The test was carried out for 90 min and the temperature distribution for the corresponding time is used in evaluating the natural convective heat transfer coefficient for air using equation (5.12) which works out to be equal to 18.5 W/m^2 ^{0}C. The ambient temperature at the time of conducting experiment was 26.2 ^{0}C. This value of natural convective heat transfer coefficient is used in the FORTRAN code for the FEM model in order to predict the temperature distribution along the length of the tube with respect to time as shown in Figure 5.5(b). The time taken to reach steady state is almost 45 min. It can be seen from Figure 5.5 that the maximum temperature obtained by experiment is 119^{0}C while that obtained from FEM model is 114.5^{0}C which is quite close to the experimental value.

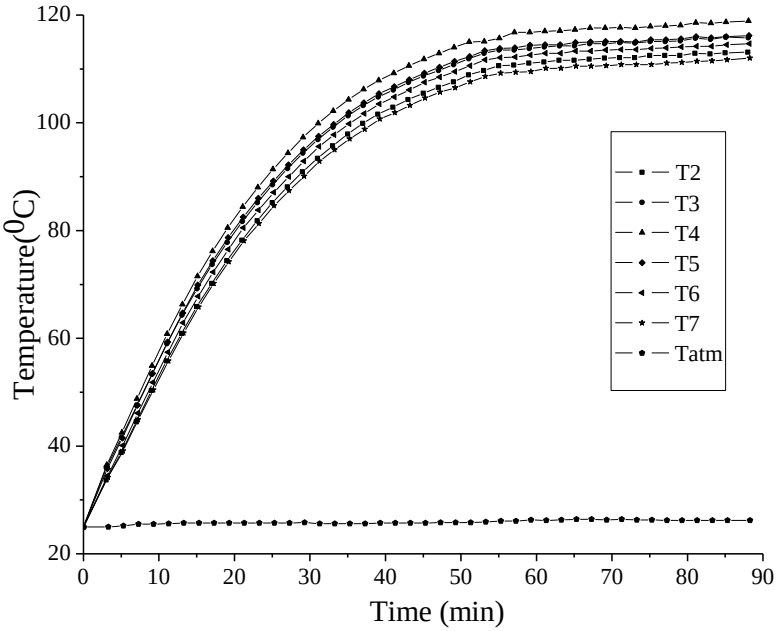

(a) Experimental data (Steady state after 56th min.).

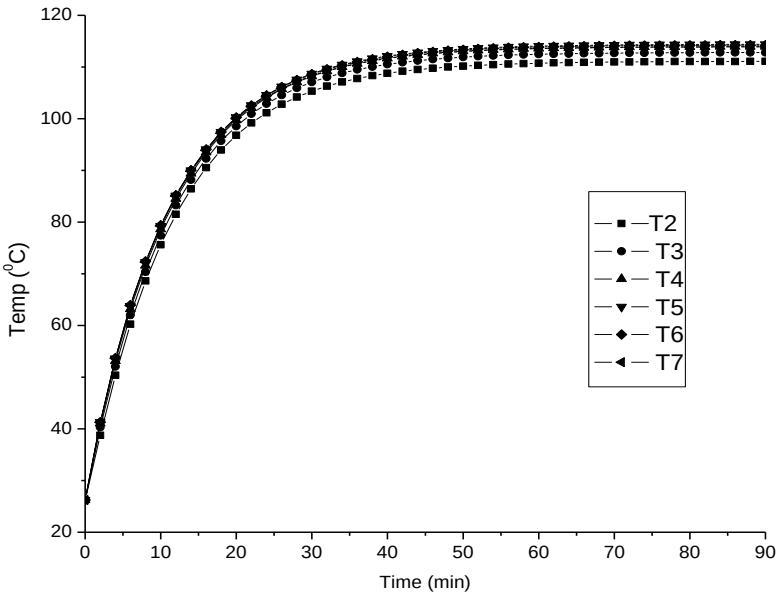

(b) FE data (Steady state after 45th min.).

Fig5.5 Temperature histories at various points along the length of tube.

The temperature distribution along the length of the beam at time equal to 90th minute is shown in Figure 5.6. It is observed from the experimental results that for the heating rate of 100 Watts, the maximum temperature is seen to occur at 210 mm from

the fixed end of tube, and is of order of 119^{O}C, but by FEM analysis the temperature obtained at same point is 114^{O}C and maximum temperature is observed at 310 mm from the fixed end of the tube. The variation in temperature is due to the assumptions made while deriving the theoretical model.

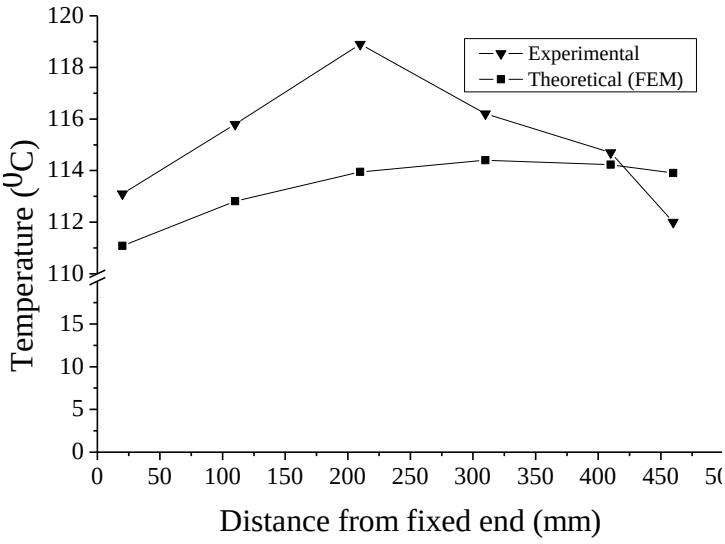

Fig. 5.6 Temperature distribution along *x* -axis of heated tube at 90th minute.

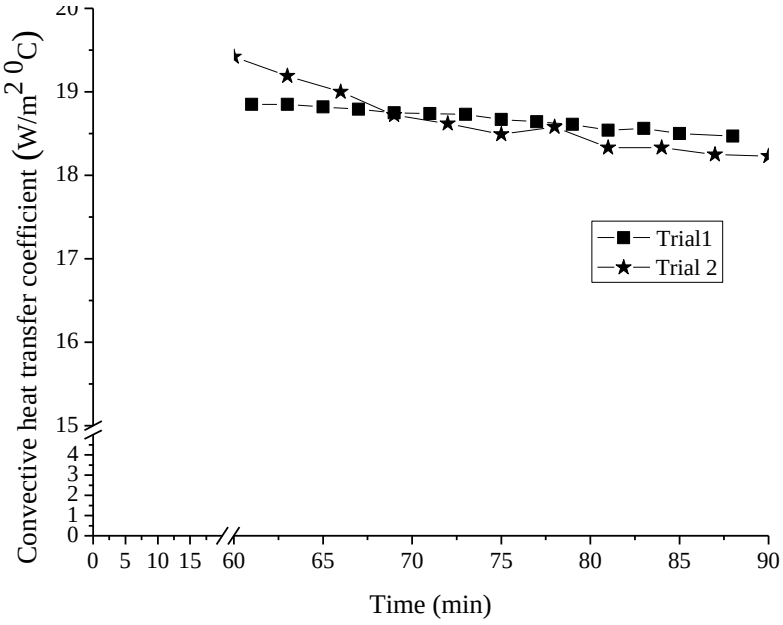

Fig. 5.7 Experimental data showing variation of convective heat transfer coefficent after attaining steady state.

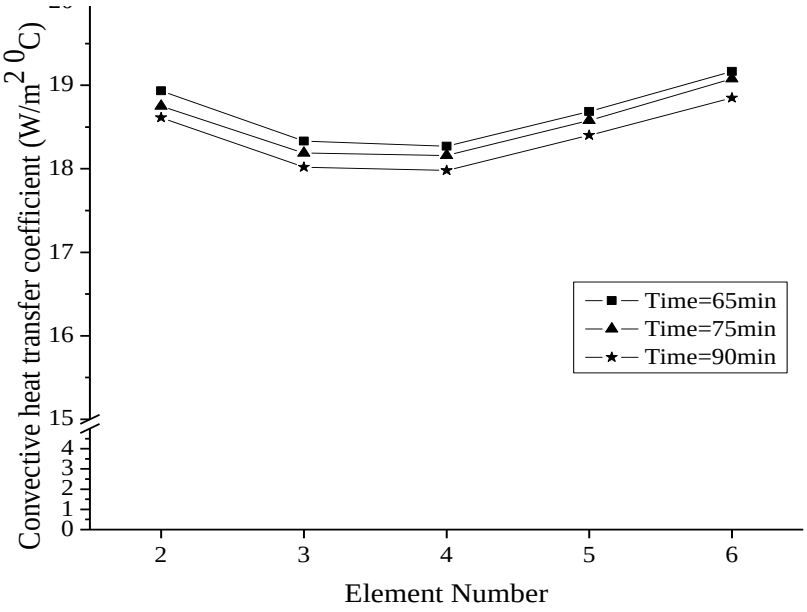

Fig. 5.8 Experimental data (Trial 1) showing variation of convective heat transfer coefficient along length of tube at various times interval.

Figure 5.7 shows the variation of natural convective heat transfer coefficient with time for the vertical copper tube after it has attained the steady state at the 56th minute. From this time onwards, it can be seen that as the time passes, the value of natural convective heat transfer coefficient decreases and maintains the steady value of about 18.5 W/m^2 ^{0}C after 90 minutes. This is because as the time passes the slope of the temperature v/s time curve shown in Figure 5.5(a) goes on decreasing and becomes almost equal to steady state value at 90th minute.

Figure 5.8 shows the variation of convective heat transfer coefficient along the length of the tube at different time interval. At any location along the length of the tube, it is observed from the Figure 5.7 that the convective heat transfer coefficient is not constant. Also, as the time passes the natural convective heat transfer coefficient decreases and takes the concave shape for variation of natural convective heat transfer coefficient along the length of the tube.

5.5.2 DISCUSSION

Comparing the experimental and theoretical results as shown in Figure 5.5 it is observed that the time taken for the tube to reach steady state predicted by FE model is 19.64% less, when compared to experimental steady state time. It is also observed that the steady state temperature obtained from the experiment is almost 4% higher than the predicted steady state temperature of 114.5 ^{0}C by FEM. Consider a temperature of 90^{0}C, the time taken by the tube to reach this temperature as predicted by FE model is 4.33% less than that of experimentally measured time. It can be seen that the temperature at the fixed end is lower than that at the free end and the maximum temperature occurs at more or less close to the centre of the tube. Though the model predicted the time taken for the steady state with considerable error, it almost predicted the steady state temperatures accurately and can be used to predict steady state temperatures at any other heating rate.

Figure 5.9 shows experimental data and theoretical data superimposed to show temperature histories for location T4. It can be seen from Figure 5.9 that though the steady state temperatures predicted by experiment and FEM model are in close agreement with each other, there is considerable difference in temperatures obtained during the transients or before the steady state. The theoretical model has predicted higher temperatures than the experiment. The variation is because, in FEM model it is assumed that the heat source is present at the nodes of the element. The nodes of the FE discretization are assumed on the outer surface of the tube. But in the real case it is not so. There is a small air gap in between the heated rod and the inner surface of the tube, thus the heater rod transmits heat by convection and radiation on to the inner surface of the tube. Hence, the tube receives less heat and hence lower values of temperatures during experiment.

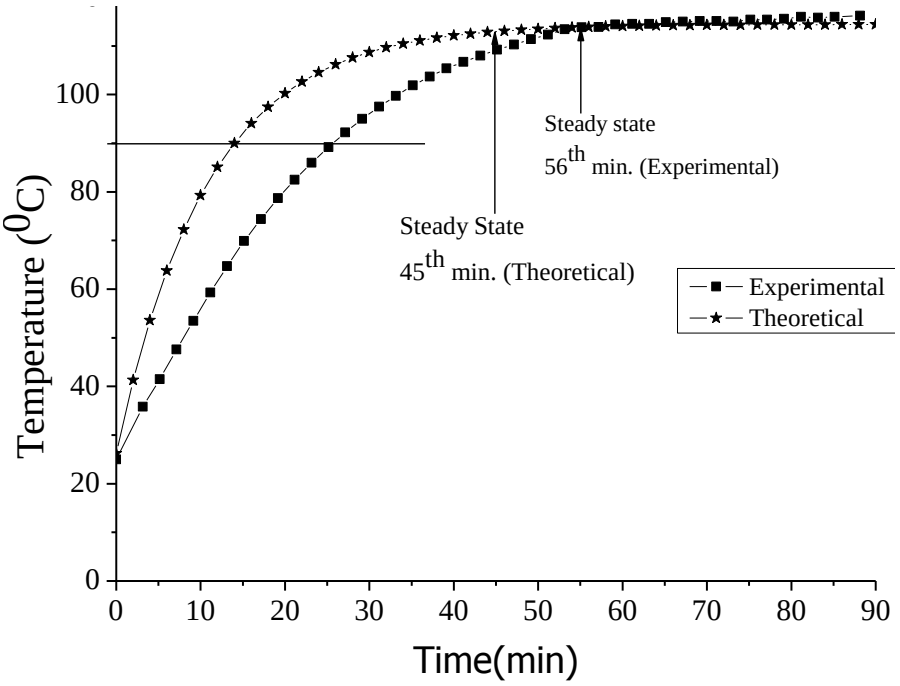

Fig 5.9 Experimental data and Theoretical data superimposed to show Temperature histories for thermocouple T4.

5.6 EXPERIMENTAL SETUP– TUBE SUBJECTED TO INTERNAL HEATING

The test specimen used for the experiment was a stainless steel SS304 tube, 500 mm long with 3 mm external diameter and 0.5 mm thickness. This experiment was carried out primarily to determine heat transfer coefficient between SS304 tube and ambient. This data would be useful for carrying out numerical studies on thermally induced vibration of beam subjected to internal heating. Five thermocouples were mounted on the tube at various points (See Table.5.1) along the length to measure the temperature at these points on the tube. The first and seventh thermocouple was used to measure the ambient temperature and it was located inside the test box.

A regulated DC power supply was used to heat the test specimen internally. The temperature readings were taken using the data acquisition system with temperature sensing module NI SCXI 1303 mounted on NI SCXI 1000 chassis. The data is sent to the computer where it is acquired using the LabVIEW software which converts the

voltage output of thermocouples through the data acquisition system in to useful temperature output. Figure 5.10 shows the front panel of LabVIEW showing various thermometers and Figure 5.11 shows the block diagram in LabVIEW showing connection diagram of various thermometers and data acquisition system.

The objective of the experiment was to gather temperature data with natural convection and to find out the time, the specimen takes to attain steady state condition. The tube was heated by means of internal heating, using the tube itself as a resistance heater. The current and voltage were adjusted to 1 ampere and 6 volts respectively in order to get heating rate of 6 Watts. The following thermal data are used for the analysis: thermal conductivity (at 100°C) k = 16.2 W/m.K, specific heat (0-100°C) c_p = 500 J/kg.K and density ρ = 8000 Kg/m^3.

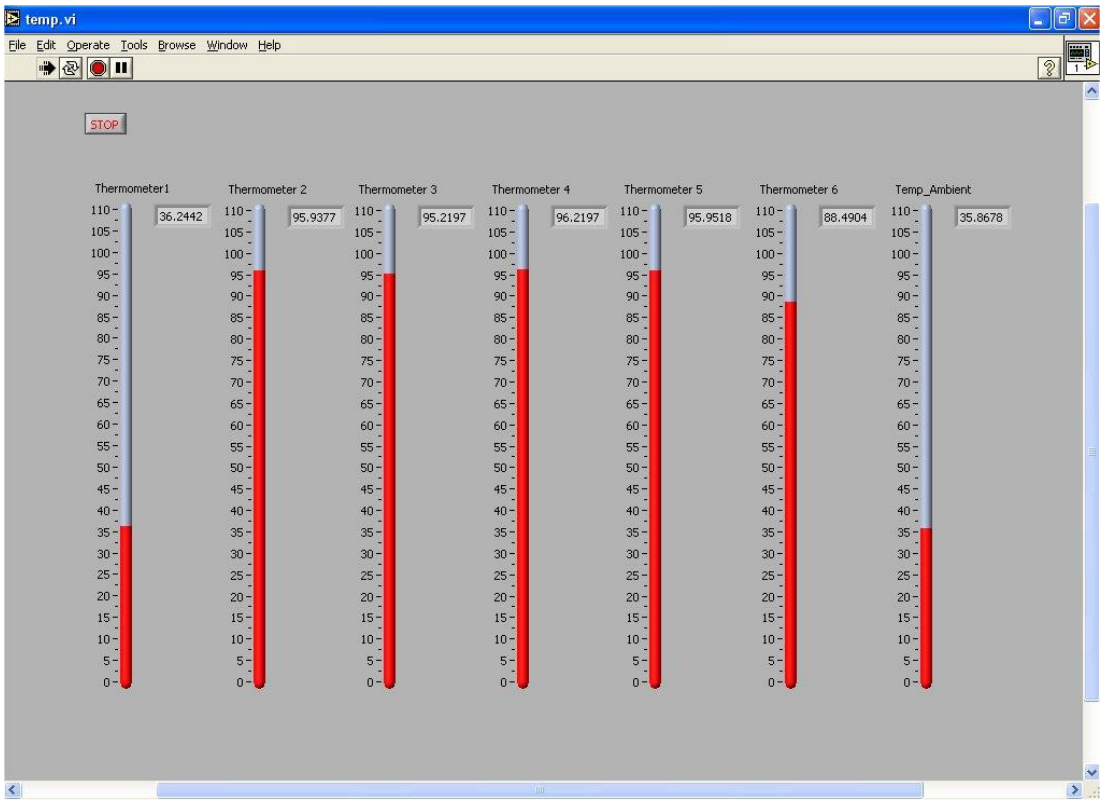

Fig 5.10 Front panel in LabVIEW showing various thermometers.

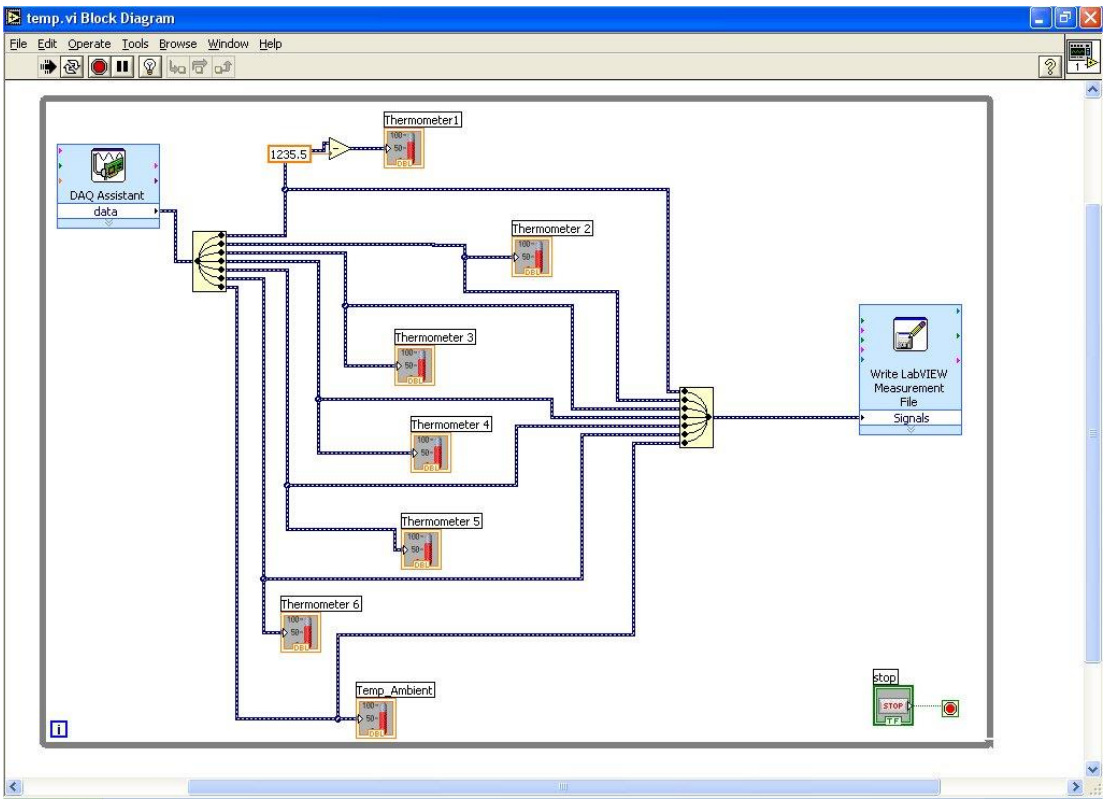

Fig 5.11 Block diagram in LabVIEW showing connection diagram of various thermometers with DAQ.

5.7 RESULTS AND DISCUSSION

5.7.1 RESULTS

For the heating rate of 6 Watts, the temperature variation on the tube surface with respect to time is shown in the Figure 5.12(a). It can be seen from Figure 5.12(a) that the tube reaches the steady state after 400 seconds and later the variation of temperature with respect to time is negligible.

The test was carried out for 600 seconds and the temperature distribution at that time is used in evaluating the natural convective heat transfer coefficient for air using equation (5.12). The ambient temperature at the time of conducting experiment was 36^0C. The heat input of 6 W corresponds to the total tube volume of

$\left(\frac{\pi}{4}\left(D^2-d^2\right)L\right)$ =1.96349×10^{-6} m^3. Hence, volumetric heating i.e. heat input per unit volume is 3055.77 kW/m^3.

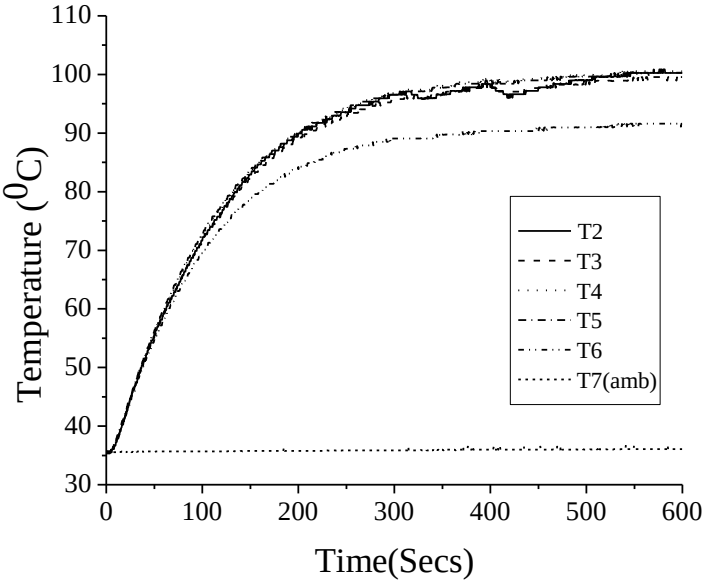

(a) Experimental data – Trial 1 (Steady state after 400 sec.).

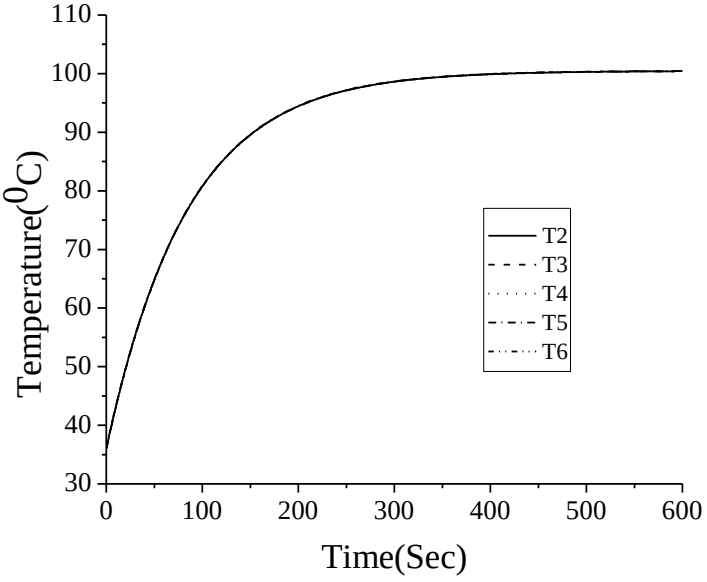

(b) Theoretical data (Steady state after 350 sec.).

Fig. 5.12 Temperature histories at various points along the length of tube.

To evaluate convective heat transfer coefficient, for convenience, the tube is divided into 5 segmental volumes, since we have 5 thermocouples located on the tube surface. Consider the segmental volume of the tube such that a thermocouple is located on its surface at the mid length of the segment i.e. T4 (T4 is the temperature measured by thermocouple, T4). Typically this segmental volume is 392.7 mm^3 for 100 mm length. Corresponding to this segment, volumetric heat is 1.2 W/m^3.

Now equating the volumetric heating for the segmental volume to the heat lost by the outer surface of the segmental volume,

$$\dot{q}_c = h_{avg} \times \pi D l_{seg} \left(T_4 - T_\infty\right),$$

$$1.2 = h_{avg} \times \pi \times 0.003 \times 0.1 \times \left(100.5 - 36\right),$$

$$h_{avg} = 19.75\,\mathrm{W/m^2\,^0C}.$$

The natural convective heat transfer coefficient for air works out to be equal to 19.75 $W/m^2\,^0C$. This value of natural convective heat transfer coefficient is used in the FORTRAN code in order to predict the temperature distribution along the length of the tube with respect to time as shown in Figure 5.12(b). The time taken to reach steady state is almost 350 seconds. It can be seen from Figure 5.12 that the maximum temperature obtained by experiment is 100.4 ^0C while that obtained from FEM model is 100.5 ^0C which is very close to the experimental value.

Similarly, for the second experimental trial, the temperature variation on the tube surface with respect to time is shown in the Figure 5.13. The test conditions are similar to trial 1 except the ambient temperature was 35 ^0C at the time of conducting the experiment. The steady state temperature attained for the second trial was 100.4^0C.

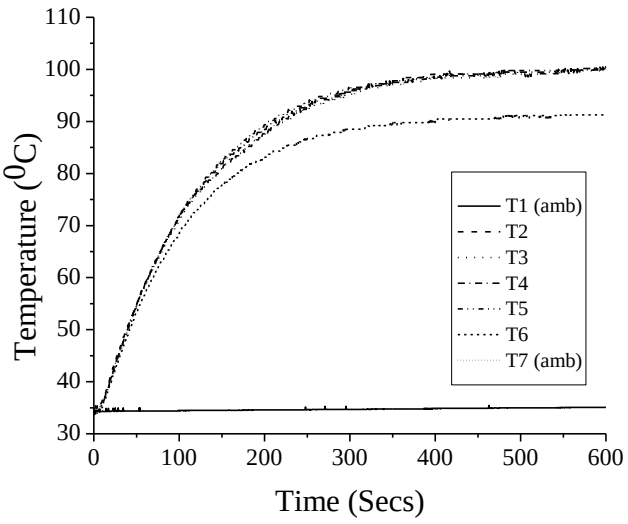

Figure 5.13 Experimental data (Trial 2) showing temperature histories at various points along the length of tube.

5.7.2 DISCUSSION

Comparing the experimental and theoretical results as shown in Figure 5.12 it is observed that the time taken for the tube to reach steady state predicted by FE model is 12.5% less than that of experimental results. Consider a temperature of 80^0C, the time taken by the tube to reach this temperature as predicted by FE model is 16.5% less than that of experimentally measured time. It is also observed that the steady state temperature obtained from experiment is almost equal to the predicted steady state temperature of 100.5 ^{0}C. Though the model predicted the time taken for steady state with some error, it predicted the steady state temperatures accurately and can be used to predict steady state temperatures at any other heating rate.

Figure 5.14 shows experimental data and theoretical data, superimposed to show temperature histories for location T4 which is 300 mm from the fixed end. It can be seen from Figure 5.14 that though the steady state temperatures obtained from experiment and predicted by FEM model are equal, there is some difference in temperatures obtained during the transients or before the steady state. The theoretical

model has predicted slightly higher temperatures than the experiment due to the assumptions made in FE analysis.

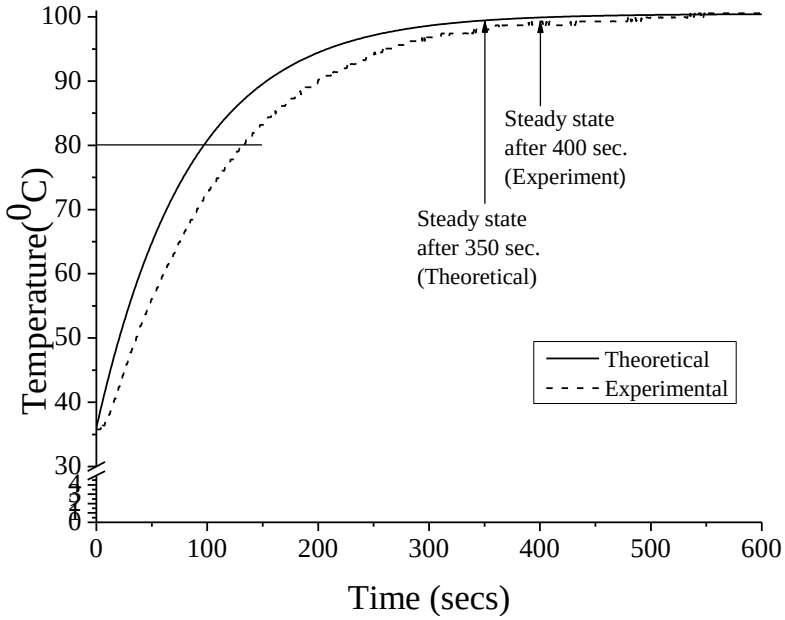

Fig. 5.14 Experimental data and theoretical data superimposed to show Temperature histories at T4 i.e. 30 cm from fixed end.

5.8 SUMMARY

The detailed study on the determination of the convective heat transfer coefficient for a stationary vertical tube with internal heating and kept in the still air under laboratory conditions were carried out. The natural convective heat transfer coefficient for air was calculated to be equal to 18.5 W/m^2 ^{0}C for copper tube and 19.75 W/m^2 ^{0}C for SS304 tube. The experimentally determined heat transfer coefficient was used in the finite element model to compute the transient temperature distribution along the length of the tube and hence steady state temperature. It is seen that the FEM model helped in predicting the steady state temperatures for the tube accurately. The FE model evaluated the transients with considerable difference when compared to experimental observed transient path.

CHAPTER 6

DYNAMIC RESPONSE OF HEATED TUBES - A THEORETICAL MODEL

6.1 INTRODUCTION

The heating of the structure may be due to constant exposure to heat source, passage of hot fluid or due to passage of electric current. When convective heat transfer varies with space and time, there will be temperature gradients in the structure. In this chapter, attempts are made to theoretically model the convection heat transfer for an oscillating cantilever tube based on Reynold's number, Prandtl number and Nusselt number. The main objective is to simulate through theoretical model, the dynamic response of the vertical cantilever tube with and without tip mass through which the electric current is passed.

The temperature distribution along the tube is solved considering heat conduction and heat convection. The temperature distribution along the tube results in the thermal moment which acts as a forcing function. Fourth order Runge-Kutta method is used to determine the transient response of heated tube. The dynamic response of the tube is studied for varying heating rates and frequencies. Further, studies are also carried out for different cross sectional areas of the tube keeping the thickness constant for a particular heating rate. The analysis showed that the rate of vibration is governed by the natural frequency of the tube and convective heat transfer coefficient.

6.2 MATHEMATICAL FORMULATION

The tube used for the study was idealized as two semicircular stainless steel tubes joined together to form a single tube with insulation in between. A metallic tip mass at one end connects the two semi-circular tubes in series so as to form a closed electric circuit in conjunction with a power supply as in Figure 6.1(a). Figure 6.2 shows the cross section of the tubes.

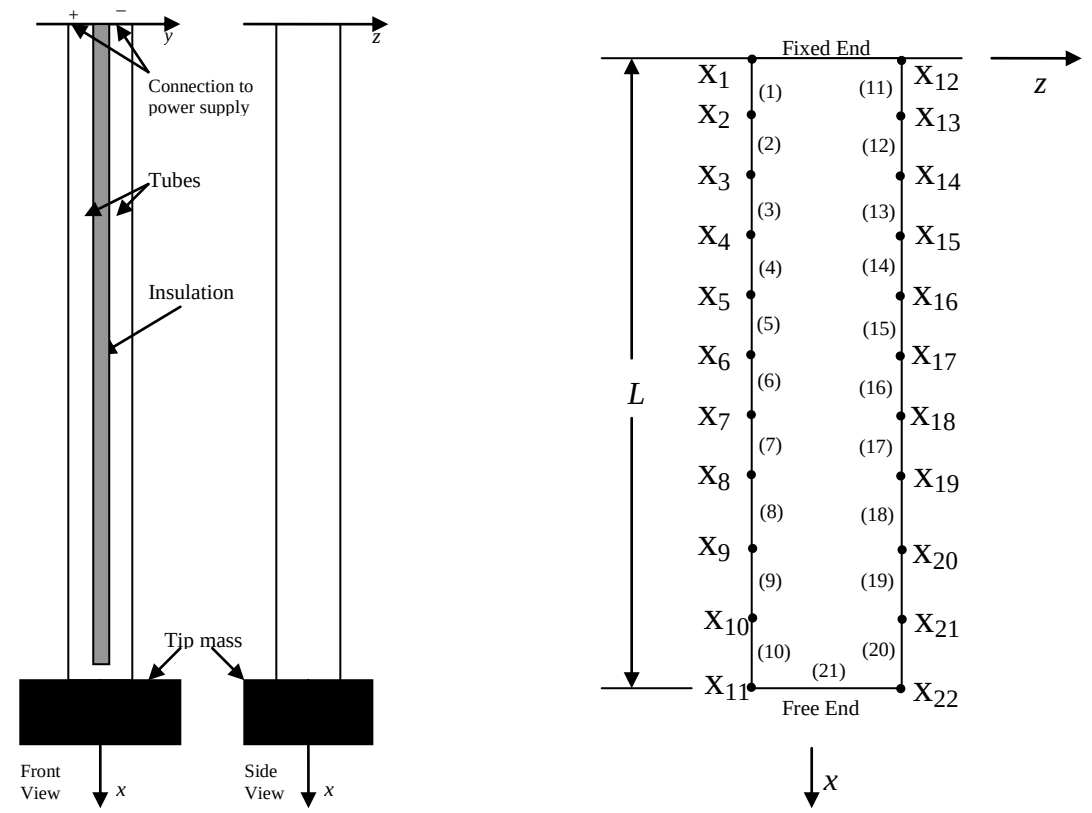

(a) Model of the tube for internal heating.

(b) Finite element idealization of the tube.

Fig.6.1FEM model for temperature computation.

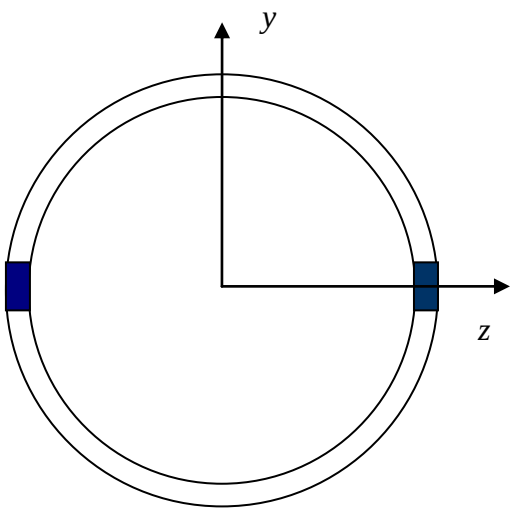

Fig. 6.2 Cross section of the tube.

The tube was heated internally by passing the current through the tubes. To analyze the vibrations set by initial excitation, the thermal and structural problems must be coupled. The two semicircular tubes are idealized using one dimensional linear finite element as shown in Figure 6.1(b). The weak form of the heat transfer governing equation for the oscillating tube with heat conduction, heat loss by convection along the tube and change in internal energy is as follows(refer Eq.(5.5):

$$-N_L^T k_x A \frac{\partial T}{\partial x}\Big|_0^l + \int k_x A \frac{\partial T}{\partial x}\frac{\partial N_L^T}{\partial x}dx + \int N_L^T h_c P T dx + \int N_L^T \rho c_p A \frac{dT}{dt}dx - \int N_L^T h_c P T_\infty dx - \int N_L^T \dot{q} A dx = 0, \tag{6.1}$$

where, A = area, P = perimeter, k_x = thermal conductivity, ρ = density, c_p = specific heat, h = convective heat transfer coefficient, T = temperature, T_∞ = environment temperature, l = element length, L = length of tube, $\dot{q}$ = heat supplied per unit volume. The boundary conditions being, heat loss by convection at end face of the tube and temperature specified at time, t = 0. Equation (6.1) can be applied to a oscillating tube provided convective heat transfer coefficient is defined as a function of space and time. Linear shape functions N_1 and N_2 are used to develop the various finite element matrices. The finite element equation for time dependent temperature is:

$$\left\{\frac{k_x A}{l}\begin{bmatrix}1 & -1\\ -1 & 1\end{bmatrix} + \frac{h_c P l}{6}\begin{bmatrix}2 & 1\\ 1 & 2\end{bmatrix} + \begin{bmatrix}0 & 0\\ 0 & h_c A\end{bmatrix}\right\}\begin{Bmatrix}T_1\\ T_2\end{Bmatrix} + \frac{\rho c_p A l}{6}\begin{bmatrix}2 & 1\\ 1 & 2\end{bmatrix}\begin{Bmatrix}\dot{T}_1\\ \dot{T}_2\end{Bmatrix} = \frac{\dot{q} A l}{2}\begin{Bmatrix}1\\ 1\end{Bmatrix} + \frac{h_c P l T_\infty}{2}\begin{Bmatrix}1\\ 1\end{Bmatrix} + h_c A T_\infty \begin{Bmatrix}0\\ 1\end{Bmatrix}, \tag{6.2}$$

$$\mathbf{K}_{\text{comb}}^e \mathbf{T} + \mathbf{K}_{\text{cap}}^e \dot{\mathbf{T}} = \bar{\mathbf{F}}_Q^e. \tag{6.3}$$

In equation (6.2), the third term on LHS and third term on RHS are considered for the second node of the elements involving boundary flux terms. $\mathbf{K}_{\text{comb}}^{\text{e}}$ = combination of elemental conduction and convection matrices, $\mathbf{K}_{\text{cap}}^e$ =elemental capacitance matrix,

$\bar{\mathbf{F}}_Q^e$ =force vector. Equation (6.3) is solved for the temperature variation in space and time domain.

6.2.1 INTERPRETATION OF FORCED CONVECTION HEAT TRANSFER COEFFICIENT AS A FUNCTION OF BEAM MOTION

Heat transfer analysis for objects in motion becomes a complex issue primarily due to the fact that the heat loss by convection which is governed by the heat transfer coefficient between the object and the surrounding medium is difficult to account for in the theoretical computation. Such related issues can be referred to the work of Blandino and Thornton (2000). Referring to the same, the convective heat transfer coefficient used for heat transfer analysis is sum of natural convective heat transfer coefficient and forced convective heat transfer coefficient. Blandino and Thornton (2000) derived the corresponding governing equations for the evaluation of temperature transients and steady state for an oscillating tube. The governing equation contains forced convection as well as natural convective heat transfer coefficient. The overall heat transfer coefficient is used based on Fourier series expansion. The heat transfer coefficients for numerical computations were input from the experimental work. Blandino and Thornton (2000) carried out exhaustive experimental studies in order to obtain the relation between Nusselt number and Reynolds number. Nusselt number is a non dimensional quantity describing a relation between the convective heat transfer coefficient and the thermal conductivity of medium along with the characteristic geometry dimension of the object. The velocity of the vibrating tube is used to compute Reynolds number, by using this Reynolds number in the experimental relation between Nusslet number and Reynolds number, the forced convective heat transfer coefficient is computed. Further they also claim that the natural convective heat transfer coefficient depends on the oscillating object. Again using experimental studies, natural convection Nusselt number of the vibrating object is related to the natural convection Nusselt number of the stationary object. Using the velocity of the moving object in the above relation produces natural convection heat transfer coefficient.

The present chapter attempts to model the variation of convection heat transfer coefficient in a different approach as detailed in the following paragraphs. The theoretical results produced in this chapter are different from that modeled by Blandino and Thornton (2000).

The variation of convection along the length of the tube is chosen to be a polynomial characterized to provide least convection at the fixed end and maximum convection at the free end and also proportional to velocity of oscillating tube. Thus, the spatial and time variation of heat transfer coefficient is:

$$h(x,t) = h_c + a\left(\frac{3x^2}{2L^2} - \frac{x^3}{2L^3}\right)h(t), \tag{6.4}$$

where, h_c = natural convective heat transfer coefficient, a = magnification factor for convection, L = length of tube, x = position along x-axis, $h(t)$ is forced convection heat transfer coefficient which depends on beam/tube velocity. Expression in the bracket $\left(\frac{3x^2}{2L^2} - \frac{x^3}{2L^3}\right)$ corresponds to the displaced shape of the cantilever beam. Forced convection is considered since the oscillating tube displaces the air. The concept of $h(t)$ is explained now. Approximating the velocity of air equals velocity of oscillating tube, the Reynolds number is computed,

$$\text{Reynolds number} \quad = \frac{\text{Inertia force}}{\textit{Viscous}\,\text{force}} \qquad \text{i.e.} \quad \mathrm{R}_{eD} = \frac{\rho_a V_o D}{\mu}, \tag{6.5}$$

where, ρ_a is the density of air at ambient temperature, V_o is the velocity of the oscillating tube, D is the external diameter of the tube (characteristic length) and μ is the viscosity of the air at ambient temperature. Using this Reynolds number, R_{eD}, the Nusselt number, N_{uD} (referred to Incropera and DeWitt, 2002) is found which helps in finding the convective of heat transfer coefficient, $h(t)$. The correlation given for computation of Nusslet number for flow over circular object is:

$$N_{uD} = CR_{eD}^{m} P_r^{n} \left(\frac{P_r}{P_{rS}} \right)^{1/4}, \qquad (6.6)$$

and the empirical correlation given for time dependent or forced convective heat transfer coefficient is:

$$h(t) = N_{uD} \frac{k_{air}}{D}, \qquad (6.7)$$

where, C = constant (C = 0.75 for P_r < 40, C = 0.51 for P_r > 40), m =constant (m = 0.4 for P_r < 40, m = 0.5 for P_r > 40), P_r is the Prandlt number evaluated at ambient temperature, T_∞, n = 0.36 for $P_r \leq 10$ and n = 0.37 for $P_r > 10$, and P_{rS} is the Prandlt number at instantaneous temperature, T_s. The Prandlt number at instantaneous temperature can be referred from the Table of thermodynamic properties of air, as reproduced in Table.6.1 (referred from Incropera and DeWitt, 2002).

Table.6.1 Thermodynamic Properties of Air, (Incropera and DeWitt 2002).

Temperature, K	ρ_a (Kg/m^3)	$\nu \times 10^6$ (m^2/s)	$k_{air} \times 10^3$ (W/mK)	Pr
300	1.1614	15.89	26.3	0.707
350	0.9950	20.92	30.0	0.700
400	0.8711	26.41	33.8	0.690
450	0.7740	32.39	37.3	0.686
500	0.6964	38.79	40.7	0.684
550	0.6329	45.57	43.9	0.683
600	0.5804	52.69	46.9	0.685
650	0.5356	60.21	49.7	0.690
700	0.4975	68.1	52.4	0.695

It is seen from the Table 6.1 that the Prandlt number is given for every 50^{0}C temperature difference, starting from temperature of 27 ^{0}C (300 K). To obtain the Prandlt number at intermediate temperatures, a polynomial fit is carried out on the

data given in Table.6.1 with instantaneous temperature, T_i, as the variable which resulted in:

$$\Pr = 0.84071 - 6.8066\times10^{-4}T_i + 8.796\times10^{-7}T_i^2 - 2.9261\times10^{-10}T_i^3. \qquad (6.8)$$

This value of Prandlt number is used in equation (6.6) to evaluate the Nusselt number. The above expression is also used to evaluate Prandlt number at ambient temperature.

The temperature T is assumed to be a superposition of the average tube temperature at the cross-section, T_{avg}, and time varying temperature at points around tube circumference, T_m, called perturbation temperature, and is expressed as:

$$T(x,\phi,t) = T_{avg}(x,t) + T_m(x,t)\cos\phi, \qquad (6.9)$$

where ϕ being radial position angle. Figure 6.3 shows the variation of temperature on either sides of the tube with respect to time i.e. perturbation temperature.

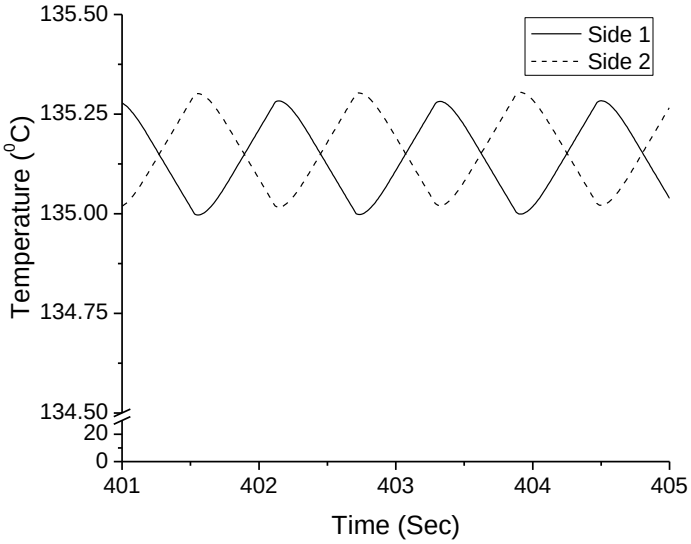

Fig. 6.3 Variation of temperature on either sides of the tube with time.

The computation of forced convection heat transfer coefficient, h(t), as a function of beam velocity was outlined in the previous paragraphs. The physical understanding for the same is illustrated in Figure 6.4. Referring to Figure 6.4(a), when the beam executes right to left motion, the windward face AB will experience rush of air past it which is likely to increases the heat transfer. Hence the forced convective heat transfer coefficient (FCHTC) for windward side AB will initially increase to maximum until the beam reaches mean position and for the later portion of the motion the FCHTC will remain constant equal to a maximum (curve pq). At the same instant the leeward face CD will have no influence of the moving air. Hence the FCHTC for the leeward face is assumed to decrease from a maximum (due to previous motion) to a minimum until it reaches the mean position and during the later stages of motion it remains constant equal to the minimum, curve rs, (greater than natural heat transfer coefficient).

Referring Figure 6.4(b), when the beam executes left to right motion, the windward face CD will experience rush of air past it which is likely to increases the heat transfer. Hence the forced convective heat transfer coefficient (FCHTC) for windward side CD will initially increase to maximum until the beam reaches mean position and for the later portion of the motion the FCHTC will remain constant equal to a maximum (curve mn). At the same instant the leeward face AB will have no influence of the moving air. Hence the FCHTC for the leeward face is assumed to decrease from a maximum (due to previous motion, explained in Figure 6.4(a) to a minimum until it reaches the mean position and during the later stages of motion it remains constant equal to the minimum, curve jk, (greater than natural heat transfer coefficient). This sequence of the variation of heat transfer coefficient repeats for subsequent oscillations of beam.

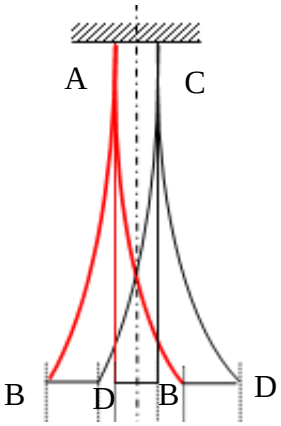

a) Variation of forced convection when beam moves from right to left or vice verse.

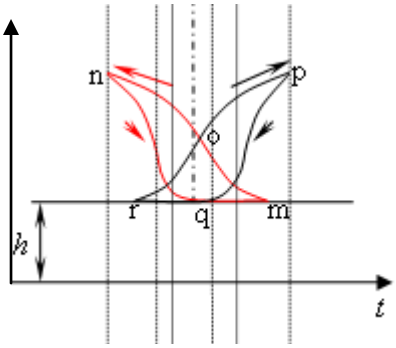

Oscillation from left to right
mn forced convection profile windward face.
pq forced convection profile leeward face.

b) Variation of forced convection when beam moves from right to left.

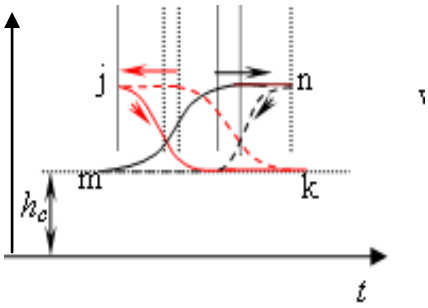

Oscillation from right to left
mn forced convection profile windward face.
jk forced convection profile leeward face.

c) Variation of forced convection when beam moves from left to right.

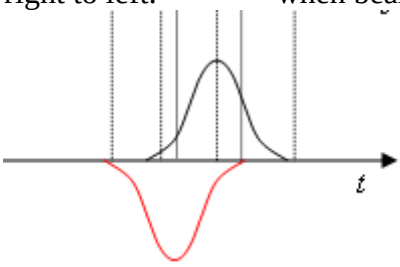

d) Velocity profile of the beam.

Fig 6.4 Description of the variation of forced convection due to beam motion.

6.2.2 STRUCTURAL EQUATION OF MOTION

The heat transfer problem is solved and the temperature output is used for calculation of thermal moment. Variation of temperature on either sides give rise to thermal moment results in a forcing function as illustrated in Figure 6.5.

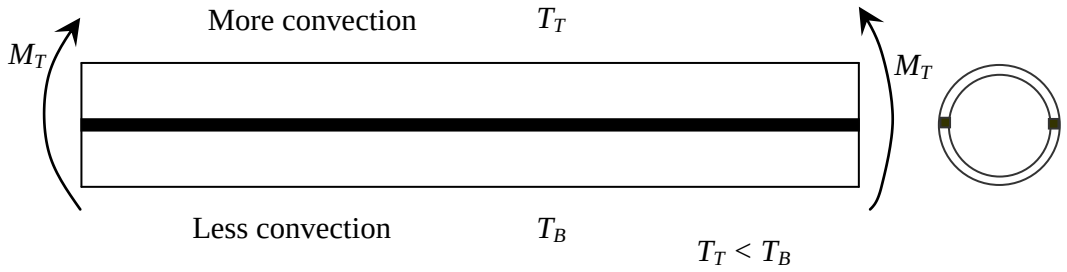

Fig. 6.5 Variation of temperature on either sides of tube gives rise to thermal moment.

Two assumptions are made in the structural formulation. The analysis considers the tube oscillating at the fundamental frequency. The effective mass of the beam is taken as a fraction of the beam mass plus the tip mass, referred from Young (2002).

$$m_e = 0.236m + m_{tip}, \tag{6.10}$$

where, m_e = equivalent mass, m = mass of tube, m_{tip} = tip mass. The bending moment M for a beam with thermal load is given as;

$$M = -EI\frac{\partial^2 \upsilon}{\partial x^2} - M_T, \tag{6.11}$$

where E is the modulus of elasticity, I is the moment of inertia and υ is the displacement at any point along beam length.

For the semicircular section of the tube as shown in Figure 6.6 the thermal moment M_T is:

$$M_T = E\alpha\int_A (T - T_\infty)ydA + E\alpha\int_A (T - T_\infty)zdA, \tag{6.12}$$

where, α = mean coefficient of thermal expansion, y and z = moment arm (refer to Figure 6.6) and T = temperature.

The thermal moment for tube cross section shown in Figure 6.6 can be evaluated as:

$$y = R\sin\phi, \qquad z = R\cos\phi, \qquad dA = RHd\phi; \tag{6.13}$$

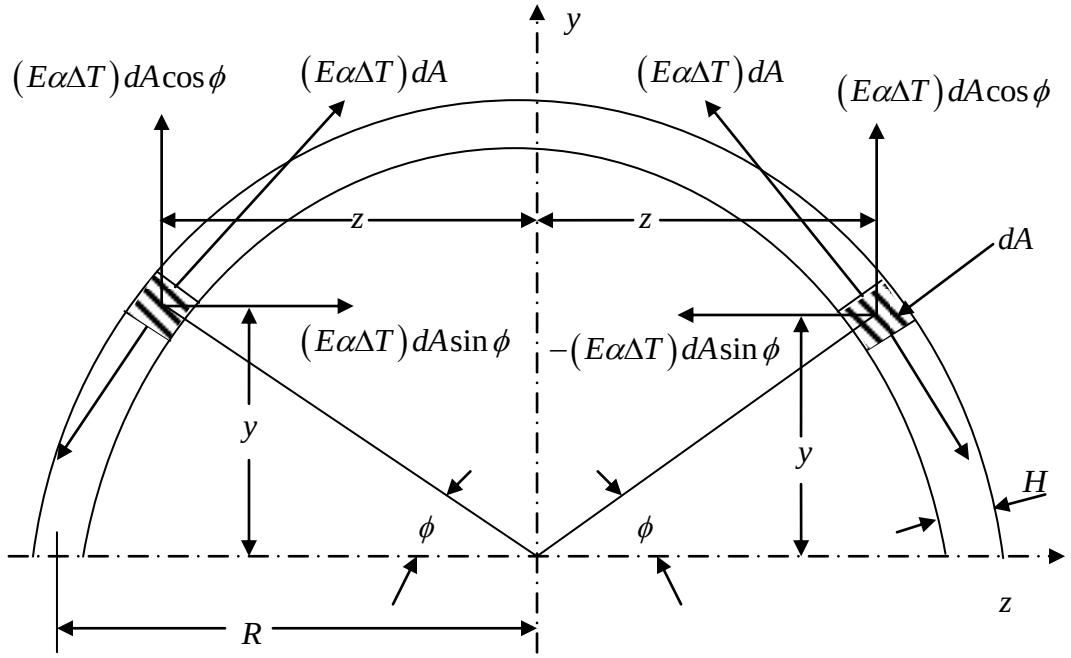

Fig 6.6 Cross section of the tube with thermal forces on differential area *dA* and corresponding moment arms.

Substituting equation (6.13) in equation (6.12) results in

$$M_T = E\alpha\int (T - T_\infty)R\sin\phi RHd\phi + E\alpha\int (T - T_\infty)R\cos\phi RHd\phi,$$

$$M_T(x,t) = E\alpha\int_0^\pi (T - T_\infty)R^2H\sin\phi d\phi + E\alpha\int_0^\pi (T - T_\infty)R^2H\cos\phi d\phi. \tag{6.14}$$

The horizontal component of the thermal moment will become zero when evaluated over 0 to π. Substituting the expression for *T*, i.e. equation (6.9), in equation (6.14) and performing the integration gives the thermal moment as:

$$M_T(x,t) = E\alpha \int_0^{\pi} \{T_{avg}(x,t) + T_m(x,t)\cos\phi - T_\infty\} R^2 H \cos\phi d\phi,$$

$$M_T(x,t) = E\alpha \left[\int_0^{\pi} T_{avg}(x,t) R^2 H \cos\phi d\phi + \int_0^{\pi} T_m(x,t) R^2 H \cos^2\phi d\phi - \int_0^{\pi} T_\infty R^2 H \cos\phi d\phi \right],$$

$$M_T(x,t) = E\alpha \int_0^{\pi} T_m(x,t) R^2 H \cos^2\phi d\phi,$$

$$\int \cos^2 x dx = \tfrac{1}{2}\left(x + \tfrac{1}{2}\sin 2x\right).$$

Solving,

$$M_T(x,t) = E\alpha T_m(x,t) R^2 H \left[\tfrac{1}{2}\left(\phi + \tfrac{1}{2}\sin 2\phi\right) \right]_0^{\pi},$$

$$M_T(x,t) = E\alpha T_m(x,t) R^2 H \left[\tfrac{1}{2}\left(\pi + \tfrac{1}{2}\sin 2\pi\right) - \tfrac{1}{2}\left(0 + \tfrac{1}{2}\sin 0\right) \right],$$

$$M_T(x,t) = E\alpha T_m(x,t) R^2 H \left[\pi/2 + 0 - 0 - 0 \right],$$

which gives the thermal moment as:

$$M_T(x,t) = \frac{\pi}{2} E\alpha T_m(x,t) R^2 H, \tag{6.15}$$

where, R = average tube radius and H = thickness of tube. Note that the thermal moment depends only on the perturbation temperature, T_m. Based on the free body diagram shown in Figure 6.7, summing moments about point O,

$$-M + (L-x)m\frac{\partial^2 \bar{V}}{\partial t^2} + (\bar{V} - \upsilon)mg = 0. \tag{6.16}$$

The equation of motion for the beam with thermal load is:

$$-EI\frac{\partial^2 \upsilon}{\partial x^2} + m\frac{\partial^2 \bar{V}}{\partial t^2}(L-x) + mg[\upsilon(L,t) - \upsilon] + M_T(x,t) = 0, \tag{6.17}$$

where, m = mass, υ is the displacement at any point along beam length and $\bar{V}$ = displacement at tip of beam (tube). The boundary and initial conditions at the clamped end of the tube are:

$$\upsilon(0,t)=\frac{\partial \upsilon}{\partial x}(0,t)=0,\ \upsilon(x,0)\neq 0,\ \ \frac{\partial \upsilon}{\partial t}(x,0)=0; \tag{6.18}$$

The beam displacement is represented approximately by using the shape function for cantilever beam with concentrated end mass as:

$$\upsilon(x,t)=\left(\frac{3x^2}{2L^2}-\frac{x^3}{2L^3}\right)\bar{V}(t), \tag{6.19}$$

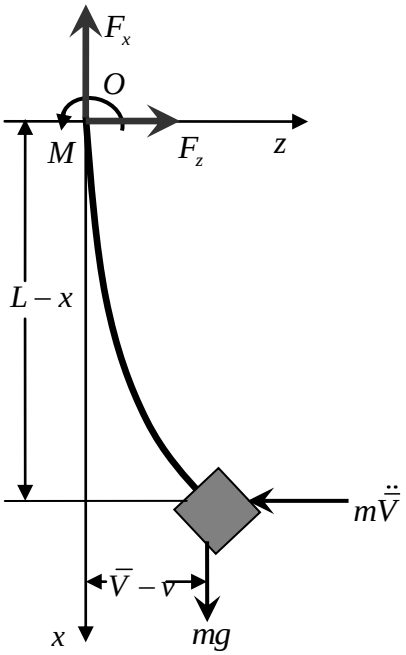

Fig 6.7 Free body diagram of the deflected beam.

where $\bar{V}(t)$ is the displacement at $x = L$, that is $\bar{V}(t)$ is the tip displacement. Figure 6.8 shows the plot of the assumed shape function which is compared with the standard Hermite shape function.

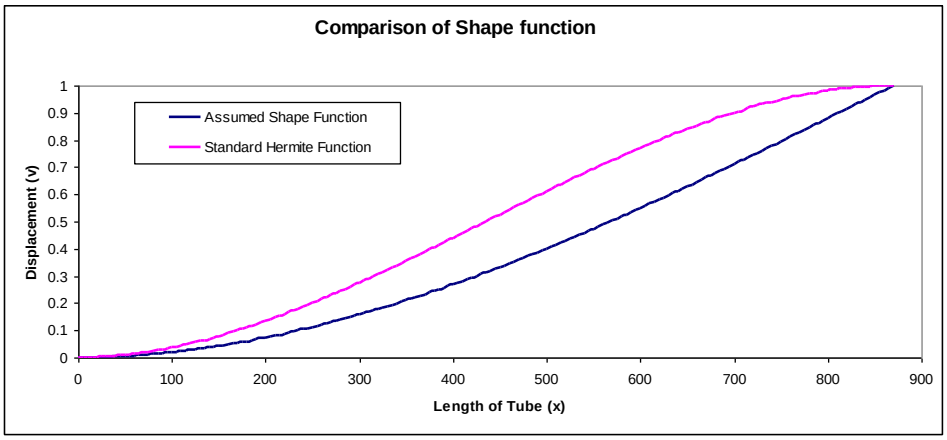

Fig. 6.8 Comparison of assumed shape function with standard Hermite function.

Substituting the shape function of equation (6.19) in equation(6.17) and integrating twice with respect to x and substituting limits 0 to L results in the ordinary differential equation of motion similar to a single degree of freedom system which can be derived as follows:

Let, $\upsilon(L,t) = \bar{V}(t)$,

$$\frac{\partial \upsilon}{\partial x} = \left(\frac{3x}{L^2} - \frac{3x^2}{2L^3}\right)\bar{V}(t) \quad \text{and} \quad \frac{\partial^2 \upsilon}{\partial x^2} = \left(\frac{3}{L^2} - \frac{3x}{L^3}\right)\bar{V}(t); \tag{6.20}$$

substituting equation (6.20) in equation (6.17)

$$EI\left(\frac{3}{L^2} - \frac{3x}{L^3}\right)\bar{V}(t) + m\ddot{\bar{V}}(L-x) + mg\left[\bar{V}(t) - \frac{3x^2}{2L^2}\bar{V}(t) + \frac{x^3}{2L^3}\bar{V}(t)\right] + M_T(x,t) = 0,$$

$$3EI\left(\frac{1}{L^2} - \frac{x}{L^3}\right)\bar{V}(t) + m\ddot{\bar{V}}(L-x) + mg\left[1 - \frac{3x^2}{2L^2} + \frac{x^3}{2L^3}\right]\bar{V}(t) + M_T(x,t) = 0.$$

Integrating with respect to (w.r.t) x,

$$3EI\left(\frac{x}{L^2} - \frac{x^2}{2L^3}\right)\bar{V}(t) + m\ddot{\bar{V}}\left(Lx - \frac{x^2}{2}\right) + mg\left[x - \frac{3x^3}{6L^2} + \frac{x^4}{8L^3}\right]\bar{V}(t) + \int_0^x M_T(x,t)dx = 0,$$

$$3EI\left(\frac{x}{L^2} - \frac{x^2}{2L^3}\right)\bar{V}(t) + m\ddot{\bar{V}}\left(Lx - \frac{x^2}{2}\right) + mg\left[x - \frac{x^3}{2L^2} + \frac{x^4}{8L^3}\right]\bar{V}(t) + \int_0^x M_T(x,t)dx = 0.$$

Integrating again w.r.t. x,

$$3EI\left(\frac{x^2}{2L^2}-\frac{x^3}{6L^3}\right)\bar{V}(t)+m\ddot{\bar{V}}\left(\frac{Lx^2}{2}-\frac{x^3}{6}\right)+mg\left[\frac{x^2}{2}-\frac{x^4}{8L^2}+\frac{x^5}{40L^3}\right]\bar{V}(t)$$
$$+\int_0^L\int_0^x M_T(x,t)dudx=0.$$

Substituting the limits: 0 to L, results in,

$$3EI\left(\frac{L^2}{2L^2}-\frac{L^3}{6L^3}\right)\bar{V}(t)+m\ddot{\bar{V}}\left(\frac{L^3}{2}-\frac{L^3}{6}\right)$$
$$+mg\left[\frac{L^2}{2}-\frac{L^4}{8L^2}+\frac{L^5}{40L^3}\right]\bar{V}(t)+\int_0^L\int_0^x M_T(x,t)dudx=0,$$

$$3EI\left(\frac{1}{2}-\frac{1}{6}\right)\bar{V}(t)+m\ddot{\bar{V}}\left(\frac{L^3}{2}-\frac{L^3}{6}\right)+mg\left[\frac{L^2}{2}-\frac{L^2}{8}+\frac{L^2}{40}\right]\bar{V}(t)+\int_0^L\int_0^x M_T(x,t)dudx=0,$$

$$3EI\left(\frac{3-1}{6}\right)\bar{V}(t)+m\ddot{\bar{V}}L^3\left(\frac{3-1}{6}\right)+mgL^2\left[\frac{20-5+1}{40}\right]\bar{V}(t)+\int_0^L\int_0^x M_T(x,t)dudx=0.$$

Dividing by mL^3

$$\frac{3EI}{mL^3}\left(\frac{2}{6}\right)\bar{V}(t)+\ddot{\bar{V}}\left(\frac{2}{6}\right)+\frac{g}{L}\left[\frac{2}{5}\right]\bar{V}(t)+\frac{1}{mL^3}\int_0^L\int_0^x M_T(x,t)dudx=0.$$

Multiplying by 3,

$$\frac{3EI}{mL^3}\bar{V}(t)+\ddot{\bar{V}}+\frac{6g}{5L}\bar{V}(t)+\frac{3}{m_eL^3}\int_0^L\int_0^x M_T(x,t)dudx=0.$$

Thus,

$$\ddot{\bar{V}}+\left(\frac{3EI}{mL^3}+\frac{6g}{5L}\right)\bar{V}(t)=-\frac{3}{mL^3}\int_0^L\int_0^x M_T(u,t)dudx. \qquad (6.21)$$

In equation (6.21) u is a dummy variable of integration, g = acceleration due to gravity, $\ddot{V}$ is acceleration and m is replaced by m_e i.e. equivalent mass of the beam. The natural frequency of the beam is square root of the coefficient of the second term on the LHS of equation (6.21). The forcing function $F(t)$ due to thermal moment is:

$$F(t)=-\frac{3}{L^3}\int_0^L\int_0^x M_T(u,t)dudx. \qquad (6.22)$$

This is the forcing function for each semicircular tube and since the tube under study consists of two identical half tubes, the total forcing function F_{tot} is, $F_{tot}(t) = 2F(t)$. Thus the final equation of motion for the internally heated tube with damping term ξ is given as:

$$\ddot{\bar{V}} + 2\xi\omega_n\dot{\bar{V}} + \omega_n^2\bar{V} = \frac{F_{tot}(t)}{m_e}. \tag{6.23}$$

The thermal-structural analysis takes into account the variation of temperature along the length of the beam because both the natural and forced convection vary with x. The tube is divided into twenty one elements as shown in Figure 6.1(b). At each time, the temperature distribution is calculated at each node section and then the thermal moment is calculated at the node. Thermal moments are assumed to vary linearly between nodes:

$$M_T(u,t) = [N(u)]\{M_T(t)\}, \tag{6.24}$$

where u_i and u_j are the locations of typical nodes i and j, and M_{Ti} and M_{Tj} are the thermal moments at nodes i and j respectively. Using linear shape functions,

$$M_T(u,t)^{(e)} = M_T(u,t)_i + M_T(u,t)_j,$$

$$M_T(u,t)^{(e)} = \left(1 - \frac{u}{l}\right)M_{T_i} + \frac{u}{l}M_{T_j}. \tag{6.25}$$

Evaluating the integrals gives the forcing function for each element which is derived as follows:

$$F_{tot}(t) = -2\frac{3}{L^3}\int_0^L\int_0^x M_T(u,t)dudx,$$

$$F_{tot}(t) = -\frac{6}{L^3}\int_0^L\int_0^x M_T(u,t)dudx,$$

$$F_{tot}(t) = \frac{-6}{L^3}\int_0^L\int_0^x\left[\left(1 - \frac{u}{l}\right)M_{T_i} + \frac{u}{l}M_{T_j}\right]dudx.$$

Integrating with respect to *u* and substituting limits 0 to *x*,

$$F_{tot}(t) = \frac{-6}{L^3}\int_0^L \left[\left(x - \frac{x^2}{2l}\right)M_{T_i} + \frac{x^2}{2l}M_{T_j}\right]dx.$$

Integrating with respect to x and substituting limits 0 to *l*,

$$F_{tot}(t) = \frac{-6}{L^3}\left[\left(\frac{l^2}{2} - \frac{l^3}{6l}\right)M_{T_i} + \frac{l^3}{6l}M_{T_j}\right],$$

$$F_{tot}(t) = \frac{-6}{L^3}\left[\frac{2l^2}{6}M_{T_i} + \frac{l^2}{6}M_{T_j}\right],$$

$$F_{tot}(t)^{(1)} = -\frac{2l^2}{L^3}\left(M_{T_1} + \frac{1}{2}M_{T_2}\right). \qquad (6.26)$$

The moments thus computed using equation (6.26) at each node section are summed up to give the final forcing function derived as:

$$F_{tot}(t) = -\frac{2l^2}{L^3}\sum_{elements}\left(M_{Ti} + \frac{1}{2}M_{Tj}\right). \qquad (6.27)$$

Fourth order Runge-Kutta method is used to solve the second order differential equation (6.23) where, equation (6.27) acts as a forcing function for the initially excited beam.

6.2.3 THE RUNGE-KUTTA METHOD FOR SOLVING SECOND-ORDER DIFFERENTIAL EQUATION OF MOTION

Many systems demonstrate oscillatory behavior, a mass suspended by a spring and a simple pendulum are common mechanical systems which come to mind. Examples of more complicated systems are sound waves and electromagnetic radiation. Typically, systems that display oscillatory behavior do so when the differential equation which describes them involves second derivatives of the unknown function. The second derivative of a function is the derivative of the first derivative of the function. Geometrically, this just means the slope of the slope of the curve representing the original function. Most second-order differential equations can be written in the form:

$$y''(x) = f\left(y'(x), y(x), x\right), \tag{6.28}$$

where, *f* is some arbitrary function of $y'(x)$, $y(x)$ and x. $y''(x)$ is the notation used for the second derivative of the function .

How do equations that have the form of equation (6.28) arise in nature? For mechanical systems, Newton's second law of motion is just such an equation. Newton's second law states that the acceleration of an object is proportional to the sum of all the forces acting on the object and inversely proportional to its mass:

$$a_c = \frac{F_T}{m}, \tag{6.29}$$

where a_c is the acceleration, F_T is the net force and *m* is the mass.

Equation (6.29) is a second-order differential equation because the acceleration is the second derivative of position $a_c(t) = x''(t)$.

Equation (6.29) can be rewritten as:

$$x''(t) = \frac{F_T(u, x, t)}{m}. \tag{6.30}$$

In general, any second-order differential equation can be written as a pair of first-order equations. Hence, equation (6.30) can be rewritten as:

$$u'(t) = \frac{F_T}{m} \text{ and } x'(t) = u(t). \tag{6.31}$$

The fourth-order Runge-Kutta solution of the first-order differential equation of the form:

$$y'(x) = f\left(x, y\right), \tag{6.32}$$

$$y_{n+1} = \frac{1}{6}\left(k_1 + 2k_2 + 2k_3 + k_4\right), \tag{6.33}$$

where the constants k_1, k_2, k_3 and k_4 are given by:

$$k_1 = \Delta x\, f\left(x_n, y_n\right), \tag{6.34}$$

$$k_2 = \Delta x\, f\left(x_n + \frac{\Delta x}{2}, y_n + \frac{k_1}{2} \right), \tag{6.35}$$

$$k_3 = \Delta x\, f\left(x_n + \frac{\Delta x}{2}, y_n + \frac{k_2}{2} \right), \tag{6.36}$$

$$k_4 = \Delta x\, f\left(x_n + \Delta x, y_n + k_3 \right). \tag{6.37}$$

On examination of equation (6.32 to 6.37), it is seen that the constant k_1 depends on only x_n and y_n, while k_2 depends on only x_n and k_1, and so forth. Therefore, the right-hand-side of equation (6.33) ultimately depends only upon x_n and y_n. Thus, the fourth-order Runge-Kutta solution of equation (6.32) is obtained by iterating equation (6.33), beginning at the known initial condition $y_0 = y(x_0)$. To solve second order differential equation by Runge-Kutta method, re-write the single second-order equation given in equation (6.30) as the pair of first-order equations given in equation (6.31). Simultaneously iterate the pair of equations in equation (6.31) using the fourth-order Runge-Kutta algorithm embodied in equation (6.33).

6.3 RESULTS AND DISCUSSION

A FORTRAN computer program is written based on the above formulation to study the dynamic response of the heated tube. The trends of the results obtained have similarities when compared with the existing literature (Blandino and Thornton 2001) for an internally heated twin tube coupled by a tip mass undergoing thermally induced vibrations. The flow chart in Figure 6.9 shows the computational steps involved in evaluating the temperature distribution along the length of the tube and the procedure for computing dynamic displacement and velocity at the tip of the cantilever tube.

Table.6.2 Thermal- Structural data for the tube used for numerical analysis.

(304 grade stainless steel)

Parameter	Symbol	Value
Beam Length	L	870 mm
Tube Diameter	D	2.76 mm
Wall thickness	H	0.22 mm
Mean Coefficient of Thermal Expansion, 0-100°C	α	17.2 μm/m/°C
Elastic Modulus	E	193 GPa
Damping ratio	ξ	0.001
Thermal Conductivity at 100°C	k	16.2 W/m.K
Specific Heat, 0-100°C	c_p	500 J/kg.K
Density	ρ	8000 Kg/m^3
Natural convective heat transfer coefficient	h_c	5 W/m$^{2.0}$K

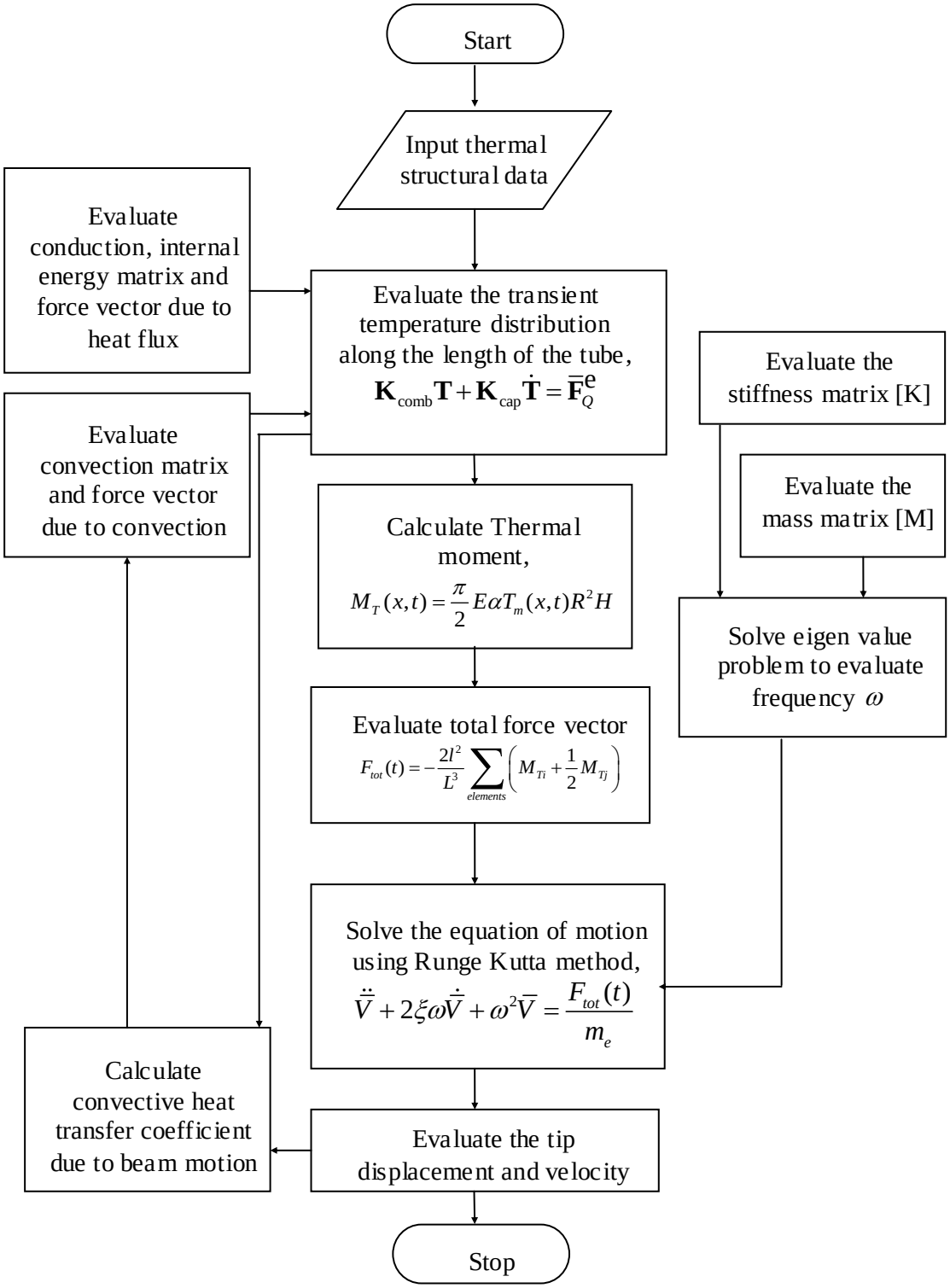

Fig 6.9 Flow chart showing the computation of temperature and dynamic displacement.

6.3.1 ISOTHERMAL FREE VIBRATIONS

The damped response of the tube is predicted in the absence of a forcing function. Displacement data for two tubes, one with natural frequency of 0.846 Hz and the second with natural frequency of 1.321 Hz are compared. The natural frequencies were determined using a FEM code for the vertical cantilever tube fixed at top with tip mass at bottom (Tip mass attached were 47.3 gm and 17.3 gm respectively). Figure 6.10(a) and 6.10(b) show the predicted tip displacement data for the free vibration. Given an initial displacement of 10 mm, the tube with natural frequency of 1.321 Hz comes to rest faster (i.e. it takes nearly half the time) than the other tube with natural frequency of 0.846 Hz.

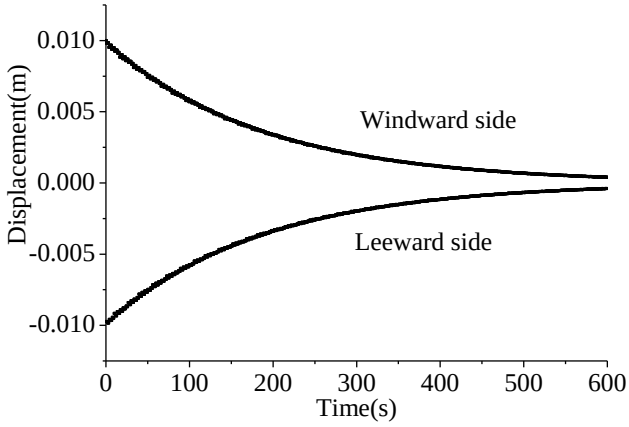

(a) 0.846 Hz tube

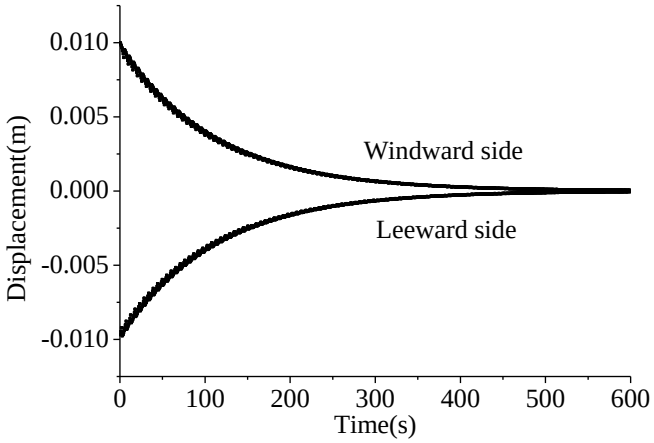

(b) 1.321 Hz tube

Fig 6.10 Isothermal free vibration displacement histories for two tubes.

6.3.2 RESPONSE OF HEATED TUBE

To find the effect of heating rate on amplitude of vibration, results are compared for three different heating rates. The beam used in the computation had a tip mass of 47.3 gm and natural frequency of 0.846 Hz. Results are compared for heating rates of 7.5 W, 10 W and 15 W as shown in Figure 6.11. The temperature histories at X=783 mm from the fixed end of the tube are illustrated in Figure 6.11(a), while Figure 6.11(b) shows the displacement histories. In evaluating the convection heat transfer coefficient, the constant a in equation (6.4) was chosen to be equal to 1.0.

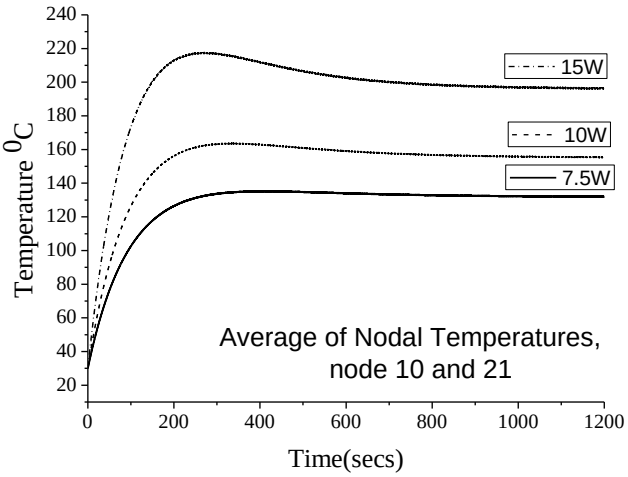

(a) Temperature histories

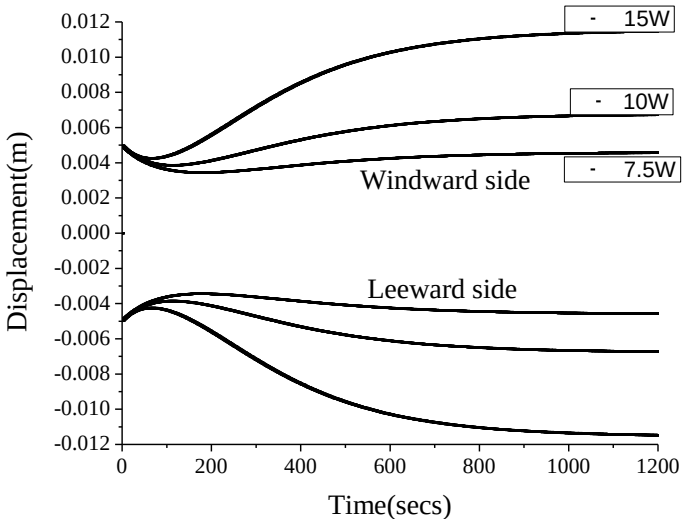

(b)) Tip displacement

Fig. 6.11 Temperature histories and Tip displacement for different heating rates.

The analysis predicts a faster amplitude growth for higher heating rates. While for lower heating rates, the amplitude of vibration decreases with time due to the fact that, the heat supplied is not sufficient to produce thermal moments that can cause thermal vibrations. From Figure 6.11(a), it is observed that, for a peak temperature of 217 ^{0}C and at approximately 200 seconds the displacement is around 6 mm, which is less than the maximum amplitude of vibration of 12 mm for a heating rate of 15 W.

Figure 6.12 shows the variation of convective heat transfer coefficient with respect to time on either sides of tube for natural frequency of 0.846 Hz and heating rate of 7.5 W. The convective heat transfer coefficient at a time instant consists of natural convective heat transfer coefficient and the forced convection generated by the to and fro motion of the tube.

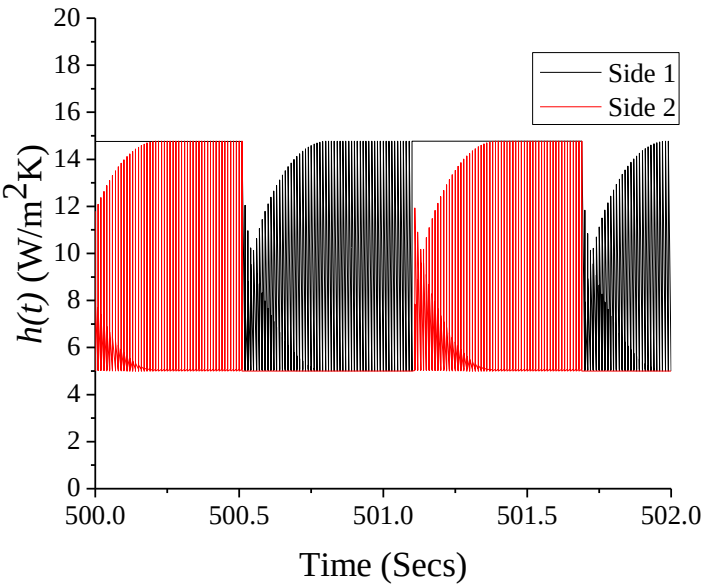

Fig. 6.12 Variation of convective heat transfer coefficient with time on either sides of tube for natural frequency of 0.846 Hz and heating rate of 7.5 W.

Figure 6.13 illustrates the variation of convective heat transfer coefficient on windward and leeward sides of tube at various points along the length of tube for natural frequency of 0.846 Hz and heating rate of 7.5 W at 500th sec. It is seen from

Figure 6.13 that, on the windward side of the tube the maximum convection is experienced by the tip of the tube and goes on decreasing towards the fixed end of the tube where it is equal to natural convective heat transfer coefficient. On the leeward side of the tube the convection throughout the length of the tube is equal to natural convection.

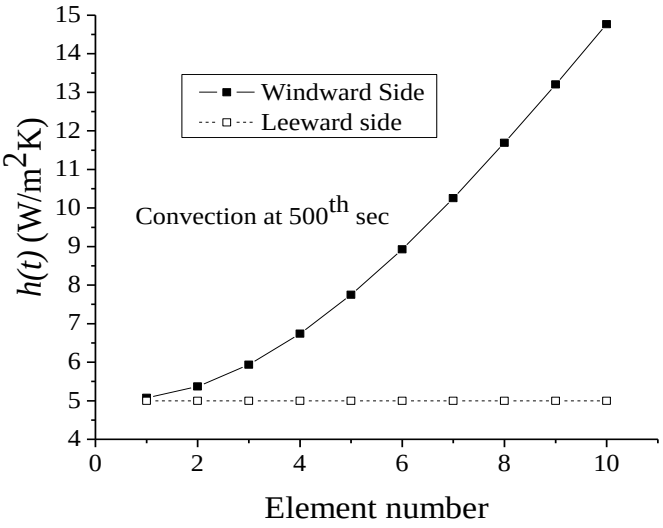

Fig. 6.13 Variation of convective heat transfer coefficient on windward and leeward sides for heating rate of 7.5 W.

The variation of temperature on either sides of tube at various points along the length of tube for natural frequency of 0.846 Hz and heating rate of 7.5 W and time instant of 500^{th} sec is illustrated in Figure 6.14. Consider side 1 as windward side. The maximum temperature on the windward side is seen at the fixed end, where the convective heat transfer coefficient is the lowest and it goes on decreasing towards the free end of the tube where the tube experiences maximum convective heat transfer coefficient. Same phenomenon is observed on the leeward side (side 2) of the tube but the absolute value of the temperature on the leeward side of the tube at particular point is slightly more than the temperature on the windward side as leeward side is exposed to less convective heat transfer coefficient.

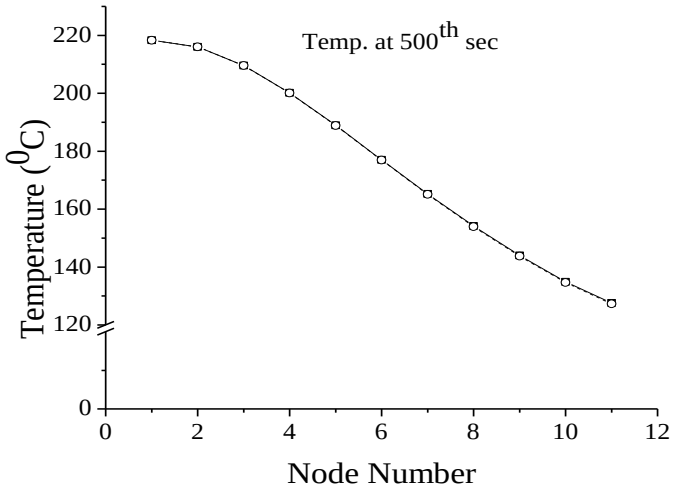

Fig 6.14 Variation of temperature on winward side for heating rate of 7.5 W.

6.3.3 THERMAL VIBRATIONS AT HIGHER FREQUENCY

The predicted displacement and temperature histories are shown in Figure 6.15 for natural frequency of 1.32 Hz. It can be seen from Figure 6.15(b) that the maximum amplitude of vibration is 8 mm in comparison to 12 mm in Figure 6.11(b) for heating rate of 15 W, which clearly indicates that the amplitude of vibration decreases with increase in natural frequency of the tube. In evaluating the convective heat transfer coefficient, the constant a in equation (6.4) was chosen to be equal to 1.

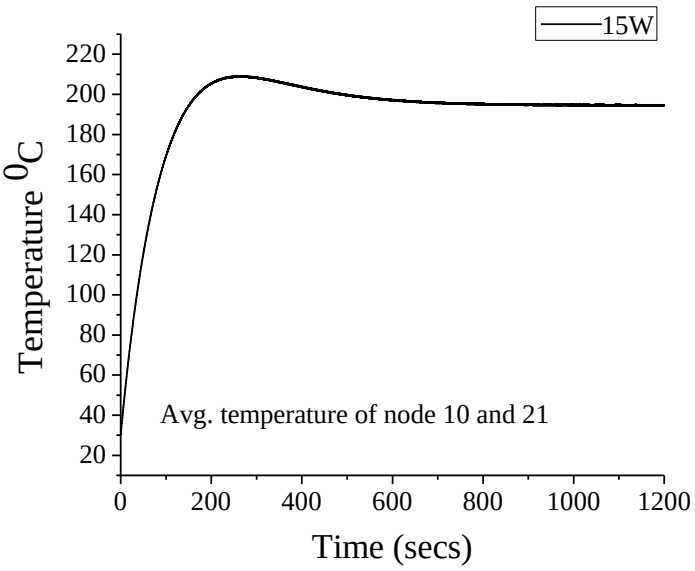

(a) Temperature histories

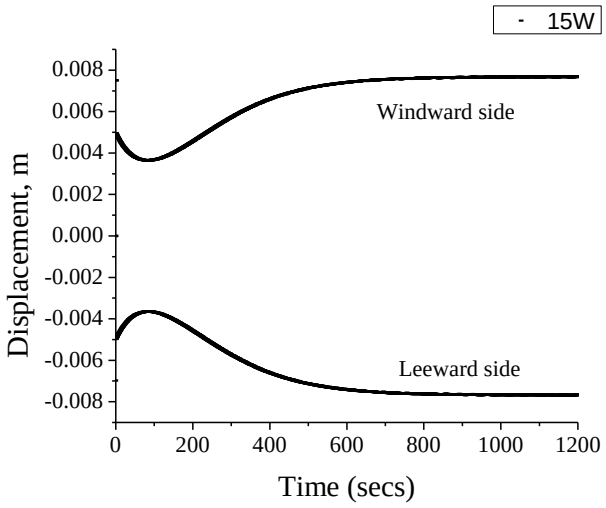

(b) Tip displacement

Fig. 6.15 Temperature histories and Tip displacement for higher frequency.

6.3.4 EFFECT OF CONVECTIVE HEAT TRANSFER COEFFICIENT ON VIBRATION AMPLITUDE

From Figure 6.16(b) it is seen that if the convective currents are low, then the heat lost by convection is less when compared to the heat generated in the tube. This result in the decay of oscillations and the tube will vibrate at lower amplitudes. If the convective currents are increased (i.e. increase the value of a in equation (6.4), where

a varies from 1 to 3) it is seen that the beam vibrates at higher amplitude as in Figure 6.16(b). The corresponding temperatures are shown in Figure 6.16(a)

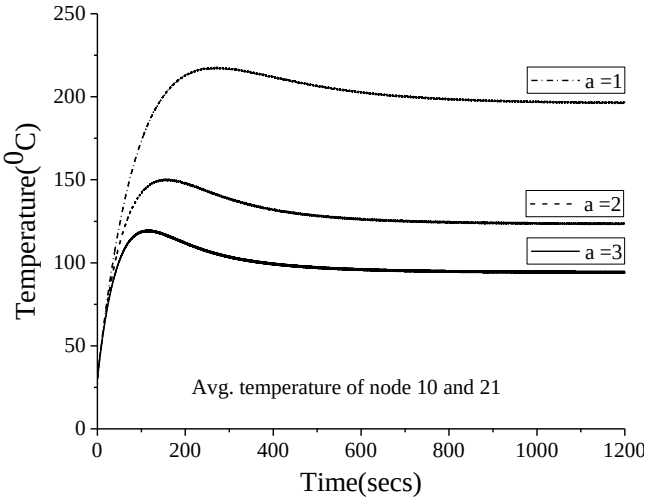

(a) Temperature histories

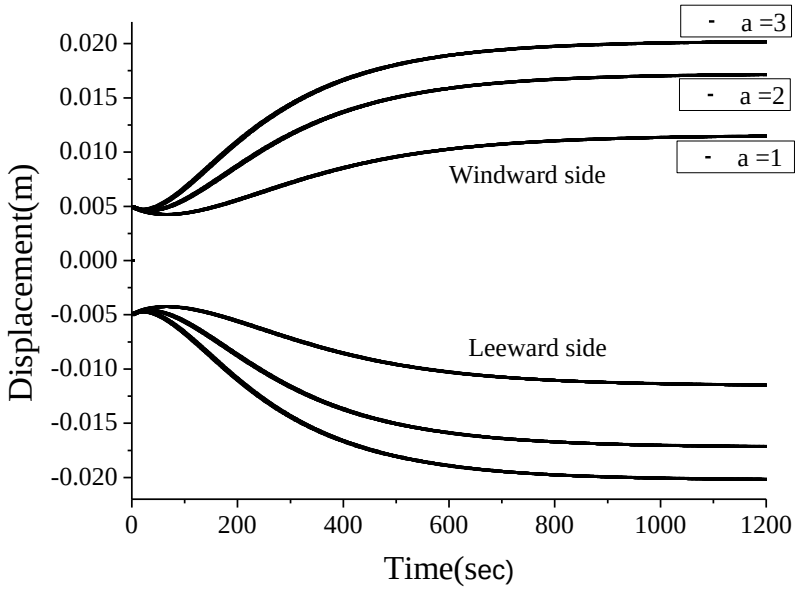

(b)Tip displacement

Fig. 6.16 Effect of Constant ‘ a ’ in Equation (6.4).

6.3.5 EFFECT OF SIZE OF TUBE ON AMPLITUDE OF VIBRATION

To study the effect of diameter of the tube on the amplitude of thermal vibration, the tubes of diameter ranging from 1.86mm to 3.0mm were considered for the study. The thickness and length of the tube was maintained constant and equal to

0.22 mm and 870mm respectively. The heating rate was 15 W and the constant a to account for convection was equal to 1.0. In all the cases, the tube was given an initial displacement of 10 mm and its response over the time period of 1200 sec was studied. The tubes had a tip mass of 47.3 gms. Figure 6.17 shows the plots of tube diameter vs. maximum dynamic tube tip displacement. From the analysis it is seen that as the size of the tube (diameter) is increased keeping thickness constant, the frequency of vibration of tube changes and hence there is decrease in amplitude of vibration for particular heating rate.

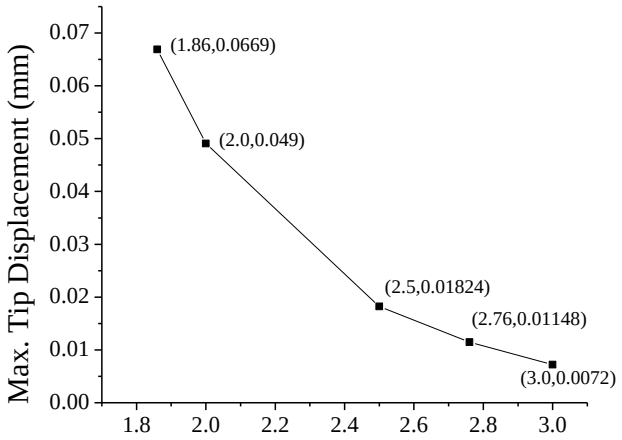

Fig 6.17 Tube diameter vs. maximum thermal dynamic tube tip displacement.

6.3.6 VIBRATION RESPONSE OF HEATED TUBE WITHOUT TIP-MASS

Figure 6.18 illustrates the dynamic response of the tube without tip mass for the heating rate of 15W. Comparing the results of tube with tip mass (refer Figure 6.11) and without tip mass it is found that a heated tube without tip mass is characterized by damped response during the initial period and subsequently the system remains unstable with oscillations remaining constant. In Figure 6.18 it is also evident that the length of the tube has its influence in increasing the final oscillatory amplitude of the system. Thus, it can be said that the natural frequency of the heated tube has a greater role on the amplitude of unstable vibration.

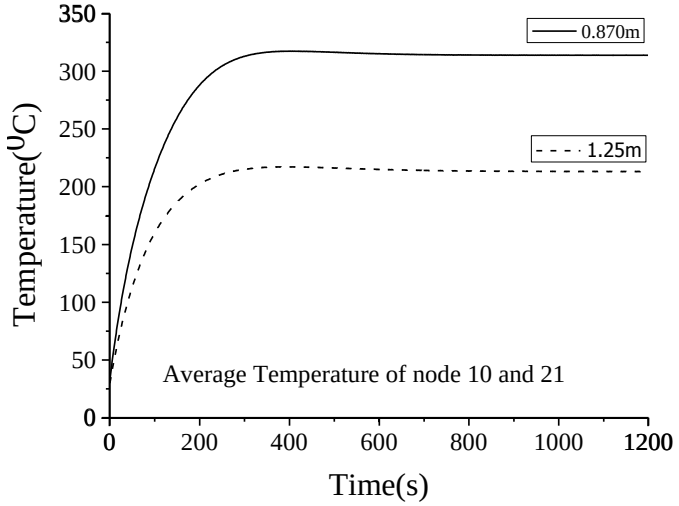

(a) Temperature Distribution for heating rate of 15W.

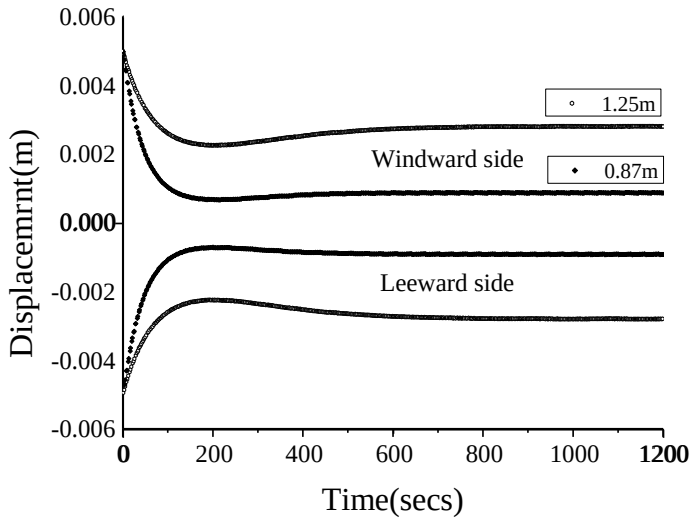

(b)Tip Displacement response of tube for heating rate of 15W.

Fig. 6.18 Temperature and displacement for a heated tube without tip mass.

Comparing the temperature plots in Figure 6.11(a) and Figure 6.18(a), it is seen that the tube without tip mass doesn't shows the sudden peak in the temperature and then gradual decrease to attain steady as seen from Figure 6.11(a) for the tube with tip mass. This is because the amplitude of vibration (refer Figure 6.11(b)) in case of tube with tip mass is higher than the one without tip mass giving rise to higher value of convective heat transfer coefficient and hence, more cooling and overall decreases in the surface temperature of the tube.

6.3.7 MECHANISM CAUSING THERMAL VIBRATIONS

The difference in the magnitude of the forced convection on the windward and leeward faces of the tube as it oscillates (to and fro motion) causes the temperature difference on either sides of the tube which causes the thermal moment. To elaborate, consider the thermal moment and velocity profiles as the tube vibrates over a time period as shown in Figure 6.19, for a beam with a natural frequency of 0.846 Hz and heating rate of 15 W. It can be seen that the absolute value of the thermal moment is at a maximum when the velocity nears to zero and vice-versa. As discussed by Blandino and Thornton 2001, it is appropriate to conclude that there exists a coupling between the thermal moment and the velocity, hence causing the vibration amplitude to grow with time. The velocity is at a maximum when the beam is in the vertical position whereas the thermal moment is minimum and nears to zero.

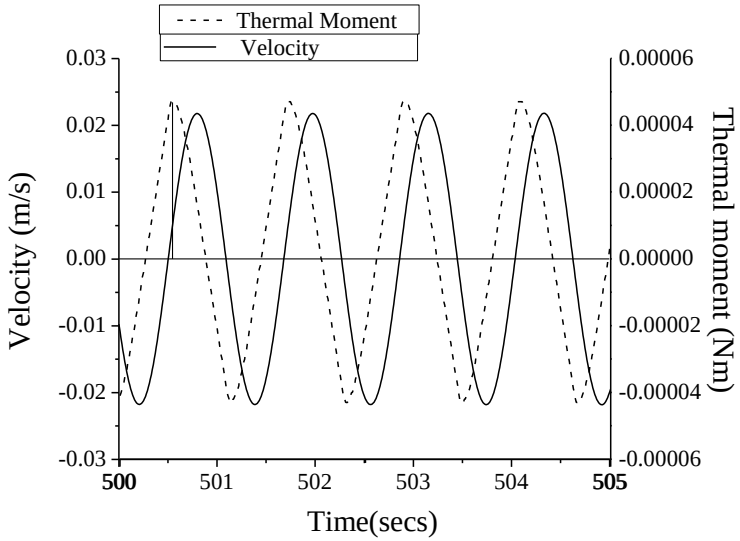

Fig. 6.19 Comparison of Velocity and Thermal moment.

6.3.8 EFFECT OF INITIAL DISPLACEMENT ON THERMAL INDUCED VIBRATION

The steady-state vibration amplitude is reached when the internal heating is balanced by convection from the tube surface. The steady-state amplitude is independent of the initial displacement. Hence it may be inferred that the thermally induced vibration fall into the category of self-sustained vibrations. The steady-state

amplitude of the vibration is the amplitude where the vibration neither grows nor decays. In this case the limit cycle is the amplitude where the energy removed by convection is equal to the energy from the internal heating.

Consider the tube of natural frequency 0.846 Hz with a heating rate of 15 W, and given an initial displacement of 20 mm, Figure 6.20 (a) shows that the vibrations decay to a limit cycle of approximately 12 mm. While in Figure 6.20 (b) the beam is given an initial displacement of only 5 mm for same heating rate where the amplitude grows to a limit cycle of approximately 12 mm. Although the initial condition varies significantly the same limit cycle is reached in both the cases.

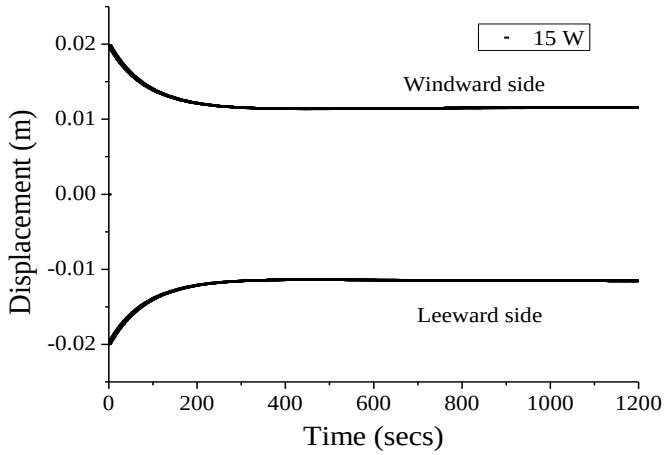

(a) Initial displacement of 20 mm.

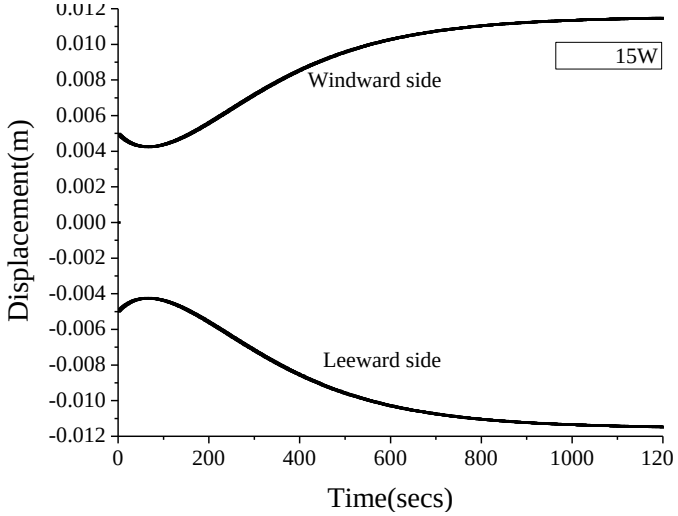

(b) Initial displacement of 5 mm.

Fig. 6.20 Tip displacement history.

6.4 SUMMARY

Computational studies are presented on the vibration behavior of a tube with internal heating with and without tip mass. The theoretical approach in simulating convection heat loss for oscillating tube has shown to provide results which have similar trends as reported in literature, Blandino and Thornton (2001). For a range of heating rates between 7.5 and 15 W, the model predicted reasonably well transient temperature distribution and hence the steady-state temperature. It is also to be noted that the amplitude of vibration depends on the tube natural frequency and heat transfer coefficient during forced convection. It is also noticed that for a particular heating rate for the tube, the amplitude of thermally induced self sustained oscillations were independent of the initial excitation.

CHAPTER 7

THEORETICAL AND EXPERIMENTAL STUDIES ON THERMALLY INDUCED VIBRATION OF TUBE WITH TIP MASS

7.1 INTRODUCTION

The main objective of this chapter is to simulate through theoretical model and validate experimentally the dynamic response of the internally heated vertical cantilever tube with tip mass. Internal heating is achieved by means of passing electric current through the tube. In the previous chapter, a mathematical formulation for the thermal-structural behavior of an internally heated tube was discussed. The formulation was verified with the results available in the literature. In the present chapter the experimental results are compared with the results evaluated from the theoretical model for an internally heated tube undergoing thermally induced vibration.

7.2 CONFIGURATION OF TUBE WITH TIP MASS AND FINITE ELEMENT DISCRETIZATION

Figure 7.1(a) shows the front and side view of the tube along with the attachments. A metallic tip mass was attached at the free end of the tube. The coated copper wire was attached to the tip mass and it was passed through the tube until it reaches the top end of the tube which acted as one lead for connecting to the power supply. The fixed end of the tube acted as another lead, thus forming a closed electric circuit in conjunction with the power supply as in Figure 7.1(a). The finite element idealization of this tube configuration for the theoretical study is shown in Figure 7.1(b). The tube was heated internally by passing current through the tube. To analyze the vibrations set by initial excitation, the thermal and structural problems are coupled. The theoretical model used for the analysis is same as that discussed in

Chapter 6 (Section 6.2) for the cantilever tube with tip mass. Thermal and structural data for the tube used for the experimental and numerical analysis is given in the Table 7.1

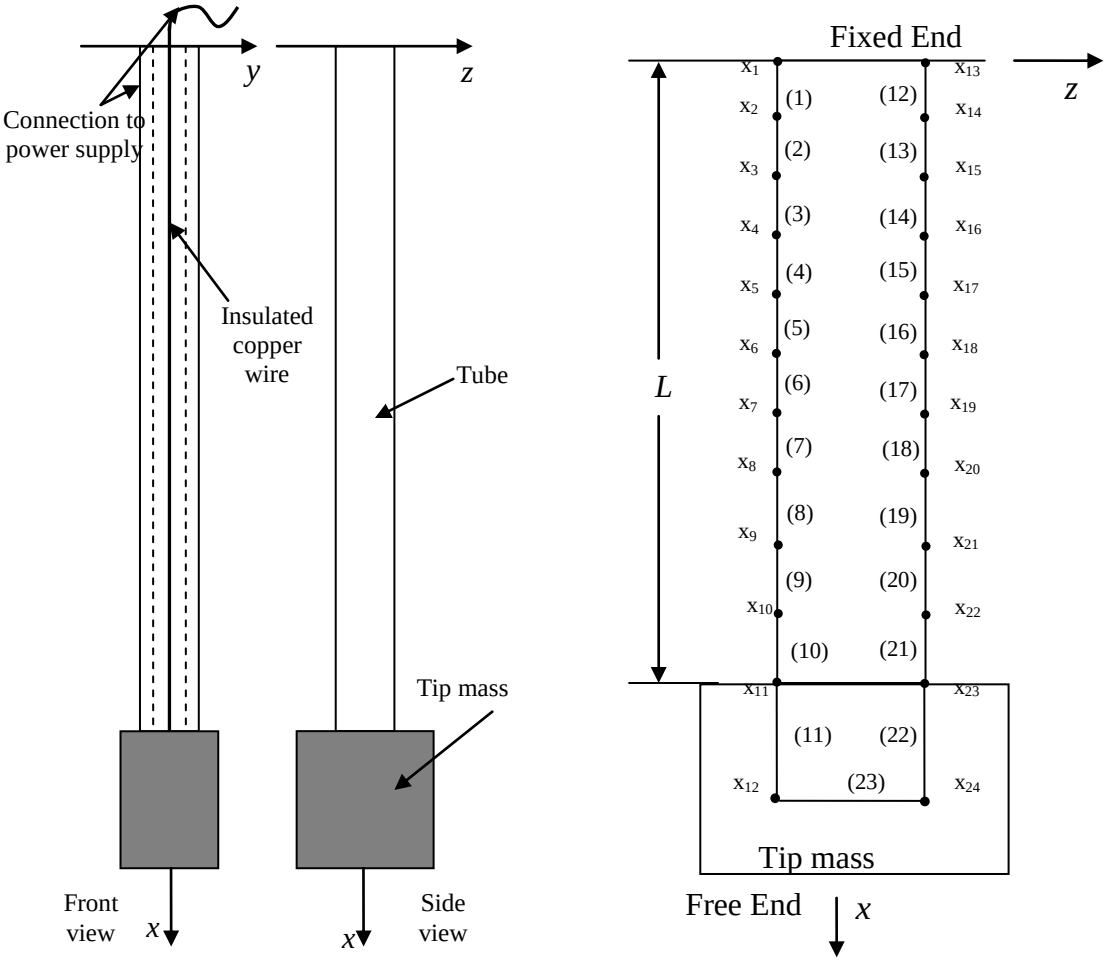

(a) Model of the tube for internal heating.

(b) Finite element idealization of the tube for temperature computation.

Fig. 7.1 Configuration of the tube with tip mass.

7.3 EXPERIMENTAL SETUP

The test specimen used for the experimental investigation was a stainless steel SS304 tube of 460 mm long with 1.86 mm external diameter and 1.42 mm internal diameter. In order to obtain the desired natural frequency, the tube was connected by a mild steel tip mass of 34 gm. The test specimen was mounted inside a wooden test box of 300 mm wide, 300 mm long and 1100 mm high with three sides of the box covered with perspex glass. The test box performed several functions: (i) the walls of the box prevented cross currents from affecting the convection heat transfer from the surface of the tube (iii) provide clamped support for holding the tube (iii) allowed for mounting of instrumentation.

Table.7.1: Thermal-Structural data for the tube used for experimental and numerical analysis (304 grade stainless steel).

Parameter	Symbol	Value
Beam Length	L	460 mm
Tube Diameter	D	1.86 mm
Wall thickness	H	0.22 mm
Mean Coefficient of Thermal Expansion, 0-100°C	α	17.2 μm/m/°C
Elastic Modulus	E	193 GPa
Damping ratio	ξ	0.001
Thermal Conductivity at 100°C	k	16.2 W/m.K
Specific Heat, 0-100°C	c_p	500 J/kg.K
Density	ρ	8000 Kg/m^3
Natural convective heat transfer coefficient	h_c	20 W/m^{2}/K

A thermocouple was mounted inside the test box to measure the ambient temperature, which was recorded by means of digital thermometer. Beam displacements were measured directly with a laser displacement sensor. The sensor head was located approximately 40 mm from the tip mass. The sensor used has ± 10 mm resolution with a response time of 1 ms. The sensor was positioned such that the

laser beam reflected off a point near the center of the tip mass. The output of the laser sensor was 5 V direct current. The output from the laser pickup was supplied to the data acquisition system. The data acquisition program in LabVIEW through a closed loop, control the acquisition of displacement data from the test specimen. Figure 7.2 is the block diagram in LabVIEW showing the data acquisition control circuit.

The power supply used to supply the current to the test beam, delivered up to 5 A and 65 V. The heating is carried out by using the tube as a resistance heater by connecting the either ends of the tube to power supply. In order to achieve this, a thin insulated copper wire was passed through the tube and connected to the tip mass at the free end of the tube. A photograph of the experimental setup with laser pickup, data acquisition system and power supply is shown in and Figure 7.3(b). The block diagram of the experimental setup is shown in Figure 7.3(a).

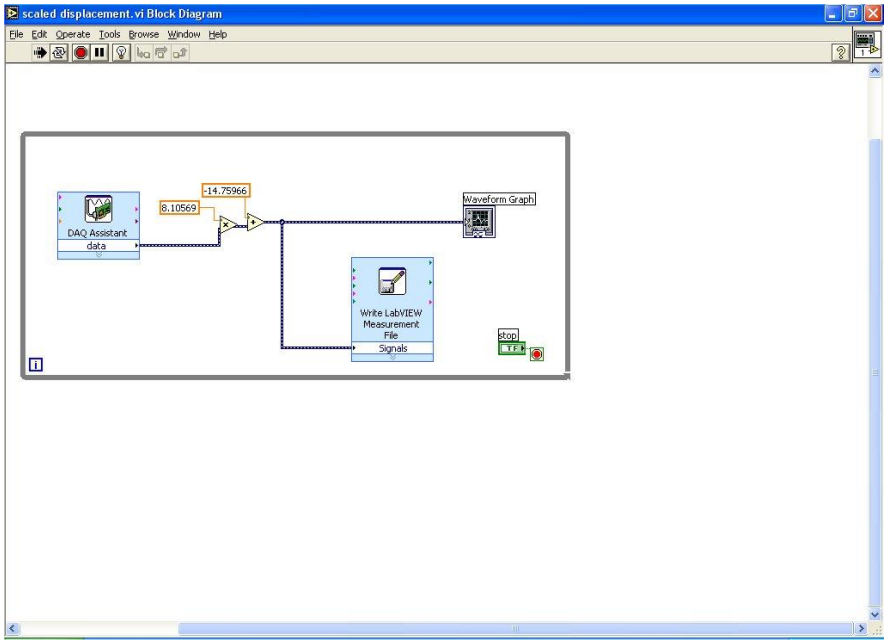

Fig. 7.2 Block diagram in LabVIEW showing the data acquisition control circuit.

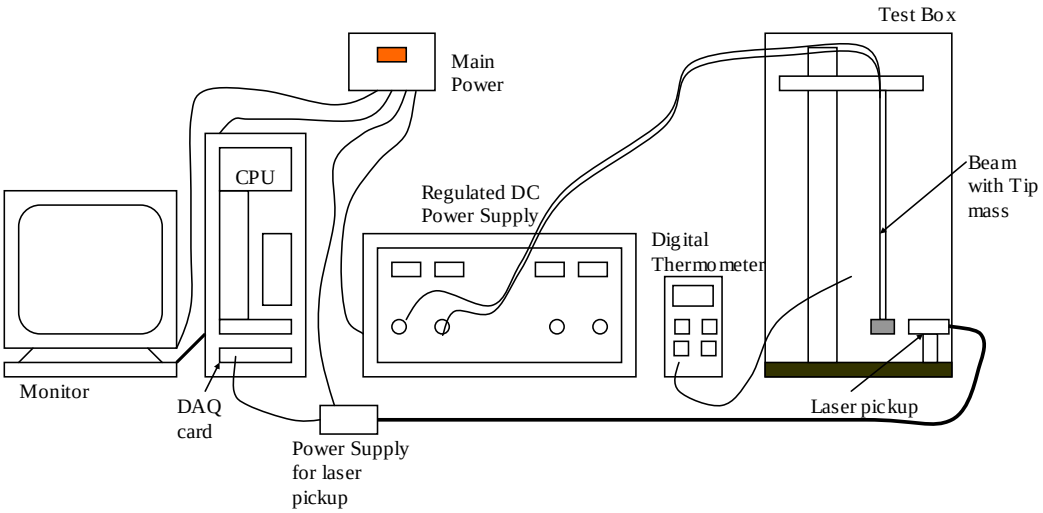

(a) Block diagram

(b) Photograph

Fig. 7.3 Experimental Setup.

7.4 RESULTS AND DISCUSSION

A FORTRAN computer program is written based on the formulation given in Chapter 6 which now incorporates the modified approach in the evaluation of forced convective heat transfer coefficient to study the dynamic response of the heated tube. The trends of the results obtained have similarities when compared with the experimental results for an internally heated tube undergoing thermally induced vibrations. The studies were carried out for the heating rates ranging from 6 W to 12

W. The displacement histories and temperature variation on the tube surface with respect to time were obtained and compared with the experimental results. The experiments for each heating rates were carried out for 1200 seconds.

7.4.1 ISOTHERMAL FREE VIBRATIONS

The damped response of the tube is predicted in the absence of a forcing function. By carrying out FFT on the experimentally obtained tip displacement data the natural frequency of the tube at the room temperature of 38^0C was calculated and is equal to 1.41 Hz. The natural frequency was also determined using a FE code for the vertical cantilever tube fixed at the top and with a tip mass at bottom and was equal to 1.395 Hz, which is close to the experimentally obtained value. Figure 7.4 shows the predicted and experimental tip displacement data for the free vibration. Given an initial displacement of approximately 10 mm, it takes 500 seconds for the tube to come to rest. It is seen that there is good agreement over the entire 500 seconds range between the predicted and experimental values for the isothermal case.

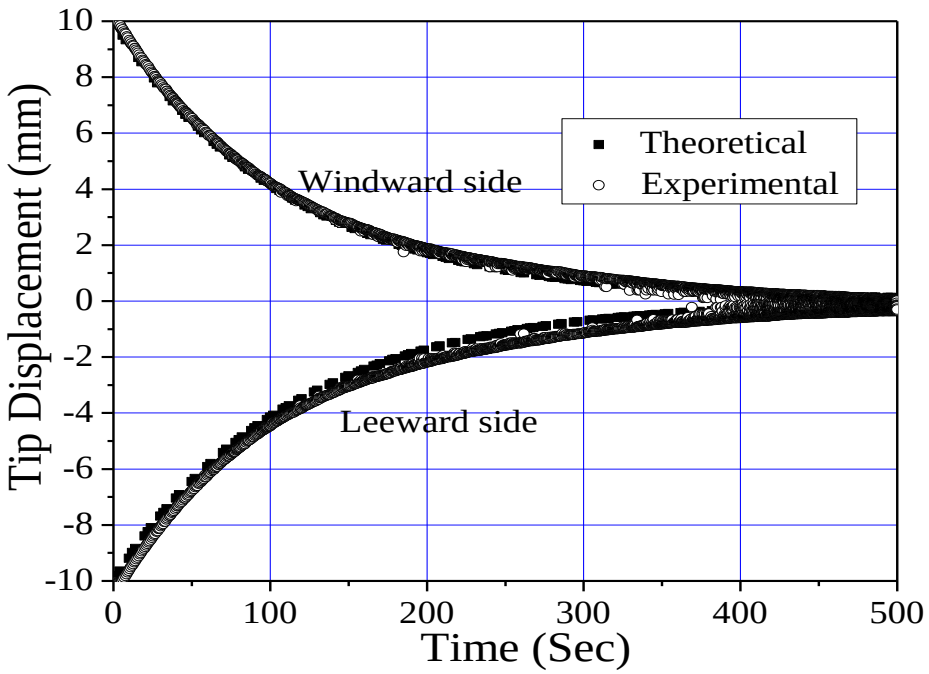

Fig. 7.4 Isothermal free vibration displacement histories for the tube.

7.4.2 RESPONSE OF HEATED TUBE AT DIFFERENT HEATING RATES

To determine the effect of heating rate on vibration growth, results are compared at six different heating rates. The tube used in the experiments had a natural frequency of 1.41 Hz. The results are compared for heating rates of 12 W, 10.8 W, 9.4 W, 9 W, 8 W and 6 W. Figure 7.5 compare the tip displacement and temperature histories obtained from the experimental investigation and the theoretical analysis for the tube which is subjected to internal heating of 12 W. Only the envelopes of the peak values are shown. Figure 7.5(a) shows the tip displacement histories, while Figure 7.5(b) shows the predicted temperature histories at X = 410 mm from the fixed end of the tube. The temperature shown is the average of the two nodal temperatures at this location. In Figure 7.5(a) the analysis predicts a faster amplitude growth, but the steady-state displacements are similar. After 1000 sec, the steady-state displacement again starts increasing and the difference in the experimental and theoretical displacements is approximately 8 percent. From Figure 7.5(a), it is observed that, for a peak temperature of 127^0C and at approximately 60 seconds, the displacement is around 5 mm, which is less than the maximum amplitude of vibration of 9 mm.

Figure 7.6 shows the assumed variation of the convection along the length on the surface of the oscillating tube. Curve AB stands for the forced convection curve for the leeward face and CD is for windward face, assuming the tube moving from left to right. The plot is obtained using the numerical data obtained from the FORTRAN code written for the tube vibration problem. As explained in Chapter 6, it is to be noted that the difference in the magnitude of the forced convection on the windward and leeward faces of the tube, as it vibrates, causes the temperature difference on either side of the tube which causes the thermal moment.

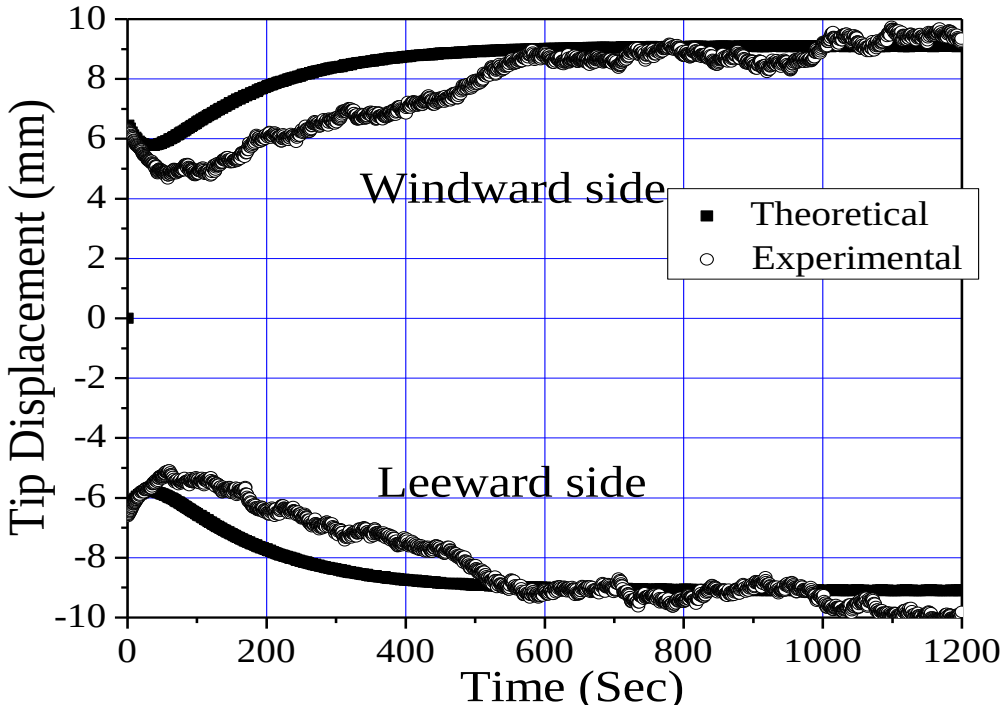

(a) Tip displacement

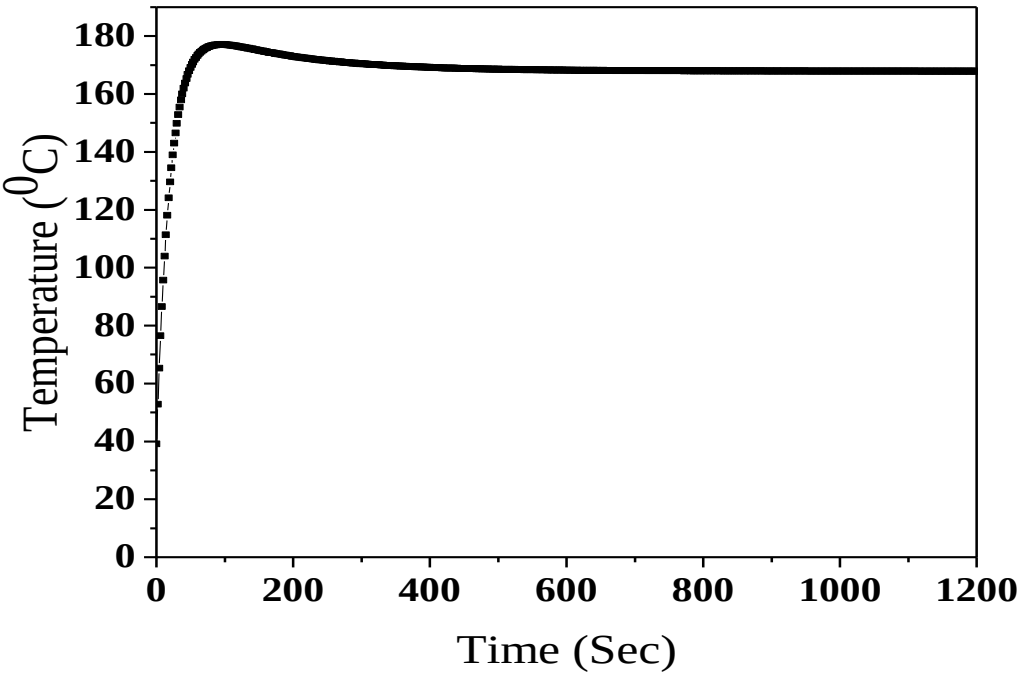

(b) Predicted temperature histories at X = 410mm

Fig 7.5 Displacement and temperature histories for the tube for heating rate of 12 W.

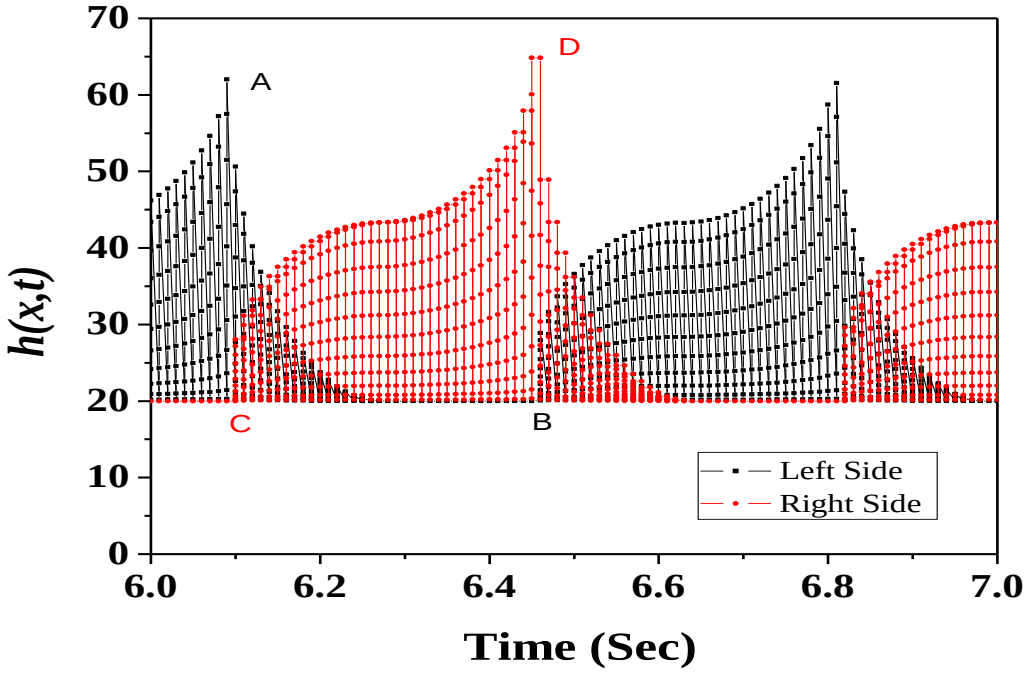

Fig 7.6 Variation of convective heat transfer coefficient on surface of the tube.

Figures 7.7 to 7.11 shows the tip displacement and temperature histories obtained from the experimental work and the numerical analysis for the tube subjected to heating rates of 10.8 W, 9.4 W, 9 W, 8 W and 6 W respectively. It is seen that the theoretical analysis predicts a faster amplitude growth for higher heating rates, while for lower heating rates, the amplitude of vibration decreases with time due to the fact that, the heat supplied is not sufficient to produce thermal moments that can cause thermal vibrations. It is also observed that as the heating rate is decrease the experimental values considerably differ from the theoretical values.

Table 7.2 and Table 7.3 produces a comparison of theoretical and experimental tip displacement at time equal to 250 seconds and 1000 seconds during the tip displacement history. The percentage error in relation to the experimental displacement is reasonably high at 250 seconds when compared to 1000 seconds. However note that the percentage error is considerably large at 1000 seconds for the heating rate of 6 W.

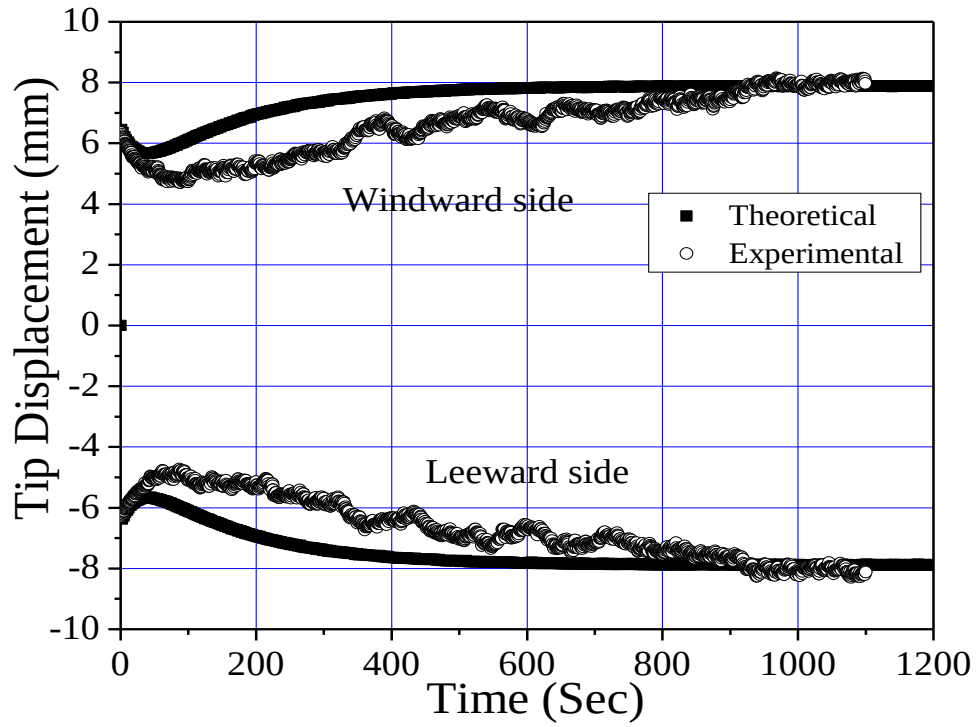

(a) Tip displacement

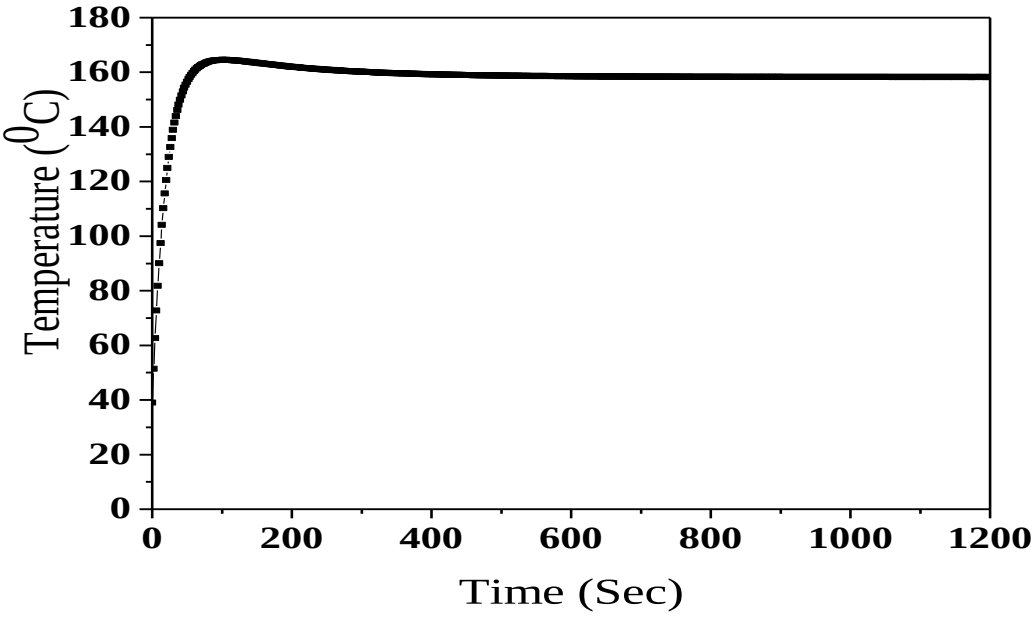

(b) Predicted temperature histories at X = 410mm

Fig 7.7 Displacement and temperature histories for tube for heating rate of 10.8 W.

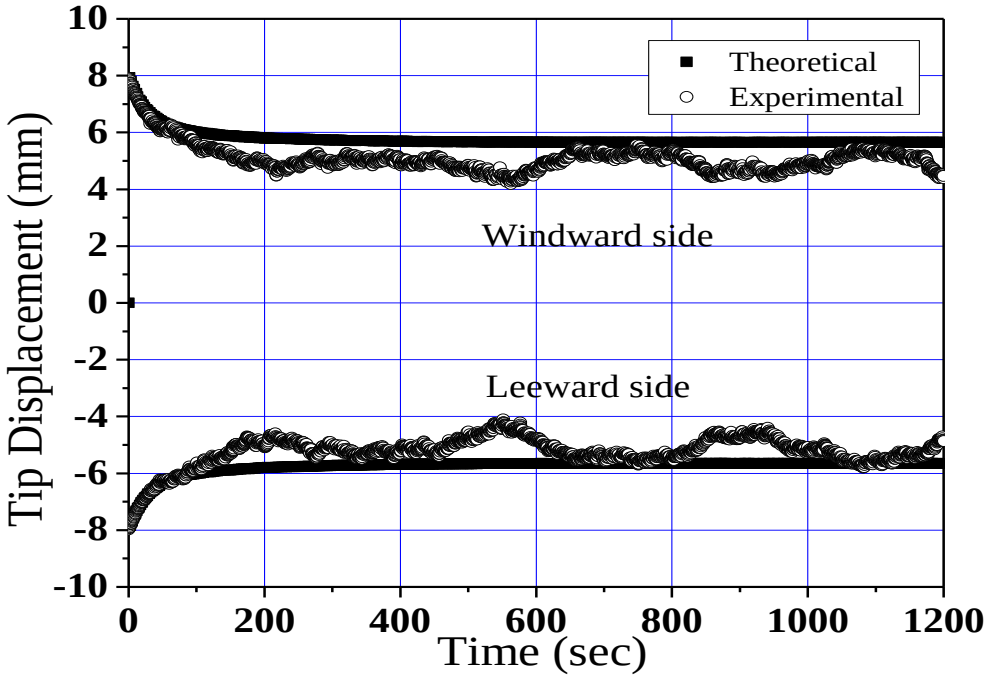

(a) Tip displacement

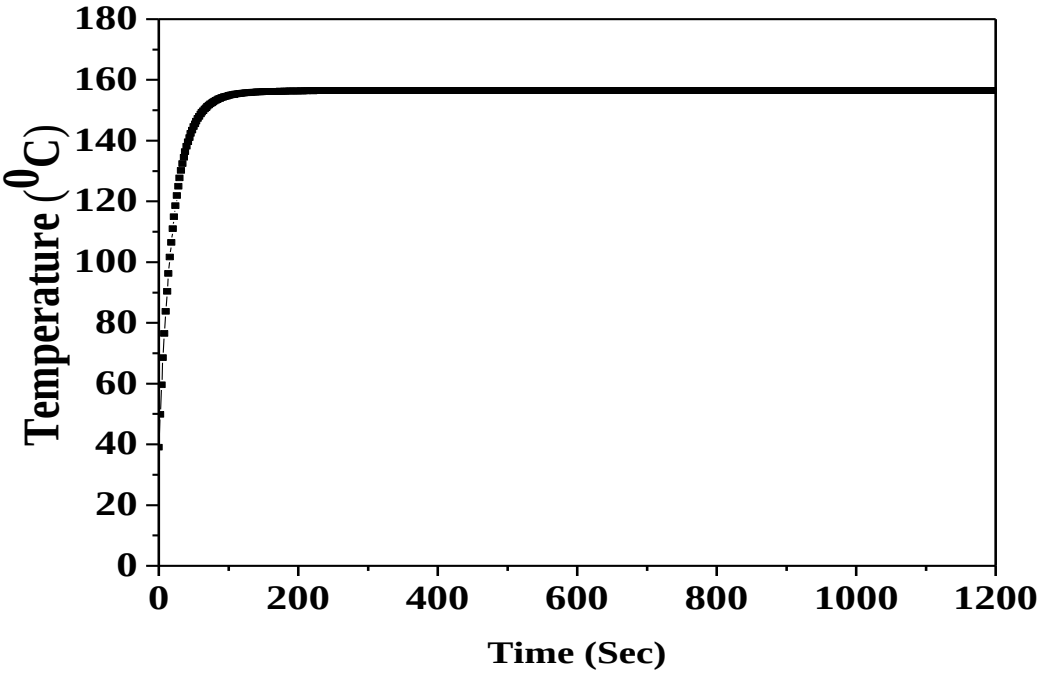

(b) Predicted temperature histories at X = 410mm

Fig. 7.8 Displacement and temperature histories for tube for heating rate of 9.4 W.

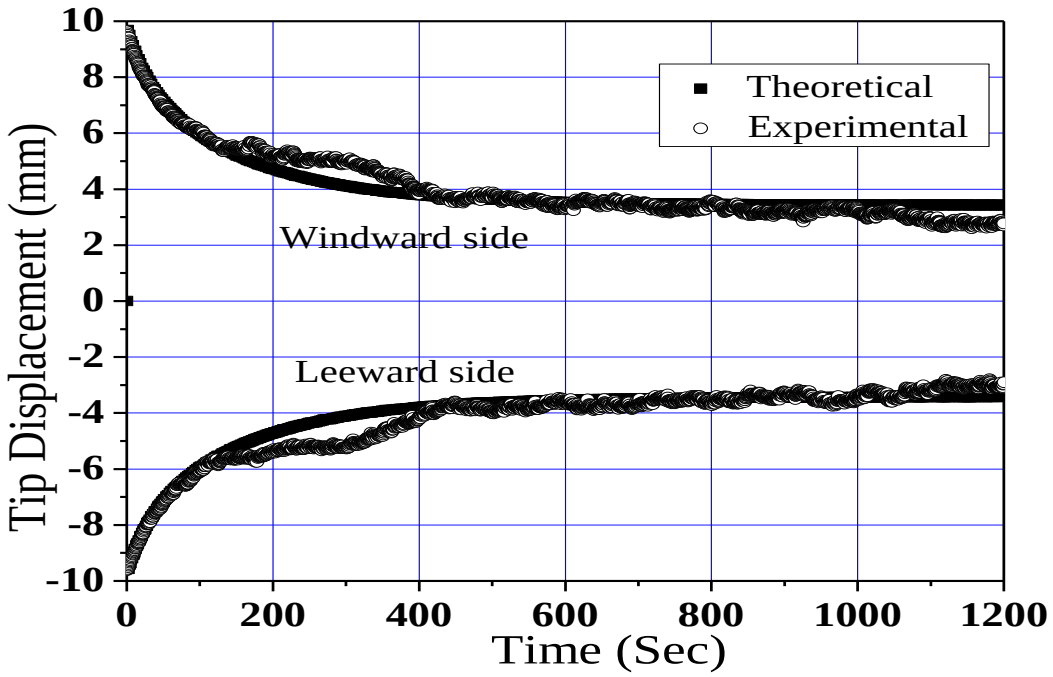

(a) Tip displacement

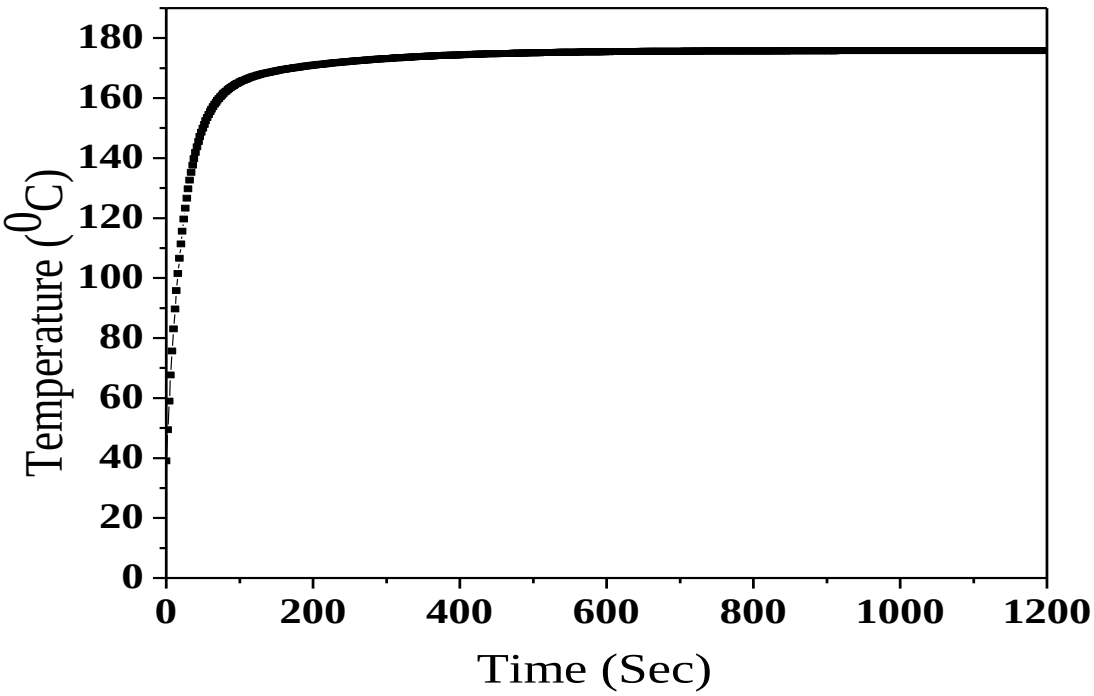

(b) Predicted temperature histories at X = 410mm

Fig. 7.9 Displacement and temperature histories for the tube for heating rate of 9 W.

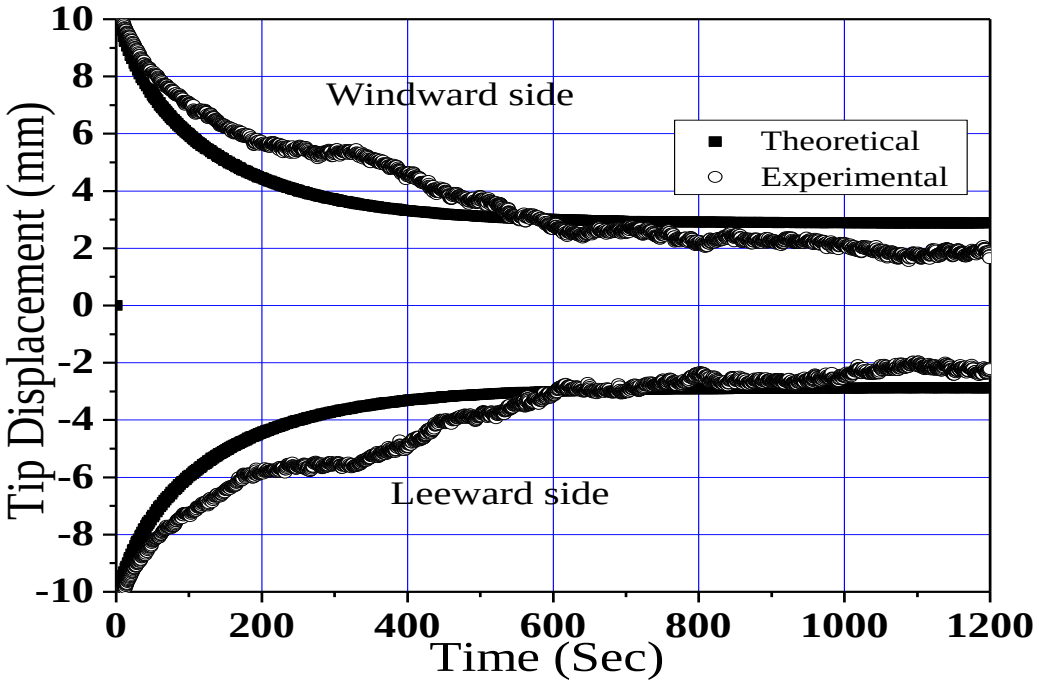

(a) Tip displacement

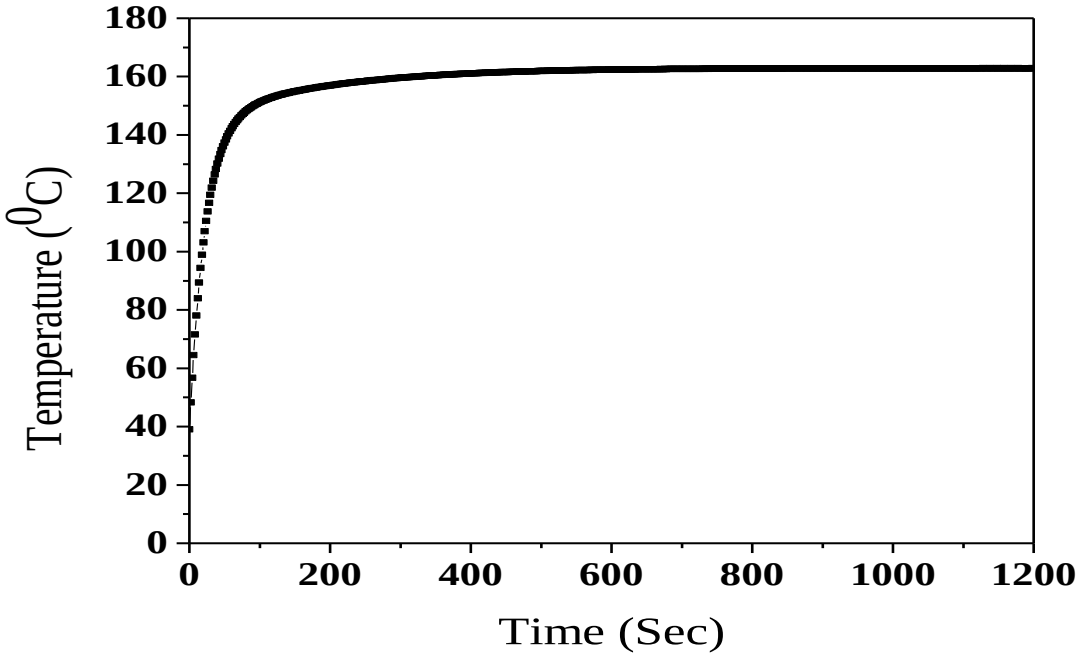

(b) Predicted temperature histories at X = 410mm

Fig. 7.10 Displacement and temperature histories for the tube for heating rate of 8 W.

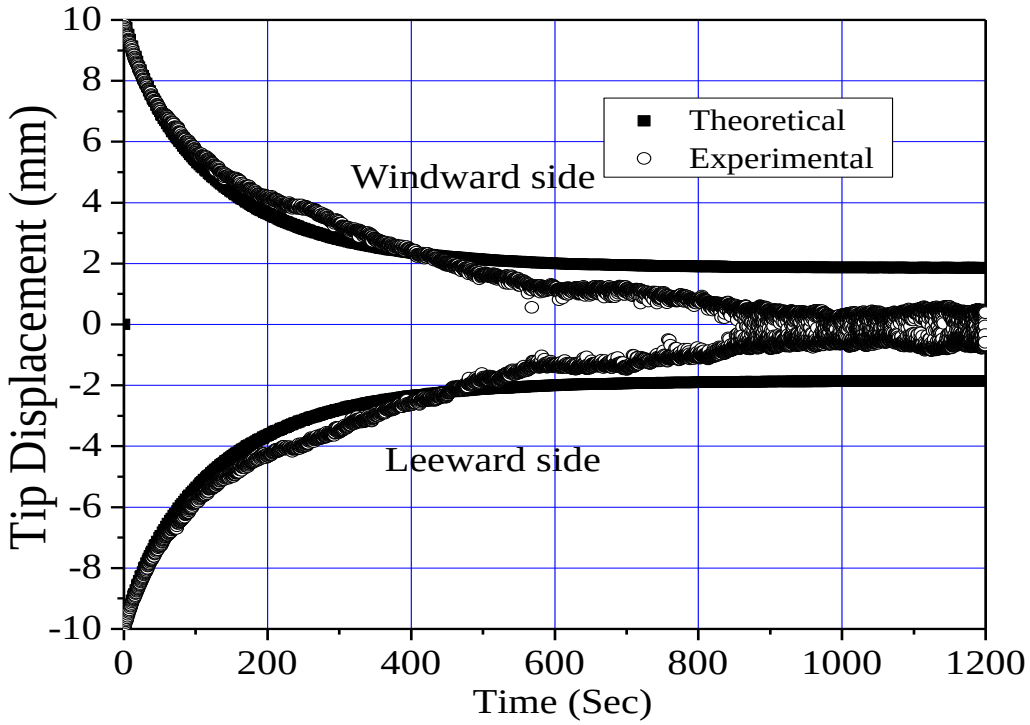

(a) Tip displacement

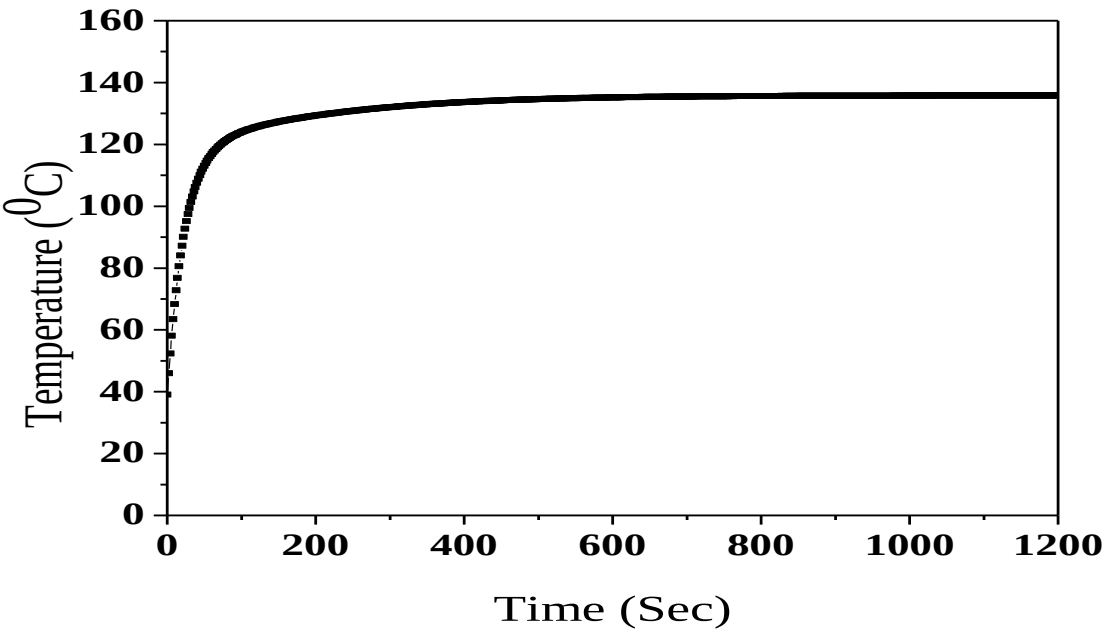

(b) Predicted temperature histories at X = 410mm

Fig 7.11 Displacement and temperature histories for the tube for heating rate of 6 W.

The following observations were made from the study: The theoretical model was used to predict the steady-state temperatures of the oscillating tube as well as the temperature variation along the length of the tube. The model predicted the steady-state displacements adequately close to the experimental displacement time history. It is seen that the temperature of the tube increases very rapidly and tries to attain steady state as time progresses, but the temperature corresponding to maximum amplitude of vibration is quite lower than the maximum temperature attained by the tube. Once initiated, the amplitude of the vibration increases until the amplitude, such that the heat removed by convection balance the internal heating.

Table 7.2: Comparison of theoretical and experimental tip displacement at 250 seconds of displacement-time history.

Sl. No	Heating rate (W)	Theoretical tip displacement (mm)	Experimental tip displacement (mm)	% Error w.r.t. experimental displacement
1	12.0	7.12	6.6974	6.04
2	10.8	6.19	5.565	8.7
3	9.4	4.77	4.931	3.3
4	9.0	4.56	4.73	3.6
5	8.0	4.52	4.35	3.8
6	6.0	3.65	3.951	7.6

Table 7.3: Comparison of theoretical and experimental tip displacement at 1000 seconds of displacement-time history.

Sl. No	Heating rate (W)	Theoretical tip displacement (mm)	Experimental tip displacement (mm)	% Error w.r.t. experimental displacement
1	12.0	9.1	9.322	2.38
2	10.8	7.89	7.874	0.203
3	9.4	5.26	5.092	3.2
4	9.0	3.44	3.462	0.635
5	8.0	2.58	2.478	3.9
6	6.0	1.87	1.715	8.3

7.5 SUMMARY

Computational studies are presented on the vibration behavior of an internally heated tube with tip mass. The theoretical approach in simulating convection heat loss for oscillating tube has shown to provide results which are in close agreement with the experimentally obtained vibration amplitude. For a range of heating rates between 6 W to 12 W, the model was used to predict the transient temperature distribution and hence the steady-state temperature. The model predicted the steady-state displacements accurately, although it predicted the displacement histories with some error for lower heating rates. It is also noted that the amplitude of vibration depends on heat transfer coefficient during forced convection. The displacement histories which are initiated due to initial displacement, with passage of time exhibit an initial decrease in the displacement and gradually increased to a maximum value depending on the heating rate and the magnitude of the sustained oscillations were governed by the fact that the heat removed by convection balanced the internal heating.

CHAPTER 8

THEORETICAL AND EXPERIMENTAL STUDIES ON THERMALLY INDUCED VIBRATION OF U-TUBES

8.1 INTRODUCTION

The main objective of this chapter is to study experimentally the dynamic response of the vertical tube bent to a U shape and compare the results with the theoretical results. The ends of the two limbs of the U tube are fixed. These two ends of the tube also serve the purpose of supplying power. The bent junction of the tube may be left free or a tip mass may be attached (Figure 8.1). The tubes were heated by means of current supplied by regulated DC power supply. The dynamic response of two different sizes of U-tubes with and without tip mass was studied. The theoretical model is the same as derived in Chapter 6 (Section 6.2) for the single tube with tip mass. The difference lies in computation of thermal moment and it amounts to twice the thermal moment obtained for a single tube. Natural frequency of the U-tube is required to be evaluated, which is input to the thermal vibration code. This has been obtained experimentally and compared with the theoretical frequency obtained from the finite element FORTRAN code for a U-tube configuration. The dynamic response of the U-tubes with tip mass in lateral direction was studied theoretically and experimentally for different heating rates. Only experimental studies were carried out on U-tube without tip mass to study the lateral and transverse displacement response.

8.2 EVALUATION OF FREQUENCY OF U-TUBE WITH AND WITHOUT TIP MASS

Figure 8.2 shows the U-tube with tip mass and the coordinate system. For this configuration of the tube, a 3-D beam element is used for the evaluation of the natural frequencies. Figure 8.3 shows the nodal degrees of freedom for a 3-D beam element. For undamped free vibration the eigenvalue problem has the following form

$$\left[\left[K\right]-\omega_n^2\left[M\right]\right]\{d\}=0, \tag{8.1}$$

where, $[K]$ is the global structural stiffness matrix, $[M]$ is the structural mass matrix, $\{d\} = \{u_i \quad v_i \quad w_i\}^T$ is the nodal degrees of freedom vector, and ω_n is the natural frequency of the beam.

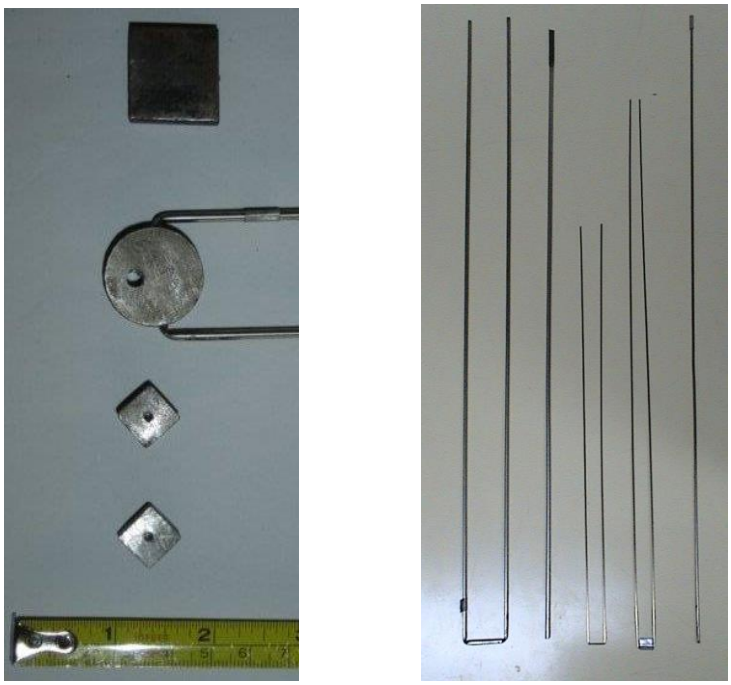

Fig. 8.1 Different tip masses and tubes used for study.

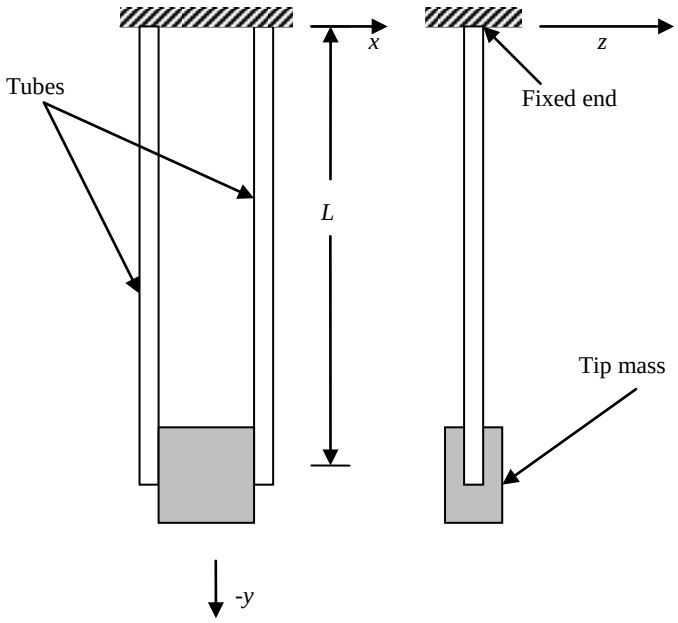

Fig. 8.2. U-tube beam with tip mass and coordinate system.

A FORTRAN computer program is written for the eigenvalue problem in order to obtain the frequency of vibration of U-tube with and without tip mass. The code is validated by comparing the theoretical values with the experimentally obtained frequency data. The U-tube is formed from three different sizes of stainless steel SS304 tubes.

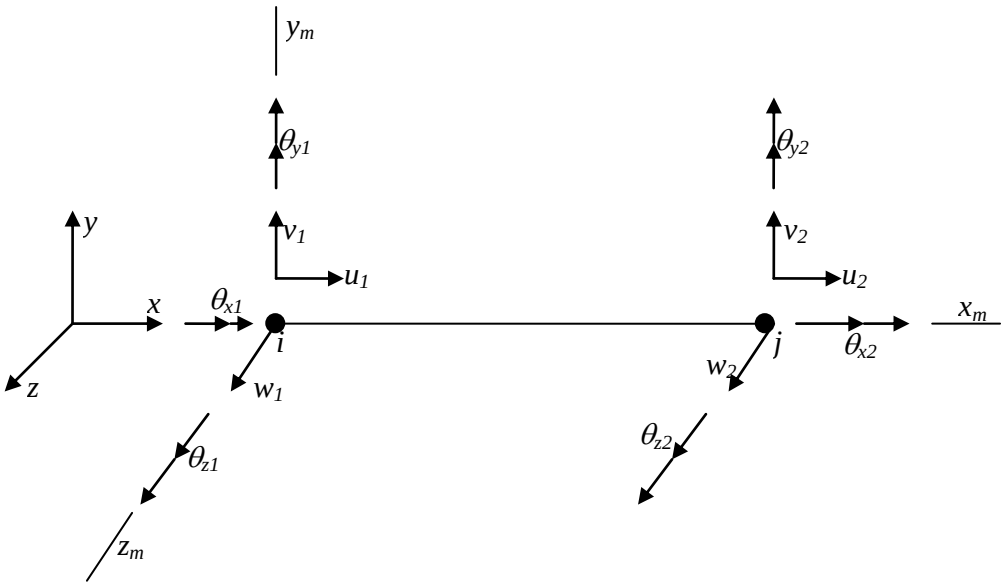

Fig. 8.3 Three dimensional beam element.

8.2.1 STIFFNESS MATRIX FOR THREE DIMENSIONAL BEAM ELEMENT

Consider a three dimensional prismatic beam element with the member axes as shown in Figure 8.4. The x_m axis coincides with the centroidal axis of the member and is positive from *i* to *j*. The y_m and z_m axes are chosen such that x_m–y_m and x_m–z_m planes are principal planes of bending. The member axes x_m, y_m and z_m are parallel to the global axes and the degrees of freedom are shown in the Figure 8.3. In this, there are six degrees of freedom at each node. Hence, total degrees of freedom are 12. It is to be noted that the rotations are about the axes but not in the directions of axes. Thus,

$$\{d\} = \begin{bmatrix} u_1 & v_1 & w_1 & \theta_{x1} & \theta_{y1} & \theta_{z1} & u_2 & v_2 & w_2 & \theta_{x2} & \theta_{y2} & \theta_{z2} \end{bmatrix}.$$

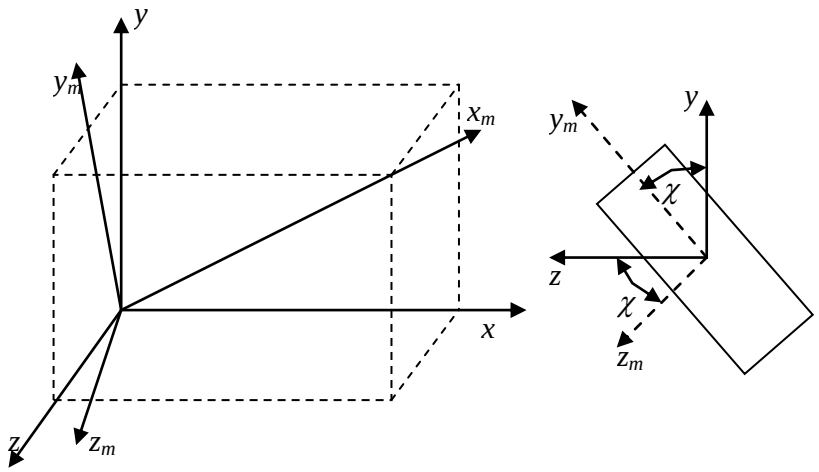

(a) Orientation of beam element (b) Orientation of principal axes about x_m axis

Fig. 8.4 Three dimensional prismatic beam element.

The stiffness matrix in local coordinates, referred to from Krishnamurthy (2001), can be written as:

$$[K_{3D}]=\begin{bmatrix}
\frac{EA}{l} & 0 & 0 & 0 & 0 & 0 & -\frac{EA}{l} & 0 & 0 & 0 & 0 & 0 \\
0 & \frac{12EI_x}{l^3} & 0 & 0 & 0 & \frac{6EI_x}{l^2} & 0 & -\frac{12EI_x}{l^3} & 0 & 0 & 0 & \frac{6EI_x}{l^2} \\
0 & 0 & \frac{12EI_y}{l^3} & 0 & -\frac{6EI_y}{l^2} & 0 & 0 & 0 & -\frac{12EI_y}{l^3} & 0 & -\frac{6EI_y}{l^2} & 0 \\
0 & 0 & 0 & \frac{GI_x}{l} & 0 & 0 & 0 & 0 & 0 & \frac{GI_x}{l} & 0 & 0 \\
0 & 0 & -\frac{6EI_y}{l^2} & 0 & \frac{4EI_y}{l} & 0 & 0 & 0 & \frac{6EI_y}{l^2} & 0 & \frac{2EI_y}{l} & 0 \\
0 & \frac{6EI_z}{l^2} & 0 & 0 & 0 & \frac{4EI_z}{l} & 0 & -\frac{6EI_z}{l^2} & 0 & 0 & 0 & \frac{2EI_z}{l} \\
-\frac{EA}{l} & 0 & 0 & 0 & 0 & 0 & \frac{EA}{l} & 0 & 0 & 0 & 0 & 0 \\
0 & -\frac{12EI_z}{l^3} & 0 & 0 & 0 & -\frac{6EI_z}{l^2} & 0 & \frac{12EI_z}{l^3} & 0 & 0 & 0 & -\frac{6EI_z}{l^2} \\
0 & 0 & -\frac{12EI_y}{l^3} & 0 & \frac{6EI_y}{l^2} & 0 & 0 & 0 & \frac{12EI_y}{l^3} & 0 & \frac{6EI_y}{l^2} & 0 \\
0 & 0 & 0 & \frac{GI_x}{l} & 0 & 0 & 0 & 0 & 0 & \frac{GI_x}{l} & 0 & 0 \\
0 & 0 & -\frac{6EI_y}{l^2} & 0 & \frac{2EI_y}{l} & 0 & 0 & 0 & \frac{6EI_y}{l^2} & 0 & \frac{4EI_y}{l} & 0 \\
0 & \frac{6EI_z}{l^2} & 0 & 0 & 0 & \frac{2EI_z}{l} & 0 & -\frac{6EI_z}{l^2} & 0 & 0 & 0 & \frac{4EI_z}{l}
\end{bmatrix} \tag{8.2}$$

8.2.2 TRANSFORMATION MATRIX

In general the member may be arbitrarily oriented in space. In the case of a three dimensional beam element, the line joining *i* and *j* define the x_m axis, but the y_m and z_m axes should be along the principal planes of bending and hence their orientation has to be specified. The global (structure) axes are brought to coincide with the local member axes by sequence of rotation about *y, z* and *x* axes respectively. This is referred to as *y-z-x* transformation. For the rotation about *y* axis, z axis and *x* axis, the transformation matrix is written respectively as:

$$\left[T_y\right]=\begin{bmatrix}\cos\beta & 0 & \sin\beta\\ 0 & 1 & 0\\ -\sin\beta & 0 & \cos\beta\end{bmatrix}, \tag{8.3}$$

$$\left[T_z\right]=\begin{bmatrix}\cos\gamma & \sin\gamma & 0\\ -\sin\gamma & \cos\gamma & 0\\ 0 & 0 & 1\end{bmatrix}, \tag{8.4}$$

$$\left[T_x\right]=\begin{bmatrix}1 & 0 & 0\\ 0 & \cos\chi & \sin\chi\\ 0 & -\sin\chi & \cos\chi\end{bmatrix}, \tag{8.5}$$

where, χ, β and γ are the angles of rotation about *x*, *y* and *z* axes respectively.
Therefore, the transformation matrix is written as:

$$\left[T'\right]=\left[T_x\right]\left[T_y\right]\left[T_z\right]. \tag{8.6}$$

As there are twelve degrees of freedom for a three dimensional beam element the rotation transformation matrix can be written as:

$$\left[T\right]=\begin{bmatrix}\left[T'\right] & 0 & 0 & 0\\ 0 & \left[T'\right] & 0 & 0\\ 0 & 0 & \left[T'\right] & 0\\ 0 & 0 & 0 & \left[T'\right]\end{bmatrix}. \tag{8.7}$$

Therefore, the stiffness matrix of the element $[K]$ with reference to global system of axes is written as:

$$[K]=[T]^T[K_{3D}][T], \tag{8.8}$$

where, $[K_{3D}]$ is the stiffness matrix for 3-D beam element with reference to the local member axes. The transformation matrix used to calculate the lateral frequency (about *x* axis) of the beam is written as follows: Referring to Figure 8.5(a), for the vertical tube on LHS, $\gamma = 90^0$

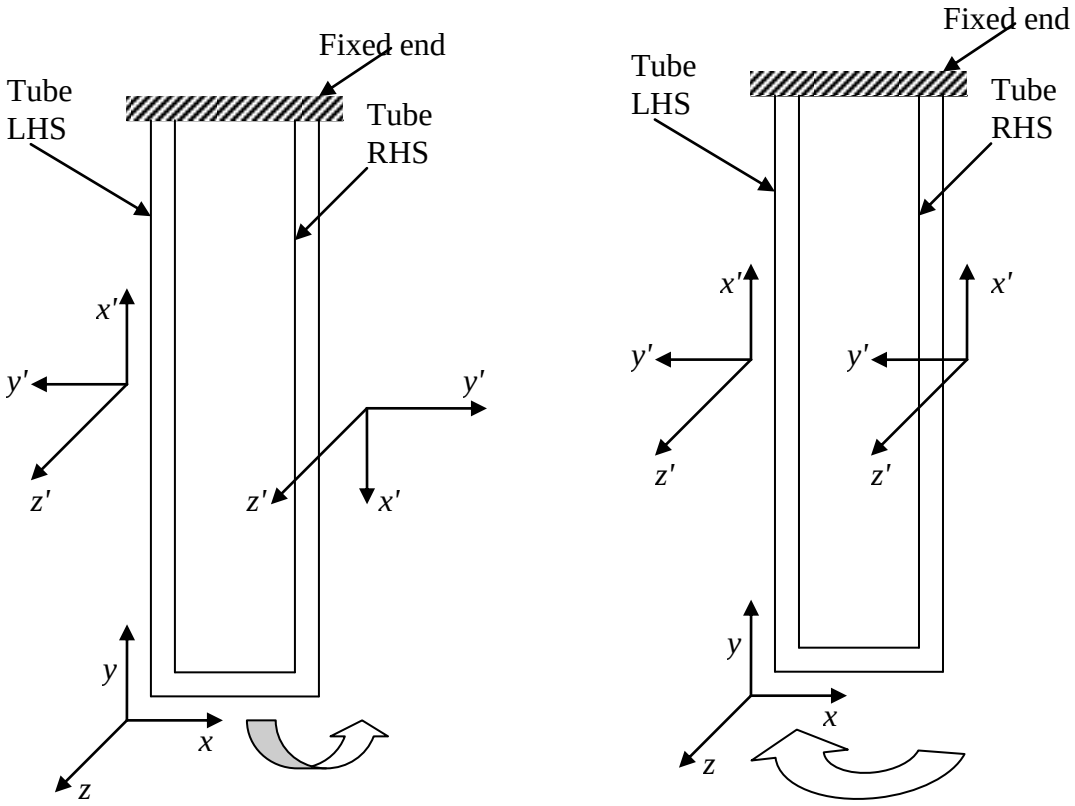

(a) Lateral motion (b) Transverse motion

Fig 8.5 Local and global co-ordinates for computing transformation matrix for U-tube configuration.

$$[T]=\begin{bmatrix} \begin{bmatrix} Cos90 & Sin90 & 0 \\ -Sin90 & Cos90 & 0 \\ 0 & 0 & 1 \end{bmatrix} & [0] & [0] & [0] \\ [0] & \begin{bmatrix} Cos90 & Sin90 & 0 \\ -Sin90 & Cos90 & 0 \\ 0 & 0 & 1 \end{bmatrix} & [0] & [0] \\ [0] & [0] & \begin{bmatrix} Cos90 & Sin90 & 0 \\ -Sin90 & Cos90 & 0 \\ 0 & 0 & 1 \end{bmatrix} & [0] \\ [0] & [0] & [0] & \begin{bmatrix} Cos90 & Sin90 & 0 \\ -Sin90 & Cos90 & 0 \\ 0 & 0 & 1 \end{bmatrix} \end{bmatrix}$$

and for the vertical tube on RHS, $\gamma = 270^0$

$$[T]=\begin{bmatrix} \begin{bmatrix} Cos270 & Sin270 & 0 \\ -Sin270 & Cos270 & 0 \\ 0 & 0 & 1 \end{bmatrix} & [0] & [0] & [0] \\ [0] & \begin{bmatrix} Cos270 & Sin270 & 0 \\ -Sin270 & Cos270 & 0 \\ 0 & 0 & 1 \end{bmatrix} & [0] & [0] \\ [0] & [0] & \begin{bmatrix} Cos270 & Sin270 & 0 \\ -Sin270 & Cos270 & 0 \\ 0 & 0 & 1 \end{bmatrix} & [0] \\ [0] & [0] & [0] & \begin{bmatrix} Cos270 & Sin270 & 0 \\ -Sin270 & Cos270 & 0 \\ 0 & 0 & 1 \end{bmatrix} \end{bmatrix}$$

For the horizontal tube, there is no need of transformation as global and local axes coincide with each other. The transformation matrix used to calculate the transverse frequency (about *z* axis) of the beam is written as follows:

Referring to Figure 8.5(b), for the vertical tube on LHS, $\gamma = 90^0$

$$[T]=\begin{bmatrix} \begin{bmatrix} Cos90 & Sin90 & 0 \\ -Sin90 & Cos90 & 0 \\ 0 & 0 & 1 \end{bmatrix} & [0] & [0] & [0] \\ [0] & \begin{bmatrix} Cos90 & Sin90 & 0 \\ -Sin90 & Cos90 & 0 \\ 0 & 0 & 1 \end{bmatrix} & [0] & [0] \\ [0] & [0] & \begin{bmatrix} Cos90 & Sin90 & 0 \\ -Sin90 & Cos90 & 0 \\ 0 & 0 & 1 \end{bmatrix} & [0] \\ [0] & [0] & [0] & \begin{bmatrix} Cos90 & Sin90 & 0 \\ -Sin90 & Cos90 & 0 \\ 0 & 0 & 1 \end{bmatrix} \end{bmatrix}$$

and for the vertical tube on RHS $\gamma = 90^0$

$$[T]=\begin{bmatrix} \begin{bmatrix} Cos90 & Sin90 & 0 \\ -Sin90 & Cos90 & 0 \\ 0 & 0 & 1 \end{bmatrix} & [0] & [0] & [0] \\ [0] & \begin{bmatrix} Cos90 & Sin90 & 0 \\ -Sin90 & Cos90 & 0 \\ 0 & 0 & 1 \end{bmatrix} & [0] & [0] \\ [0] & [0] & \begin{bmatrix} Cos90 & Sin90 & 0 \\ -Sin90 & Cos90 & 0 \\ 0 & 0 & 1 \end{bmatrix} & [0] \\ [0] & [0] & [0] & \begin{bmatrix} Cos90 & Sin90 & 0 \\ -Sin90 & Cos90 & 0 \\ 0 & 0 & 1 \end{bmatrix} \end{bmatrix}$$

For the horizontal tube, there is no need of transformation as global and local axes coincide with each other.

8.2.3 MASS MATRIX FOR THREE DIMENSIONAL BEAM ELEMENT

The mass matrix for 3-D beam element is as follows:

$$[M]=\frac{\rho Al}{420}\begin{bmatrix} 140 & 0 & 0 & 0 & 0 & 0 & 70 & 0 & 0 & 0 & 0 & 0 \\ 0 & 156 & 0 & 0 & 0 & 22l & 0 & 54 & 0 & 0 & 0 & -13l \\ 0 & 0 & 156 & 0 & -22l & 0 & 0 & 0 & 54 & 0 & 13l & 0 \\ 0 & 0 & 0 & 140I_x & 0 & 0 & 0 & 0 & 0 & 0 & 0 & 0 \\ 0 & 0 & -22l & 0 & 4l^2 & 0 & 0 & 0 & 13l & 0 & -3l^2 & 0 \\ 0 & 22l & 0 & 0 & 0 & 4l^2 & 0 & -13l & 0 & 0 & 0 & -3l^2 \\ 70 & 0 & 0 & 0 & 0 & 0 & 140 & 0 & 0 & 0 & 0 & 0 \\ 0 & 54 & 0 & 0 & 0 & -13l & 0 & 156 & 0 & 0 & 0 & -22l \\ 0 & 0 & 54 & 0 & 13l & 0 & 0 & 0 & 156 & 0 & 22l & 0 \\ 0 & 0 & 0 & 0 & 0 & 0 & 0 & 0 & 0 & 140I_x & 0 & 0 \\ 0 & 0 & 13l & 0 & -3l^2 & 0 & 0 & 0 & 22l & 0 & 4l^2 & 0 \\ 0 & -13l & 0 & 0 & 0 & -3l^2 & 0 & -22l & 0 & 0 & 0 & 4l^2 \end{bmatrix} \tag{8.9}$$

The horizontal element is taken as the tip mass in computing the theoretical frequency of the U-tube with tip mass.

8.2.4 NUMERICAL RESULTS

Tables 8.1, 8.2 and 8.3 compares the theoretical frequencies obtained from FORTRAN code written for the eigenvalue problem with the experimentally obtained natural frequencies of the U-tubes with and without tip mass in lateral (x axis) and transverse (z axis) direction. By carrying out FFT on the experimentally obtained displacement-time data in ORIGIN software the natural frequency of the U-tube was computed under laboratory conditions. As seen from Tables 8.1, 8.2 and 8.3, a minimum of 2.6% and a maximum of 6.8% error is found between the theoretical and experimentally obtained natural frequencies.

Table.8.1: Comparison of theoretical and experimental frequencies for U-tube with tip mass (Lateral frequency about *x*-axis).

Sl. No	Tube Length, *L* (mm)	Width (mm)	Tube Diameter *D* (mm)	Tip mass Weight (gm)	Frequency (Hz)		Error %
					Theoretical	Experimental	
1	460	30	1.86	58.1	1.3833	1.4487	3.95
2	465	31	2.5	58.1	2.3041	2.415	4.59
3	280	10	1.05	13	2.2635	2.357	3.96

Table.8.2: Comparison of theoretical and experimental frequencies for U-tube without tip mass (Lateral frequency about *x*-axis).

Sl. No	Tube Length, *L* (mm)	Width (mm)	Tube Diameter *D* (mm)	Frequency (Hz)		Error %
				Theoretical	Experimental	
1	465	30	1.86	6.9783	6.6677	4.65
2	475	31	2.5	9.1609	8.7729	4.42
3	400	10	1.05	4.9635	4.7	5.6

Table.8.3: Comparison of theoretical and experimental frequencies for U-tube without tip mass (Transverse frequency about *z*-axis).

Sl. No	Tube Length, *L* (mm)	Width (mm)	Tube Diameter *D* (mm)	Frequency (Hz)		Error %
				Theoretical	Experimental	
1	465	30	1.86	11.175	10.554	5.55
2	475	31	2.5	14.127	13.157	6.8
3	400	10	1.05	10.12	9.85	2.6

8.3 THERMALLY INDUCED VIBRATION OF U-TUBE WITH TIP MASS IN LATERAL DIRECTION

This section presents a comparison studies between theory and experiment on the thermally induced motion of U-tube with tip mass. The displacement response was measured in the lateral (x axis) direction.

8.3.1 EXPERIMENTAL SETUP

The U-tube cantilever beam with tip mass is shown in Figure 8.2. The test specimen used for the experimental investigation was a stainless steel SS304 tube with 1.86 mm and 1.05 mm external diameter and 0.22 mm thick, each bent to a U shape to form cantilever beam as shown in Figure 8.2. The tube was connected either by a mild steel tip mass or without tip mass. The test specimen was mounted inside a wooden test box 300 mm wide, 300 mm long and 1100 mm high with three sides of the box covered with perspex glass which performed the same functions as mentioned in earlier Chapter 6. A photograph of the experimental setup with U-tube, with tip mass, laser pickup and power supply is shown in Figure 8.6.

Fig 8.6 Experimental setup of U-tube cantilever beam with tip mass.

8.3.2 RESULTS AND DISCUSSION

8.3.2.1 FOR 1.86 MM DIAMETER U-TUBE WITH TIP MASS

The test specimen used for the experimental investigation was a stainless steel SS304 tube 960 mm long with 1.86 mm external diameter and 1.42 mm internal diameter bent in U form with effective length L = 465 mm and width b = 30 mm as shown in Figure 8.6 . The tubes were connected by a mild steel tip mass of 58.1 gm. The studies were carried out for the heating rates ranging from 3 W to 32 W. The displacement histories at the centre of the tube were obtained in each case. The temperature variation at the fixed end on the tube surface with respect to time was noted in each case using digital thermometer. For different heating rates the experiment was carried out for about 600 seconds. The ambient temperature during the experiment was 37^0C.

Isothermal free vibrations of U-tube with tip mass

The damped response in the absence of a forcing function of the U-tube with tip mass was predicted and the natural frequency calculated to be equal to 1.3833 Hz. By carrying out FFT on the experimentally obtained displacement data, the natural frequency of the tube at the room temperature of 37^0C calculated to be equal to 1.5564 Hz. Figure 8.7 shows the experimentally obtained displacement data, along with the theoretical data for the free vibration. Given an initial displacement of approximately 9.5 mm, it takes 450 seconds for the tube to come to rest. It is seen that there is good agreement over the entire 500 seconds range between the predicted and experimental values for the isothermal case.

Response of heated U-tube with tip mass for different heating rates

To determine the effect of heating rate on vibration growth, results are compared at two different heating rates of 24.5 W and 27.2 W. The ambient temperature during the experiments was 37^0C. Figures 8.8 and 8.9 compares the tip displacement and temperature histories obtained from the experimental data and the numerical data for different heating rates. Only the envelopes of the peak values are shown. Figure 8.8(a)

shows the displacement histories for the heating rate of 24.5 W, while Figure 8.9(a) shows the displacement histories for the heating rate of 27.2 W. The corresponding predicted temperature histories at X = 410 mm from the fixed end of the tube is illustrated in Figure 8.8(b) and Figure 8.9(b) respectively. The temperature shown is the average of the two nodal temperatures at this location. In both the cases, the initial displacement of 10 mm was given to the beam. It is seen that for the higher heating rate of 27.2 W, the beam attains the steady state amplitude of 7.1mm rapidly within 50 second but as the heating rate is reduced (24.5W) as shown in Figure 8.8(a), it takes almost 650 seconds to achieve steady state amplitude of 3 mm. The theoretical results are in close agreement with the experimentally obtained displacement histories.

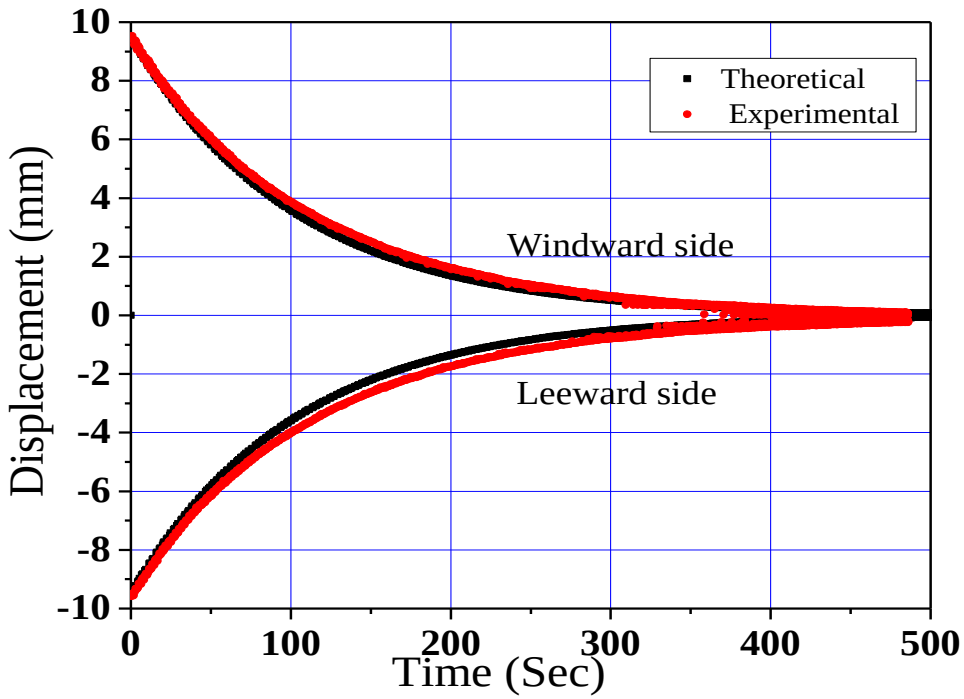

Fig 8.7 Isothermal lateral free vibration displacement histories for the U-tube with tip mass.

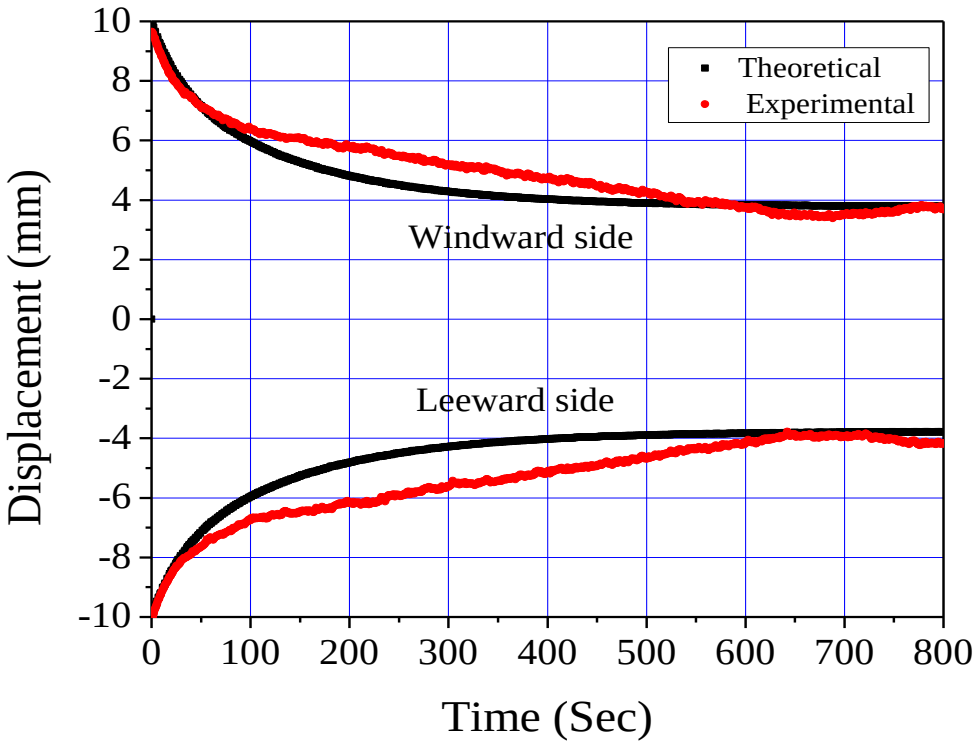

(a) Displacement histories

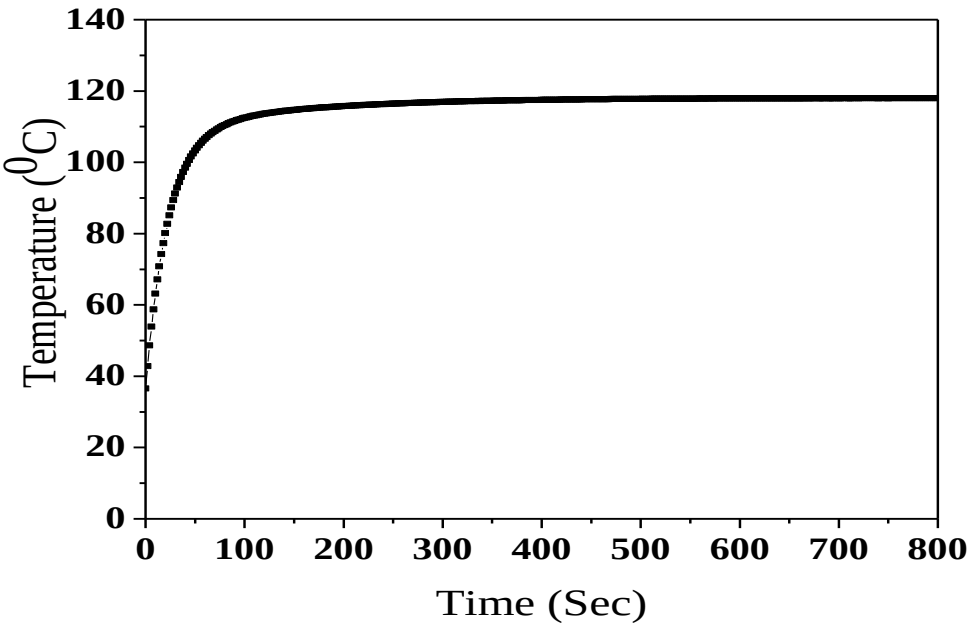

(b) Temperature histories

Fig. 8.8 Lateral displacement and temperature histories for heating rate of 24.5 W.

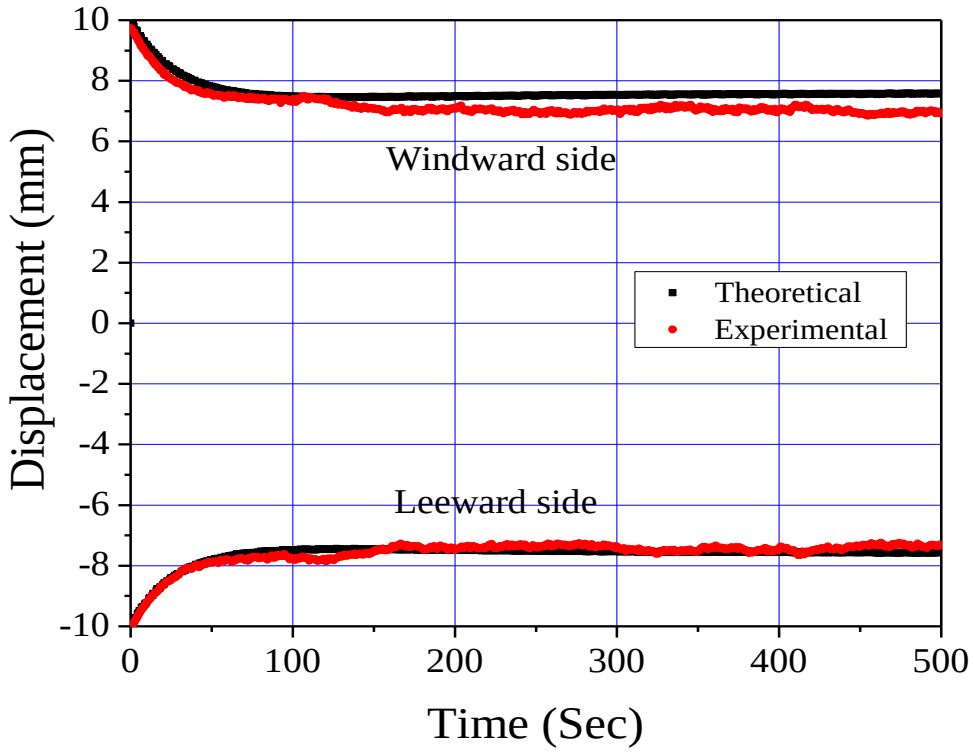

(a) Displacement histories

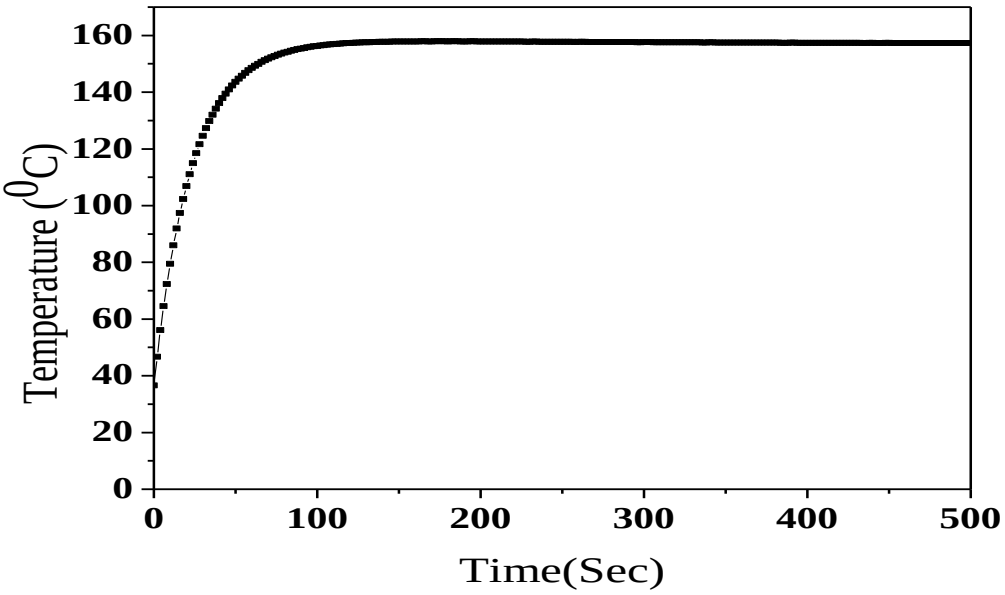

(b) Temperature histories

Fig. 8.9 Lateral displacement and temperature histories for heating rate of 27.2 W.

The studies were also carried out for other heating rate ranging from 3 W to 32 W. Figure 8.10 shows the plot comparing the steady state displacement for various heating rates. It is seen from the Figure 8.10 that, there is some value of threshold heating rate upto which the self induced vibrations will not be seen. In the present study the threshold heating rate was found to be equal to 22 W. As the heating rate is increased above 22 W the self induced vibrations are observed. It was not possible to measure vibration amplitude for the heating rate of 31.5 W which exceeded 10 mm, because the maximum value which can be measured by the laser pickup is ± 10 mm.

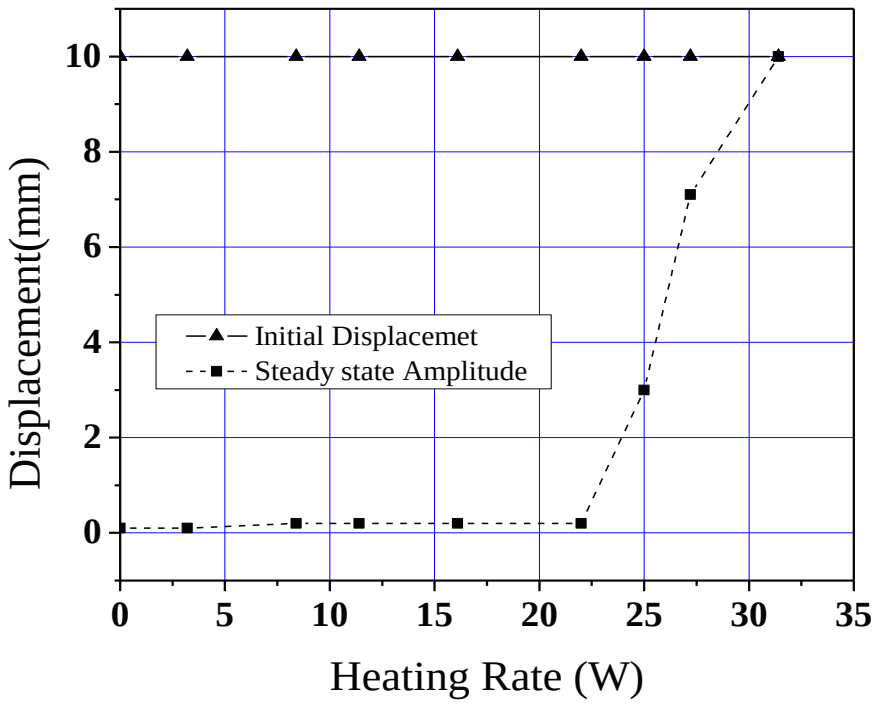

Fig 8.10 Variation of lateral displacement at 290 mm from the fixed end for different heating rates.

The temperature variation at the fixed end of the U-tube with respect to heating rate is shown in Figure 8.11. It is observed that, as the heating rate is increased the temperature increases and shows almost the linear trend.

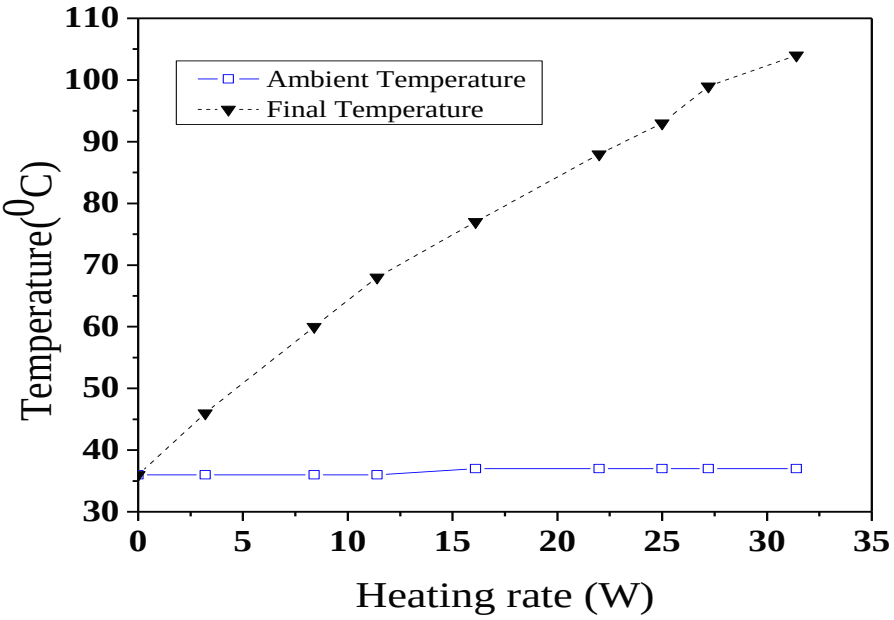

Fig.8.11 Variation of temperature at fixed end of U-tube with heating rate.

8.3.2.2 FOR 1.05 MM DIAMETER U-TUBE WITH TIP MASS

The test specimen used for the experimental investigation was a stainless steel SS304 tube of 570 mm long with 1.05 mm external diameter and 0.61 mm internal diameter bent in the U form, with effective length L = 280 mm and width b =10 mm as shown in Figure 8.2 . The tubes were connected by a mild steel tip mass of 13 gm. The studies were carried out for the heating rate ranging from 1.7 W to 13 W. The displacement histories at the tip mass were obtained in each case. The ambient temperature was 37^0C during the experiment.

Isothermal free vibrations of U-tube with tip mass

The damped response of the U-tube is predicted in the absence of a forcing function. By carrying out FFT on the experimentally obtained tip displacement data the natural frequency of the tube at the room temperature of 37^0C was calculated to be equal to 2.357 Hz. Figure 8.12 shows the predicted and experimentally obtained displacement data for the free vibration. Given an initial displacement of approximately 6 mm, it takes approximately 250 seconds for the U-tube to come to

rest. There is a considerable error in the displacement histories between the predicted and experimental values.

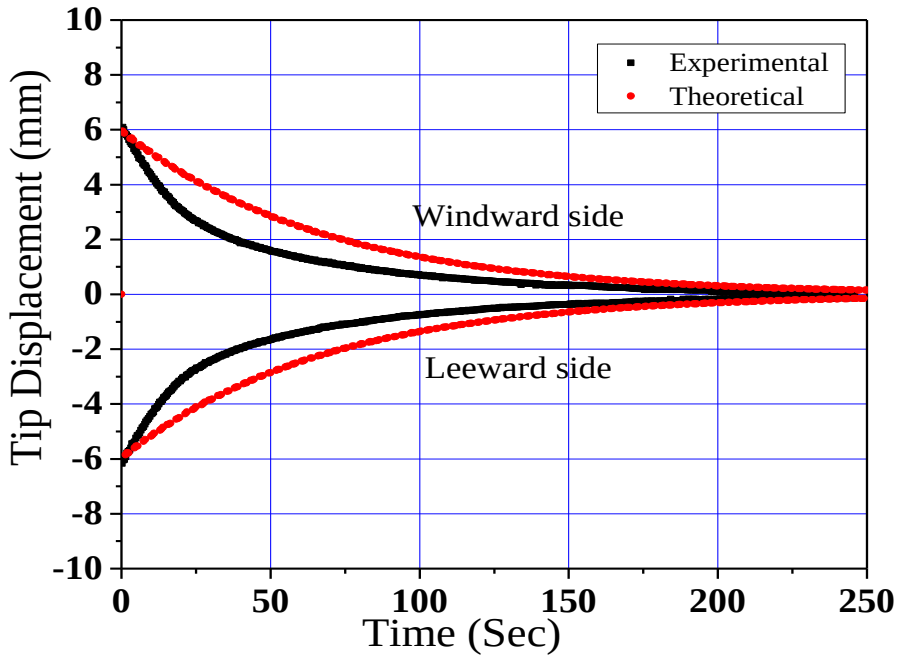

Fig 8.12 Isothermal lateral free vibration displacement histories for the U-tube with tip mass.

Response of heated U-tube with tip mass for different heating rates

To determine the effect of heating rate on vibration growth, results are compared at four different heating rates. The U-tube used in the experiments had a natural frequency of 2.357 Hz. Results are compared for heating rates of 9.62 W, 9.0 W, 7.8 W and 5.2 W. Figure 8.13 compares the tip displacement and temperature histories obtained from the experimental data and the numerical data for a U-tube heated with 9.62 W. Only the envelopes of the peak values are shown. Figure 8.13(a) shows the displacement histories, while Figure 8.13(b) shows the predicted temperature history at X = 250 mm from the fixed end of the tube. The temperature shown is the average of the two nodal temperatures at this location. In Figure 8.13(a) the theoretical analysis predicts a faster amplitude growth, but the steady-state displacements are close to the experimental values. After 900 seconds, the steady-state displacement again starts increasing and differs by 4 percent w.r.t. experimental

value. From Figure 8.13(a), it is observed that, for a peak temperature of 178^{0}C and at approximately 60 seconds the displacement is around 4 mm, which is less than the maximum amplitude of vibration of 9 mm.

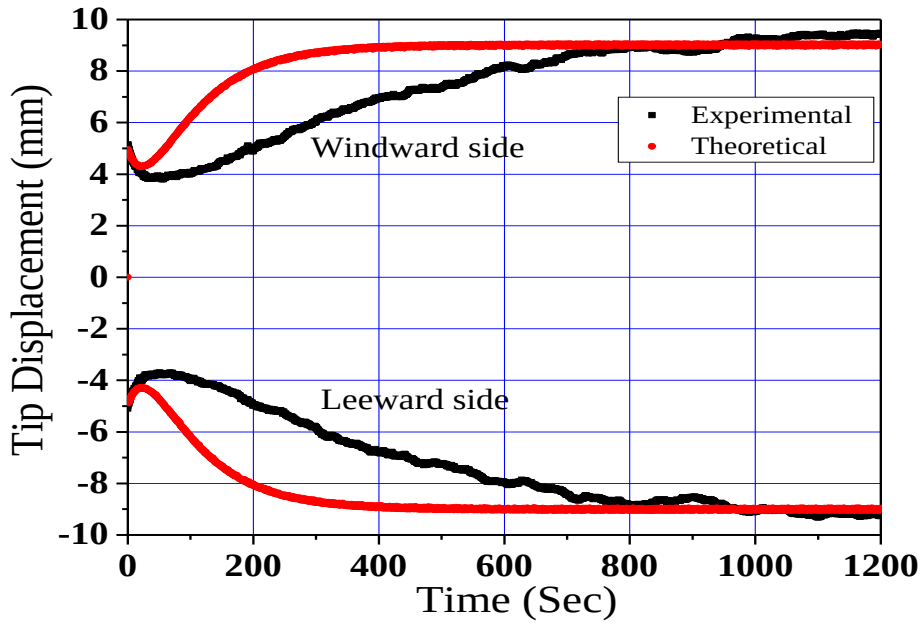

(a) Tip displacement

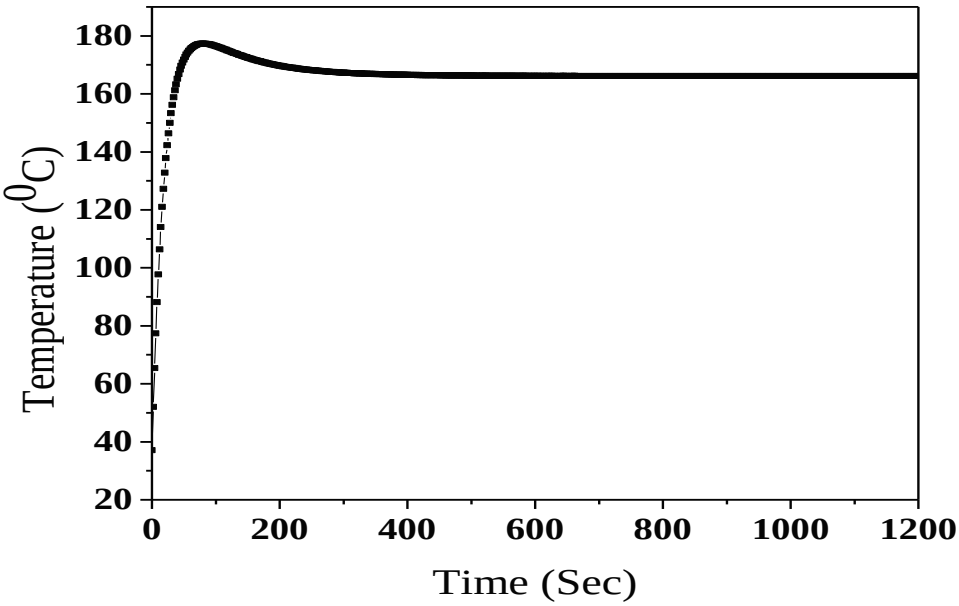

(b) Predicted temperature histories at X = 250 mm

Fig.8.13 Displacement and temperature histories for the U-tube for heating rate of 9.62 W.

Figures 8.14 to 8.16 shows the tip displacement and temperature histories obtained from the experiments and theoretical analysis for the U-tubes for heating rates of 9.0 W, 7.8 W and 5.2 W respectively. It is seen that the theoretical analysis predicts the displacement transients with considerable error during the initial time periods but predicted the steady state amplitude with reasonable accuracy. It is seen from the figures that the theoretical analysis predicts the steady state amplitude within short time duration but experimentally it is found that considerable time is required for the amplitudes to grow towards the steady state.

The studies were also carried out for other heating rate ranging from 1.7 W to 13 W. Figure 8.17 shows the plot comparing the steady state displacement histories for various heating rates. It is seen from the Figure 8.17 that, there is a threshold value of heating rate, below which the self induced vibrations will not be seen. In the present study the threshold heating rate was found to be equal to 4 W. As the heating rate is increased above 4 W the self induced vibrations are observed. It was not possible to measure vibration amplitude for the heating rate of 12.9 W which exceeded 10 mm because the maximum value which can be measured by the laser pickup is ± 10 mm.

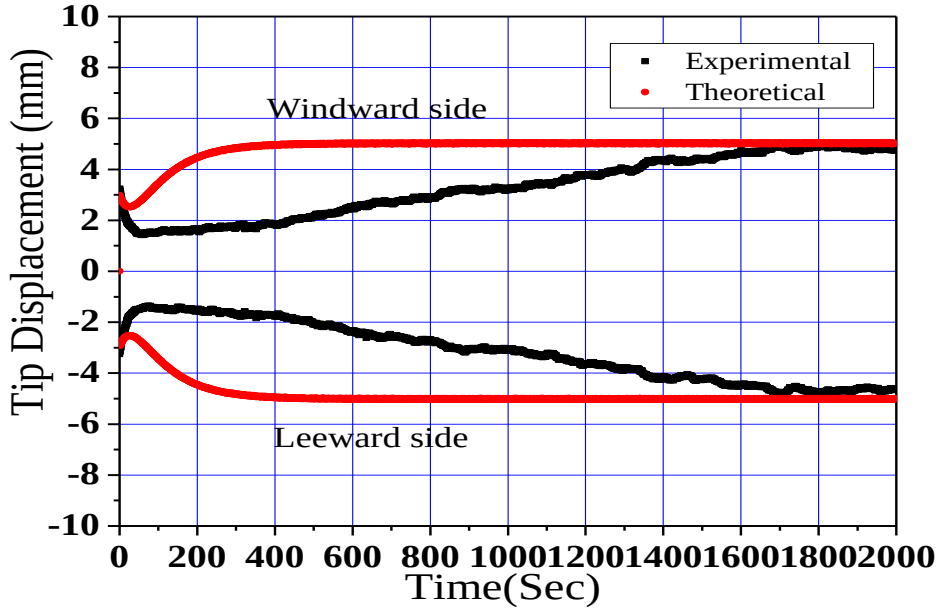

(a) Tip displacement

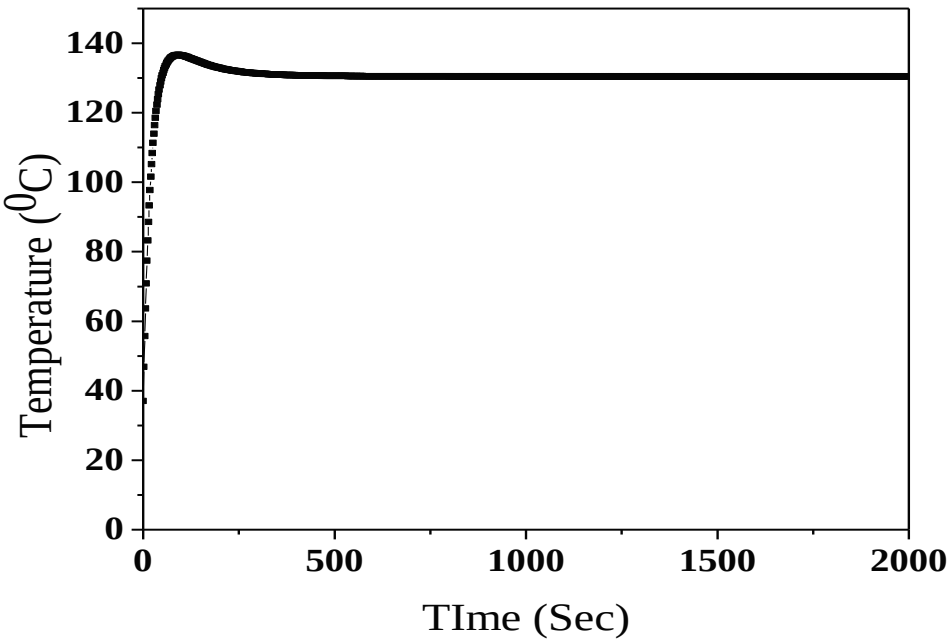

(b) Predicted temperature histories at X= 250 mm

Fig.8.14 Lateral displacement and temperature histories for the U-tube for heating rate 9.0 W.

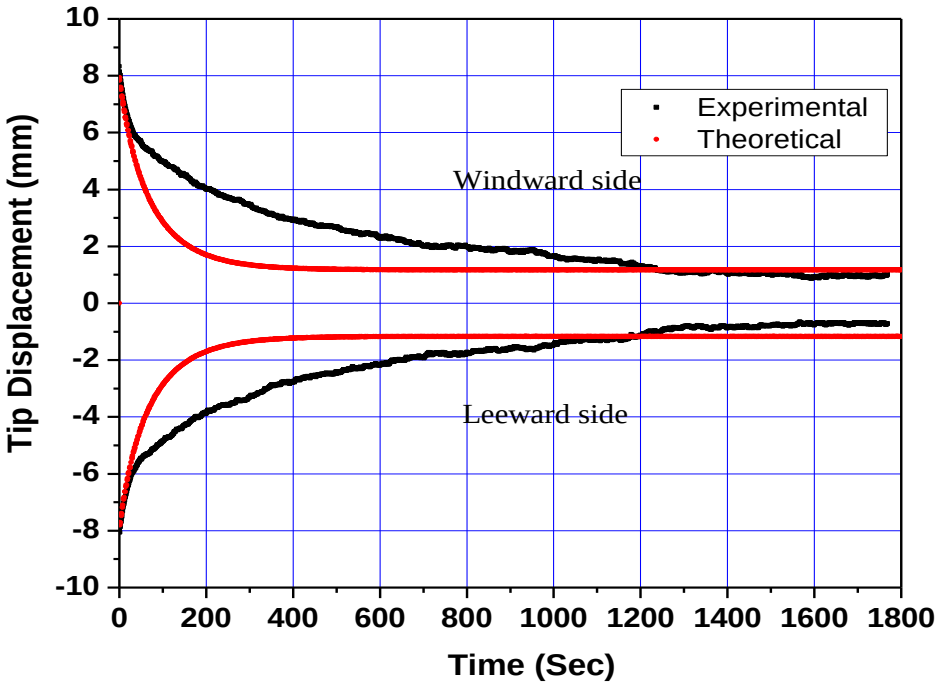

(a) Tip displacement

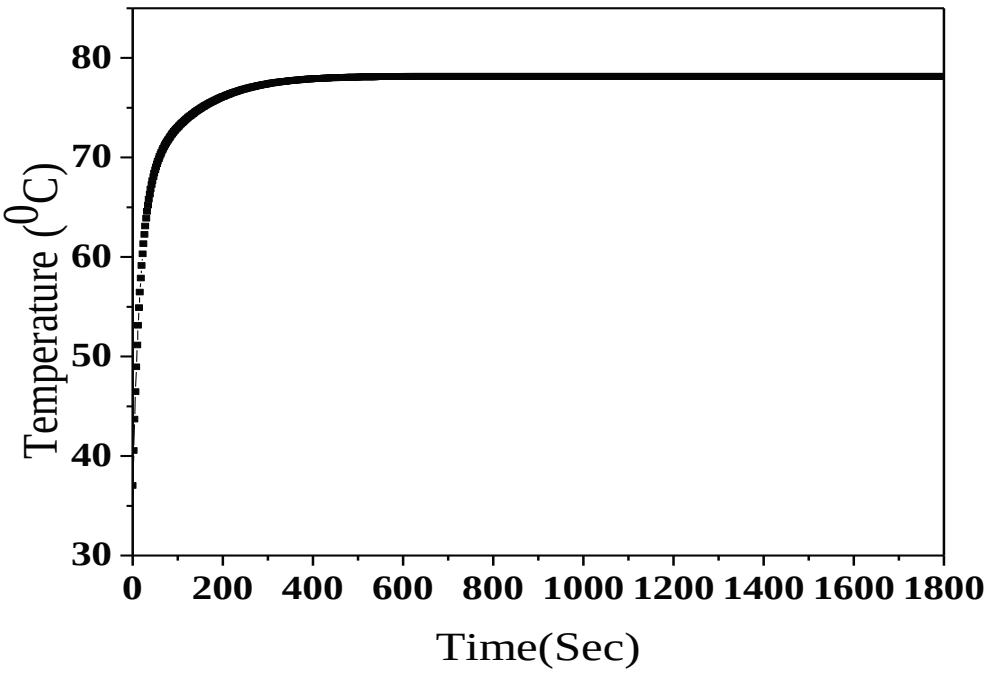

(b) Predicted temperature histories at X= 250 mm

Fig.8.15 Lateral displacement and temperature histories for the U-tube for heating rate 7.2 W.

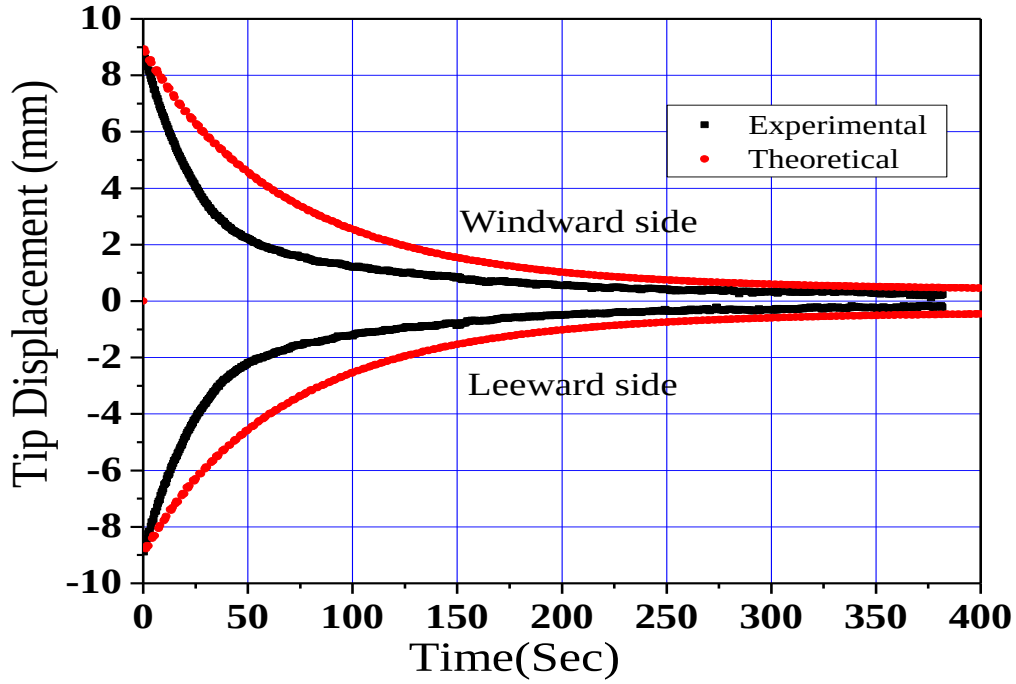

(a) Tip displacement

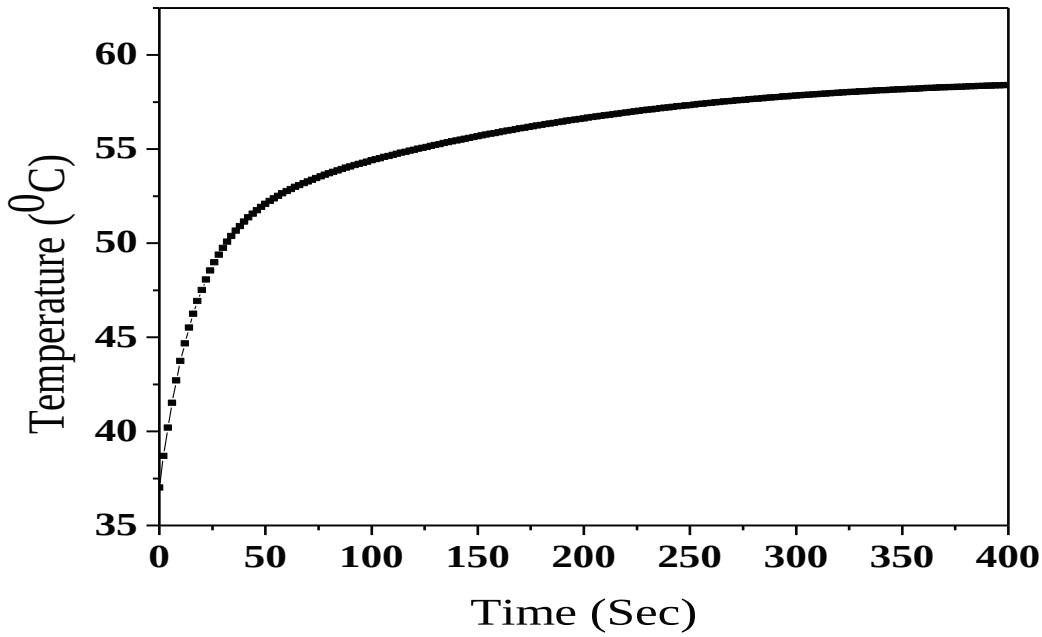

(b) Predicted temperature histories at X= 250 mm

Fig.8.16 Lateral displacement and temperature histories for the U-tube for heating rate 5.8 W.

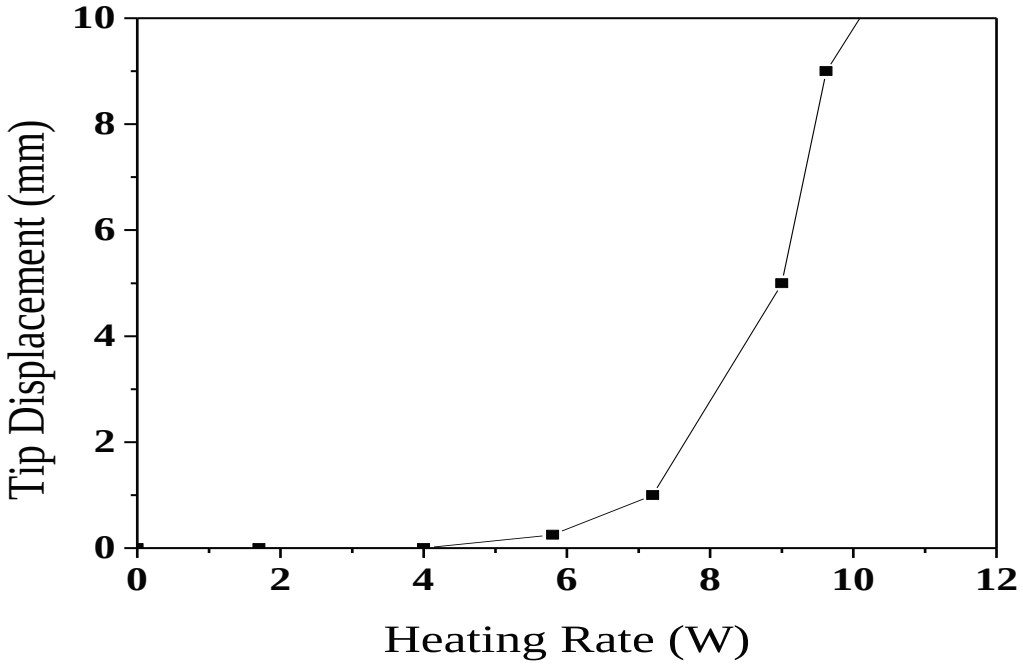

Fig 8.17 Effect of heating rate on U-tube lateral tip displacement.

8.4 THERMALLY INDUCED VIBRATION OF U-TUBE WITHOUT TIP MASS IN LATERAL AND TRANSVERSE DIRECTION

This section presents the experimental investigations on the lateral and transverse thermally induced motion of heated U-tube without tip mass.

8.4.1 EXPERIMENTAL SETUP

The U-tube cantilever beam without tip mass is shown in Figure 8.5. The test specimen used for the experimental investigation was a stainless steel SS304 tube with 1.86 mm and 1.05 mm external diameter and 0.22 mm thick bent in the U shape to form cantilever beam as shown in Figure 8.5. The experimental setup is same as explained in Section 8.3.1.

8.4.2 RESULTS AND DISCUSSION

8.4.2.1 FOR 1.86 MM DIAMETER U-TUBE WITHOUT TIP MASS

The test specimen used for the experimental investigation was a stainless steel SS304 tube 960 mm long with 1.86 mm external diameter and 1.42 mm internal diameter bent in U form with effective length l = 465 mm and width w =30 mm as shown in Figure 8.5. The studies were carried out for the heating rates ranging from 8.4 W to 25 W. The displacement histories at the tip (free end) of the beam were obtained in each case. The experiment was carried out for about 250 seconds. The ambient temperature during the experiment was 35.5^0C.

Isothermal transverse free vibrations of U-tube without tip mass

The experimentally obtained damped response of the U-tube in the transverse direction (about z axis) in the absence of a forcing function is shown in Figure 8.18. By carrying out FFT on the experimentally obtained displacement data the natural frequency of the tube at the room temperature of 35.5^0C was found to be equal to 10.454 Hz. Given an initial displacement of approximately 10 mm, it takes 100 seconds for the tube to come to rest.

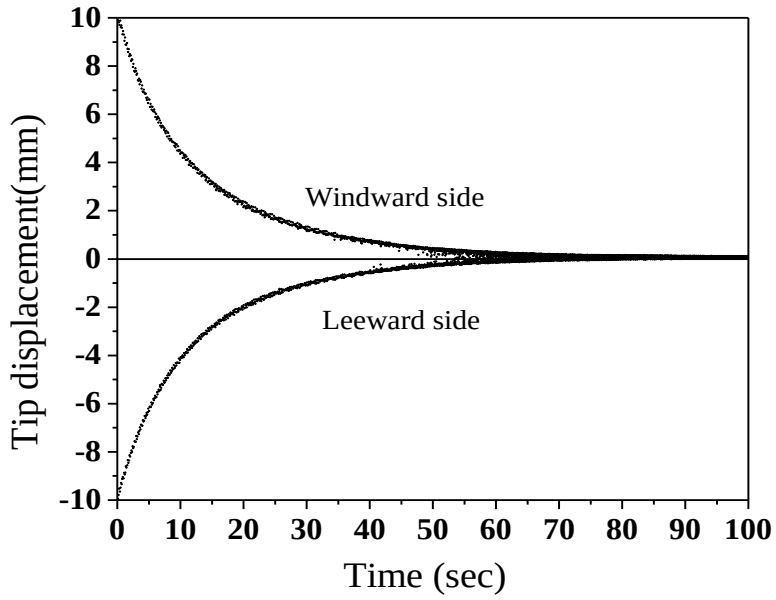

Fig.8.18 Isothermal transverse free vibration displacement histories for the U-tube without tip mass.

Response of heated U-tube without tip mass for different heating rates

To determine the effect of heating rate on vibration growth in transverse direction, results are compared for two different heating rates of 15.6 W and 25 W. The ambient temperature during the experiment was 35.5^0C.

Figures.8.19 and 8.20 compares the experimental transverse displacement histories for the two different heating rates. Only the envelopes of the peak values are shown. Figure 8.19 shows the displacement histories for the heating rate of 15.6 W, while Figure 8.20 shows the displacement histories for the heating rate of 25 W. In both the cases the initial displacement of 4 mm was given to the U-tube. It is seen that for the higher heating rate i.e. 25 W, the U-tube attains rapidly the steady state amplitude of 3 mm within 70 seconds but as the heating rate is reduced, it takes almost 150 sec to achieve steady state amplitude of 2.25 mm as shown in Figure 8.19.

Fig.8.19 Transverse displacement histories for the U tube beam for heating rate of 15.6 W.

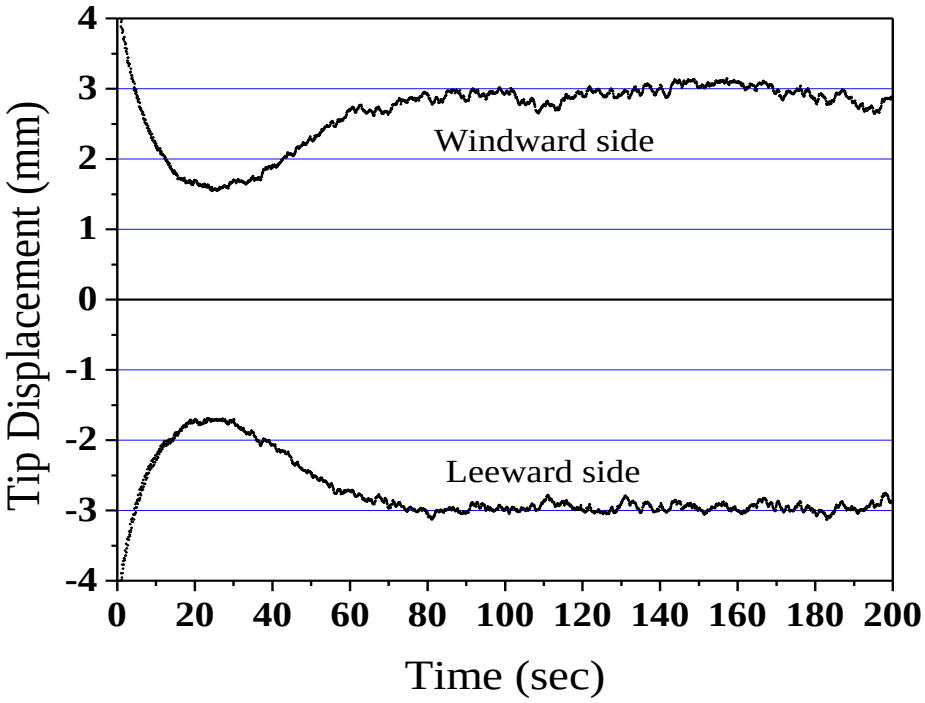

Fig 8.20 Transverse displacement histories for U tube beam for heating rate of 25 W.

The studies were also carried out for other heating rate ranging from 8.4 W to 25 W. Figure 8.21 shows the plot comparing the steady state transverse tip displacement histories for various heating rates. It is seen from the Figure 8.21 that as the heating rate is increased above 8.4 W, the self induced vibrations are observed. This value corresponds to threshold heating rate below which the self induced vibrations will not be seen. Studies were not possible for higher heating rates beyond 25 W since the maximum current that can be supplied by the DC power supply unit is limited to 5 A.

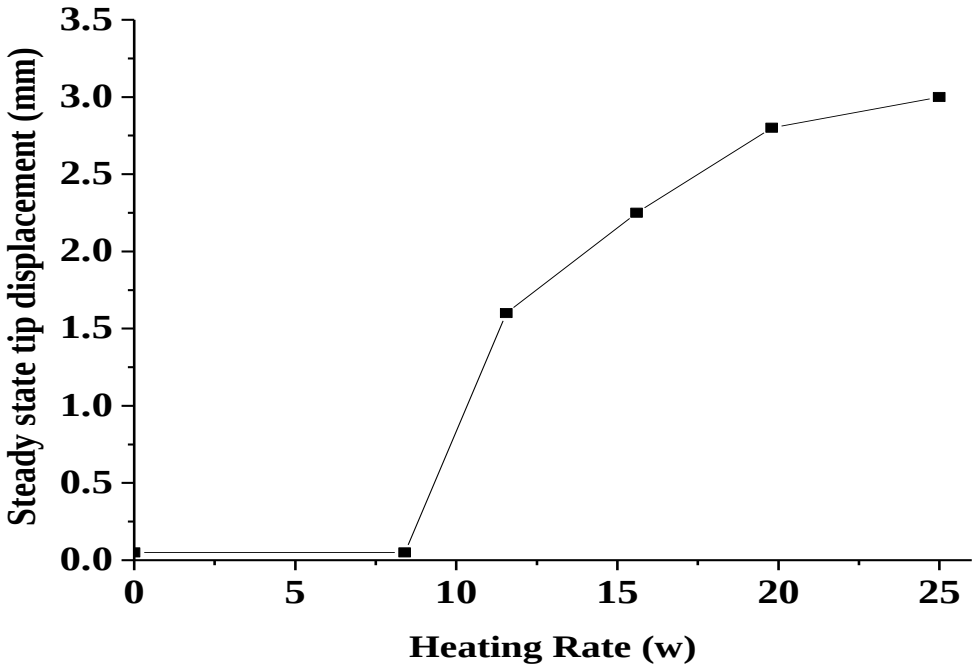

Fig. 8.21 Effect of heating rate on U-tube tip displacement in transverse (z axis) direction.

Figure 8.22 shows the plot comparing the time required to achieve steady state tip displacement histories for various heating rates. It is seen from the Figure 8.22 that as the heating rate is increased, the time taken to achieve steady state increases up to a certain value of heating rate (in this case 11.5W) and then starts decreasing. This is because the vibration amplitudes are less and the self induced motion of the beam is not able to give rise to forced convection which will remove the heat from the tube surface faster and helps in achieving the steady state.

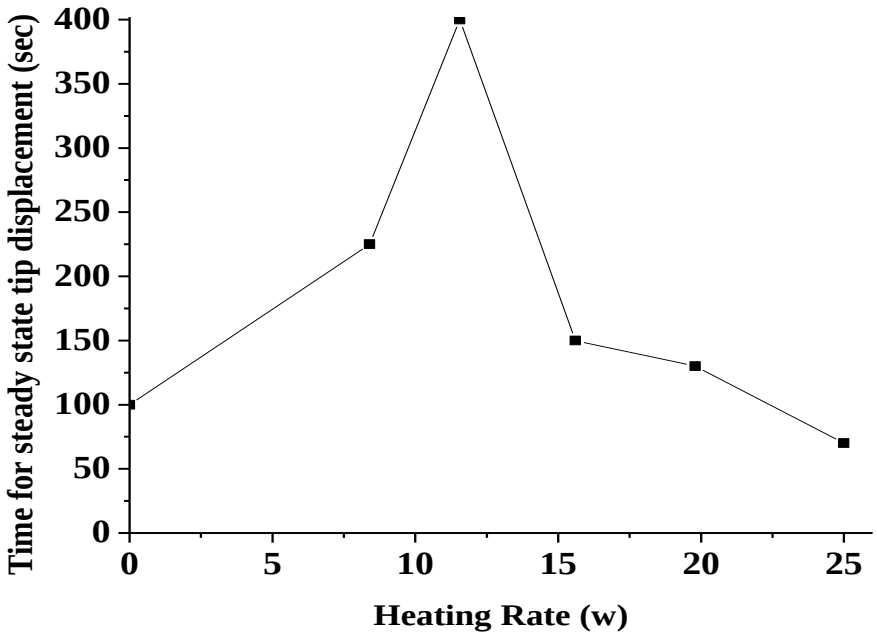

Fig 8.22 Effect of heating rate on time to achieve steady state transverse displacement.

8.4.2.2 FOR 1.05 MM DIAMETER U-TUBE WITHOUT TIP MASS

The test specimen used for the experimental investigation was a stainless steel SS304 tube 810 mm long with 1.05 mm external diameter and 0.61 mm internal diameter. The bent tube in the U shape had an effective length L = 400 mm and width b =10 mm as shown in Figure 8.2. The studies were carried out for the heating rates ranging from 8.4 W to 25 W. The lateral displacement histories at the tip (free end) of the U-tube were obtained in each case. The experiment was carried out for about 400 seconds for each of the heating rates. The ambient temperature during the experiment was 37^0C.

Isothermal lateral free vibrations for U-tube without tip mass

The experimentally obtained damped response of the U-tube in the lateral direction (about x axis) in the absence of a forcing function is shown in Figure 8.23. By carrying out FFT on the experimentally obtained displacement data, the natural frequency of the tube at the room temperature of 36.5^0C was found to be equal to 4.7

Hz. Given an initial displacement of approximately 5 mm, it takes 80 seconds for the tube to come to rest.

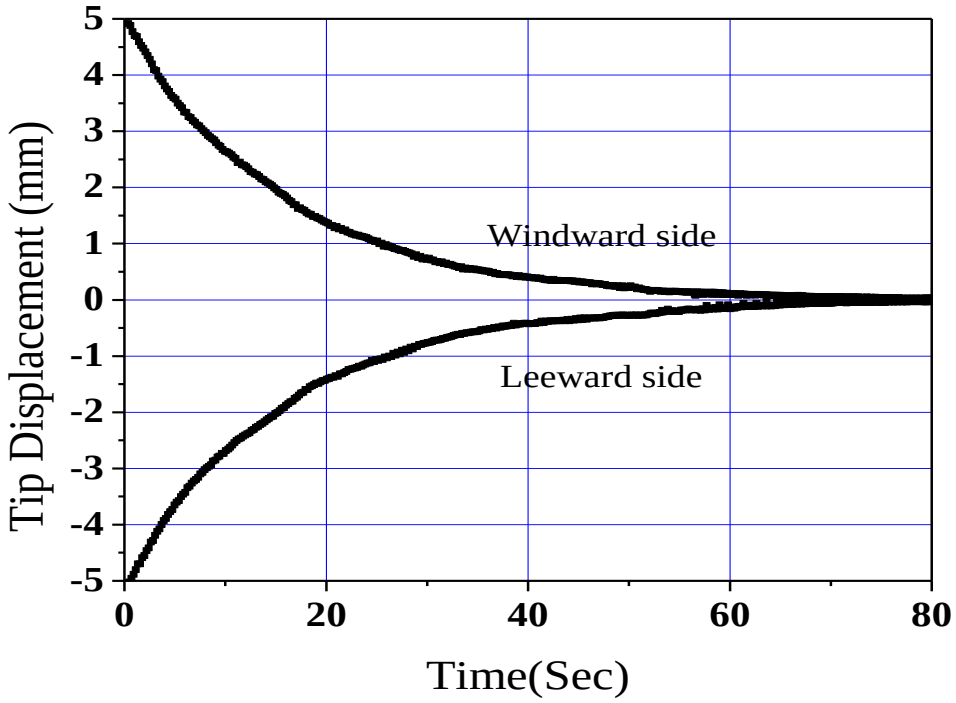

Fig 8.23 Isothermal lateral free vibration tip displacement histories for the U-tube without tip mass.

Lateral response of the heated U-tube without tip mass for different heating rates

To determine the effect of heating rate on vibration growth, results are compared for various heating rates ranging from 1.9 W to 35.55 W. The ambient temperature on the day when experiments were carried out was 37^0C. Figure 8.24 to Figure 8.27 shows the lateral tip displacement histories obtained from the experiment for the heating rates of 15.9 W, 21.7 W, 28.8 W and 35.55 W respectively. Only the envelopes of the peak values are shown. In both the cases the initial displacement of about 5 mm was given to the U-tube. For the heating rate of 15.9 W, U-tube beam showed the damped response as shown in Figure 8.24. It is to be noted that for the heating rates below 15.9 W, thermal induced motions will not occur. Threshold heating rate which will cause thermally induced motion is greater than 15.9 W. It is seen that for the higher heating rates, Figure 8.25, the amplitude of vibration first

decreases to a minimum and later on as the time progresses, the amplitude starts increasing to attain steady state, governed by the amount of heat input.

As shown in Figures 8.24 to 8.26, it is observed during the experiments that for higher heating rates, the beam initially vibrates at the frequency of 4.7 Hz. At the same frequency it shows the damped response until the amplitude of oscillation become minimum. Later from this time onwards the amplitude of vibration starts increasing and attain a maximum (refer to region 1 and 2 in Figure 8.25 and 8.26). Further, from this time onwards the amplitude of oscillation decreases and with the progress of time the amplitudes become steady with the frequency of oscillation being 28.515 Hz, i.e. region 3. It is found that there exists a transition from first mode frequency of 4.7 Hz to a second mode frequency of 28.515 Hz during the time when the amplitude of oscillation starts decreasing towards final steady state amplitude. The amplitude of vibration at steady state occurring at beam frequency of 28.515 Hz is less than the maximum amplitude attained by the beam at frequency of 4.7 Hz. The change of mode of vibration of beam with respect to time is illustrated in Figure 8.27.

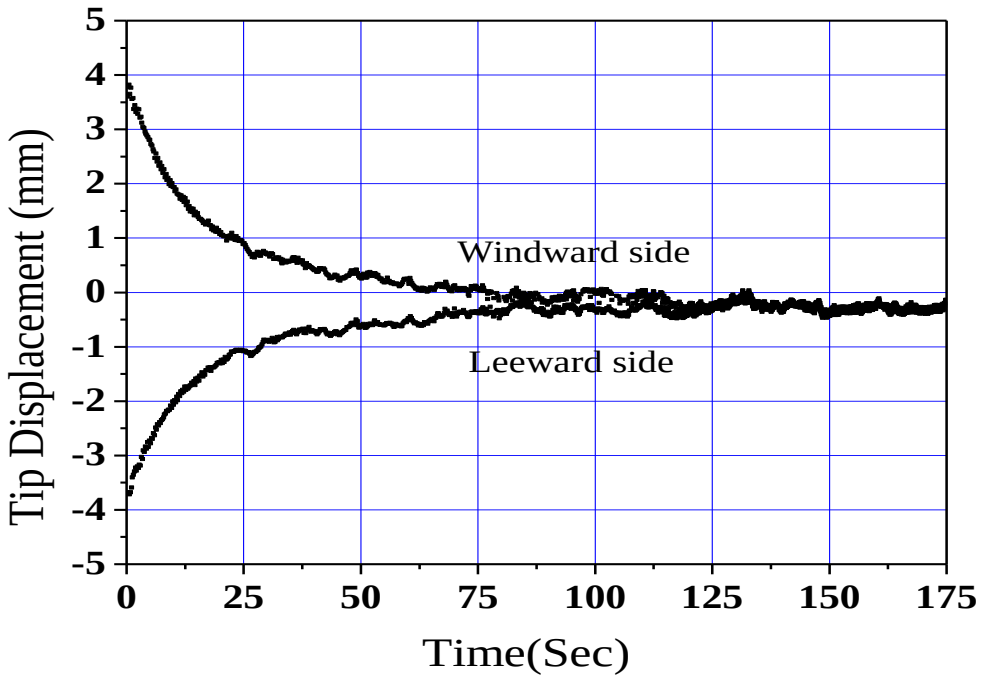

Fig. 8.24 Lateral displacement histories for U-tube beam for heating rate of 15.9W.

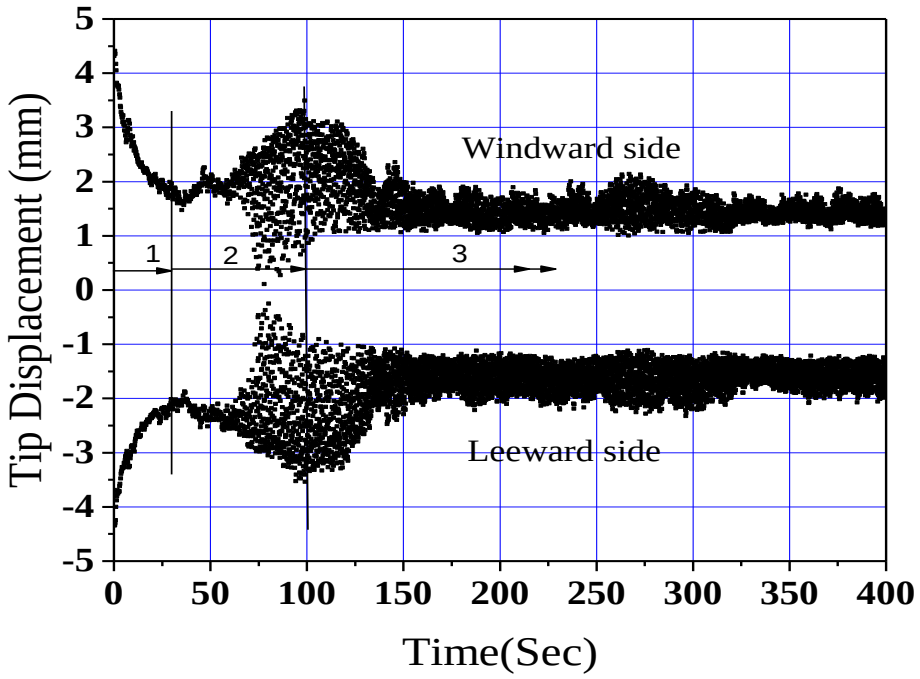

Fig.8.25 Lateral displacement histories for the U tube beam for heating rate of 28.8 W.

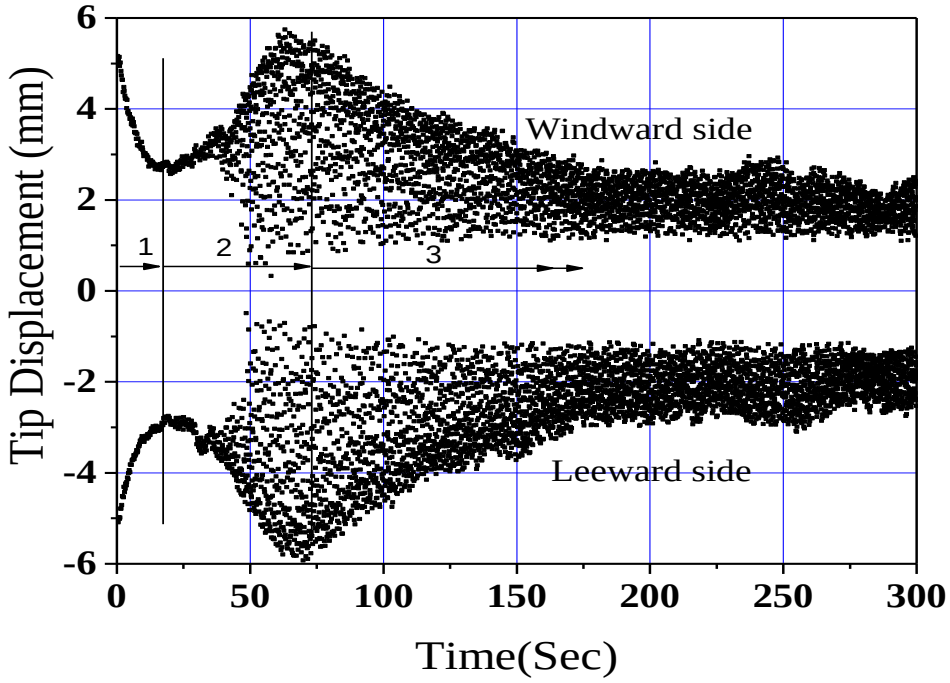

Fig.8.26 Lateral displacement histories for the U- tube beam for heating rate of 35.55 W.

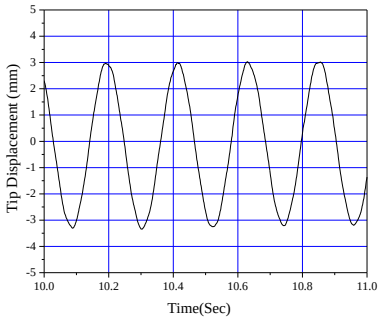

(a)First mode

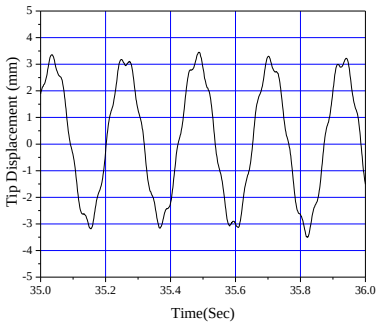

(b)Second mode

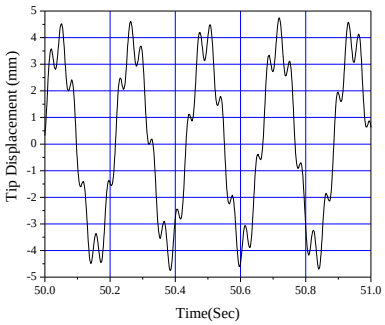

(c) Third mode

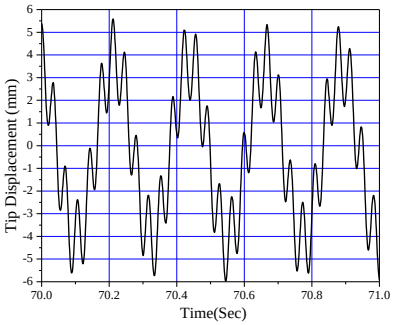

(d) Forth mode

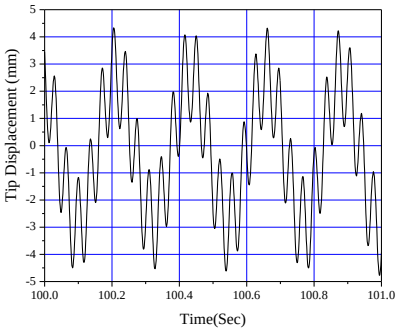

(e) Fifth mode

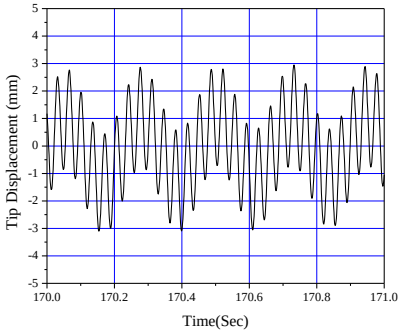

(f) Sixth mode

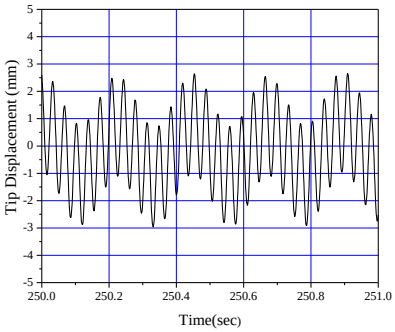

(g) Seventh mode

Fig.8.27 Change in mode of vibration with time for a U-tube without tip mass.

8.5 SUMMARY

The dynamic response of the U-tubes in lateral direction was studied theoretically and experimentally for the vertical tube bent to a U shape with tip mass for different heating rates and two different sizes of the U-tubes. Only experimental studies were carried out on U-tube without tip mass and displacement response was observed both in lateral (x axis) and transverse (z axis) direction. Natural frequency of the U-tube was obtained experimentally and compared with the theoretical results obtained by the FORTRAN code written for frequency computation of a U-tube. Experimental results when compared with theoretical results for the lateral displacement response of U-tubes with tip mass had the following observations:

(i) the steady state amplitudes were reasonably in close agreement

(ii) during the initial period of the displacement response, the theoretical results showed a rapid rise when compared to the slow and gradual growth of displacement from the experiment

(iii) there exists a threshold heating rate to produce thermal induced motion for U-tube.

Observations on the experimental results for the displacement response of U-tubes without tip mass are as follows

(i) for lower heating rates, it took considerable amount of time to attain steady state amplitude when compared to higher heating rates

(ii) there exists a threshold heating rate to produce thermal induced motion for U-tube

(iii) for the displacement response of the U-tube in the lateral direction, during the initial period, the beam motion occurred in the first mode and with progress of time the displacement response changed to second mode with amplitude of vibrations being lower than that observed in first mode.

CHAPTER 9
COMBINED EFFECT OF FLUID AND THERMAL INDUCED VIBRATION

9.1 EXPERIMENTAL SETUP

An experimental setup is fabricated in the laboratory to demonstrate the fluid thermal interaction in a thin slender tube. The setup consists of two narrow tubes of diameter 3 mm. The tubes are connected through an orifice. The orifice assembly produces an additional load due to fluid expansion. The orifice size can be changed to obtain different hole diameter. Experiments were conducted for 1 mm and 1.5 mm orifice hole sizes. The one end of the first tube is for the entry of the compressed air. The other end of this tube is connected to another tube through orifice assembly. The other end of the second tube is exposed to atmosphere. These two tube assemblies are in such away that one end is fixed and other end is free with orifice assembly. The setup is mounted inside a test stand. The test stand acts as a means to hold the two ends of the tube as shown in Figure 9.1. The supply pressure is controlled by the pressure regulator. The air is passed through stainless steel heating box of cylindrical shape of diameter 200 mm and the arrangement is suitable for generating pressurized air at required temperature. The stainless steel heating box contain 200 watt heating coil connected through 220 V, 5 amp AC source with a voltage regulator. The voltage regulator is required to vary the power supply to the heating coil in order to vary the supply air temperature. As the air flows, the heat from the compressed air is lost by conduction through the tube and by convection from the tube surface to atmosphere. The tube surface temperature is measured using thermocouple and DAQ through LabVIEW as explained in Chapter 5. Due to pressurized air, there exert fluid load in the structure and an additional load due to sudden expansion of the air through an orifice. The air enters into one chamber of the sudden expansion assembly and flow through an orifice plate having small hole. Thus, flow results in sudden expansion of air and hence additional load at the tube tip. From the second chamber, air exits through the second tube to atmosphere. To obtain the transient and steady state response of the tube, a piezoelectric accelerometer AD1221 N605 with sensitivity 10 mv/g is used. In order to acquire the signals NIPXI 1050 chassis containing NIPXI

4472 DAQ with 24 bit having 8 analog input channels and 2 analog output channel is used as shown in Figure 9.1. Then, instrument is connected to CPU and monitor to display of the output. The programming was done to acquire response signals through LabVIEW 8.0.

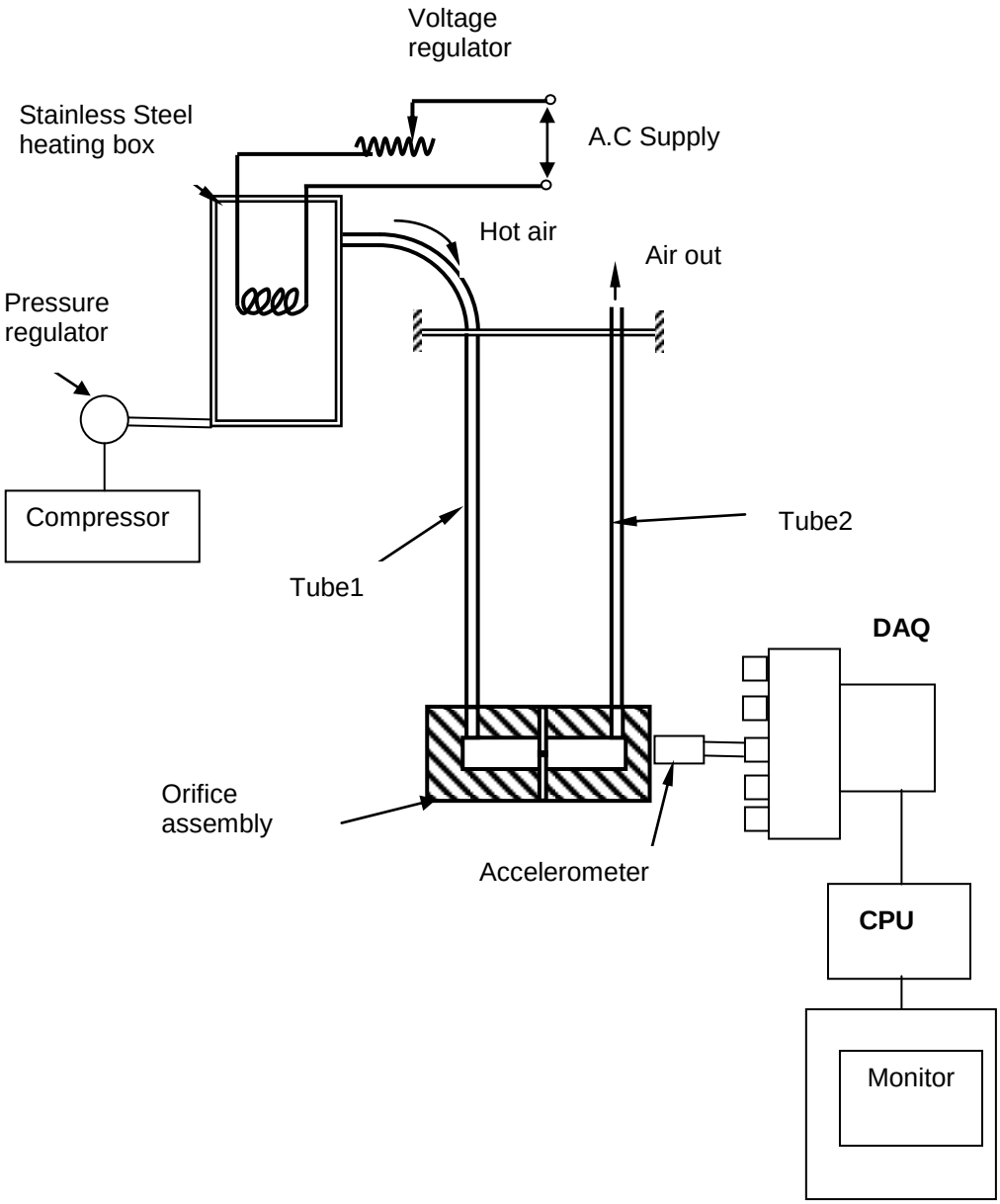

Fig 9.1. Experimental Setup.

9.2 TUBE SPECIFICATIONS

A high carbon steel of 3 mm diameter tube is used to study the response of the structure due to fluid and thermal load. The tube material characteristics are important for the numerical computation. In this respect the dimensions and strength characteristics of the tube are determined. Outer diameter of the tube is 3 mm and inner diameter of the tube 2.24 mm. Inner diameter of the tube is accurately measured using a tool maker's microscope. The tensile tests were conducted on the specimen to evaluate Young's modulus. The other data are measured using proper instruments. These tube data are tabulated in the Table 9.1

Table 9.1 Tube specifications table.

Parameters	Value
Length	800 mm
Young's modulus	2.61×10^{11} N/mm^2
Density	6.9 gm/cc
Outer diameter	3.0 mm
Inner diameter	2.24mm

9.3 TEMPERATURE PROFILE ON THE TUBE

Figures 9.2 and 9.3 shows the temperature distribution obtained through experiment in the first tube before expansion when hot air is passed. The air entry temperature was maintained at 78^0C and experiment is repeated for air pressure varied from 2, 3, 4 and 5 bars. Experiment is alsoconducted for inlet air temperature 58^0C and ambient temperature of 31^0C. From Figures 9.2 and 9.3, as the hot air moves along the length of the tube, the temperature decreases due to heat transfer to ambient by natural convection. It is also observed that the temperatures along the tube are less when the working air pressure increases. This is due to larger flow rate which enhance the convection heat transfer. The temperature gradient is nonlinear, indicating that the variation in overall heat transfer coefficient along the tube varies. However, during the finite element modeling, the overall heat transfer coefficient is taken as a constant.

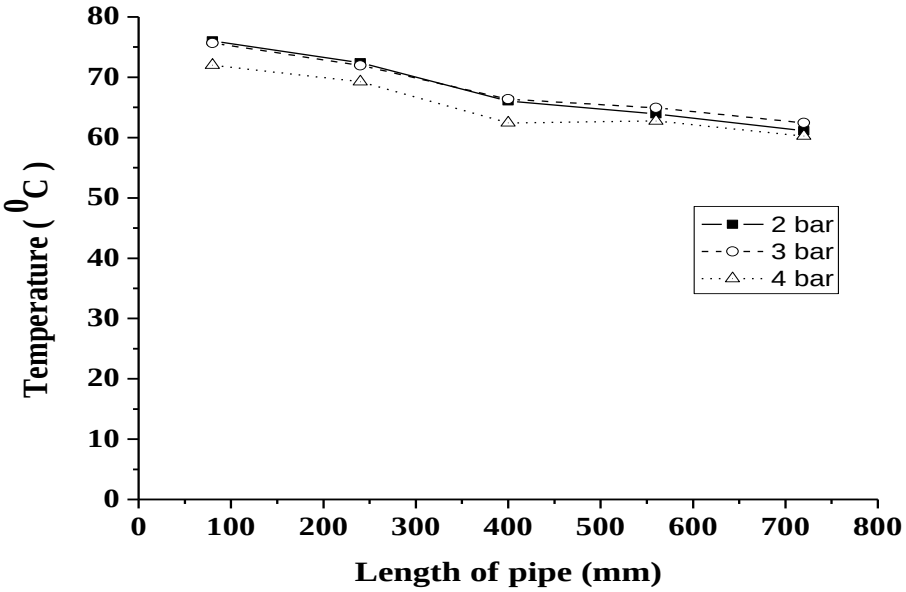

Fig. 9.2. Experimentally obtained temperature distributions along the tube at 78^0C inlet temperature.

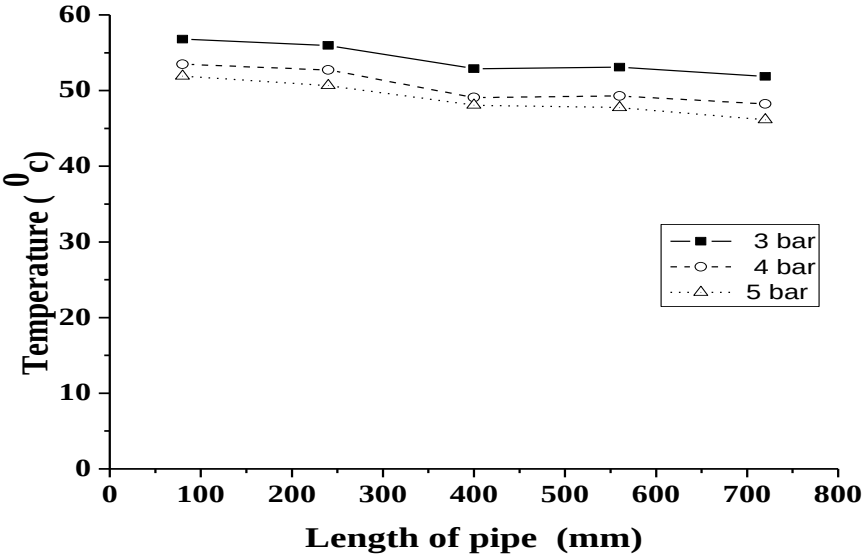

Fig. 9.3 Experimentally obtained temperature distributions along the tube at 58^0C inlet temperature.

9.4 RESPONSE OF THE TUBE SYSTEM

Figures 9.4 and 9.5 indicate the transient response of the tube at supply air pressure of 2 bar and 5 bar respectively. This shows that as the pressure increases the response becomes more oscillatory and takes more time to attain steady state. Experiments were conducted for 1 bar, 2 bar, 3 bar and 4 bar. The steady state response were obtained in each case and frequency spectrum also obtained as explained earlier (Refer Chapter 2). The compressed air temperature is at ambient temperature 31^0C. Figures 9.6 and 9.7 show transient response for the supply air pressure of 1 bar and 2 bar at a temperature 58^0 C. This also indicates that load coming on the tube increases with pressure and response takes more time to attain steady state value. Moreover, small variation in temperature has negligible effect on the frequency of vibration.

Figures 9.8 and 9.9 shows steady state vibration for the supply air pressure of 1 bar and 2 bar respectively at 58^0C temperature. Experiments were also conducted for the air temperature 78^0C and ambient temperature 31^0C for various pressures.

It is observed that orifice used to give a shift of the tube from the initial position. As the pressure increases, the shift position also increases. It is observed that, as the size of the orifice decreases initial shift also increases. This is due to thrust produced on the orifice increases as the sudden expansion of the air take place. However, the shifts are negligibly small compared to deformation of the tube due to temperature and fluid structure interaction. From the steady state response, the frequency response data is obtained as explained earlier and hence the frequency of vibration of the system for different supply pressure and temperature. Experiments were repeated for different supply air pressure of 1 bar, 2 bar, 3 bar, 4 bar and 5 bar. Experiments were also repeated at different air supply temperature 31^0C, 58^0C and 78^0C. Response curve obtained in each case is similar in pattern. However there is variation in displacement and natural frequency.

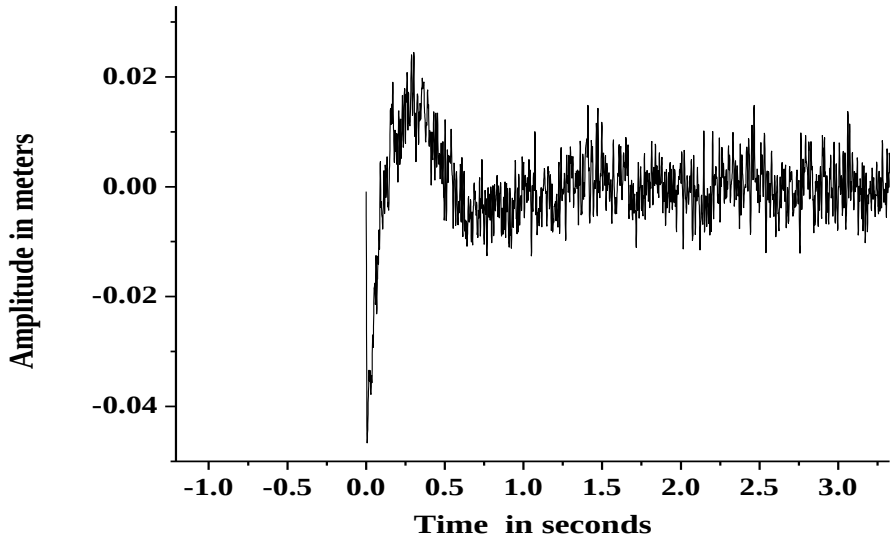

Fig 9.4 Transient response of the tube at 2 bar pressure and ambient temperature 31^0C.

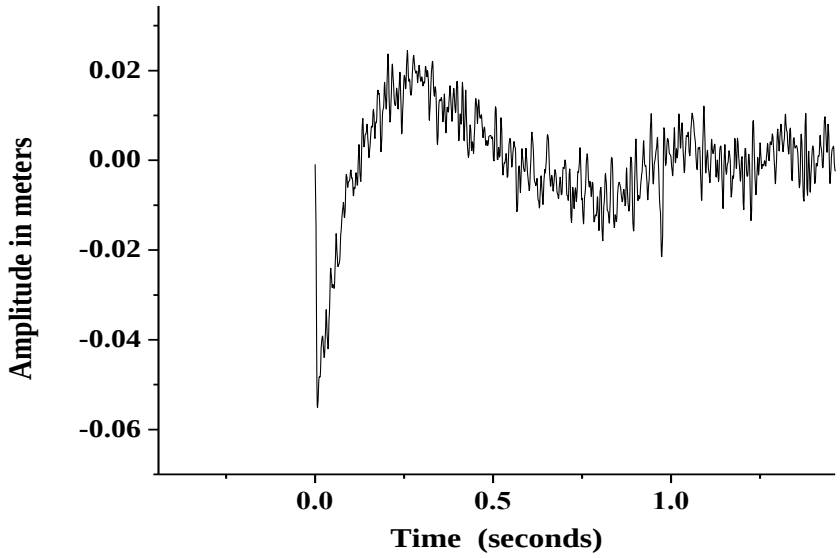

Fig 9.5 Transient response of the tube at 5 bar pressure and ambient temperature 31^0C.

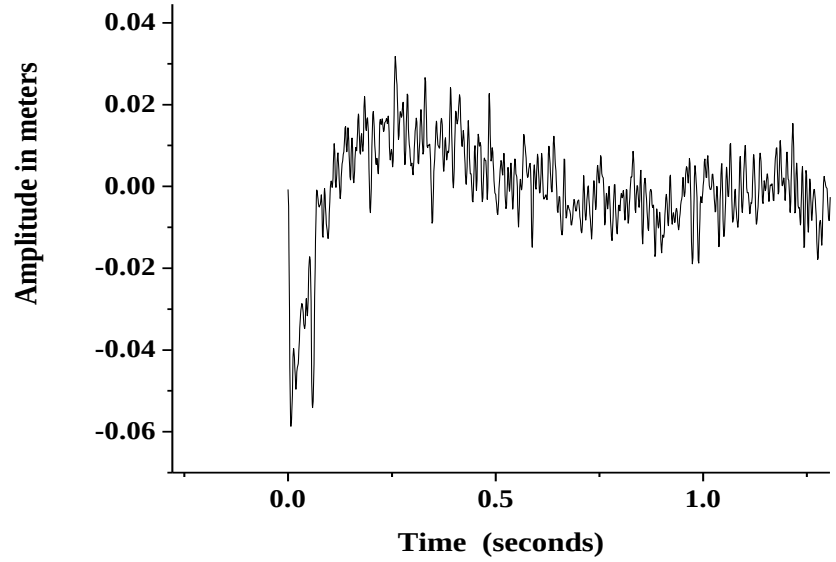

Fig 9.6 Transient response of the tube at 1 bar pressure and inlet temperature 58^0C.

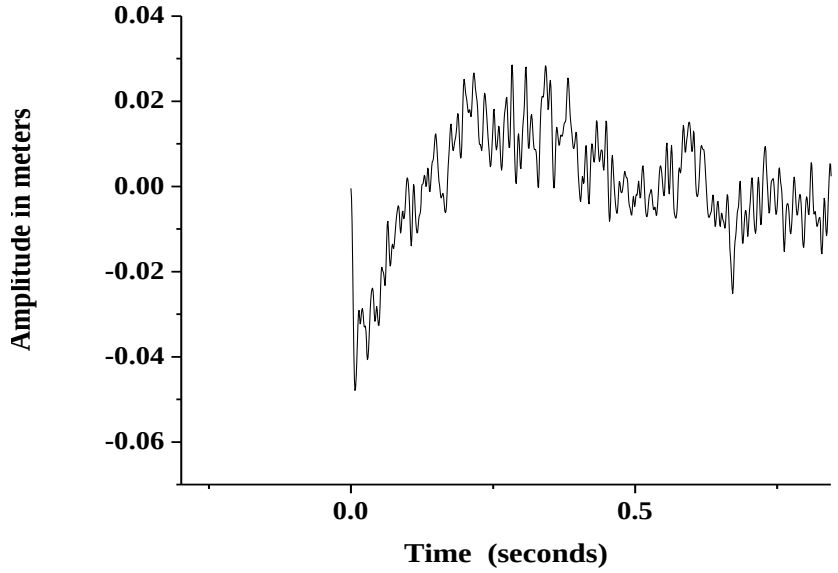

Fig 9.7 Transient response of the tube at 2 bar pressure and inlet temperature 58^0C.

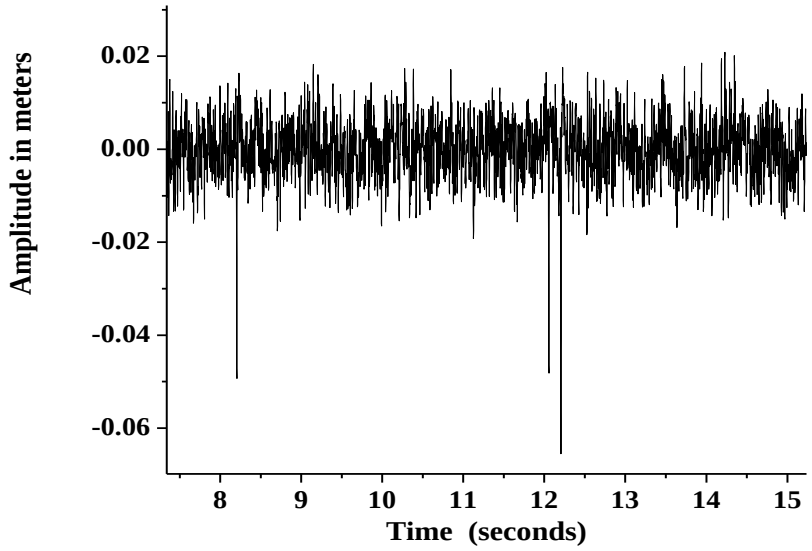

Fig 9.8 Steady state response of the tube at 1 bar pressure and inlet temperature 58^0C.

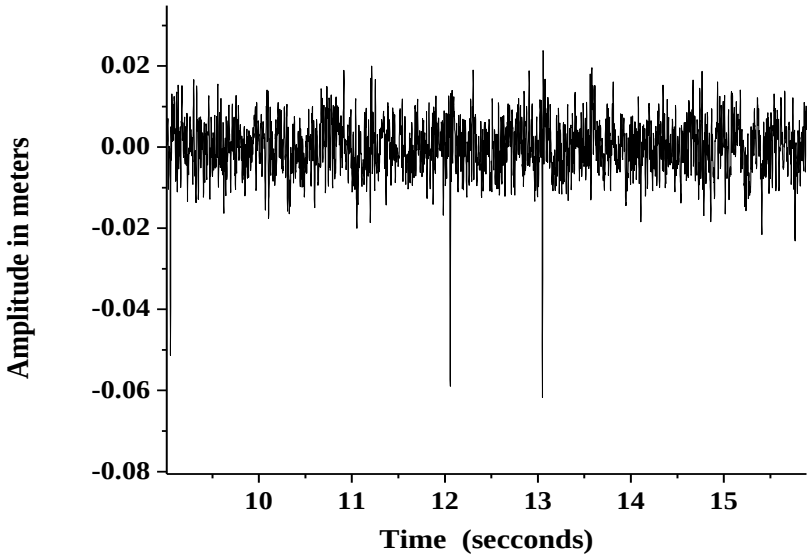

Fig 9.9 Steady state response of the tube at 2 bar pressure and inlet temperature 58^0C.

9.5 EXPERIMENTAL COMPARISION OF VIBRATION OF SLENDER TUBE FOR DIFFERENT END MASS, LENGTH AND SURFACE TEMPERATURE

Experiments were also conducted on single tube with two different end masses, various pressure, length and temperature. The tube specification used for the experiment is same as explained in the Section 9.2. Figure 9.10 shows the response of the tube for two different end masses, namely 46.2 grams and 22.6 grams. The tube length in this case 800 mm and air supply pressure is 3 bar. The maximum displacement of the tube having 46.2 grams end mass is about 6 mm from -2 mm to +4 mm (Refer the red color graph from Figure 9.10) and for 22.6 grams end mass is about 10 mm from -4 mm to +6 mm. As the end mass of the tube increases the displacement decreases, this may be due to increase in inertia effect. The vibration amplitude is reduced for larger end mass in a thin slender tube vibration. Experiments were repeated for different supply air pressure and a same phenomenon was observed.

Figure 9.11 shows the response of the 46.2 grams end mass with tube length 800 mm and working pressure of 1 bar (Refer the red color graph from Figure 9.11) and 4 bar. The maximum displacement of the tube for 1 bar pressure is about 9 mm from -2 mm to +7 mm and for 4 bar pressure is about 14 mm (from -5mm to +9mm). As pressure increases the displacement also increases, due to more force applied on the tube by the air. The supply air pressure multiplied by the projected area of the tube gives the force acting on the tube. This shows that there is a variation in displacement when the air pressure varies. However, it is observed that the variation in natural frequency of the system is not significant.

Figure 9.12 shows the response of the tube for 46.2 grams end mass with supply air pressure, 5 bar and two different length of the tube, 700 mm (Refer the red color graph from Figure 9.12) and 800 mm. The maximum displacement of the tube for 700 mm length is about 8 mm from -3mm to +5mm and for 800 mm length is about 12 mm from -5 mm to +7 mm. As the length of the tube increases the

displacement also increases due to increase in overhanging length of cantilever tube and hence more deflection. It is observed that there is significant effect on the natural frequency of the system due to variation in length of the tube.

Figure 9.13 shows the response of the tube for 22.6 grams end mass and length 800 mm at supply air pressure of 5 bar with ambient temperature, 31^0C and 58^0C (Refer the red color graph from Figure 9.13). The maximum displacement of the tube at ambient temperature is about 8 mm from -3 mm to +5 mm and for 58^0 C temperature is about 11 mm from -2 mm to +4 mm. It is observed that as the temperature of the tube increases the displacement increases due to larger thermal moment. However, the displacement is not significant compared to fluid structure interaction. For a higher temperature, the displacement may be more.

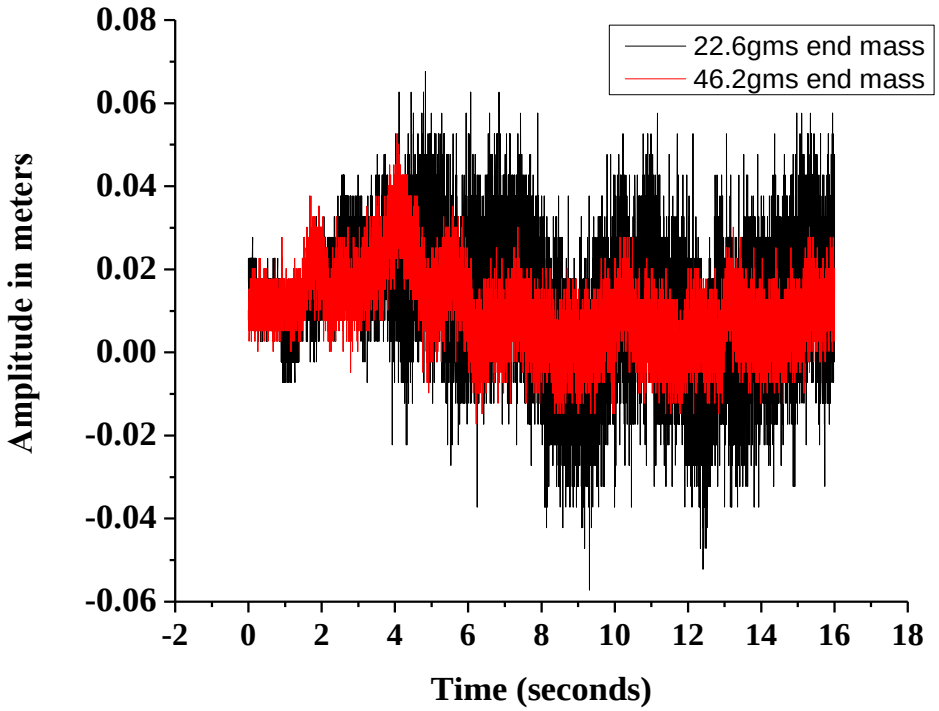

Fig 9.10 Reponses of the tube for different end mass with 3 bar and 800 mm length.

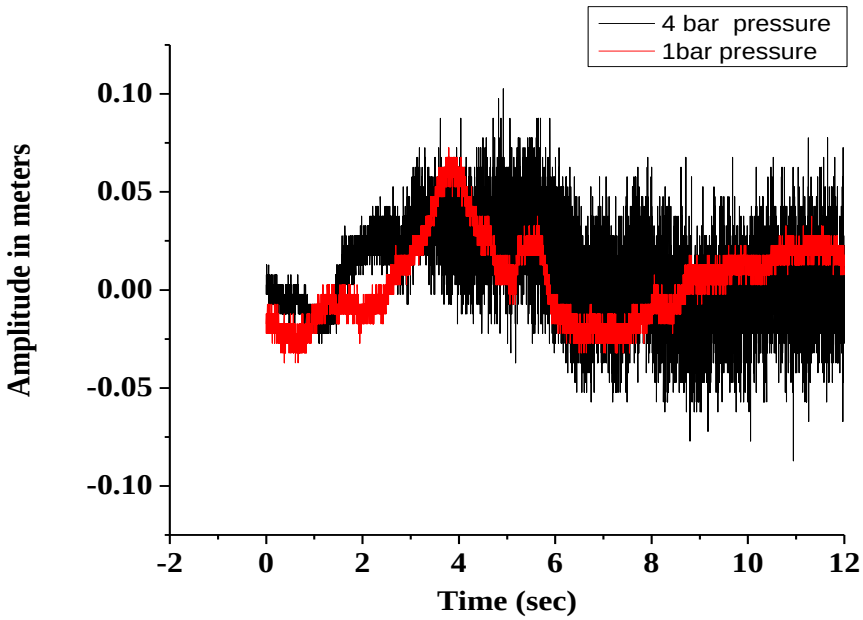

Fig 9.11 Reponses of the tube for different pressures with end mass 46.2 grams and 800 mm length.

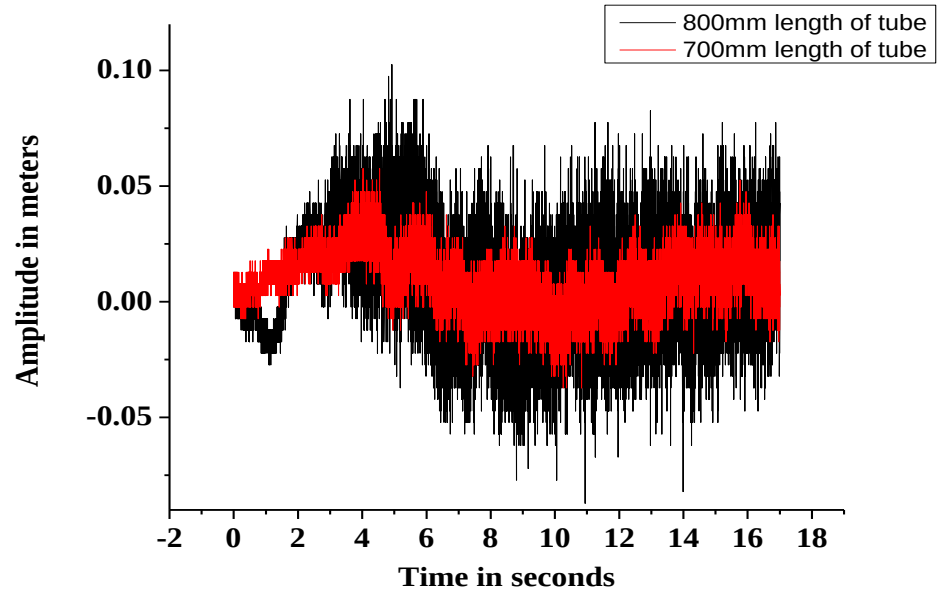

Fig 9.12 Reponses of the tube for different length with end mass 46.2 grams and 5 bar pressure.

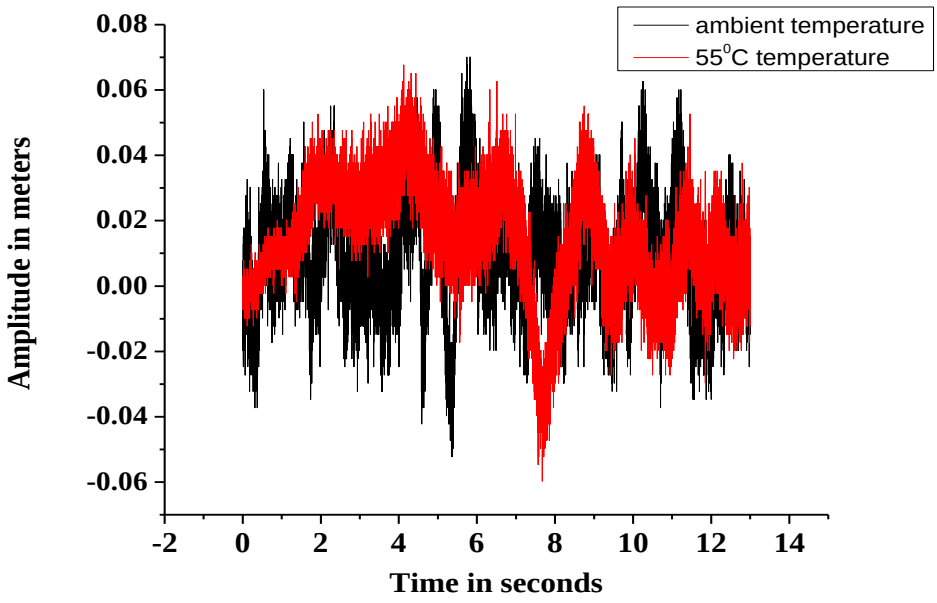

Fig 9.13 Reponses of the tube for different temperature with end mass 46.2 grams and 5 bar pressure.

9.6 NUMERICAL COMPUTATION OF NATURAL FREQUENCY

A fluid flowing through a tube can impose pressure on the tube wall which deflects the tube. A steady high velocity flow through a thin walled tube can either buckle the tube or cause it to oscillate about its axis. These deflections are called instabilities of fluid conveying tube. Similarly, the change in internal temperature of the tube due to temperature change in fluid or change in ambient temperature outside the tube can cause instability. The details of the fluid structure interaction and thermal structure interaction are explained in Chapter 1 to 4 and Chapter 5 to 8 respectively. If sudden expansion of the fluid takes place, it also causes vibration and failure of the tube. Experimental set up explained in Section 9.1 incorporated fluid thermal structure interaction as well as sudden expansion model. In this section, Finite element method is used to investigate the frequency of vibration due to the combined effect.

Considering fluid structure interaction, referring the governing equation (1.23), and rewriting the governing equation as:

$$E I \frac{\partial^4 w}{\partial x^4} + \left[m_f U^2 - \bar{T} + \bar{p} A(1-2\upsilon) \right] \frac{\partial^2 w}{\partial x^2} + 2 m_f U \frac{\partial^2 w}{\partial x \partial t} + (m_f + m) \frac{\partial^2 w}{\partial t^2} = 0 \qquad (9.1)$$

where w is the transverse deflection, x is the distance from fixed end of the tube, E is the Young's modulus, I is the moment of inertia, m is the mass of structure per unit length, A is the area of cross section, $\bar{T}$ is the initial tension. The force induced by the acceleration of the structure can be represent as $\left(m_f + m\right)\frac{\partial^2 w}{\partial t^2}$. As explained by Blevins (2001), the term, $\left(\bar{p}A(1-2\nu) - \bar{T}\right) = 0$ for all x since the fluid pressure at the end of the pipe is the ambient pressure which is taken as zero and also tension, $T_o = 0$ at x = l. If the pipe end is fitted with a convergent nozzle the conservation of momentum gives $\rho AU(U_j - U)$ where U_j is the exit velocity of the air at the orifice and U *i*s the approach velocity (air flow velocity inside the tube). The approach velocity for different supply pressure, U is given in the Figure 4.1. Using the mass conservation equation, $\rho_1 A_1 U = \rho_j A_j U_j$ the exit velocity, U_j is computed for different orifice diameter and it is given in Table 9.2 Here, the density of the air is assumed constant before entering to the orifice and exit from orifice since the flow is through a thin slender tube.

Table 9.2 Thrust force generated through sudden expansion in the orifice.

Supply pressure (bar)	Flow velocity (m/sec)	Exit velocity of orifice (m/sec)			Force generated (N)		
		Diameter= 0.5 mm	Diameter = 1 mm	Diameter= 1.5 mm	Diameter= 0.5 mm	Diameter= 1.0 mm	Diameter =1.5 mm
0.5	5.3	116.3	23.54	12.89	0.00303	0.000498	0.0002076
1	8.7	190.86	47.63	21.17	0.00817	0.001747	0.0005598
2	12.56	275.5	58.76	36.56	0.01704	0.002994	0.0011666
3	19.84	427.36	107.1	48.28	0.04171	0.008933	0.0029115
4	27.56	604.63	150.8	67.1	0.08206	0.017525	0.0056229
5	38.9	853.42	212.97	94.66	0.16349	0.034940	0.0111924

From the Table 9.2, it is noted that for the orifice diameter of 0.5 mm only have the significant effect on thrust generated through sudden expansion. However, for experimental work 1 mm and 1.5 mm orifice is used and hence the effect on sudden expansion of the fluid is negligibly small and not considered in the FEM model.

Considering the thermal structure interaction, the moment acting on the tube is given by:

$$M_T = E\,\alpha\,\Delta T\,\frac{\partial^2 w}{\partial x^2} \tag{9.2}$$

All the terms in the equation (9.2) are explained in Chapter 6.

Combining fluid thermal structure as well as for fluid expansion, the governing differential equation is:

$$E\,I\,\frac{\partial^4 w}{\partial x^4} + \left[m_f U^2 - \bar{T} + \bar{p}\,A(1-2\nu) \right] \frac{\partial^2 w}{\partial x^2} + 2 m_f U \frac{\partial^2 w}{\partial x \partial t} + (m_f + m)\frac{\partial^2 w}{\partial t^2} + M_T = 0 \tag{9.3}$$

The last term, M_T considers deformation due to thermal load which include conduction and convection of the heat through the tube. All the terms in the equation (9.1) are defined earlier and finite element formulation are obtained for the equation (9.1) in Chapter 3. Finite element formulation for the combined effect of fluid thermal structure interaction for the equation (9.3) is explained in Appendix E and natural frequency of the system is obtained for various pressures and temperatures. The natural frequency obtained through the FEM analysis and experimentally obtained results are closely in agreement and results are tabulated in Table 9.3.

9.7 CONCLUSIONS

From the response analysis it is observed that frequency of vibration for 800mm tube length increases from 2.614 to 6.217 Hz for an increase in pressure 1 bar to 5 bar. As the temperature of the fluid increases, the frequency decreases, however it is not predominant compared to the fluid structure interaction. Table 9.3 shows the concluding remarks obtained experimentally and theoretically on the fundamental

frequencies of the pipe conveying hot air. From the Table 9.3, it is observed that the frequency of vibration increases with the increase in pressure and decreases with increase in temperature. The increase in pressure increases the velocity of the fluid flow and reduces the damping effect. Temperature has an effect on displacement as well as frequency, since thermal contraction and expansion increases due to high heat transfer rate at high velocity. Displacement also varies from 22.2 mm to 25.3 mm as the pressure increases from 2 bar to 5 bar (Refer Figure 9.8 and 9.9).

Table 9.3 Experimental and theoretical natural frequency for various temperature and pressure.

Pressure in bar	Fundamental natural frequency (Hz)					
	Experimental results			Theoretical results		
	Ambient temperature 31^0C	Inlet temperature of the air 58^0C	Inlet temperature of the air 78^0C	Ambient temperature 31^0C	Inlet temperature of the air 58^0C	Inlet temperature of the air 78^0C
1	2.614	2.481	2.134	2.511	2.428	2.156
2	3.834	3.356	3.224	3.656	3.512	3.236
3	4.291	3.935	3.434	4.412	3.921	3.351
4	5.811	4.365	3.564	5.122	4.421	3.641
5	6.317	5.8238	4.458	6.516	5.974	4.259

CHAPTER 10
SUMMARY AND SCOPE FOR FURTHER WORK

The purpose of this chapter is to review the significant results obtained during the research work and to make suggestions for future work.

10.1 FLUID INDUCED VIBRATION

Summary drawn from the theoretical and experimental work on fluid-structure interaction of thin slender tube conveying air can be briefly summarized as follows.

Theoretical results of fluid induced vibration

Using Newtonian's approach, the equation of motion for cantilever pipe conveying fluid is derived. The finite element equations are formulated to study the effect of boundary conditions, effect of flow velocity, effect of fluid pressure on the free vibration characteristics of the cantilevered pipe conveying fluid. The FORTRAN codes are written based on the finite element formulation in order to obtain the response of the cantilevered pipe conveying fluid. This code is validated with problems reported journal papers.

The natural frequencies for isotropic steel pipe are compared with the analytical results detailed in Blevins (2001) and numerical results detailed in Lee and Oh (2003) at different conditions like empty pipeline, stagnant fluid and pipe line conveying fluid at various flow velocities and pipe axial tension. It is observed that there is very close comparison between these values (i.e. within 1% of error).

- The natural frequencies for isotropic aluminum pipe are also compared with the analytical results detailed in Blevins (2001) and numerical results detailed in Sinha et al. (2001) at different conditions like empty pipeline, stagnant fluid and fluid velocity 0.55 m/s and 1.1 m/s. It is observed that there is close comparison between these values (i.e. within 12% of error).
- Similarly natural frequencies are compared with numerical results obtained by Zou et al. (2005) for cement coated steel pipe for the simply supported, cantilever and clamped-simply supported pipeline. There is a good comparison of result for simply supported and clamped simply supported pipe, with the

percentage error of 0.12% and for the clamped free tube, the percentage of error is about 5%.

Experimental result of fluid induced vibration

- An experimental set up has been prepared in the laboratory to analyze response of the cantilever tube with vertical and horizontal position conveying compressed air. Experiments are conducted for different air pressure, velocity and length of tube. This experimental data is analyzed through LabVIEW in the time domain plot and frequency domain plot extracted in Origin Pro software.
- It is observed that as the air pass through the tube at certain pressure, the tube deflects from its initial position to some other position and oscillates in that position with certain amplitude. The amount of deflection and amplitude of vibration depends on pressure of air and length of tube.
- From the response plot it is clear that, by increasing the length of cantilever tube will increase the amplitude of transverse displacement and decrease the fundamental frequency of tube, whether it may be in vertical or horizontal position. Also by increasing the pressure, will increase transverse response of cantilever tube and there is no significant change in frequency.
- Experimental results are very closely in agreement to FEM results. By analyzing the tube response due to air flow, it is observed that the response of the tube varies as the fluid pressure, tube initial tension, fluid velocity and length of the tube are varying.

10.2 THERMALLY INDUCED STRUCTURAL MOTION

Transient and convective heat transfer coefficients were determined for vertical tube and theoretical and experimental results were obtained. The following are the summary during the experimental and theoretical model.

- The natural convective heat transfer coefficient for air was calculated to be equal to 18.5 $W/m^{2\ 0}C$ for a copper tube and 19.75 $W/m^{2\ 0}C$ for SS304 tube

kept in a closed box which prevented the cross currents and hence forced convection.

- The experimentally determined heat transfer coefficient was used in the finite element model to compute the transient temperature distribution along the length of the tube and hence steady state temperature.
- The FEM model helped in predicting the steady state temperatures for the tube and can be used to predict steady state temperatures at any other heating rate.
- The theoretical approach is presented to simulate forced convection heat loss for oscillating tube by using the velocity of moving tube for computing Reynold's number, Prandlt number and Nusselt number using which the time dependent heat transfer coefficient is calculated. This approach has shown to provide results which have similar trends as reported by Blandino and Thornton (2001).
- For a range of heating rates between 7.5 and 15 W, the model predicted the transient temperature distribution reasonably well and hence the steady-state temperature and it was observed that the amplitude of thermal induced vibrations increases with increase in heating rate.
- Studies were carried out for higher heating rates and it was observed that the amplitude of vibration depends on the tube natural frequency and heat transfer coefficient during forced convection.
- When the diameter of the tube was increased keeping the thickness and length constant, it was observed that as the tube diameter increases, there is decrease in the amplitude of steady state vibration for a particular heating rate.
- It is noticed that for a particular heating rate for the tube, the amplitude of thermally induced self sustained oscillations were independent of the initial excitation.

The detailed result comparison experimental and theoretical studies on thermally induced vibration of single tube cantilever beam with tip mass subjected to internal heating is presented below:

- Computational studies were presented on the vibration behavior of an internally heated thin circular tube with tip mass. The modified theoretical approach in simulating convection heat loss for oscillating tube has shown to provide results which are in close agreement with the experimentally obtained vibration amplitude.
- For a range of heating rates between 6W to 12W, the model was used to predict the transient temperature distribution and hence the steady-state temperature. The model predicted the steady-state displacements adequately, although it predicted the displacement histories with some error for lower heating rates.
- It is also noted that the amplitude of vibration depends on heat transfer coefficient during forced convection.
- The displacement histories which were initiated due to initial displacement with the passage of time exhibited a initial decrease in the displacement and gradually increased to a maximum value depending on the heating rate and the magnitude of the sustained oscillations were governed by the fact that the heat removed by convection balanced the internal heating.

Experimental and theoretical studies on thermally induced vibration of U-tube cantilever beam with and without tip mass subjected to internal heating is presented below:

- The dynamic response of the U-tubes in lateral direction was studied theoretically and experimentally with tip mass for different heating rates and two different sizes of the U-tubes.
- Natural frequency of the U-tube was obtained experimentally and compared with the theoretical frequency obtained from the FORTRAN code.
- Experimental results when compared with theoretical results for the lateral displacement response of U-tubes with tip mass were as follows: (i) the steady state amplitudes were reasonably in close agreement (ii) during the initial period of the displacement response, the theoretical results showed a rapid raise whereas the experimental displacement response had a slow and gradual growth especially for higher heating rates (iii) for internally heated U-tubes, a

threshold value of heating rate should be exceeded in order to observe thermally induced vibrations.

- Observations on the experimental results for the transverse displacement response of U-tubes without tip mass were as follows (i) for lower heating rates, it took considerable amount of time to attain steady state amplitude when compared to higher heating rates (ii) there exists a threshold heating rate to produce thermal induced motion for U-tube (iii) the time required for steady state thermally induced oscillations depends on the amount of heat input. As the heating rate is increased, the time for steady state increases upto a certain value of heating rate and later on time for steady state oscillations gradually decreases as the heating rate is further increased.

- Observations on the experimental results for the lateral displacement response of U-tubes without tip mass were as follows: (i) lower the heating rates, larger is the time to attain steady state amplitude and vice-versa (ii) there exists a threshold heating rate to produce thermal induced motion for U-tube (iii) during the initial period of the response, the beam motion occurred in the first mode and with progress of time, the displacement response changed to second mode with amplitude of vibration lower than that observed in first mode.

From the experimental and theoretical analysis it is concluded that amplitude of vibration depends on the heat transfer coefficient and structure. And decrease in the displacement is observed for an oscillatory tube due to the increase in heat transfer rate by forced convection.

10.3 FLUID THERMAL STRUCTURE INTERACTION

The combined effect of fluid induced vibration and thermal effect on the oscillation of the tube is studied both experimentally and numerically. The experiments were conducted for different end mass, different length of the tube as well as the fluid passing through the tube at different temperature. It is observed that the displacement and frequency of vibration increases with the increase in pressure

and frequency of vibration decreases with increase in temperature. However, the displacement of the structure is dominant for the variation in pressure compared to the variation in temperature. Experiment and analysis is performed for the temperature of the air varying from 31^0C to 78^0C. Similarly the natural frequency variation is also very small for change in the supply air temperature. The length of the tube has significant effect on the natural frequency of the structure.

Finite element formulation is performed for fluid thermal structure interaction and natural frequency of the system is compared for different air supply pressure and temperature which are closely in agreement with the experimental results. For the variation in pressure from 1 bar to 5 bar for the supply air at ambient temperature 31^0C, maximum error is within 6%. At the higher temperature of the supply air (78^0C), the maximum percentage of error is 8.8%.

10.4 SCOPE FOR FUTURE WORK

- The FEM modeling has to be modified for a compressible fluid like gases where it is flow through large diameter tube. Some investigation in this area is required.
- Thermal induced vibration in the tube conveying fluid at very low temperature and very high temperature is to be investigated.
- Fluid and thermal induced vibration for different composite materials to be investigated.

REFERENCES

1. Ashley H. and Haviland G. (1950), "Boundary vibration of a pipe line containing flowing fluid", *Journals of Applied Mechanics*, 17, 229-232.
2. Baker J.G. (1933), "Self induced vibration", *Transactions of ASME*, 55, 5-13.
3. Bar-Avi P. (2000), Dynamic response of risers conveying fluid, *Transactions of ASME*, 22, 188-193.
4. Beam R. M**.** (1969) ''On the Phenomenon of Thermo elastic instability (thermal flutter) of booms with open cross section,'' *NASA TN D-5222*.
5. Blandino J. R and Thornton E. A. (2001), "Thermally induced vibration of an internally heated beam", *Journals of vibration and acoustics*, 123, 67-74.
6. Blandino J. R. and Thornton E. A**.** (2000) ''Determination of heat transfer coefficients from a vertical vibrating beam'' *Proceedings of the AIAA 34th Thermophysics Conference*, June 19-22, Denver, CO, 1-14.
7. Blandino J. R. and Thornton E. A**.** (2001) "Thermally induced vibration of an internally heated beam" *ASME Journal of Vibration and Acoustics*, 123, 67-75.
8. Blevins R.D. (2001), Flow Induced Vibration, *Krieger Publishing*, Melbourne, USA.
9. Boley, B.A. and Weiner J.H**.** (1960), "Theory of thermal stresses", *Robert E. Krieger Publishing*, Malabar, FL, 313, 339–345.
10. Boley B. A., and Barber A. D**.** (1957) "Dynamic response of beams and plates to rapid heating", *Journal of Applied Mechanics*, 24, 413-416.
11. Boley B. A. (1972) "Approximate analysis of thermally Induced vibrations of beams and plates", *Journal of Applied Mechanics*, 39, 212-216.
12. Boley B.A. (1956), "Thermally induced vibration of beam", *Journal of Aeronaut. Science*, 23, 179-181.
13. Carne J. B. (1937) "Heat loss by natural convection from vertical cylinders", *Philosophical Magazine and Journal of Science*, 24, 635-653.
14. Carslaw H. S. and Jaeger J. C. (1959)**,** "Conduction of heat in solids", Second Edition, *Clarendon Press*, Oxford.
15. Chen,S.S. (1973), "Out of–plane vibration and stability of curved tubes conveying fluid", *Journal of Applied Mechanics*, 40(2), 362-368.

16. Chen T. S. and Yuh C. F. (1980)**,** "Combined heat and mass transfer in natural convection along a vertical cylinder", *International Journal of Heat and Mass Transfer*, 23, 451-461.
17. Cheng Lejin, Xue Mingde, Tang Yuye and Yao Haimin, (2004) "Thermal-dynamic analysis of large scale space structures by FEM", *Chinese Journal of Applied Mechanics.*
18. Chu C.L. and Lin Y.H (1955), "Finite Element Analysis of fluid conveying Timoshenko pipe", *Journal of Shock and Vibration*, 2, 247-255.
19. Crede C.E. and Ruzccku J.E (1990), "Shocks and Vibration Handbook", *McGraw Hill Publications.*
20. Curling L.R. and Païdoussis M.P. (2003), "Analyses of random flow-induced vibration of cylindrical structures subjected to turbulent axial flow", *Journal of Sound and Vibration*, 264, 795-833.
21. De Langre E., Païdoussis M.P, Doare O & Modarres-Sadeghi Y (2007), "Flutter of long flexible cylinders in axial flow", *Journal of Fluid Mechanics*, 571, 371-389.
22. Devid W.U., Gulick and Thornton E. A. (1995), "Thermally induced vibration in spacecraft boom", *Journals of Astronautic*, 36, 163-176.
23. Edelstein W.S. Chen S.S and Jendrzeijezyk J.A (1986), "A finite element computation of the flow induced oscillation in a cantilever tube", *Journal of sound and vibration*, 107, 121-129.
24. Frisch H.P**.** (1970), "Thermally induced vibrations of long thin walled cylinders of open section", *Journal of Spacecraft and Rockets*, 8, 897-905.
25. Friswell M. I., Inman D. J. and Rietz R. W**.** (1997)**,** "Active damping of thermally induced vibration", *Journal of Intelligent Material Systems and Structures*, 8(8), 678-685.
26. Graham J. D. (1970)**,** "Solar induced bending vibrations of a flexible member", *AIAA Journal*, 8(11), 2031-2036.
27. Gulick D.W. and Thornton E.A. (1995), "Thermally induced vibration of an axial boom on a spin stabilized spacecraft", *Journal of Acta Austronaut*, 36, 163-176.

28. Guo C.Q. , Zhang C.H and Paıdoussis M.P. (2010), "Modification of equation of motion of fluid-conveying pipe for laminar and turbulent flow profiles", *Journal of Fluids and Structures*, 26(5), 793-803.
29. Gupta A. K., Johri Tripti and Vats R.P. (2007), "Thermal effect on vibration of non-homogeneous orthotropic rectangular plate having bi-directional parabolically varying thickness" *Proceedings of the World Congress on Engineering and Computer Science 2007, San Francisco, USA.*
30. Hama F. R., Recesso J. V. and Christiaens J. (1959)**,** "The axisymmetric free-convection temperature field along a vertical thin cylinder", *Journal of the Aerospace Sciences*, 26(6), 335-342.
31. Hellum A.M., Mukherjee R and Hull A.J (2010), "Dynamics of pipes conveying fluid with non-uniform turbulent and laminar velocity profiles", *Journal of Fluids and Structures*, 26(5), 804-813.
32. Hill, J.L, and Davis C.G. (1974), "The effect of internal forces on the hydro elastic vibration and stability of planar curved tubes", *Journals of Applied Mechanics*, 255-359.
33. Hills J.L, and Swanson C.P (1970), "Effect of lumped masses on the stability of fluid conveying tubes", *Journals of Applied Mechanics*, 37(4), 494-497.
34. Holmes P.J. (1978), "Pipe supported at both ends can not flutter", *Journal of Applied Mechanics*, 45, 619-622.
35. Hong C. C., Liao H. W., Lee L. T., Ke J. B. and Jane K. C.(2005)**,** "Thermally induced vibration of a thermal sleeve with the GDQ method", *International Journal of Mechanical Sciences*, 47, 1789–1806,.
36. Incropera Frank P. and DeWitt David P**.** (2002)**,** "Fundamentals of heat and mass transfer", Fifth Edition, *John Wiley and Sons*, 399-414.
37. Johnston J. D. and Thornton E. A. (2000)**,** "Thermally induced dynamics of satellite solar panels", *Journal of Spacecraft and Rockets*, 37(5).
38. Johnston J. D. and Thornton E. A.(1996)**,** ''Thermal response of radiantly heated spinning spacecraft booms,'' *Journal of Thermophysics and Heat Transfer*, 10, 60–68.

39. Johnston J. D. and Thornton E.A. (1996),"Thermal response of radiantly heated spinning spacecraft boom", *Journal of thermo physics and heat transfer*, 10, 60-68.
40. Kaneko S, Nakamura T, Inada F, Kato M and Mureithi N.W, (2008), "Flow induced vibrations", *Elsevier Publishing Company*, 145-176.
41. Karagiozis K.N., Païdoussis M.P., Misra A.K. and Grinevich E. (2005), "An experimental study of the nonlinear dynamics of cylindrical shells with clamped ends subjected to axial flow", *Journal of Fluids and Structures*, 20, 801-816.
42. Karagiozis K.N., Païdoussis M.P., Amabili M. and Misra A.K. (2008), "Nonlinear stability of cylindrical shells subjected to axial flow: Theory and experiments", *Journal of Sound and Vibration*, 309, 637-676.
43. Karagiozis K.N., Païdoussis M.P and Misra A.K (2007), "Transmural pressure effects on the stability of clamped cylindrical shells subjected to internal fluid flow: Theory and experiments", *International Journal of Non-Linear Mechanics*, 42, 13-23.
44. Khulief Y.A., Al-Sulliaman F.A. and Bashmal S. (2007), "Vibration analysis of drill strings with self excited stick-slip oscillations", *Journal of Sound and Vibration*, 299, 552-558.
45. Kidawa-Kukla (1997), "Vibration of a beam induced by harmonic motion of a heat source", *Journals of Sounds and Vibration*, 205(2), 213-222.
46. Kidawa-Kukla J. (2003), "Application of green function to the problem of thermally induced vibration of a beam", *Journal of Sound and Vibration*, 262, 865-878.
47. Kim Yool A. (1998)**,** "Thermal crack induced dynamics of space structures", Ph.D thesis, Department of Aeronautics and Astronautics, Massachusetts Institute of Technology.
48. Ko K. E. and Kim Ji-Hwan (2003), "Thermally induced vibrations of spinning thin-walled composite beam", *AIAA Journal*, 41(2).
49. Kohnke P.C. (1978), "Large deflection analysis of frame structures by fictitious forces", *Journal of Numerical Method in Engineering*, 12, 1279-1294.
50. Kong Changduk, Park Hyunbum and Lee Haseaung (2010), " Study on Comparison of Atmospheric and Vacuum Environment of Thermally-Induced

Vibration Using Vacuum Chamber" *International Journal of Aeronautical & Space Sciences*, 11(1), 26-30.

51. Kraus H. (1996)**,** "Thermally induced vibrations of thin nonshallow spherical shells", *AIAA Journal*, 4, 500-505.
52. Krishnamoorty C. S. (2001)**,** "Finite Element Analysis-Theory and Programming", 2001, Second Edition, *Tata McGraw Hill*, Noida, India.
53. Kuiper G.L. and Metrikire A.V. (2008), Experimental investigation of dynamic stability of a cantilever pipe aspirating fluid, *Journal of Fluid and Structure*, 24, 541-558.
54. Lee U. and Kwon K. (2008) "Spectral element modeling of the thermally induced vibration of an axially moving plate" Journal *of Achievements in Materials and Manufacturing Engineering*, 26, 65-72.
55. Lee U. and Oh H. (2003), "The spectral element model for pipelines conveying internal steady flow", *Journal of Engineering Structures*, 25, 1045-1055.
56. Lewis R.W., Nithiarasu P. and Seetharumu K. N. (2004)**,** "Fundamentals of Finite Element Method for Heat and Fluid Flow", John *Wiley and Sons*.
57. Lin W. and Qiao N. (2008), "Vibration stability of an axially moving beam immersed in fluid", *Journals of Solids and Structures*, 45, 1445-1457.
58. Lin Yih-Hwang and Tsai Yau-Kun (1996), "Non linear vibration of Thimoshenko pipe conveying fluid", *Journals of Solids Structure*, 34, 2945-2956.
59. Logan D. L. (2002)**,** "A First Course in the Finite Element Method", Third Edition, *Brooks/Cole, Thomson Learning*, USA.
60. Long R.H. (1955), "Experimental and theoretical study of transverse vibration of a tube containing flowing fluid", *Journal of Applied Mechanics*, 22, 65-68.
61. Lyons W.C. (1966)**,** "Comments on heat induced vibrations of Elastic beams, plates and shells", *AIAA Journal*, 4, 1502-1503.
62. Manolis and Beskos (1981), "Thermally induced vibrations of Beam structures", *Computer methods in Applied Mechanics and Engineering*, 21, 337-355.
63. Mao Qing, Zing, Zhang Jinghui, Leeo Yushan, Wang Haijen and Duan Quan (2006), "Experimental studies of orifice induced wall pressure flections and pipe vibration", *International Journals of Pressure Vessels and Piping*, 86, 505-511

64. Modarres-Sadeghi Y., Païdoussis M.P & Semler C. (2005), "A nonlinear model for an extensible slender flexible cylinder subjected to axial flow", *Journal of Fluids and Structures*, 21, 609-627.
65. Modarres-Sadeghi Y., Païdoussis M.P & Semler C. (2008), "Three-dimensional oscillations of a cantilever pipe conveying fluid", *International Journal of Non-Linear Mechanics*, 43, 18-25.
66. Modarres-Sadeghi Y., Païdoussis M.P., Semler C. and Grinevich E. (2008), "Experiments on vertical slender flexible cylinders clamped at both ends and subjected to axial flow", *Philosophical Transactions of the Royal Society A* , 366, 1275-1296.
67. Murozono M. (1995), "Thermally induced bending vibration of internally heated beam in air", Ph.D thesis, Kyuisha university.
68. Murozono M. and Thornton E.A. (1998), "Buckling and quasi-static thermal structure response of an asymmetric rolled-up solar array", *Journal of Spacer and Rockets*, 35, 147-155.
69. Naguleswaran S and Williams C.J.H. (1968), "Lateral vibration of a pipe conveying a fluid", *Journals of Mechanical Engineering Science*, 10, 228-238.
70. Namkong K, Ghoi H.G. and Yoo J.Y. (2005), "Computation of dynamic fluid-structure interaction in two dimensional flows using combined formulation, *Journal of fluids and structures*, 20, 51-69.
71. Paidoussis, M.P., Matuascu D. and Sim W.G. (1999), "Dynamics and stability of a flexible cylinder in a narrow co-axial cylinder duct subjecting to annular flow", *Journals of Applied Mechanics*, 57, 232-240.
72. Paidoussis M.P and Issid N.T. (1974), "Dynamics stability of pipes conveying fluid", *Journal of Sound and Vibration*, 33, 267-294.
73. Paidoussis M.P and Tetreault-Friend M. (2009), "Aspirating cantilevers and reverse sprinklers", *American Journal of Physics*, 77, 349-353.
74. Paidoussis M.P and Li G.X (1993), "Pipe conveying fluid: A model dynamic problem", *Journal of fluids and structures*, 7,137-204.
75. Paidoussis M.P., Luu T.P and Laithier B.E. (1986), "Dynamics of finite length tubular beam conveying fluid", *Journal of Sound and Vibration*, 106, 311-331.

76. Paidoussis M.P., Grinevich E., Adamovic D. and Semler C. (2002) "Linear and nonlinear dynamics of cantilevered cylinders in axial flow. Part 1: Physical dynamics", *Journal of Fluids and Structures*, 16, 691-713.
77. Paidoussis M.P., Luu T.P. and Prabhakar S. (2008), "Dynamics of a long tubular cantilever conveying fluid downwards, which then flows upwards around the cantilever as a confined annular flow", *Journal of Fluids and Structures*, 24, 111-128.
78. Paidoussis M.P., Sarkar A. and Semler C. (2005), "A horizontal fluid-conveying cantilever: Spatial coherent structures, beam modes and jumps in stability diagram", *Journal of Sound and Vibration*, 280, 141-157.
79. Paidoussis M.P., Semler C. and Wadham-Gagnon M. (2005), "A reappraisal of why aspirating pipes do not flutter at infinitesimal flow", *Journal of Fluids and Structures*, 20, 147-156.
80. Paidoussis M.P., Semler C., Wadham-Gagnon M. and Saaid S. (2007), "Dynamics of cantilevered pipes conveying fluid. Part 2: Dynamics of the system with intermediate spring support", *Journal of Fluids and Structures*, 23, 569-587.
81. Paidoussis M.P. (1966), "Dynamics of flexible slender cylinder in axial flow", *Journal of fluid mechanics*, 26, 717-736.
82. Paidoussis M.P. (1998) , "Fluid-Structure interactions(Slender structures and axial flow)" Volume 1, , *Academic press*, California, USA.
83. Paidoussis M.P. (2008), "The canonical problem of the fluid-conveying pipe and radiation of the knowledge gained to other dynamics problems in Applied Mechanics", *Journal of Sound and Vibration*, 310, 462-492.
84. Paidoussis M.P. and Laithier B.E. (1976), "Dynamics of Timoshanko beam conveying fluid", *Journal of Mechanical Engineering Science*, 18, 210-220.
85. Paidoussis M.P. and Semler C. (1998), "Non-linear dynamics of a fluid conveying cantilever pipe with a small mass attached at the free end", *International Journal of Non-linear Mechanics*.33, 15-32.
86. Rajeev Kumar, Mishra B.K. and Jain S.C**.** (2005)**,** "Thermally induced vibration suppression of antenna reflector with piezoelectric sensors and actuators", Proceedings of ISSS 2005, *International Conference on Smart Materials Structures and Systems*, India.

87. Reddy J. N. (2005)**,** "An Introduction to the Finite Element Method", Second Edition, *Tata McGraw-Hill*, New Delhi.
88. Rimrott R.P.J. and Abdel–Sayed R. (1977), "Flexural thermal flutter under laboratory conditions", *Trans. of CSME*, 4, 187-196.
89. Rinaldi S, and Païdoussis M.P. (2010), "Dynamics of cantilevered pipe discharging fluid, fitted with a stabilized end piece", *Journal of fluids and structures*, 2, 517-525.
90. Rousselet J. and Herrmann G. (1981), "Dynamics behavior of continuous cantilever pipe conveying fluid near the critical velocity", *Journal of Applied Mechanics*, 48, 943-947.
91. Segerlind L. J. (2004)**,** "Applied Finite Analysis", Second Edition, *John Wiley and Sons.*
92. Seibert A. G. and Rice J. S. (1973)**,** "Coupled thermally induced vibrations of beams", *AIAA Journal*, 7(7), 1033-1035.
93. Sheshu P. (2003) "Text book of Finite Element Analysis", *Prentice Hall of India Private Limited*.
94. Silver M.J. (2001)**,** "Picometer scale spontaneous vibrations in a precision deployable boom under thermal loading" Master's thesis, Department of Aerospace Engineering Sciences, *University of Colorado at Boulder*.
95. Sinha J.K, Singh S and Rama Rao A (2001), "Finite element simulation of dynamic behavior of an open ended cantilever pipe conveying fluid", *Journal of Sound and Vibration*, 240(1), 189-194.
96. Srejith B, Jayaraj K, Ganesan N, Padmanaba P, Chellapandi P. and Selvaraj P (2004), "Finite element method analysis of fluid-structure interaction in pipeline system", *Journal of Nuclear Engineering and Design*, 227, 313-322.
97. Stroud R.C. and Mayers J**.** (1971)**,** "Dynamic response of rapidly heated plate elements", *AIAA Journal*, 9 (1), 76-83.
98. Taleb I.A. and Misra A.K. (1981), "Dynamics of an axially moving beam submerged in a fluid", *Journal of hydronautics*, 15, 62-66.
99. Tang L. and Païdoussis M.P. (2008), "The influence of the wake on the stability of cantilevered flexible plates in axial flow", *Journal of Sound and Vibration*, 310, 512-526.

100. Tang L.and Païdoussis M.P. (2007), "On the instability and the post-critical behaviour of two-dimensional cantilevered flexible plates in axial flow", *Journal of Sound and Vibration*, 305, 97-115.
101. Teixira P.R.F. and Awruch A.M. (2005), "Numerical simulation of fluid structure interaction using finite element method", *Journal of Computers and Fluids*, 34, 249-273.
102. Thornton E. A**.** and Kim Y. A**.** (1993), "Thermally induced bending vibrations of a flexible rolled-up solar array,'' *Journal of Spacecrafts and Rockets*, 30, 438– 448.
103. Thornton E.A., Chini G.P. and Gulick D.W. (1995), "Thermally induced vibration of a self-shadowed split blanket solar array", *Journal of Spacer and Rocket*, 32, 302-311.
104. Thornton E.A. (1993), "Thermal buckling of plates and shells", *Journals of Applied mechanics*, 46, 485-506.
105. Thornton E.A. (1996) "Thermal structure for aerospace application", Ph.D thesis, *American Institute of Aeronautics & Astronautics*, Washington.
106. Thornton E.A. and Foster R.S. (1992), "Dynamic response of rapidly heated space structures", *Computational Non-linear Mechanics in Aerospace Engineering*. 146, 451- 477.
107. Tienfuan K., Lee J.J and Weelford L.C (1998), "Finite element analysis of fluid motion with an oscillating structural system", *Journal of Advances in Engineering. Software*, 29,717-722.
108. Tran T.Q.N, Lee H.P. and Lim S.S. (2007), "Structural intensity analysis of thin laminated composite plate subjected thermally induced vibration", *Journal of Composite Structure*, 78, 70-83.
109. Wang, X.Q. So R.M.C. and Liu Y. (2001), "Flow induced vibration of an Euler Bernoulli beam", *Journals of Sounds and Vibration*, 243 (2), 241-268.
110. Wang Bao-Lin and Mai Yiu-Wing (2005), "Transient one-dimensional heat conduction problems solved by finite element", *International Journal of Mechanical Sciences*, 47, 303–317.

111. Wang S., Lui Y. and Huang W. (1998), "Research on solid-liquid coupling dynamics of pipe conveying fluid", *Applied Mathematics and Mechanics*, 19, 1065-1071.
112. Xia J.X., Ni J.R. and Nendoza C (2004), "Hydraulic lifting of manganese nodules through a riser", *Journal of Offshore Mechanics and Arctic Engineering*, 126, 72-77.
113. Young W. C. (2002)**,** "Roark's Formulas for Stress and Strain", Seventh Edition *McGraw-Hill*, New York, NY, 765–766.
114. Yu Yi-Yuan (1969), "Thermally induced vibration and flutter of a flexible boom", *Journal of Spacecraft and Rockets*, 6, 502-510,
115. Zou G.P., Cheraghi N., and Taheri F. (2005), "Fluid induced vibration of composite natural gas pipeline", *International Journals of Solids and Structures*, 42, 1253-1268.

APPENDIX A

LOGARITHMIC DECREMENT METHOD

For damped free vibration general equation is (Crede and Ruzccku 1990),

$$m\frac{d^2x}{dt^2}+C\frac{dx}{dt}+Kx=0 \tag{A1}$$

Figure A1 shows under damped vibration due to fluid resistance to the motion of the body. The fluid resistance is proportional to relative velocity of piston and cylinder. Many non-linearity like internal frictional resistance of materials can lead to deviation in predicted values of vibration.

General solution for equation (A1) is

$$x(t)=Ae^{r_1t}+Be^{r_2t} \tag{A2}$$

Where $r_{1,2}=-\omega_n\left[\xi\pm\sqrt{\xi^2-1}\right]$ (A3)

For under damped system of vibration, roots will be complex conjugate.

$$x(t)=\frac{Ae^{-\omega_n\xi t}}{\sqrt{1-\xi^2}}\sin\left(\omega_n\sqrt{1-\xi^2}t+\phi\right) \tag{A4}$$

where $\sin\phi=\sqrt{1-\xi^2}$ (A5)

The motion is oscillatory with exponentially decaying amplitude. To experimentally determine damping factor ξ, two successive maxima X_m and X_{m+1} are found from the experimentally obtained graph.

Amplitude ratio $\frac{X_m}{X_{m+1}}=e^{2\pi\xi/\sqrt{1-\xi^2}}$ (A6)

$$\delta=\ln\left(\frac{X_m}{X_{m+1}}\right)=\frac{2\pi\xi}{\sqrt{1-\xi^2}} \tag{A7}$$

Damping factor $\xi=\frac{\delta}{\sqrt{\delta^2+4\pi^2}}$ (A8)

Using this equation (A8) damping ratio ξ is determined experimentally.

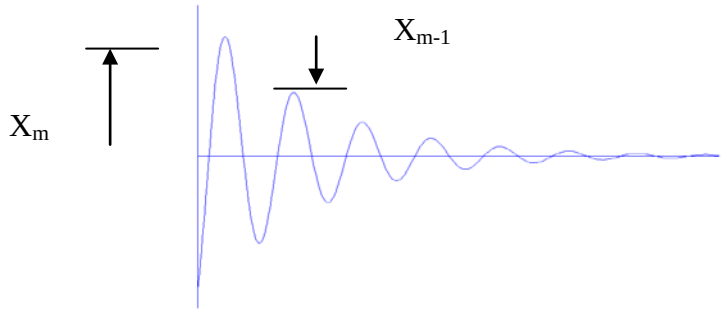

Fig. A1 Response of an under damped vibratory system.

APPENDEX B

Computation of constants of θ matrix

Trail 1:

When U = 28.88 m/s , $\overline{p}$ = 4 bar, l =500 mm

$$C_1 = \left[\frac{261*10^{9}*2.825*10^{-12}}{0.5^2}\right]\left[\frac{0.05*28.8^2}{30*0.5}\right]\left[\frac{7.361*10^{-6}}{30*0.5}\right]\left[\frac{4*3.23*10^{-6}(1-2*0.3)}{30*0.5}\right] = 41.6$$

$$C_2 = \left[\frac{(0.5+3.68*10^{-6})0.5}{420}\right] = 0.0034$$

Trail 2:

When U = 28.88 m/s, $\overline{p}$ = 4 bar, l =600 mm

$$C_1 = \left[\frac{261*10^{9}*2.825*10^{-12}}{0.6^2}\right]\left[\frac{0.5*28.8^2}{30*0.6}\right]\left[\frac{7.361*10^{-6}}{30*0.6}\right]\left[\frac{4*3.23*10^{-6}(1-2*0.3)}{30*0.6}\right] = 24.9$$

$$C_2 = \left[\frac{(0.5+3.68*10^{-6})0.6}{420}\right] = 0.004$$

Trail 3:

When U = 28.88 m/s , $\overline{p}$ = 4 bar, l =700 mm

$$C_1 = \left[\frac{261*10^{9}*2.825*10^{-12}}{0.7^2}\right]\left[\frac{0.5*28.8^2}{30*0.7}\right]\left[\frac{7.361*10^{-6}}{30*0.7}\right]\left[\frac{4*3.23*10^{-6}(1-2*0.3)}{30*0.7}\right] = 16.5$$

$$C_2 = \left[\frac{(0.5+3.68*10^{-6})0.7}{420}\right] = 0.005$$

Trail 4:

When U = 28.88 m/s , $\overline{p}$ = 4 bar, l =800 mm

$$C_1 = \left[\frac{261*10^{9}*2.825*10^{-12}}{0.8^2}\right]\left[\frac{0.5*28.8^2}{30*0.8}\right]\left[\frac{7.361*10^{-6}}{30*0.8}\right]\left[\frac{4*3.23*10^{-6}(1-2*0.3)}{30*0.8}\right] = 11.68$$

$$C_2 = \left[\frac{(0.5+3.68*10^{-6})0.8}{420}\right] = 0.006$$

Trail 5:

When U = 40.8 m/s , $\overline{p}$ = 5 bar, l =500 mm

$$C_1 = \left[\frac{261*10^{9}*2.825*10^{-12}}{0.5^2}\right]\left[\frac{0.5*40.8^2}{30*0.5}\right]\left[\frac{7.361*10^{-6}}{30*0.5}\right]\left[\frac{5*3.23*10^{-6}(1-2*0.3)}{30*0.5}\right] = 43.5$$

Trail 6:

When U = 40.8 m/s, $\bar{p}$ = 5 bar, l =600 mm

$$C_1 = \left[\frac{261*10^{9}*2.825*10^{-12}}{0.6^2}\right]\left[\frac{0.5*40.8^2}{30*0.6}\right]\left[\frac{7.361*10^{-6}}{30*0.6}\right]\left[\frac{5*3.23*10^{-6}(1-2*0.3)}{30*0.6}\right] = 26.9$$

Trail 7:

When U = 40.8 m/s , $\bar{p}$ = 5 bar, l =700 mm

$$C_1 = \left[\frac{261*10^{9}*2.825*10^{-12}}{0.7^2}\right]\left[\frac{0.5*40.8^2}{30*0.7}\right]\left[\frac{7.361*10^{-6}}{30*0.7}\right]\left[\frac{5*3.23*10^{-6}(1-2*0.3)}{30*0.7}\right] = 18.5$$

Trail 8:

When U = 40.8 m/s , $\bar{p}$ = 5 bar, l =800 mm

$$C_1 = \left[\frac{261*10^{9}*2.825*10^{-12}}{0.8^2}\right]\left[\frac{0.5*40.8^2}{30*0.8}\right]\left[\frac{7.361*10^{-6}}{30*0.8}\right]\left[\frac{5*3.23*10^{-6}(1-2*0.3)}{30*0.8}\right] = 13.68$$

Trail 9:

When U =57.6 m/s , $\bar{p}$ = 6 bar, l =500 mm

$$C_1 = \left[\frac{261*10^{9}*2.825*10^{-12}}{0.5^2}\right]\left[\frac{0.5*57.6^2}{30*0.5}\right]\left[\frac{7.361*10^{-6}}{30*0.5}\right]\left[\frac{6*3.23*10^{-6}(1-2*0.3)}{30*0.5}\right] = 47.68$$

Trail 10:

When U =57.6 $/s$, $\bar{p}$ = 6 bar, l =600 mm

$$C_1 = \left[\frac{261*10^{9}*2.825*10^{-12}}{0.6^2}\right]\left[\frac{0.5*57.6^2}{30*0.6}\right]\left[\frac{7.361*10^{-6}}{30*0.6}\right]\left[\frac{6*3.23*10^{-6}(1-2*0.3)}{30*0.6}\right] = 30.98$$

Trail 11:

When U = 57.6 m/s , $\bar{p}$ = 6 bar, l =700 mm

$$C_1 = \left[\frac{261*10^{9}*2.825*10^{-12}}{0.7^2}\right]\left[\frac{0.5*57.6^2}{30*0.7}\right]\left[\frac{7.361*10^{-6}}{30*0.7}\right]\left[\frac{5*3.23*10^{-6}(1-2*0.3)}{30*0.7}\right] = 22.58$$

Trail 12:

When U = 57.6 $/s$, $\bar{p}$ = 6 bar, l =800 mm

$$C_1 = \left[\frac{261*10^{9}*2.825*10^{-12}}{0.8^2}\right]\left[\frac{0.5*57.6^2}{30*0.8}\right]\left[\frac{7.361*10^{-6}}{30*0.8}\right]\left[\frac{5*3.23*10^{-6}(1-2*0.3)}{30*0.8}\right] = 17.7$$

APPENDEX C

Computation of constants of ψ matrix

Trail 1:

When U = 28.88 m/s , $\overline{p}$ = 4 bar, l =500 mm

$$C_3 = \left[\frac{0.5*28.8}{30}\right] = 0.0558$$

Trial 2:

When U = 40.8 m/s , $\overline{p}$ = 5 bar, l =500 mm

$$C_3 = \left[\frac{0.5*40.8}{420}\right] = 0.0788$$

Trial 3:

When U = 57.6 m/s , $\overline{p}$ = 6 bar, l =500 mm

$$C_3 = \left[\frac{0.5*57.6}{420}\right] = 0.1114$$

APPENDIX D

Theoretical frequency (Hz) computed for different pressure and length

Table D1: Natural frequency for 4 bar pressure and velocity 28.88 m/s.

U = 28.88 m/s $\bar{p}$ = 4 bar l = 500 mm	U = 28.88 m/s $\bar{p}$ = 4 bar l =600 mm	U = 28.88 m/s $\bar{p}$ = 4bar l =700 mm	U = 28.88 m/s $\bar{p}$ = 4 bar l =800 mm
4.5402	-0.0094	2.8317	2.4115
4.2902	-0.0094	-2.7014	2.3899
-3.9690	3.7201	2.5800	-2.1550
-3.5690	-3.4807	-2.4058	-2.0550
-2.8729	3.1317	1.0627	0.0047
2.4742	2.4962	1.0627	0.0047
0.6530	-2.9455	-1.1314	-1.7536
0.6530	-2.6603	-1.1314	1.5404
0.9744	0.8225	-0.9085	0.5943
-1.0624	-0.9218	0.6467	-0.6757
-0.5830	0.1251	0.6467	-0.3811
-0.5830	-0.2501	0.5392	0.1940
-0.5447	-0.1194	-0.4207	-0.0451
0.3008	-0.1194	-0.4207	-0.0451
-0.0000	-0.0001	-0.0000	-0.0000
-0.0000	0.0000	-0.0000	0.0000

Eigen-values for other cases are computed in similar line and the result is presented in Table 4.3 in the Chapter 4. For a clamped pipe the results indicate that the first frequency is zero and it was noted in the reference (Zou et al. 2005).

APPENDIX E

Theoretical frequency (Hz) computed for fluid thermal structure interaction

State space representation of the fluid structure interaction is given in equation (3.19). Rewriting the equation (3.19):

$$[\mathbf{\Theta}]\left\{\dot{\xi}\right\}-[\mathbf{\Psi}]\{\xi\}=0 \tag{E1}$$

where, $[\mathbf{\Theta}]=\begin{bmatrix}[\mathbf{K}]_{nsmax} & \mathbf{0}\\ \mathbf{0} & [-\mathbf{M}]_{nsmax}\end{bmatrix}_{nsmax2}$, $[\Psi]=\begin{bmatrix}[\mathbf{0}] & [\mathbf{K}]_{nsmax}\\ [\mathbf{K}]_{nsmax} & [\mathbf{G}]_{nsmax}\end{bmatrix}_{nsmax2}$

$[\mathbf{K}]_{nsmax}=[\mathbf{K}_s^e+\mathbf{K}_f^e+\mathbf{K}_t^e+\mathbf{K}_p^e]_{nsmax}$.

Due to thermal load, the stiffness matrix $[\mathbf{K}]_{nsmax}$ has one more additional stiffness matrix due to thermal load. Hence,

$$[\mathbf{K}]_{nsmax}=[\mathbf{K}_s^e+\mathbf{K}_f^e+\mathbf{K}_t^e+\mathbf{K}_p^e+\mathbf{K}_{Thermal}^e]_{nsmax} \tag{E2}$$

$[\mathbf{K}_{Thermal}^e]$ is obtained from equation (9.2) as:

$$\mathbf{K}_{thermal}^e=\frac{E\alpha\Delta T}{30l}\begin{bmatrix}36 & 3l & -36 & 3l\\ 3l & 4l^2 & -3l & -l^2\\ -36 & -3l & 36 & -3l\\ 3l & -l^2 & -3l & 4l^2\end{bmatrix} \tag{E3}$$

Then,

$$[\mathbf{K}]_{nsmax}=\left(\left(\frac{EI}{l^3}\right)+\left(\frac{m_fU^2}{30l}\right)+\left(\frac{\bar{T}}{30l}\right)+\left\{\frac{\bar{p}A(1-2\upsilon)}{30l}\right\}+\left(\frac{E\alpha\Delta t}{30l}\right)\right)$$
$$\begin{bmatrix}156 & 18l & -156 & 18l & 0 & 0 & 0 & 0\\ 18l & 20l^2 & -18l & -2l^2 & 0 & 0 & 0 & 0\\ -156 & -18l & 312 & 0 & -156 & 18l & 0 & 0\\ 18l & -2l^2 & 0 & 40l^2 & -18l & -2l^2 & 0 & 0\\ 0 & 0 & -156 & -18l & 312 & 0 & -156 & 18l\\ 0 & 0 & 18l & -2l^2 & 0 & 40l^2 & -18l & -2l^2\\ 0 & 0 & 0 & 0 & -156 & -18l & 156 & -18l\\ 0 & 0 & 0 & 0 & 18l & -2l^2 & -18l & 20l^2\end{bmatrix} \tag{E4}$$

The eigenvalues for the state space representation of the system defined in equation (E1) where obtained for identifying the frequency spectrum. For the comparison purpose, the frequency spectrum obtained for temperature 58^0C and 78^0C are given in Table E1. Length of the tube in this case is 800 mm and air supply pressure is 5 bar. Similarly, computation is carried fr different pressures and temperature.

Table E1 Theoretical frequency (Hz) computed for different Temperature.

U = 40.8 m/s Air temperature at 58^0C	U = 40.8 m/s Air temperature at 78^0C
5.9742	4.2595
5.9704	2.1374
2.9435	3.2260
2.8926	2.1121
1.2286	1.5326
1.2318	1.5301
0.6308	0.5454
0.6256	0.5458
0.3832	0.0028
0.3843	0.0028
0.0008	0.0008
0.0008	0.0008
0.0044	0.0010
0.0004	0.0007
0.0000	0.0000
0.0000	0.0000

BIO-DATA

Name: NARASIMHA MARAKALA

Academic Qualification: M.Tech. (Manufacturing Engineering)

Address: Assistant Professor

Department of Mechanical Engineering,

N.M.A.M.Institute of Technology,

Nitte-574 110

Karkala Taluk, Udupi Dist.

Karnataka, India.

E-mail: nmarakala@rediffmail.com

Phone No.: +919945771735

LIST OF PAPER PUBLISHED AND COMMUNICATED

1. Narasimha Marakala, Kondaiah, Appukuttan K.K and Ravikiran Kadoli, (2009) "Experimental studies on dynamic behavior of slender cantilever pipe conveying compressed air", *54th congress of ISTAM (An Iternational Meet)*, Nethaji Shubhas Institute of Technology, New Delhi.
2. Narasimha Marakala, Appukuttan K.K and Ravikiran Kadoli, (2010) "Thermally induced vibration of a simply supported beam using finite element method", *International Journal of Engineering Science and Technology*, 2(12), 7874-7879.
3. Narasimha Marakala, Appukuttan K.K and Ravikiran Kadoli, (2010) "Experimental investigation on dynamic response of slender steel cantilever pipe conveying compressed air", *International Journal on Mechanical and Automobile Engineering*, 09, 14-20.
4. Narasimha Marakala, Appukuttan K.K and Ravikiran Kadoli, (2010) "Experimental studies on dynamic behaviour of slender pipe conveying compressed air at different pressure", *FIME-2010 International conference*, NITK, Surathkal.

5. Narasimha Marakala, Suma H., Appukuttan K.K and Ravikiran Kadoli (2011), “Numerical and experimental study on transient response of a vertical thin sender tube subjected to internal surface heating”, *National Conference on Advances in Mechanical Engineering*, M.I.T. Manipal.